National Library of Canada
Acquisitions and Bibliographic Services Branch
395 Wellington Street
Ottawa, Ontario
K1A 0N4

Bibliothèque nationale du Canada
Direction des acquisitions et des services bibliographiques
395, rue Wellington
Ottawa (Ontario)
K1A 0N4

Your file Votre référence

Our file Notre référence

NOTICE

The quality of this microform is heavily dependent upon the quality of the original thesis submitted for microfilming. Every effort has been made to ensure the highest quality of reproduction possible.

If pages are missing, contact the university which granted the degree.

Some pages may have indistinct print especially if the original pages were typed with a poor typewriter ribbon or if the university sent us an inferior photocopy.

Reproduction in full or in part of this microform is governed by the Canadian Copyright Act, R.S.C. 1970, c. C-30, and subsequent amendments.

AVIS

La qualité de cette microforme dépend grandement de la qualité de la thèse soumise au microfilmage. Nous avons tout fait pour assurer une qualité supérieure de reproduction.

S'il manque des pages, veuillez communiquer avec l'université qui a conféré le grade.

La qualité d'impression de certaines pages peut laisser à désirer, surtout si les pages originales ont été dactylographiées à l'aide d'un ruban usé ou si l'université nous a fait parvenir une photocopie de qualité inférieure.

La reproduction, même partielle, de cette microforme est soumise à la Loi canadienne sur le droit d'auteur, SRC 1970, c. C-30, et ses amendements subséquents.

Canadä

UNIVERSITY OF ALBERTA

A COMPUTATIONAL STUDY OF THE LATERAL DISCHARGE CHARACTERISTICS OF TRANSIENT COMPOUND CHANNEL FLOW

BY

MANAS LAL SHOME ©

A THESIS
SUBMITTED TO THE FACULTY OF GRADUATE STUDIES AND RESEARCH
IN PARTIAL FULFILLMENT OF THE REQUIREMENTS FOR THE DEGREE OF
DOCTOR OF PHILOSOPHY
in
WATER RESOURCES ENGINEERING

DEPARTMENT OF CIVIL ENGINEERING

EDMONTON, ALBERTA
SPRING 1995

National Library
of Canada

Acquisitions and
Bibliographic Services Branch

395 Wellington Street
Ottawa, Ontario
K1A 0N4

Bibliothèque nationale
du Canada

Direction des acquisitions et
des services bibliographiques

395, rue Wellington
Ottawa (Ontario)
K1A 0N4

Your file Votre référence

Our file Notre référence

THE AUTHOR HAS GRANTED AN IRREVOCABLE NON-EXCLUSIVE LICENCE ALLOWING THE NATIONAL LIBRARY OF CANADA TO REPRODUCE, LOAN, DISTRIBUTE OR SELL COPIES OF HIS/HER THESIS BY ANY MEANS AND IN ANY FORM OR FORMAT, MAKING THIS THESIS AVAILABLE TO INTERESTED PERSONS.

L'AUTEUR A ACCORDE UNE LICENCE IRREVOCABLE ET NON EXCLUSIVE PERMETTANT A LA BIBLIOTHEQUE NATIONALE DU CANADA DE REPRODUIRE, PRETER, DISTRIBUER OU VENDRE DES COPIES DE SA THESE DE QUELQUE MANIERE ET SOUS QUELQUE FORME QUE CE SOIT POUR METTRE DES EXEMPLAIRES DE CETTE THESE A LA DISPOSITION DES PERSONNE INTERESSEES.

THE AUTHOR RETAINS OWNERSHIP OF THE COPYRIGHT IN HIS/HER THESIS. NEITHER THE THESIS NOR SUBSTANTIAL EXTRACTS FROM IT MAY BE PRINTED OR OTHERWISE REPRODUCED WITHOUT HIS/HER PERMISSION.

L'AUTEUR CONSERVE LA PROPRIETE DU DROIT D'AUTEUR QUI PROTEGE SA THESE. NI LA THESE NI DES EXTRAITS SUBSTANTIELS DE CELLE-CI NE DOIVENT ETRE IMPRIMES OU AUTREMENT REPRODUITS SANS SON AUTORISATION.

ISBN 0-612-01760-5

Canada

UNIVERSITY OF ALBERTA

RELEASE FORM

NAME OF AUTHOR: MANAS LAL SHOME

TITLE OF THESIS: A COMPUTATIONAL STUDY OF THE LATERAL DISCHARGE CHARACTERISTICS OF TRANSIENT COMPOUND CHANNEL FLOW

DEGREE: DOCTOR OF PHILOSOPHY

YEAR THIS DEGREE GRANTED: SPRING 1995

Permission is hereby granted to the University of Alberta Library to reproduce single copies of this thesis and to lend or sell such copies for private, scholarly, or scientific research purposes only.

The author reserves all other publication and other rights in association with the copyright in the thesis, and except as hereinbefore provided, neither the thesis nor any substantial portion thereof may be printed or otherwise reproduced in any material form whatever without the author's prior written permission.

Manas Lal Shome

PERMANENT ADDRESS:
Village: Uttarsur
Post Office: Srimangal
District: Moulvibazar
Bangladesh.

Dated: March 17, 1995.

UNIVERSITY OF ALBERTA

FACULTY OF GRADUATE STUDIES AND RESEARCH

The undersigned certify that they have read, and recommend to the Faculty of Graduate Studies and Research for acceptance, a thesis entitled A COMPUTATIONAL STUDY OF THE LATERAL DISCHARGE CHARACTERISTICS OF TRANSIENT COMPOUND CHANNEL FLOW submitted by MANAS LAL SHOME in partial fulfillment of the requirements for the degree of DOCTOR OF PHILOSOPHY in Water Resources Engineering.

P. M. STEFFLER, SUPERVISOR

N. RAJARATNAM

F.E. Hicks
F. E. HICKS

D. M. ROGOWSKY

Y. FENG

V. M. PONCE, EXTERNAL EXAMINER

DATE: March 16, 1995

To the memory of my father

ABSTRACT

During a flood event, the volume of a flood plain reach is filled up by lateral flow from the main channel and by longitudinal flow from the upstream end of the flood plain. A comprehensive investigation of the hydraulic characteristics of this lateral flow may lead to some estimates of the transfer of materials from the main channel to the flood plain. An order of magnitude analysis of the governing two-dimensional depth-averaged shallow water equations shows that the inertial terms can be neglected for most flood flows. A zero-inertia computational model is then developed based on a control volume method with an alternating direction implicit scheme. The numerical stability and accuracy of the scheme are investigated by using Fourier Stability Analysis. The model is tested against experimental data and good agreement is found. Also, the relative performance of the model and the FESWMS-2DH (Finite Element Surface Water Modeling System) for hypothetical floods shows that the zero-inertia model produces comparable results with much less computational effort.

A pseudo-steady state form of the zero-inertia model is then applied to investigate the characteristics of lateral flows for two-dimensional monoclinal waves. A theoretical equation is derived to relate the contribution of the lateral flows in filling up the flood plain with the properties of the compound channel and the monoclinal flood wave. Extensive numerical experiments are conducted for straight, prismatic, and symmetric compound channels and the analysis of data produces a similarity profile of the distribution of lateral flows. The scales are the peak lateral discharge and two length scales chosen such that the magnitude of the lateral discharge on each side of the profile is half of the peak discharge. Analysis of the various scales and empirical regression equations for practical purposes are presented.

Finally, two theoretical equations are derived for flow exchange between the main channel and the flood plain in terms of the local channel and flood plain flow depths for fully and partially flooded flood plains. Data from numerical experiments support the trend of these equations reasonably well and empirical regression equations are proposed for practical purposes.

ACKNOWLEDGEMENTS

The author gratefully acknowledges his profound gratitude and indebtedness to Dr. P. M. Steffler, Professor, Department of Civil Engineering, University of Alberta, Edmonton, Alberta, Canada for his supervision, assistance, and encouragement throughout the course of this work. His active interest in this topic and valuable advice throughout the study were of immense help. Supervision and encouragement provided by late Professor R. Gerard at the early stage of this research are gratefully acknowledged.

Sincere thanks are extended to Dr. V. M. Ponce for agreeing to be the external examiner. The valuable suggestions for improvements extended by the examination committee are highly appreciated.

Thanks are also extended to friends and colleagues with whom the author had many fruitful discussions throughout the study.

The financial support provided by the Canadian International Development Agency (CIDA) through the BUET-U of A Linkage Project is gratefully acknowledged.

Finally, special thanks are extended to my beloved wife, Nandita, who made this work possible with her love, support, and forbearance. Satisfaction and happiness brought by our little daughter, Epsita, through her sweet smile and joyful presence are greatly appreciated.

TABLE OF CONTENTS

1 INTRODUCTION

1.1 Background and the objectives of the present study 1

1.2 Presentation of the research work 4

2 GOVERNING EQUATIONS AND THEORETICAL ANALYSIS

2.1 Introduction 7

2.2 Continuity and Reynolds equations for turbulent flow....................8

2.3 Derivations of the depth-averaged flow equations 10

   2.3.1 Evaluation of bed stresses 17

   2.3.2 Modeling of effective shear stresses....................19

2.4 Approximations to the Full Dynamic Equations 25

   2.4.1 Introduction....................25

   2.4.2 Order of magnitude analysis 25

   2.4.3 The two-dimensional zero-inertia model and its mathematical characteristics....................33

2.5 Theoretical analysis of monoclinal waves....................36

   2.5.1 Average wave velocity....................37

   2.5.2 Volume of lateral flows and theoretical analysis....................40

2.6 Non-dimensional form of the governing flow equations....................43

3 NUMERICAL MODEL

3.1 Introduction....................56

3.2 Review of numerical modeling of the compound channel flow....................57

   3.2.1 Modeling of steady flow in compound channel 57

3.2.2 Modeling of unsteady flow in compound Channel 58
3.3 Review of unsteady flow models in overland flow 61
3.4 Development of the two-dimensional zero-inertia model.........................62
3.4.1 Model equations...63
3.4.2 Initial and boundary flow conditions...63
3.4.3 Control volume formulation and the numerical scheme..............64
3.4.4 Small depth problems...73

4 STABILITY AND ACCURACY ANALYSES OF THE NUMERICAL MODEL

4.1 Introduction 78
4.2 Consistency and convergence...79
4.3 Stability and accuracy...80
4.3.1 Linearization of the governing equations......................................80
4.3.2 Numerical amplification factor...86
4.3.3 Analytical amplification factor..92
4.3.4 Amplitude and phase errors analysis..95

5 VALIDATION OF THE NUMERICAL MODEL

5.1 Introduction..119
5.2 Numerical simulation of floods 119
5.3 Conclusion...127

6 APPLICATION OF THE MONOCLINAL WAVE MODEL

6.1 Introduction..158
6.2 Model equations... 159

6.2.1 Initial and boundary flow conditions....159

6.2.2 Numerical experiments....159

6.3 Analysis of results....160

6.3.1 General discussion....160

6.3.2 Non-dimensional analysis of lateral discharge distribution....162

6.4 Expressions for lateral flow exchange....165

6.4.1 Flow into a fully flooded flood plains....165

6.4.2 Flow into a partially flooded flood plains....168

6.4.3 Regression equations for lateral flow exchange....171

7 CONCLUSIONS AND RECOMMENDATIONS

7.1 Summary....197

7.2 Conclusions....198

7.3 Recommendations....200

REFERENCES....202

LIST OF FIGURES

Figure 2.1 Schematic representation of the approximation of the various derivative terms for the order of magnitude analysis....47

Figure 2.2 Monoclinal flood hydrograph....48

Figure 2.3 Half of the plan view of the compound channel....49

Figure 2.4 Effect of width ratio on the ratio of the average wave velocity to the average flow velocity....50

Figure 2.5 Effect of roughness ratio on the ratio of the average wave velocity to the average flow velocity....51

Figure 2.6 Distribution of pseudo-steady flow in the flood plain....52

Figure 2.7 Variation of the non-dimensional volume per unit length filled by lateral discharge with depth ratios for different width ratios....53

Figure 2.8 Variation of the percentage of flood plain volume per unit length filled by lateral discharge with depth ratios for different width ratios....54

Figure 2.9 Variation of the percentage of flood plain volume per unit length filled by lateral discharge with depth ratios for different roughness ratios....55

Figure 3.1 Typical Control Volume....76

Figure 3.2 Relationship between discharge and downstream water surface elevation in small depth situation; a. Increasing slope dominates; b. Decreasing cross sectional area dominates....77

Figure 4.1 Numerical Amplification factor for C_{rx}=0.5, and r_x=0.25....97

Figure 4.2 Numerical Amplification factor for C_{rx}=0.5, and r_x=0.5....98

Figure 4.3 Numerical Amplification factor for C_{rx}=0.5, and r_x=1.0....99

Figure 4.4 Numerical Amplification factor for C_{rx}=0.5, and r_x=5.0....100

Figure 4.5 Numerical Amplification factor for C_{rx}=1.0, and r_x=0.25 101

Figure 4.6 Numerical Amplification factor for C_{rx}=1.0, and r_x=0.5 102

Figure 4.7 Numerical Amplification factor for C_{rx}=1.0, and r_x=1.0 103

Figure 4.8 Numerical Amplification factor for C_{rx}=1.0, and r_x=5.0 104

Figure 4.9a Amplitude Portraits for C_{rx}=0.5, and r_x= 0.25 105

Figure 4.9b Phase Portraits for C_{rx}=0.5, and r_x= 0.25........................106

Figure 4.10a Amplitude Portraits for C_{rx}=0.5, and r_x=0.5........................107

Figure 4.10b Phase Portraits for C_{rx}=0.5, and r_x=.5........................108

Figure 4.11a Amplitude Portraits for C_{rx}=0.5, and r_x=1.0........................109

Figure 4.11b Phase Portraits for C_{rx}=0.5, and r_x=1.0........................110

Figure 4.12a Amplitude Portraits for C_{rx}=1.0 and r_x= 0.25........................111

Figure 4.12b Phase Portraits for C_{rx}=1.0, and r_x= 0.25........................112

Figure 4.13a Amplitude Portraits for C_{rx}=1.0, and r_x= 0.5 113

Figure 4.13b Phase Portraits for C_{rx}=1.0, and r_x=0.50........................114

Figure 4.14a Amplitude for Portraits for C_{rx}=1.0, and r_x=1.0........................115

Figure 4.14b Phase Portraits for C_{rx}=1.0, and r_x=1.0........................116

Figure 4.15a Amplitude for Portraits for C_{rx}=.5 and a_r=100........................117

Figure 4.15b Phase Portraits for C_{rx}=1.0 and a_r=100........................118

Figure 5.1 Inflow discharge hydrograph for Case 1........................128

Figure 5.2 Simulated variation of the depth of flow with time at the inflow boundary for Case 1 129

Figure 5.3 Simulated longitudinal water surface profiles at the various stages of the unsteady flow for Case 1........................130

Figure 5.4 Cross section and longitudinal profile of the Treske's prismatic compound channel (1980)........................131

Figure 5.5 Measured discharge hydrograph at the inflow boundary of Treske's experiment (1980)........................132

Figure 5.6 Measured depth hydrograph at the downstream end of the Treske's experiment (1980)....133

Figure 5.7 Comparison of the downstream discharge hydrograph simulated by zero- inertia model with Treske's data....134

Figure 5.8 Comparison of the upstream depth hydrograph simulated by zero-inertia model with Treske's data....135

Figure 5.9 Cross section of the prismatic compound channel for Case 3....136

Figure 5.10 Various longitudinal discharge hydrographs at 50 km downstream from the inflow boundary along with inflow discharge hydrograph for Case 3....137

Figure 5.11 Simulated depth hydrographs at 50 km downstream from the inflow boundary for Case 3....138

Figure 5.12 Stage-discharge relationship at 50 km downstream from the inflow boundary for Case 3....139

Figure 5.13 Cross-section of the prismatic compound channel for Case 4....140

Figure 5.14 Plan view of the half of the symmetric and prismatic compound channel for Case 4. 141

Figure 5.15 Comparison of the main channel longitudinal discharge hydrographs per unit width at 16 km downstream from the inflow boundary and 150 m off the center line for Case 4....142

Figure 5.16 Comparison of the flood plain longitudinal discharge hydrographs per unit width at 16 km downstream from the inflow boundary and 500 m off the center line for Case 4....143

Figure 5.17 Comparison of the main channel depth hydrographs at 16 km downstream from the inflow boundary and 150 m off the center line for Case 4....144

Figure 5.18 Comparison of the flood plain depth hydrographs at 16 km downstream from the inflow boundary and 500 m off the center line for Case 4..145

Figure 5.19 Comparison of the lateral discharge hydrographs per unit length at 15 km downstream from the inflow boundary and 350 m off the center line for Case 4......................146

Figure 5.20 Comparison of the lateral discharge hydrographs at 15 km downstream from the inflow boundary and 550 m off the center line for Case 4..147

Figure 5.21 Cross-section of the prismatic compound channel for Case 5...............148

Figure 5.22 Plan view of the half of the symmetric and prismatic compound channel for Case 5. 149

Figure 5.23 Comparison of the main channel longitudinal discharge hydrographs per unit width at 60 km downstream from the inflow boundary and 150 m off the center line for Case 5............150

Figure 5.24 Comparison of the flood plain longitudinal discharge hydrographs per unit width at 60 km downstream from the inflow boundary and 500 m off the center line for Case 5............151

Figure 5.25 Comparison of the main channel depth hydrographs at 60 km downstream from the inflow boundary and 150 m off the center line for Case 5...152

Figure 5.26 Comparison of the flood plain depth hydrographs at 60 km downstream from the inflow boundary and 500 m off the center line for Case 5..153

Figure 5.27 Comparison of the depth of flow across the compound channel section at 60 km downstream from the inflow boundary at 24 hours for Case 5...154

Figure 5.28 Comparison of the lateral distribution of the longitudinal velocity across the compound channel section at 60 km downstream from the inflow boundary at 24 hours for Case 5 155

Figure 5.29 Comparison of the lateral discharge hydrographs per unit length at 58 km downstream from the inflow boundary and 350 m off the center line for Case 5 156

Figure 5.30 Comparison of the lateral discharge hydrographs at 58 km downstream from the inflow boundary and 550 m off the center line for Case 5 157

Figure 6.1 Steady water surface profile along the center line of the channel and the initial assumed water surface profile 173

Figure 6.2 Effects of roughness ratio on the main channel water surface profiles 174

Figure 6.3 Effects of roughness ratio on the main channel depth hydrographs 175

Figure 6.4 Effects of roughness ratio on the flood plain water surface profiles 176

Figure 6.5 Spatial distribution of the longitudinal main channel velocity along the wave 177

Figure 6.6 Spatial distribution of the longitudinal flood plain velocity along the wave 178

Figure 6.7 Spatial distribution of the total discharge along the wave 179

Figure 6.8 Monoclinal discharge hydrograph 180

Figure 6.9 Profiles of lateral discharges at various locations across the flood plain 181

Figure 6.10 Variation of peak lateral discharge across the flood plain 182

Figure 6.11 Effect of roughness ratio on the spatial distribution of lateral discharge profile at the interface 183

Figure 6.12 Effect of roughness ratio on the lateral discharge hydrographs at the interface....184
Figure 6.13 Effect of the longitudinal bed slope on the lateral discharge profile at the interface....185
Figure 6.14 Effect of the flood plain width on the lateral discharge profile at the interface....186
Figure 6.15 Similarity profiles of the lateral discharge....187
Figure 6.16 Non-dimensional plot of the peak lateral discharge across the flood plain....188
Figure 6.17 Non-dimensional plot of the left length scale....189
Figure 6.18 Non-dimensional plot of the right length scale....190
Figure 6.19 Comparison of the fitted and the numerical experimental lateral discharge at the interface of the main channel and the flood plain....191
Figure 6.20 Control volume of a fully flooded flood plain....192
Figure 6.21 Control volume of a partially flooded flood plain....193
Figure 6.22 Comparison of the data obtained through the theoretical equations with the simulated data for lateral flow exchange....194
Figure 6.23 Comparison of the data obtained through the regression equation with the simulated data for lateral flow exchange....195
Figure 6.24 Comparison of the data obtained through the linear regression equation with the simulated data for lateral flow exchange....196

LIST OF SYMBOLS

a,b	coefficients
a_r	ratio of longitudinal grid size to lateral grid size
$A, A_o, A_1, A_2, A_3, A_4$	coefficients
$[\mathbf{A}]$	Jacobian matrix
b_t	width of the shear layer
$[\mathbf{B}]$	Jacobian matrix
c	constant
C	dimensional Chezy roughness coefficient
C_*	non-dimensional Chezy roughness coefficient
C_{*c}	non-dimensional Chezy roughness coefficient for the main channel
C_{*p}	non-dimensional Chezy roughness coefficient for the flood plain
C_{cu}	dimensional Chezy roughness coefficient in the main channel at the final stage of flood
C_{pu}	dimensional Chezy roughness coefficient in the flood plain at the final stage of flood
C_{cd}	dimensional Chezy roughness coefficient in the main channel at the initial stage of flood
C_{rx}	Courant number in the longitudinal direction
C_{ry}	Courant number in the lateral direction
c_μ, c'_μ	empirical coefficients
c_v	non-dimensional eddy viscosity
D	main channel depth below flood plain level
D_x	apparent longitudinal diffusion coefficient
D_y	apparent lateral diffusion coefficient

dx	differential distance
dt	differential time
f	friction factor
F_τ	boundary shear force
F_o	reference Froude number
$\{\mathbf{F}_{i,j}\}$	residual vector
g	acceleration due to gravity
$\{\mathbf{G}_{i,j}\}$	residual vector
h	stage at any point
$\hat{h}$	depth perturbation
H_o	uniform flow depth
H	flow depth
H_1	depth in the main channel above the flood plain level
H_2	depth at the outer edge of the flood plain
H_c	main channel depth at the final stage of the flood
H_f	average flood plain depth
H^*	non-dimensional flow depth
$I = \sqrt{-1}$	
I_1, I_2, I_3, I_4	coefficients
i, j, n	integer indices
k	turbulent kinetic energy
k_s	equivalent sand roughness
k_{sc}	effective bed roughness in the main channel
k_{sp}	effective bed roughness in the flood plain
k_1	longitudinal wave number
k_2	lateral wave number
K_{ox}	longitudinal conveyance for uniform flow

K_{oy}	lateral conveyance for uniform flow
K_x	longitudinal conveyance
K_y	lateral conveyance
K_{xx}, K_{xy}, K_{yy}	components of effective stresses
l_s, L_s, L_o	length scale
L	length of a monoclinal wave
L_x	wave length in the longitudinal direction
L_y	wave length in the lateral direction
L_r	wave length ratio
L_{ls}	left length scale
m	iteration number
M	number of control volumes along a row
M_l	convective momentum
N	number of control volumes along a column
n	Manning roughness coefficient
p	hydrostatic pressure
P_a	atmospheric pressure
P_1	hydrostatic pressure at the interface
P_2	hydrostatic pressure at the outer edge of the flood plain
q_m	peak longitudinal discharge per unit width
Q_m	peak longitudinal total discharge
q_o	lateral flow exchange
q_x	longitudinal discharge per unit width
q_{xin}	longitudinal inflow into a control volume
q_{xout}	longitudinal outflow from a control volume
q_x^*	non-dimensional longitudinal discharge per unit width
q_y	lateral discharge per unit length

q_{yin}	lateral flow into a control volume
q_{yout}	lateral flow from a control volume
q_y^*	non-dimensional longitudinal discharge per unit length
q_{ypeak}	peak lateral discharge per unit length at any point
q_{yedge}	peak lateral discharge per unit length at the interface of the main channel and the flood plain
Q_{inflow}	inflow discharge
Q_o	total steady discharge across the flood plain as seen by the moving observer
r_x	non-dimensional longitudinal diffusion coefficient
r_y	non-dimensional lateral diffusion coefficient
R	hydraulic radius
R_1, R_2, R_3, R_4	coefficients
R_d	ratio of the numerical amplification to the analytical amplification
R_θ	ratio of the numerical wave celerity to analytical wave celerity
R_{ls}	right length scale
R.	shear Reynolds number
R^2	coefficient of determination
S	friction slope
S_{ox}	longitudinal bed slope
S_{oy}	lateral bed slope
S_{fx}	longitudinal friction slope
S_{fy}	lateral friction slope
t	time coordinate
t^*	non-dimensional time coordinate
T	wave period
T_c	response time of the channel
T_o	time scale

T_{xx}, T_{xy}, T_{yy}	components of effective stresses
u	time averaged longitudinal velocity at a point
u^*	non-dimensional longitudinal velocity
u'	longitudinal velocity fluctuation
u_*	longitudinal shear velocity
u_s	longitudinal velocity at surface
u_b	longitudinal velocity at the bed
U	depth-averaged longitudinal velocity at a point
U'	longitudinal kinematic wave velocity
U_o	longitudinal uniform flow velocity
U_{ave}	cross-sectional average velocity at the final stage of flood
U_{cu}	uniform longitudinal main channel velocity at the final stage of flood
U_{cd}	uniform longitudinal main channel velocity at the initial stage of flood
U_{pu}	uniform longitudinal flood plain velocity at the final stage of flood
v	time averaged lateral velocity at a point
v_s	lateral velocity at surface
v_b	lateral velocity at the bed
V	depth-averaged lateral velocity at a point
v^*	non-dimensional lateral velocity
v'	lateral velocity fluctuation
V'	lateral kinematic wave velocity
V_o	lateral uniform flow velocity
V_w	wave velocity
V_r	resultant flow velocity
Vol	volume of flood plain per unit length
$Vol\%$	percentage of the volume of flood plain per unit length
W	length scale for the lateral direction

W_c	half-width of the main channel
W_p	width of the flood plain
W_r	ratio of the flood plain width to the half-main channel width
w_s	vertical velocity at water surface
w_b	vertical velocity at the bed
w'	vertical velocity fluctuation
x	longitudinal coordinate
x^*	non-dimensional longitudinal distance
y	lateral coordinate
y^*	non-dimensional lateral distance
y'	distance from the wall
z	vertical coordinate
z_b	bed elevation
α	angle of the bed in the longitudinal direction
α'	constant
α_1	real part of the numerical amplification factor
α_2	real part of the analytical amplification factor
β	diffusion flow number
β'	constant
β_1	imaginary part of the numerical amplification factor
β_2	imaginary part of the analytical amplification factor
ρ	fluid density
υ	kinematic viscosity of the fluid
$\sigma_{xx}, \sigma_{yy}, \sigma_{zz}$	normal stresses
$\nu_t, \nu_{t_1}, \nu_{t_2}, \nu_{t_3}$	eddy viscosity coefficients
γ_y^n	numerical amplification factor for the first half time step
γ_x^n	numerical amplification factor for the second half time step

γ^n	numerical amplification factor for the complete one time step
γ^a	analytical amplification factor
θ	angle between total bed shear stress and the longitudinal component of bed shear stress
θ^n	numerical wave celerity
θ^a	analytical wave celerity
τ_o	wall shear stress
τ_{bx}	component of bed shear stress in the longitudinal direction
τ_{by}	component of bed shear stress in the lateral direction
τ_{xx}	longitudinal shear stress
τ_{xy}	lateral shear stress
τ_b	resultant bed shear stress
ξ	convergence criteria
ε	turbulent energy dissipation rate
η	variable
ω	weighting factor
Δh	change in stage
ΔU	velocity difference across the shear layer
Δx	grid size in the longitudinal direction
Δy	grid size in the lateral direction
Δt	time step
$\{\Delta \mathbf{h}\}$	stage correction vector
Λ	length of the reach of interest

1 INTRODUCTION

1.1 BACKGROUND AND OBJECTIVES OF THE PRESENT STUDY

A compound channel is comprised of a relatively deep channel and one or more flood plains. Many natural rivers and man made drainage and irrigation canals fall under the category of compound channels. During natural and man-made floods, the adjacent flood plain areas get inundated, resulting in serious damage into agricultural fields, properties and lives. As a result, an adequate knowledge of the hydraulics of compound channel flows is required for the proper design and management of rivers, drainage and irrigation canals. Consequently, extensive numerical and experimental investigations have been carried out to study the various aspects of compound channel flows. It has been established that a strong interaction between the faster moving main channel flow and the slower moving flood plain flow takes place (Sellin, 1964; Ahmadi, 1979; Bhowmik and Demissie, 1982). This interaction results in a lateral transfer of a significant amount of longitudinal momentum which affects the velocity, discharge, and bed shear stress distribution. These hydraulic parameters, in turn, affect the transport of sediments and pollutants through the compound channel system.

Geomorphological, environmental and ecological concerns are also associated with floods. As the volume of flow in the flood plain is filled up by the lateral flows from the main channel as well as by the longitudinal flows from the upstream end of a flood plain reach during a flood, suspended sediments, nutrients, and contaminants are transferred from the main channel and get deposited on the flood plain. An adequate knowledge and understanding of the transfer mechanism, quantification of the total volume of the laterally transferred materials, and their distribution is needed to assess the potential risk of environmental and ecological hazards resulting from this process.

As pointed out by Walling, Quine, and He (1989), the dearth of field data on this particular aspect clearly demonstrates the practical problems and difficulties associated with the techniques for measuring the deposition and the distribution of such materials. Walling et al. (1989) discussed the commonly adopted techniques used to measure the deposition rates in the field. These approaches can be broadly classified into two groups based on the time scale involved. One group of approaches measures the deposition rate for an individual flood and the other approaches estimate the deposition rates averaged over a number of years. Among the many other investigators, Leopold (1973), Kesel, Dunne, Mcdonald, Allison and Spicer (1974), Walling and Lambert (1986), attempted to measure the deposition rates of sediments on the flood plains. Investigations of Walling and Lambert (1986) showed that a significant amount of suspended sediment gets deposited on the flood plain during a flood. Walling et al. (1989) discussed the limitations and difficulties involved in implementing the traditional techniques and the reliability of the sampled data. They also proposed a new technique to measure the rate as well as the distribution of the sediments using Caesium-137, a man- made radio nuclide. According to their opinion, this technique seems to be more usable than the other methods but it is also not free from limitations and problems. It is very time consuming and sometimes may underestimate the deposition of coarse sediment or overestimate the fine sediment. The above discussion clearly demonstrates that to make an attempt to quantify the volume and the distribution of the transferred materials which are highly variable in space and time directly in the field is a very difficult and complicated task.

Apart from these field studies, James (1985, 1987) applied a finite difference model to quantify the transfer of sediments from the main channel to the flood plain for steady uniform flow. Pizzuto (1987) developed an analytical model based on a sediment diffusion equation to quantify the deposition of sediment and its distribution in the flood plain. By comparing the field observations, he concluded that suspended sediments are transported by lateral convection as well as by diffusion.

In the present research, attention is devoted to examine and analyze the hydraulic characteristics of the lateral flows that take place between the main channel and the flood plain during floods. A comprehensive investigation of the characteristics of such flow may lead to some simple estimates of the quantity and the distribution of the laterally transferred materials. As it is prohibitively difficult to study this aspect by laboratory experiments, numerical experiments are needed. Solving the full dynamic two-dimensional shallow water equations numerically, however, requires considerable computational time and effort and also special techniques are needed for the dry bed situation. Therefore, simplified equations which are relatively easier to implement but produce comparable results under some conditions are often used. Hence, one of the objectives of this study is to develop a two-dimensional zero-inertia computational model for simulating unsteady compound channel flows. The second objective is to examine the hydraulic characteristics of the lateral discharge component in the flood plain and the contribution of the lateral discharge from the main channel to the flood plain in the filling process. The third objective of the present study is to develop a relationship for flow exchange between the main channel and the flood plain in terms of the local channel and flood plain flow depths.

In order to accomplish these objectives, this study begins with an order of magnitude analysis of the governing two-dimensional depth-averaged shallow water equations. This analysis shows that the inertial terms can be neglected for most flood flows. A two-dimensional zero-inertia computational model is then developed based on the control volume method which is simple, easy to understand, and follows from a direct physical interpretation. The computational domain is discretized into a finite number of non-overlapping control volumes. The depth and all other scalar variables are defined in the center of each control volume. The velocity or the discharge components are defined at the interfaces of each control volume. Consistent flow approximations between control volumes lead to mass conservation at the discrete level. The model solution uses an alternating direction implicit scheme which is robust and computationally very efficient.

The zero-inertia model is then used to develop a methodology to quantify the volume of the lateral flows from the main channel to the flood plain and its distribution along the flood wave and across the flood plain. A pseudo-steady state form of the zero-inertia model (monoclinal wave model) is applied to investigate the hydraulic characteristics of the lateral flows for a two-dimensional monoclinal wave. Application of the monoclinal wave approximation from the point of view of a moving observer makes it possible to analyze the characteristics of the lateral discharge within the wave instead of investigating through the whole length of the compound channel system. It is also possible to use large time steps for numerical experiments.

1.2 PRESENTATION OF THE RESEARCH WORK

The derivation of the depth-averaged shallow water equations and the underlying assumptions are presented in Chapter 2. As the effect of momentum transfer mechanism will be taken into account through the use of an eddy viscosity, the literature on the modeling of the eddy viscosity in the compound channel is reviewed. By order of magnitude analysis, the simplified, zero-inertia model equations are obtained and their properties and limitations are discussed. The terms, ' diffusion ', diffusive ', and ' zero-inertia ' will be used interchangeably in this thesis. The formation and the derivations of the various properties of the two-dimensional monoclinal wave are provided. A theoretical analysis of this wave produces a simple equation which relates the contribution of the lateral flows in filling up the flood plain with the properties of the compound channel and the flood wave. This theoretical analysis is supported by data obtained through extensive numerical experiments conducted for straight, prismatic and symmetric compound channels. The pertinent non-dimensional variables are obtained by non-dimensionalizing the simplified equations and these variables will be used for designing numerical experiments.

In Chapter 3, the description of the development of the proposed model is provided. While doing so, the existing literature on the modeling of compound channel and overland flows is reviewed.

In Chapter 4, the results of linear stability and accuracy analyses for the zero-inertia scheme are presented. These analyses are carried out to examine the amplification and phase portraits of the numerical scheme employed. The purpose of these analyses is also to make effective use of the model by determining discretization parameters which give acceptable accuracy with minimum effort.

In Chapter 5, the performance of the present model is verified. The zero-inertia model is tested against experimental data. The relative performance of the model is also compared with the results obtained from one of the commonly used models in the professional domain, namely, FESWMS-2DH (Finite Element Surface Water Modeling System) developed by U. S. Federal Highways Administration (1989) for two hypothetical flood events to investigate the effect of neglect of inertial terms.

Chapter 6 presents the application of the monoclinal wave model and the analysis of the data obtained through this model. The effects of various physical parameters and flood properties on the hydraulic characteristics of lateral discharge are critically investigated. The data is also analyzed to produce a similarity profile of the distribution of the lateral flows. The scales are the peak lateral discharge and two length scales chosen such that the magnitude of the lateral discharge on each side of the profile is half of the peak discharge. An analysis of the various scales is presented and empirical regression equations are proposed for practical purposes. The spatial distributions of the lateral discharges along the flood wave can be transferred to the lateral discharge hydrographs using the average flood wave velocity as seen by a stationary observer. These findings could be used for an approximate estimate of the volume and the distribution of suspended sediment or other substances transferred from the main channel to the flood plain during a flood.

Finally, a theoretical analysis is carried out to derive a relationship for flow exchange between the main channel and the flood plain in terms of the local channel and flood plain flow depths. Two theoretical equations are derived for different flood plain flow situations, namely, for fully flooded and partially flooded plains. Numerical experimental data support the trend of these theoretical equations reasonably well. Empirical equations obtained through regression analysis are proposed for practical purposes. These equations may be useful for specifying the lateral flow exchange between the main channel and the flood plain flows presently handled by weir type equations in one-dimensional compound channel flow models.

Based on the above mentioned studies, general conclusions and recommendations are provided in Chapter 7.

2 GOVERNING EQUATIONS AND THEORETICAL ANALYSIS

2.1 INTRODUCTION

For many practical open channel flow problems and particularly where the depth of flow is small compared with the horizontal length scales of the area concerned, knowledge of the full three-dimensional flow structure is not always necessary; rather, mean flow variables in two orthogonal horizontal directions are sufficient (Leendertse, 1967; Ponce and Yabusaki, 1981; and Rijn, 1990). For the study under consideration, flow in a compound channel can be investigated from this point of view. The flow is predominantly two-dimensional in plan and the three- dimensional governing equations of flow can be simplified to the depth- averaged flow equations (Jenkins and Keller, 1990). In this chapter, these depth-averaged two-dimensional flow equations are derived from the continuity and Reynolds equations for mean turbulent flow which are introduced in Section 2.2. Having derived the depth-averaged full dynamic flow equations in Section 2.3, the evaluation of bed shear stresses and the representation and the modeling of effective stresses are discussed in Sections 2.3.1 and 2.3.2 respectively. An order of magnitude analysis of the governing equations is carried out in Section 2.4.

Using the information obtained from this scaling process, the full dynamic equations are simplified to zero-inertia approximations and their properties are discussed in Sections 2.4.3. The properties of monoclinal waves and the theoretical analysis of the lateral discharge are then discussed in Section 2.5. Finally, non-dimensional variables are obtained by performing dimensional analysis to the simplified equations in Section 2.6 and these will be used for numerical experiments.

2.2 CONTINUITY AND REYNOLDS EQUATIONS FOR TURBULENT FLOW

The derivations of the continuity and the three dimensional Reynolds equations for an incompressible fluid element can be found in any open channel flow text such as Rijn (1990) or Chaudhry (1993). They are reproduced here as follows. A Cartesian coordinate system, with x, y, and z are the longitudinal, lateral, and vertical directions, respectively, is considered.

The continuity equation for a fluid element in a turbulent flow can be written as:

$$\frac{\partial u}{\partial x}+\frac{\partial v}{\partial y}+\frac{\partial w}{\partial z}=0 \qquad [2.1]$$

and the Reynolds equations for a fluid element in a turbulent flow in the x, y, and z directions, respectively, are written as:

$$\frac{\partial u}{\partial t}+\frac{\partial uu}{\partial x}+\frac{\partial uv}{\partial y}+\frac{\partial uw}{\partial z}=-\frac{1}{\rho}\frac{\partial p}{\partial x}+\frac{1}{\rho}\left(\frac{\partial \sigma_{xx}}{\partial x}+\frac{\partial \tau_{xy}}{\partial y}+\frac{\partial \tau_{xz}}{\partial z}\right) \qquad [2.2]$$

$$\frac{\partial v}{\partial t}+\frac{\partial vu}{\partial x}+\frac{\partial vv}{\partial y}+\frac{\partial vw}{\partial z}=-\frac{1}{\rho}\frac{\partial p}{\partial y}+\frac{1}{\rho}\left(\frac{\partial \tau_{yx}}{\partial x}+\frac{\partial \sigma_{yy}}{\partial y}+\frac{\partial \tau_{yz}}{\partial z}\right) \qquad [2.3]$$

$$\frac{\partial w}{\partial t}+\frac{\partial wu}{\partial x}+\frac{\partial wv}{\partial y}+\frac{\partial ww}{\partial z}=-\frac{1}{\rho}\frac{\partial p}{\partial z}+\frac{1}{\rho}\left(\frac{\partial \tau_{zx}}{\partial x}+\frac{\partial \tau_{zy}}{\partial y}+\frac{\partial \sigma_{zz}}{\partial z}\right)-g \qquad [2.4]$$

where u, v, and w are the time averaged longitudinal, lateral, and vertical velocities, respectively; ρ is the density of fluid, and g is the acceleration due to gravity. The stresses can be expanded as:

$$\sigma_{xx} = 2\rho\upsilon\frac{\partial u}{\partial x} - \rho\overline{u'u'} \qquad [2.5]$$

$$\sigma_{yy} = 2\rho\upsilon\frac{\partial v}{\partial y} - \rho\overline{v'v'} \qquad [2.6]$$

$$\sigma_{zz} = 2\rho\upsilon\frac{\partial w}{\partial z} - \rho\overline{w'w'} \qquad [2.7]$$

$$\tau_{xy} = \rho\upsilon\left(\frac{\partial u}{\partial y} + \frac{\partial v}{\partial x}\right) - \rho\overline{u'v'} \qquad [2.8]$$

$$\tau_{xz} = \rho\upsilon\left(\frac{\partial u}{\partial z} + \frac{\partial w}{\partial x}\right) - \rho\overline{u'w'} \qquad [2.9]$$

$$\tau_{yz} = \rho\upsilon\left(\frac{\partial v}{\partial z} + \frac{\partial w}{\partial y}\right) - \rho\overline{v'w'} \qquad [2.10]$$

where u', v', and w' are the fluctuating part of the instantaneous longitudinal, lateral, and vertical velocities at a point, respectively; and υ is the kinematic viscosity of the fluid.

In equations [2.5] to [2.10], each stress term is comprised of a viscous and turbulent part. The turbulent stresses are known as Reynolds stresses and they appear as additional unknown variables. Experimental investigations have shown that these stresses are much larger than their laminar counterparts except in the viscous sub-layer near a smooth bed surface. For engineering purposes, viscous effects can be neglected for shear Reynolds number, $\mathbf{R}_*$, greater than 30 or 40 (Adeff, 1988). The shear Reynolds number, $\mathbf{R}_*$, is defined by the following:

$$\mathbf{R}_* = \frac{u_* y'}{\nu} \qquad [2.11]$$

where

y' is the distance from the wall,

$u_*(=\sqrt{\frac{\tau_o}{\rho}})$ is the shear velocity, and

τ_0 is the wall shear stress.

In the present study, the viscous stresses are thus neglected.

2.3 DERIVATION OF THE DEPTH-AVERAGED EQUATIONS

The depth averaged flow equations are derived by integrating the continuity and the Reynolds equations over the flow depth as described in this section. The derivation of these flow equations are also found in Jansen, Bendegom, Berg, deVries, and Zanen (1979), Samuels (1985), and Rijn (1990).

The following assumptions are made in order to derive the governing depth averaged flow equations:

1. The flow is incompressible.
2. The fluid is homogeneous i.e., density is uniform across the depth.
3. The stream bed does not change with time.
4. The channel bed slope is small so that sin α= tan α where, α is the angle the bed makes with longitudinal direction.
5. The effect of the rotation of the earth can be neglected.
6. The spatial variation of atmospheric pressure can be neglected.
7. The vertical acceleration is negligible compared with the acceleration due to gravity (g).
8. The frictional resistance formulae for unsteady non-uniform flow are the same as that for steady uniform flow.

9. The momentum correction coefficient is 1.
10. No seepage inflow/outflows, evaporation, or rainfall inflows occur.
11. There are no tangential stresses on the water/ air interface.

The following kinematic boundary condition is applied at the surface. It implies that no flow occurs across the specified boundary (Rijn, 1990):

$$\frac{\partial h}{\partial t}+u_s\frac{\partial h}{\partial x}+v_s\frac{\partial h}{\partial y}-w_s=0, \qquad [2.12]$$

at the bed, no slip condition,

$$u_b=v_b=w_b=0, \qquad [2.13]$$

is applied where u_s, v_s, and w_s are the longitudinal, lateral, and vertical velocities at the water surface, respectively and u_b, v_b, and w_b are the longitudinal, lateral, and vertical velocities at the bed, respectively.

The depth-averaged velocity components in the horizontal x and y directions, respectively, are defined as:

$$U=\frac{1}{H}\int_{z_b}^{h}u\,dz \qquad [2.14]$$

and

$$V=\frac{1}{H}\int_{z_b}^{h}v\,dz \qquad [2.15]$$

where $h=z_b+H$ is the water surface elevation, z_b is the bed elevation, and H is the water depth.

Integrating the continuity equation over the depth,

$$\int_{z_b}^{h}\left(\frac{\partial u}{\partial x}+\frac{\partial v}{\partial y}+\frac{\partial w}{\partial z}\right)dz=0 \qquad [2.16]$$

Considering each term and applying Liebnitz rule,

$$\int_{z_b}^{h}\left(\frac{\partial u}{\partial x}\right)dz=\frac{\partial}{\partial x}\int_{z_b}^{h}udz-u_s\frac{\partial h}{\partial x}+u_b\frac{\partial z_b}{\partial x}=\frac{\partial(HU)}{\partial x}-u_s\frac{\partial h}{\partial x} \qquad [2.17]$$

$$\int_{z_b}^{h}\left(\frac{\partial v}{\partial y}\right)dz=\frac{\partial(HV)}{\partial y}-v_s\frac{\partial h}{\partial y}+v_b\frac{\partial z_b}{\partial y}$$

$$=\frac{\partial(HV)}{\partial y}-v_s\frac{\partial h}{\partial y}$$

[2.18]

$$\int_{z_b}^{h}\left(\frac{\partial w}{\partial z}\right)dz=w_s-w_b=w_s \qquad [2.19]$$

Adding all the terms, rearranging, and applying equation [2.12], the following depth-averaged continuity equation is obtained:

$$\frac{\partial h}{\partial t}+\frac{\partial(HU)}{\partial x}+\frac{\partial(HV)}{\partial y}=0 \qquad [2.20]$$

Using assumption (3) that the bed elevation does not change with time, the water surface elevation, h may be substituted by the water depth, H in the above equation.

Applying assumption (7) that vertical acceleration is negligible, the $z-$momentum equation becomes:

$$\frac{\partial p}{\partial z}+\rho g=0 \qquad [2.21]$$

Integrating the $z-$ momentum equation over the depth

$$\int_{z_b}^{h}\left(\frac{\partial p}{\partial z}+\rho g\right)dz=0 \qquad [2.22]$$

which results in

$p(z)+\rho gz=$ constant [2.23]

The boundary condition at the water surface, i.e., at $z = h$, $p = P_a$, where, P_a is the atmospheric pressure at the water surface, results in

$$p = P_a + \rho g(h - z) \qquad [2.24]$$

which shows the hydrostatic distribution of pressure across the depth.

Integrating the $x-$ momentum equation over the depth gives

$$\int_{z_b}^{h} \frac{\partial u}{\partial t} dz + \int_{z_b}^{h} \left(\frac{\partial uu}{\partial x} + \frac{\partial uv}{\partial y} + \frac{\partial uw}{\partial z} \right) dz = -\frac{1}{\rho} \int_{z_b}^{h} \frac{\partial}{\partial x} [P_a + \rho g(h - z)] dz$$

$$+\frac{1}{\rho} \int_{z_b}^{h} \left(\frac{\partial \sigma_{xx}}{\partial x} + \frac{\partial \tau_{xy}}{\partial y} + \frac{\partial \tau_{zx}}{\partial z} \right) dz \qquad [2.25]$$

Integrating each term and applying Liebnitz rule,

$$\int_{z_b}^{h} \frac{\partial u}{\partial t} dz = \frac{\partial}{\partial t} \int_{z_b}^{h} u dz - u_s \frac{\partial h}{\partial t} + u_b \frac{\partial z_b}{\partial t} = = \frac{\partial (UH)}{\partial t} - u_s \frac{\partial h}{\partial t} \qquad [2.26]$$

$$\int_{z_b}^{h} \frac{\partial uu}{\partial x} dz = \frac{\partial}{\partial x} \int_{z_b}^{h} u^2 dz - u_s^2 \frac{\partial h}{\partial x} + u_b^2 \frac{\partial z_b}{\partial x}$$

$$= \frac{\partial}{\partial x} \int_{z_b}^{h} [U - (U - u)]^2 dz - u_s^2 \frac{\partial h}{\partial x}$$

$$= \frac{\partial}{\partial x} \int_{z_b}^{h} U^2 dz + \frac{\partial}{\partial x} \int_{z_b}^{h} (U - u)^2 dz - u_s{}^2 \frac{\partial h}{\partial x} \qquad \left(\text{since } \frac{\partial}{\partial x} \int_{z_b}^{h} U(U - u) dz = 0\right)$$

$$= \frac{\partial (U^2 H)}{\partial x} + \frac{\partial}{\partial x} \int_{z_b}^{h} (U - u)^2 dz - u_s{}^2 \frac{\partial h}{\partial x} \qquad [2.27]$$

$$\int_{z_b}^{h} \frac{\partial uv}{\partial y} dz = \frac{\partial}{\partial y} \int_{z_b}^{h} uv dz - (u_s v_s) \frac{\partial h}{\partial y} + (u_b v_b) \frac{\partial z_b}{\partial y}$$

$$= \frac{\partial}{\partial y} h \int_{z_b}^{z_b + H} [U - (U - u)][V - (V - v)] dz - (u_s v_s) \frac{\partial h}{\partial y}$$

$$= \frac{\partial}{\partial y} \int_{z_b}^{h} UV dz + \frac{\partial}{\partial y} \int_{z_b}^{h} (U - u)(V - v) dz - (u_s v_s) \frac{\partial h}{\partial y}$$

$$= \frac{\partial (UVH)}{\partial y} + \frac{\partial}{\partial y} \int_{z_b}^{h} (U - u)(V - v) dz - (u_s v_s) \frac{\partial h}{\partial y} \qquad [2.28]$$

$$\int_{z_b}^{h} \frac{\partial (uw)}{\partial z} dz = u_s w_s - u_b w_b = u_s w_s \qquad [2.29]$$

Now adding all the terms on the L.H.S. of the $x-$ momentum equation, the following is obtained:

$$\frac{\partial (UH)}{\partial t} + \frac{\partial (U^2 H)}{\partial x} + \frac{\partial}{\partial x} \int_{z_b}^{h} (U - u)^2 dz + \frac{\partial (UVH)}{\partial y} + \frac{\partial}{\partial y} \int_{z_b}^{h} (U - u)(V - v) dz$$

$$-u_s \left(\frac{\partial h}{\partial t} + u_s \frac{\partial h}{\partial x} + v_s \frac{\partial h}{\partial y} - w_s \right)$$

$$= \frac{\partial (UH)}{\partial t} + \frac{\partial (U^2 H)}{\partial x} + \frac{\partial}{\partial x} \int_{z_b}^{h} (U - u)^2 dz + \frac{\partial (UVH)}{\partial y} + \frac{\partial}{\partial y} \int_{z_b}^{h} (U - u)(V - v) dz \qquad [2.30]$$

Since the last two terms are zero according to boundary conditions, [2.12] and [2.13].

Considering the first term on the R.H.S. of the $x-$ momentum equation,

$$\frac{1}{\rho}\int_{z_b}^{h}\frac{\partial}{\partial x}[P_a+\rho g(h-z)]dz=\frac{1}{\rho}[\int_{z_b}^{h}\frac{\partial P_a}{\partial x}dz+\rho g\int_{z_b}^{h}\frac{\partial h}{\partial x}dz-\rho g\int_{z_b}^{h}\frac{\partial z}{\partial x}]dz \qquad [2.31]$$

Using assumption (6) that the spatial variation of atmospheric pressure is negligible, the first term is zero. Since z is an independent variable, the third term is also zero.

Hence,

$$\frac{1}{\rho}\int_{z_b}^{h}\frac{\partial}{\partial x}[P_a+\rho g(h-z)]dz=g\int_{z_b}^{h}\frac{\partial h}{\partial x}dz=gH\frac{\partial h}{\partial x} \qquad [2.32]$$

Integrating the second term on the R.H.S. of $x-$ momentum equation over the depth and applying the Liebnitz rule,

$$\frac{1}{\rho}\int_{z_b}^{h}\left(\frac{\partial\sigma_{xx}}{\partial x}+\frac{\partial\tau_{yx}}{\partial y}+\frac{\partial\tau_{zx}}{\partial z}\right)dz$$

$$=\frac{1}{\rho}\left[\frac{\partial}{\partial x}\int_{z_b}^{h}\sigma_{xx}dz+\frac{\partial}{\partial y}\int_{z_b}^{h}\tau_{yx}dz+\left(\tau_{zx}-\sigma_{xx}\frac{\partial h}{\partial x}-\tau_{yx}\frac{\partial h}{\partial y}\right)\Bigg|_{h}+\left(\tau_{zx}-\sigma_{xx}\frac{\partial z_b}{\partial x}-\tau_{yx}\frac{\partial z_b}{\partial y}\right)\Bigg|_{z_b}\right]$$

[2.33]

Using assumption (11) that the shear stress at wind-water interface is negligible, the second term on the R.H.S. of the $x-$ momentum equation becomes:

$$\frac{1}{\rho}\left(\frac{\partial}{\partial x}\int_{z_b}^{h}\sigma_{xx}dz+\frac{\partial}{\partial y}\int_{z_b}^{h}\tau_{xy}dz-\tau_{bx}\right) \qquad [2.34]$$

where τ_{bx} is the component of bed shear stress acting along the x-direction.

Defining the following:

$$T_{xx} = \frac{1}{H}\int_{z_b}^{h} \sigma_{xx} dz \qquad [2.35]$$

$$T_{xy} = \frac{1}{H}\int_{z_b}^{h} \tau_{xy} dz \qquad [2.36]$$

$$T_{yy} = \frac{1}{H}\int_{z_b}^{h} \sigma_{yy} dz \qquad [2.37]$$

$$K_{xx} = -\frac{1}{H}\int_{z_b}^{h} \rho (U-u)^2 dz \qquad [2.38]$$

$$K_{xy} = -\frac{1}{H}\int_{z_b}^{h} \rho (U-u)(V-v) dz \qquad [2.39]$$

and

$$K_{yy} = -\frac{1}{H}\int_{z_b}^{h} \rho (V-v)^2 dz \qquad [2.40]$$

T_{xx}, T_{xy}, and T_{yy} are effective stresses due to turbulence and K_{xx}, K_{xy}, and K_{yy} are effective stresses due to the depth-averaging of the non-uniform distributions of velocity in the vertical.

Finally, using the continuity equation and simplifying, the depth-averaged $x-$momentum equation takes the following form:

$$\frac{\partial U}{\partial t} + U\frac{\partial U}{\partial x} + V\frac{\partial U}{\partial y} + g\frac{\partial (z_b + H)}{\partial x} = -\frac{\tau_{bx}}{\rho H} + \frac{1}{\rho H}\frac{\partial (HT_{xx})}{\partial x} + \frac{1}{\rho H}\frac{\partial (HT_{xy})}{\partial y}$$

$$+\frac{1}{\rho H}\frac{\partial (HK_{xx})}{\partial x} + \frac{1}{\rho H}\frac{\partial (HK_{xy})}{\partial y} \qquad [2.41]$$

In a similar fashion, the depth-averaged *y*- momentum equation takes the following form:

$$\frac{\partial V}{\partial t} + U\frac{\partial V}{\partial x} + V\frac{\partial V}{\partial y} + g\frac{\partial(z_b + H)}{\partial y} = -\frac{\tau_{by}}{\rho H} + \frac{1}{\rho H}\frac{\partial(HT_{xy})}{\partial x} + \frac{1}{\rho H}\frac{\partial(HT_{yy})}{\partial y}$$

$$+\frac{1}{\rho H}\frac{\partial(HK_{xy})}{\partial x} + \frac{1}{\rho H}\frac{\partial(HK_{yy})}{\partial y} \qquad [2.42]$$

Equations [2.41] and [2.42] are known as the full dynamic equations.

Rastogi and Rodi (1978) have demonstrated that the effective stresses resulting from the depth-averaging process are much smaller compared to the other terms in boundary layer type flows. While studying the near field of a side discharge into open channel flow, McGuirk and Rodi (1978) also showed that the effect of these terms is negligible. However, Flokstra (1977) showed that these terms can be significant in circulating flows and flows with strong stream line curvatures. Lean and Weare (1979), and Ponce and Yabusaki (1981) also drew similar conclusions by performing numerical experiments on a circulating flow using a two-dimensional depth-averaged flow model. In the case of compound channel flows, these terms are, however, neglected by Keller and Rodi (1984, 1988), and Djordjevic (1993). In the present study, these terms will also be neglected.

2.3.1 EVALUATION OF BED STRESSES

The resultant bed stress generated by friction at the boundary between the flowing fluid and the fixed boundary can be evaluated using several empirical resistance formulae (Henderson, 1966). This bed stress can be evaluated by using dimensional Chezy coefficient and the local depth-averaged resultant velocity written as follows:

$$\tau_b = \frac{\rho g}{C^2} V_r^2 \qquad \text{(Rijn, 1990)} \qquad [2.43]$$

where the resultant velocity is given by

$$V_r = \sqrt{(U^2 + V^2)} \qquad [2.44]$$

and C is the dimensional Chezy coefficient.

The bed stress acting along the x-direction is given by:

$$\tau_{bx} = \tau_b \cos\theta = \frac{\rho g}{C^2} V_r U \qquad \text{(Rijn, 1990)} \qquad [2.45]$$

where θ is the angle between τ_b and τ_{bx}.

Similarly, the bed stress acting along the y-direction can be expressed as:

$$\tau_{by} = \tau_b \sin\theta = \frac{\rho g}{C^2} V_r V \qquad \text{(Rijn, 1990)} \qquad [2.46]$$

The dimensional Chezy coefficient, C can be expressed by the following (Jansen et al., 1979)

$$C = 18\log(\frac{12H}{k_s}) \qquad [2.47]$$

where k_s is the equivalent sand roughness of Nikuradse.

The above equation can also be written in terms of non-dimensional Chezy coefficient, C_*, which is related to, C by the following expression:

$$C_* = \frac{C}{\sqrt{g}} \qquad [2.48]$$

The bed shear stress can also be evaluated by estimating friction slope using Manning equation which can be written as:

Manning equation, $U = \frac{1}{n} R^{\frac{2}{3}} \sqrt{S}$ (for SI units) (Chow, 1959) [2.49]

where n is the Manning roughness coefficient, R is the hydraulic radius, and S is the friction slope.

The following relationships can be used for relating various parameters (Henderson, 1966):

$$C = \frac{1}{n} R^{\frac{1}{6}} \qquad [2.50]$$

$$n = \frac{k_s^{\frac{1}{6}}}{8.25\sqrt{g}} \qquad [2.51]$$

$$C = \sqrt{\frac{8g}{f}} \qquad [2.52]$$

where f is the friction factor.

The values of equivalent sand roughness of Nikuradse, k_s, and the Manning roughness, n, are to be estimated from the field observations. Typical values of Manning roughness coefficient for artificial and natural channels , as well as for flood plains, can be found in Chow (1959) and Henderson (1966), and Barnes (1987). Typical values of k_s can be found in Rijn (1990) and Chaudhry (1993).

2.3.2 MODELING OF EFFECTIVE SHEAR STRESSES

In order to evaluate the effective stresses resulting from time and depth averaging processes, the Boussinesq approximation is normally used. In this approximation, turbulent stresses, similar to viscous stresses, are assumed to be proportional to the gradients of the local depth-averaged velocities. Using this concept, the following expressions can be used for the effective shear stresses:

$$T_{xx} = 2\rho\nu_t \frac{\partial U}{\partial x} \qquad [2.53]$$

$$T_{xy} = T_{yx} = \rho\nu_t (\frac{\partial V}{\partial x} + \frac{\partial U}{\partial y}) \qquad [2.54]$$

where ν_t is the eddy viscosity coefficient which is a property of flow instead of the property of the fluid. In the above expressions, it is also assumed that this coefficient is isotropic. Various turbulence models have been used to estimate the eddy viscosity. These models can be classified into following categories:

I. Zero equation models

II. One equation models

III. Two equation models

IV Stress models

Models belonging to classes I to III use the Boussinnesq eddy viscosity concept and the models under class IV utilize a differential equation for determining Reynolds stresses. A brief description is given herein. A detail review of turbulence models and their applications can be found in Rodi (1984) and the ASCE Task Committee (1988).

I ZERO EQUATION MODELS

In these types of models, eddy viscosity is related to the local gradient of flow velocity following Prandtl's mixing length hypothesis. Using this hypothesis, an equation for logarithmic velocity distribution can be derived. Applying this distribution, an expression for the vertical distribution of eddy viscosity can be obtained. Then, depth-averaging this distribution, the depth-averaged eddy viscosity coefficient can be obtained as:

$$\nu_t = 0.067 u_* H \qquad [2.55]$$

Fischer, List, Koh, Imberger and Brooks (1979) have shown that expression for lateral distribution of the eddy viscosity resulting from bed generated turbulence can be given by

$$\frac{\nu_t}{u_* H} = c_v \qquad [2.56]$$

where c_v is the non-dimensional eddy viscosity coefficient and its value is given by

$$c_v = 0.15 \pm 50\% \qquad [2.57]$$

Lean and Weare (1979) used this formulation with, $c_v = 0.16$, to determine eddy viscosity for circulating flow in a rectangular channel. Wark, Samuels and Ervine (1990) used equation [2.56] to determine the distribution of longitudinal velocity in a compound channel. They found that the stage-discharge relationship is more sensitive to the roughness coefficient rather than to the non-dimensional eddy viscosity. They showed that c_v lies in the range of 0.16 ± 0.08 for the cases studied. They also concluded that the eddy viscosity can be modeled with reasonable accuracy using only this bed generated turbulence.

Vreugdenhil and Wijbenga (1982) suggested that the eddy viscosity for the compound channel be estimated by using either of the following two equations:

$$\nu_t = 0.014 b_t \Delta U \qquad [2.58]$$

$$\nu_t = 0.014 \Delta y^2 \left| \frac{\partial u}{\partial y} \right| \qquad [2.59]$$

where b_t is the width of the shear layer and ΔU is the velocity difference across the shear layer. The limitation of this equation is that it gives a constant eddy viscosity in the shear layer whereas Rajaratnam and Ahmadi (1981) showed that this viscosity varies strongly across the shear layer. They also proposed an expression for eddy viscosity based on the experimental investigation of compound channel flows. They derived an equation for estimating the width of the mixing zone as:

$$b_t = 5.97 D \qquad [2.60]$$

where D is the depth of the main channel below the flood plain level. This mixing width is measured from the location where U begins to decrease laterally in the main channel to the location in the flood plain where U reaches the steady uniform value.

Ogink (1985) investigated the effect of eddy viscosity on flood plain flows for a branch of the river Rhine and concluded that the eddy viscosity estimated by equation [2.58] using equation [2.60] is a reasonable first estimate.

Mckeogh, Kiely, and Javan (1989) postulated that the lateral eddy viscosity can be expressed by the following:

$$\nu_t = \nu_{t_1} + \nu_{t_2} + \nu_{t_3} \qquad [2.61]$$

where

ν_t is the total eddy viscosity,

ν_{t_1} is the contribution from bed generated shear given by $\nu_{t_1} = 0.16\ u_* H$ [2.62]

ν_{t_2} is the contribution from lateral velocity gradient , given by $\nu_{t_2} = 0.013\ l_s U_s$. [2.63]

ν_{t_3} is the contribution from the secondary current (not considered),

l_s is the characteristic length scale for lateral velocity gradient generated shear and it is calculated from the variance of the velocity gradient, and

U_s is the mean velocity in each sub-region, i. e., in the flood plain and main channel.

Mckeogh et al. (1989) also proposed a relationship relating the turbulence intensity and the eddy viscosity as follows:

$$\nu_t = c\sqrt{\overline{u'^2}}\, l_s \qquad [2.64]$$

where c is an empirical constant and l_s is the length scale. Using equations [2.61] to [2.64], they determined the average values of c for the main channel and the flood plain as 0.28 and 0.33 respectively.

Kiely, Javan, and McKeogh (1990) adopted the following equation for the eddy viscosity in order to predict the lateral distribution of longitudinal velocity.

$$\nu_t(y) = U(y)\sqrt{\frac{f(y)}{8}}H \qquad [2.65]$$

where $f(y)$ is the friction factor determined from the *Colebrook-White* equation. Equation [2.65] can be expressed in the form of the equation [2.56] with $c_v = 1$.

II ONE EQUATION MODELS

In these types of models, the eddy viscosity is related to the locally available turbulent kinetic energy (k) and a length scale (L_s). An equation governing the temporal and the spatial variation of k is introduced and the variation of a length scale is used. The eddy viscosity is then calculated as:

$$\nu_t = c'_\mu \sqrt{k} L_s \qquad [2.66]$$

where c'_μ is an empirical constant.

III TWO EQUATIONS MODELS

In this group of turbulence models, the eddy viscosity coefficient is expressed as a function of the locally available depth-averaged turbulent kinetic energy (k) and the local depth-averaged dissipation rate of turbulent energy (ε). Consequently, in addition to the governing flow equations, two additional equations governing the temporal and spatial variation of k and ε are introduced. Then, the expression for eddy viscosity becomes:

$$\nu_t = c_\mu \frac{k^2}{\varepsilon} \qquad [2.67]$$

where, c_μ is a constant.

Rastogi and Rodi (1978) used the depth-averaged version of this relationship for depth-averaged flow and transport in open channels. Moreover, Keller and Rodi (1984, 1988) applied this model in the steady uniform compound channel flow. They found that the velocity distribution was predicted well but the boundary shear stress was overestimated.

Radojkovic and Djordjevic (1985) compared the two-equation models and the zero equation model for compound channel flow using the experimental data of Knight and Demetriou (1983). They demonstrated that in some cases of flows, the non-dimensional eddy viscosity model (equation 2.55) with varying c_v may give better agreement with the experimental data than does the depth-averaged $k-\varepsilon$ model with its standard coefficients.

Pasche, Rouve, and Evers (1985) also investigated the adequacy of the $k-\varepsilon$ model with its standard coefficients for hydraulically smooth and rough compound channels. They concluded that the coefficients have to be calibrated to get better agreement with the experimental data.

IV STRESS MODELS

In all the above cases, isotropic turbulence has been assumed. In order to consider the anisotropic nature of turbulence, higher order models are applied. These are called Reynolds stress models and the turbulent transport terms are determine directly. There are differential transport equations for each of the Reynolds stress components along with the equation for dissipation rate, ε. In order to minimize the complicity and computational effort, Rodi (1984) proposed an algebraic relationship, whereby, the transport of stresses are assumed to be proportional to the transport of kinetic energy.

For the case of compound channel flows, among many other researchers, Krishnappan, and Lau (1986), Tominaga, Nezu, and Kobatake (1989), and Prinos (1989) applied these kinds of models for steady three dimensional flood plain flows.

As seen from the above discussion, no conclusive results has been found regarding the estimation of the eddy viscosity coefficient. However, the dimensionless eddy viscosity model, equation [2.55] is simpler than the popular $k-\varepsilon$ model. Hence, it is decided that in the present study, the eddy viscosity coefficient will be determined using equation [2.55] which is simple and no additional equations are required to solve it numerically.

2.4 APPROXIMATIONS TO THE FULL DYNAMIC EQUATIONS

2.4.1 INTRODUCTION

The derived full dynamic equations represent the combined effects of inertial, gravity, pressure and friction forces on open channel flow. Various approximations to these governing equations for solving open channel flow problems can be obtained by considering the relative magnitude of each of the terms. These simplified forms of the equations represent many physical flow phenomena (Henderson ,1966).

2.4.2 ORDER OF MAGNITUDE ANALYSIS

The various flow approximations can be derived from the continuity and the full dynamic equations by applying a scaling process to non-dimensionalize the equations. Hicks(1990) and many others performed similar analysis for one dimensional flood wave approximations. A detailed description of the procedure for the two-dimensional case will be presented here. The governing equations are reproduced below for easy reference.

$$\frac{\partial H}{\partial t}+\frac{\partial (HU)}{\partial x}+\frac{\partial (HV)}{\partial y}=0 \qquad [2.20]$$

$$\frac{\partial U}{\partial t}+U\frac{\partial U}{\partial x}+V\frac{\partial U}{\partial y}+g\frac{\partial H}{\partial x}=gS_{ox}-\frac{\tau_{bx}}{\rho H}$$
$$+\frac{1}{\rho H}\frac{\partial}{\partial x}\left(2\rho v_t H\frac{\partial U}{\partial x}\right)+\frac{1}{\rho H}\frac{\partial}{\partial y}\left[\rho v_t H\left(\frac{\partial V}{\partial x}+\frac{\partial U}{\partial y}\right)\right] \qquad [2.41]$$

$$\frac{\partial V}{\partial t}+U\frac{\partial V}{\partial x}+V\frac{\partial V}{\partial y}+g\frac{\partial H}{\partial y}=gS_{oy}-\frac{\tau_{by}}{\rho H}$$

$$+\frac{1}{\rho H}\frac{\partial}{\partial x}\left[\rho\nu_t H\left(\frac{\partial V}{\partial x}+\frac{\partial U}{\partial y}\right)\right]+\frac{1}{\rho H}\frac{\partial}{\partial y}\left(2\rho\nu_t H\frac{\partial V}{\partial y}\right) \qquad [2.42]$$

In the present analysis, the following non-dimensional variables are used.

$$x^*=\frac{x}{L_o}\ ,\ y^*=\frac{y}{W}\ ,\ H^*=\frac{H}{H_o}\ ,\ t^*=\frac{t}{T_o}\ ,\ U^*=\frac{U}{U_o}\ ,\ \text{and } V^*=\frac{V}{V_o} \qquad [2.68]$$

L_o is the length scale for the longitudinal direction which could represent the wave length of a disturbance or the length of the reach of interest or natural length scale of the channel, H_o/S_{ox}. The depth scale, H_o could represent the normal depth, critical depth, or some other imposed depth condition. The velocity scale, U_o could represent the uniform flow velocity in the longitudinal direction, or it could be derived from the discharge and depth scale, H_o or it could also be wave velocity $\sqrt{gH_o}$. The lateral length scale, W can be represented by any relevant length in the lateral direction such as the flood plain width or the channel width. For the present analysis, however, two different length scales are chosen for the lateral direction. The depth of flow below the flood plain level can be taken as the appropriate length scale for the shear layer region and the width of the flood plain as the length scale for the region outside the shear layer. Scale approximations of the various derivative terms of the governing equations are shown in Figure 2.1. The approximate ranges of various hydraulic variables are necessary for a scaling analysis. Samuels (1985) presented ranges of some hydraulic variables for British rivers and they are reproduced herein:

Width of the channel ~ 5 to 200 m; typical 30 m.

Width of the flood plain ~ 0 to 2000 m; typical 500 m.

Depth of flow in the channel ~ 1 to 10 m; typical 5 m.

Depth of flow in the flood plain ~ 0 to 4 m; typical 1 m.

Velocity in the channel ~ 0.5 to 3 m/s; typical 1 m/s.

Velocity in the flood plain ~ 0 to 2 m/s; typical 0.3 m/s.

The typical wave length of a flood wave ~ 100 km (Rijn, 1990).

The non-dimensional Chezy coefficient, C_*=10 (Rijn, 1990).

It is seen that if the length of the flood wave is taken as the longitudinal length scale and the width of the flood plain as the lateral length scale, then $W << L_o$.

The time scale, T_o, could be evaluated from hydrologic consideration, such as time of concentration for a basin or storm duration (Linsley, Kohler and Paulhus, 1982). The time scale could also be obtained by applying the response time of the channel (Linsley et al, 1982),

$$T_c = \frac{L_o}{U_o} \qquad [2.69]$$

The remaining velocity scale in the lateral direction, V_O could be obtained from H_o, U_o, and W using continuity equation as described in the sequel.

Considering each term of the continuity equation,

$$\frac{\partial H}{\partial t} = \frac{H_o}{T_o}\frac{\partial H^*}{\partial t^*} \qquad [2.70]$$

$$\frac{\partial (UH)}{\partial x} = \frac{U_o H_o}{L_o}\frac{\partial (U^* H^*)}{\partial x^*} \qquad [2.71]$$

$$\frac{\partial (VH)}{\partial y} = \frac{V_o H_o}{W}\frac{\partial (V^* H^*)}{\partial y^*} \qquad [2.72]$$

Substituting in the continuity equation,

$$\frac{H_o}{T_o}\frac{\partial H^*}{\partial t^*}+\frac{U_oH_o}{L_o}\frac{\partial(U^*H^*)}{\partial x^*}+\frac{V_oH_o}{W}\frac{\partial(V^*H^*)}{\partial y^*}=0 \qquad [2.73]$$

Dividing through by $\frac{U_oH_o}{L_o}$, the following non-dimensional continuity equation is obtained:

$$\frac{L_o}{T_oU_o}\frac{\partial H^*}{\partial t^*}+\frac{\partial(U^*H^*)}{\partial x^*}+\frac{V_oL_o}{WU_o}\frac{\partial(V^*H^*)}{\partial y^*}=0 \qquad [2.74]$$

Using equation [2.69], equation [2.73] can be written as:

$$\frac{T_c}{T_o}\frac{\partial H^*}{\partial t^*}+\frac{\partial(U^*H^*)}{\partial x^*}+\frac{V_oL_o}{WU_o}\frac{\partial(V^*H^*)}{\partial y^*}=0 \qquad [2.75]$$

Hence, if $\frac{T_c}{T_o}<<1$, then the time derivative term can be neglected and consequently, steady flow can be assumed. Furthermore, if $\frac{V_oL_o}{WU_o}<<1$, then one-dimensional steady flow can be assumed.

On the other hand, if, $\frac{T_c}{T_o}\approx 1$, and $\frac{V_oL_o}{WU_o}\approx 1$, then all of the three terms in equation [2.75] are equally significant. In this case, the flow can be considered as an unsteady two-dimensional flow.

From the above discussion, a scale for V_o can be obtained as:

$$V_o=\frac{W}{L_o}U_o \qquad [2.76]$$

Using this scale velocity, the resultant velocity, V_r, can be expressed as:

$$V_r = U_o \sqrt{\left[U^{*2} + \left(\frac{W}{L_o}\right)^2 V^{*2} \right]} \qquad [2.77]$$

It is seen that the second term is smaller than the first term by $\left({}^{W}\!/\!{}_{L_o} \right)^2$. Hence, the resultant velocity can be approximated by

$$V_r = U \qquad [2.78]$$

The various terms in the x-momentum equation [2.41] can be non dimensionalized in a similar way and the following is obtained:

$$\frac{U_o}{T_o}\frac{\partial U^*}{\partial t^*} + \frac{U_o^2}{L_o}U^*\frac{\partial U^*}{\partial x^*} + \frac{U_o^2}{L_o}V^*\frac{\partial U^*}{\partial y^*} + \frac{gH_o}{L_o}\frac{\partial H^*}{\partial x^*} = gS_{ox} - \frac{U_o^2 U^{*2}}{H_o H^* C_*^2}$$
$$+ \frac{U_o}{L_o^2}\frac{1}{H^*}\frac{\partial}{\partial x}\left(2\nu_t H^* \frac{\partial U^*}{\partial x^*}\right) + \frac{U_o}{W^2}\frac{1}{H^*}\frac{\partial}{\partial y}\left(\nu_t H^* \frac{\partial U^*}{\partial y^*}\right) + \frac{U_o}{L_o^2}\frac{1}{H^*}\frac{\partial}{\partial y^*}\left(\nu_t H^* \frac{\partial V^*}{\partial x^*}\right)$$

[2.79]

Dividing through by $\frac{U_o^2}{L_o}$, this equation becomes

$$\frac{\partial U^*}{\partial t^*} + U^*\frac{\partial U^*}{\partial x^*} + V^*\frac{\partial U^*}{\partial y^*} + \frac{gH_o}{U_o^2}\frac{\partial H^*}{\partial x^*} = \frac{gL_o S_{ox}}{U_o^2} - \frac{L_o U^{*2}}{H_o H^* C_*^2}$$
$$+ \frac{1}{U_o L_o}\frac{1}{H^*}\frac{\partial}{\partial x}\left(2\nu_t H^* \frac{\partial U^*}{\partial x^*}\right) + \frac{L_o^2}{W^2}\frac{1}{U_o L_o}\frac{1}{H^*}\frac{\partial}{\partial y}\left(\nu_t H^* \frac{\partial U^*}{\partial y^*}\right) + \frac{1}{U_o L_o}\frac{1}{H^*}\frac{\partial}{\partial y^*}\left(\nu_t H^* \frac{\partial V^*}{\partial x^*}\right)$$

[2.80]

Comparing the coefficients of the effective shear stress terms with those of the other terms, as long as $W << L_o$, the above equation can be simplified as:

$$\frac{\partial U^*}{\partial t^*} + U^* \frac{\partial U^*}{\partial x^*} + V^* \frac{\partial U^*}{\partial y^*} + \frac{gH_o}{U_o^2}\frac{\partial H^*}{\partial x^*} = \frac{gL_o S_{ox}}{U_o^2} - \frac{L_o U^{*2}}{H_o H^* C_*^2} + \frac{L_o^2}{W^2}\frac{1}{U_o L_o}\frac{1}{H^*}\frac{\partial}{\partial y}\left(v_t H^* \frac{\partial U^*}{\partial y^*} \right) \qquad [2.81]$$

The above equation can also be further simplified as:

$$\frac{\partial U^*}{\partial t^*} + U^* \frac{\partial U^*}{\partial x^*} + V^* \frac{\partial U^*}{\partial y^*} + \frac{1}{\mathrm{F}_o^{\,2}}\frac{\partial H^*}{\partial x^*} = \beta\left(\frac{S_{ox} C_*^2}{\mathrm{F}_o^{\,2}} - \frac{U^{*2}}{H^*} \right) + \frac{L_o^2}{W^2}\frac{1}{U_o L_o}\frac{\partial}{\partial y}\left(v_t \frac{\partial U^*}{\partial y^*} \right) \qquad [2.82]$$

where

Scale Froude number, $\mathbf{F}_o = \dfrac{U_o}{\sqrt{gH_o}}$ [2.83]

and

$$\beta = \frac{L_o}{H_o C_*^2} \qquad [2.84]$$

If L_o is defined as the length of the reach, then β is known as the kinematic flow number (Liggett, 1975). If U_o and H_o are defined in terms of uniform flow, then the above equation can be further simplified as:

$$\frac{\partial U^*}{\partial t^*} + U^* \frac{\partial U^*}{\partial x^*} + V^* \frac{\partial U^*}{\partial y^*} + \frac{1}{\mathrm{F}_o^{\,2}}\frac{\partial H^*}{\partial x^*} = \beta\left(1 - \frac{U^{*2}}{H^*} \right) + \frac{L_o^2}{W^2}\frac{1}{U_o L_o}\frac{\partial}{\partial y}\left(v_t \frac{\partial U^*}{\partial y^*} \right) \qquad [2.85]$$

Considering the y - momentum equation, [2.42] and using a similar procedure, the following non-dimensionalized form is obtained:

$$\frac{WU_o^2}{L_o^2}\frac{\partial V^*}{\partial t^*}+\frac{WU_o^2}{L_o^2}U^*\frac{\partial V^*}{\partial x^*}+\frac{WU_o^2}{L_o^2}V^*\frac{\partial V^*}{\partial y^*}+\frac{gH_o}{W}\frac{\partial H^*}{\partial y^*}=gS_{oy}-\frac{WU_o^2}{L_oH_oC_*^2}\frac{U^*V^*}{H^*}$$

$$+\frac{WU_o}{L_o^3}\frac{1}{H^*}\frac{\partial}{\partial x^*}\left(\nu_tH^*\frac{\partial V^*}{\partial x^*}\right)+\frac{U_o}{L_oW}\frac{1}{H^*}\frac{\partial}{\partial x^*}\left(\nu_tH^*\frac{\partial U^*}{\partial y^*}\right)+\frac{U_o}{L_oW}\frac{1}{H^*}\frac{\partial}{\partial y^*}\left(\nu_tH^*\frac{\partial V^*}{\partial y^*}\right)$$

[2.86]

Multiplying through by $\frac{W}{U_o^2}$, equation [2.86] becomes

$$\left(\frac{W}{L_o}\right)^2\left(\frac{\partial V^*}{\partial t^*}+U^*\frac{\partial V^*}{\partial x^*}+V^*\frac{\partial V^*}{\partial y^*}\right)+\frac{gH_o}{U_o^2}\frac{\partial H^*}{\partial y^*}=\frac{WgS_{oy}}{U_o^2}-\frac{W^2}{L_oH_oC_*^2}\frac{U^*V^*}{H^*}$$

$$+\left(\frac{W}{L_o}\right)^2\frac{1}{U_oL_o}\frac{1}{H^*}\frac{\partial}{\partial x^*}\left(\nu_tH^*\frac{\partial V^*}{\partial x^*}\right)+\frac{1}{U_oL_o}\frac{1}{H^*}\frac{\partial}{\partial x^*}\left(\nu_tH^*\frac{\partial U^*}{\partial y^*}\right)+\frac{1}{U_oL_o}\frac{1}{H^*}\frac{\partial}{\partial y^*}\left(\nu_tH^*\frac{\partial V^*}{\partial y^*}\right)$$

[2.87]

Equation [2.87] shows that the coefficients of the effective shear stress terms are much smaller in comparison to the other terms and hence these terms can be neglected.

Making further simplifications, the following non-dimensional form of the $y-$ momentum equation is obtained:

$$\left(\frac{W}{L_o}\right)^2\left(\frac{\partial V^*}{\partial t^*}+U^*\frac{\partial V^*}{\partial x^*}+V^*\frac{\partial V^*}{\partial y^*}\right)+\frac{1}{\mathrm{F}_o^2}\frac{\partial H^*}{\partial y^*}=\beta\left(\frac{W}{L_o}\right)^2\left(\frac{C_*^2S_{oy}L_o}{\mathrm{F}_o^2W}-\frac{U^*V^*}{H^*}\right) \quad [2.88]$$

where F_o and β are defined before.

The scaling analysis results in three non-dimensional parameters, namely, $\mathbf{F}_o$, β, and W/L_o. Depending on the magnitude of the each of these parameters, various approximations to the governing equations can be developed. In doing so, the scale variables need to be defined. In the present analysis, L_o is considered as the wave length and T_o as the wave period. The depth below the flood plain level is considered as the lateral length scale for the shear layer region and the width of the flood plain as a scale for the region outside the shear layer. Hence, in the present analysis, the term, β is defined as the diffusion flow number.

By comparing the relative magnitudes of the various terms of the equations [2.85] and [2.88], it is apparent that the inertial terms in the $y-$ momentum equation, [2.88] are smaller by $\left({W}/{L_o}\right)^2$. If the magnitudes of β and ${1}/{F_o^2}$ are much larger than 1 and the magnitude of the ratio ${W}/{L_o}$ is much less than 1, then it is apparent from [2.85] and [2.88] that the inertial terms are much smaller than the pressure, gravity , and friction terms. Considering the range of values of the various hydraulic variables as cited earlier, the magnitude of each of the non-dimensional parameters can be estimated as:

$\mathbf{F}_o \approx 0.1 \sim 0.3$; typical 0.15;

$\beta \approx 200 \sim 1000$, typical 500;

$\dfrac{W}{L_o} \approx 0.001 \sim 0.02$, typical 0.005;

Considering the magnitudes of these parameters, it can easily be concluded that the inertial terms are much smaller than the other terms for some flood flows and consequently, the two - dimensional zero-inertia approximation to the full dynamic equations can be applied for simulating most flood flows.

Ponce, Li, and Simons (1978) investigated and assessed the applicability of the one-dimensional zero-inertia wave approximation by comparing its celerity and wave attenuation with those of the full dynamic equations. They proposed the following criteria for practical purposes:

$$TS_{ox}\sqrt{\frac{g}{H_o}} \geq 30 \qquad [2.89]$$

where T is the wave period.

This criteria can be expressed using the non-dimensional parameters, $\mathbf{F}_o$ and β as follows:

$$\beta\,\mathbf{F}_o \geq 45 \tag{2.90}$$

From the cited typical values of various parameters, it is evident that this criteria is also satisfied. Therefore, it can be concluded that the two - dimensional zero-inertia model can be confidently applied for simulating flood flows with magnitudes of the non-dimensional parameters lying in the above mentioned ranges.

2.4.3 THE TWO-DIMENSIONAL ZERO-INERTIA MODEL AND ITS MATHEMATICAL CHARACTERISTICS

As the scaling analysis shows that the zero-inertia approximation can be applied to some flood flows, the governing flow equations reduce to the following forms:

$$\frac{\partial h}{\partial t}+\frac{\partial q_x}{\partial x}+\frac{\partial q_y}{\partial y}=0 \tag{2.91}$$

$$g\frac{\partial h}{\partial x}=-\frac{\tau_{bx}}{\rho H}+\frac{1}{\rho H}\frac{\partial}{\partial y}\left(\rho v_t H\frac{\partial U}{\partial y}\right) \tag{2.92}$$

$$g\frac{\partial h}{\partial y}=-\frac{\tau_{by}}{\rho H} \tag{2.93}$$

q_x and q_y are the longitudinal and the lateral discharge components respectively.

In order to investigate the mathematical characteristics of these partial differential equations, the effective stress term is neglected for simplicity. The continuity and momentum equations can be written as:

$$\frac{\partial H}{\partial t}+U\frac{\partial H}{\partial x}+H\frac{\partial U}{\partial x}+V\frac{\partial H}{\partial y}+H\frac{\partial V}{\partial y}=0 \qquad [2.94]$$

Substitution of the expression for τ_{bx} in equation [2.92] results in

$$\frac{\partial H}{\partial x}=S_{ox}-\frac{U^2}{gHC_*^2} \qquad [2.95]$$

then,

$$\frac{\partial^2 H}{\partial x^2}=-\frac{2U}{gHC_*^2}\frac{\partial U}{\partial x}+\frac{U^2}{gH^2C_*^2}\frac{\partial H}{\partial x} \qquad \text{for constant } S_{ox} \text{ and } C_* \qquad [2.96]$$

Rearranging and simplifying , this reduces to

$$\frac{\partial U}{\partial x}=-\frac{gHC_*^2}{2U}\frac{\partial^2 H}{\partial x^2}+\frac{U}{2H}\frac{\partial H}{\partial x} \qquad [2.97]$$

Similarly , substitution of the expression for τ_{by} in equation [2.93] yields

$$\frac{\partial H}{\partial y}=S_{oy}-\frac{UV}{gHC_*^2} \qquad [2.98]$$

then,

$$\frac{\partial^2 H}{\partial y^2}=-\left(\frac{U}{gHC_*^2}\frac{\partial V}{\partial y}+\frac{V}{gHC_*^2}\frac{\partial U}{\partial y}+\frac{VU}{gH^2C_*^2}\frac{\partial H}{\partial y}\right) \qquad [2.99]$$

Rearranging and simplifying, equation [2.99] gives

$$\frac{\partial V}{\partial y}=-\frac{gHC_*^2}{U}\frac{\partial^2 H}{\partial y^2}-\frac{V}{U}\frac{\partial U}{\partial y}+\frac{V}{H}\frac{\partial H}{\partial y} \qquad [2.100]$$

Again, differentiating equation [2.95] with respect to y and simplifying, the following is obtained:

$$\frac{\partial U}{\partial y} = -\frac{gHC_*^2}{2U}\frac{\partial^2 H}{\partial x \partial y} + \frac{U}{2H}\frac{\partial H}{\partial y} \qquad [2.101]$$

An order of magnitude analysis shows that the first term on the R.H.S. is much smaller than the second term and thus can be neglected. Hence,

$$\frac{\partial U}{\partial y} = \frac{U}{2H}\frac{\partial H}{\partial y} \qquad [2.102]$$

Substituting equations [2.97], [2.100], and [2.102] in the continuity equation [2.94], the following is obtained:

$$\frac{\partial H}{\partial t} + U\frac{\partial H}{\partial x} + H\left(-\frac{gHC_*^2}{2U}\frac{\partial^2 H}{\partial x^2} + \frac{U}{2H}\frac{\partial H}{\partial x}\right) + V\frac{\partial H}{\partial y}$$

$$+H\left(-\frac{gHC_*^2}{U}\frac{\partial^2 H}{\partial y^2} - \frac{V}{2H}\frac{\partial H}{\partial y} + \frac{V}{H}\frac{\partial H}{\partial y}\right) = 0 \qquad [2.103]$$

After simplifying, this can be reduced to

$$\frac{\partial H}{\partial t} + \frac{3}{2}U\frac{\partial H}{\partial x} + \frac{3}{2}V\frac{\partial H}{\partial y} - \frac{gH^2C_*^2}{2U}\frac{\partial^2 H}{\partial x^2} - \frac{gH^2C_*^2}{U}\frac{\partial^2 H}{\partial y^2} = 0 \qquad [2.104]$$

Therefore, after rearranging, the following equation for two-dimensional open channel flow is obtained:

$$\frac{\partial H}{\partial t} + \alpha' U \frac{\partial H}{\partial x} + \beta' V \frac{\partial H}{\partial y} = D_x \frac{\partial^2 H}{\partial x^2} + D_y \frac{\partial^2 H}{\partial y^2} \qquad [2.105]$$

where

$$\alpha' = \frac{3}{2} \qquad [2.106]$$

$$\beta' = \frac{3}{2} \qquad [2.107]$$

$$D_x = \frac{gH^2 C_*^2}{2U} \qquad [2.108]$$

and

$$D_y = \frac{gH^2 C_*^2}{U} \qquad [2.109]$$

The longitudinal diffusion coefficient, D_x can also be expressed as ${}^{q_x}\!/\!{}_{(2S_{ox})}$, originally derived by Hayami (1951) for a one-dimensional diffusive wave formulation. From equation [2.105], it can be noticed that the zero-inertia approximation to the full dynamic equations results in a two-dimensional convection-diffusion equation for open channel flow in a wide rectangular prismatic channel. It is also seen that the effective diffusion coefficient in the lateral direction is twice the coefficient in the longitudinal direction.

2.5 THEORETICAL ANALYSIS OF MONOCLINAL WAVES

The movement of floods in the natural rivers has been a great concern to the researchers. Among the many investigators, Seddon (1900) discussed the movement of flood waves in detail on the Mississippi river and showed that the major portion of the flood moves with a kinematic wave velocity. Later, Lighthill and Whitham (1955) studied theoretically the properties of kinematic waves and their role in the movement of floods in a long river. They showed that the kinematic wave velocity depends on the depth of flow, and that successive kinematic waves may lead to the formation of a steep front. However, as the wave front becomes steeper the roles of other slope terms in the governing momentum equations become prominent introducing attenuation and dispersion to the waves and thereby retarding the steepening tendency of the wave front. Lighthill and Whitham (1955) described the resulting flood wave as a kinematic shock wave or monoclinal wave which moves with the kinematic wave velocity but retains its shape unchanged as it moves downstream. A monoclinal wave approximation is applicable to a long river where the length of the reach should be greater than the natural length scale of the channel, D / S_{ox} (Lighthill and Whitham, 1955). The various properties of this wave are discussed in the sequel.

2.5.1 AVERAGE WAVE VELOCITY

A detailed analysis of the properties of the kinematic wave velocity for the case of a rectangular channel is available in the literature (Chow, 1959; and Henderson, 1966). Dingman (1984) discussed the properties of the kinematic wave velocity for the case of a compound channel by considering only the storage effects of the flood plain areas. Following a similar theoretical concept, a detailed analysis of the movement of a monoclinal wave in a compound channel considering both the storage and the conveyance of the flood plains is presented herein. In pursuing this analysis for the monoclinal wave, the flood wave can be considered as steady from the point of view of an observer moving with the wave velocity, V_w instead of analyzing an unsteady phenomena. This can be achieved by the superposition of a velocity equal and opposite to the wave velocity, V_w. Two further assumptions are also used to analyze the properties of a monoclinal flood wave. One of them is that the flood plain is initially dry and the second is that the compound channel system is straight, symmetric, and prismatic.

Figure 2.2 shows the monoclinal flood hydrograph. The plan view of the half of the compound channel along with other useful sections are shown in Figure 2.3. The initial and the final condition of the flood events are also shown.

In order to derive an expression for the average wave velocity, a one-dimensional flow condition is assumed to prevail. To satisfy the criteria for the stationary steady wave, the total discharge at every compound channel section must be constant. Mathematically, this can be expressed as follows:

$$\int_0^{W_c+W_p} (U - V_w) H dy = \text{constant} \qquad [2.110a]$$

where W_c is one half of the main channel width and W_p is the width of the flood plain.

Applying this equation between Section 1 and Section 2 as shown in Figure 2.3, this can be written as:

$$\int_0^{W_c+W_p} (U - V_w) H dy \Big|_{\text{sec}\,1} = \int_0^{W_c+W_p} (U - V_w) H dy \Big|_{\text{sec}\,2} \qquad [2.110b]$$

Using the notations of the Figure 2.3, neglecting lateral momentum transfer, and simplifying, the expression for average wave velocity can be derived as:

$$V_w = \frac{U_{cu} + U_{pu}\left(\dfrac{H_c - D}{H_c}\right) W_r - U_{cd}\dfrac{D}{H_c}}{\left(\dfrac{H_c - D}{H_c}\right)(W_r + 1)} \qquad [2.111]$$

where U_{cu} is the longitudinal main channel flow velocity at the final stage of the flood, U_{cd} is the longitudinal initial main channel flow velocity, U_{pu} is the longitudinal flood plain flow velocity at the final stage of a flood, H_c is the main channel flow depth at the final stage of a flood, D is the main channel flow depth at the beginning of a flood, W_r is the width ratio $\left(= {W_p}/{W_c}\right)$, W_p is the width of the flood plain, and W_c is one half of the main channel width.

The average flow velocity at the peak stage of a flood can be expressed as:

$$U_{ave} = \frac{U_{cu} + U_{pu}\left(\dfrac{H_c - D}{H_c}\right)W_r}{1 + \left(\dfrac{H_c - D}{H_c}\right)W_r} \qquad [2.112]$$

Hence, the ratio of the wave velocity to the average flow velocity can be expressed by the following:

$$\frac{V_w}{U_{ave}} = \frac{\left[1 + \left(\dfrac{H_c - D}{H_c}\right)W_r\right]\left[1 + \dfrac{C_{pu}}{C_{cu}}\left(\dfrac{H_c - D}{H_c}\right)^{\frac{3}{2}} W_r - \dfrac{C_{cd}}{C_{cu}}\left(\dfrac{D}{H_c}\right)^{\frac{3}{2}}\right]}{\left(\dfrac{H_c - D}{H_c}\right)(W_r + 1)\left[1 + \dfrac{C_{pu}}{C_{cu}}\left(\dfrac{H_c - D}{H_c}\right)^{\frac{3}{2}} W_r\right]} \qquad [2.113]$$

where ${V_w}/{U_{ave}}$ is the ratio of the average wave velocity to the average flow velocity, ${(H_c - D)}/{H_c}$ is the ratio of the flood plain depth to the total depth in the channel at the peak stage of a flood and it is denoted as the depth ratio hereafter, C_{pu} is the dimensional Chezy coefficient for the flood plain at the peak stage of a flood, C_{cu} is the dimensional

Chezy coefficient for the main channel at the peak stage of a flood, and C_{cd} is the dimensional Chezy coefficient in the main channel for the initial stage of a flood.

Equation [2.113] shows that the velocity ratio is a function of depth ratio, width ratio, and roughness ratio. Figure 2.4 shows the variation of the velocity ratio with depth ratio for different width ratios (W_r=1, 2, 10, and 20) and a particular roughness ratio of 1. It is seen that as the width of the flood plain increases, the velocity decreases for a particular depth ratio. However, it is also seen that the effect of width increase on the velocity ratio becomes less pronounced for larger depth ratios. The effects of depth ratio on the velocity ratio for a rectangular channel with constant Chezy coefficient is also shown. It is noticed that the velocity ratio varies from 1.5 to 1.

Figure 2.5 shows the variation of velocity ratio with depth ratio for different roughness ratios (ratio = 1, 10, 20) and a particular width ratio of 1. It appears that the effect of roughness ratio is similar to that of width ratio. In all cases, for low flood plain depths, the velocity ratio is significantly less than 1. Similar phenomena were also observed in the field (Henderson, 1963).

2.5.2 VOLUME OF LATERAL FLOWS AND THEORETICAL ANALYSIS

Application of conservation of mass in the flood plain portion of the compound channel results in a simple equation for determining the volume of flow entering from the main channel to the flood plain. This equation is derived in this section using the control volume shown in Figure 2.6. This figure shows the plan view of a flood plain on which the distributions of the steady longitudinal and lateral velocities as will be seen by a moving observer are indicated. For this part of the stationary wave, the total longitudinal discharge across the upstream section of the flood plain which appears as an outflow must be equal to the total lateral inflow from the main channel to the flood plain. Mathematically, this can be expressed as:

$$Q_o = -\int_{W_c}^{W_c+W_p}(U_{pu} - V_w)(H - D)dy = \int_0^L q_y dx \qquad [2.114]$$

where Q_0 is the total steady discharge across the flood plain as seen by the moving observer, q_y is the lateral discharge per unit length, U_{pu} is the longitudinal flood plain flow velocity at the final stage of a flood, V_w is the average wave velocity, and L is the length of the wave along the channel.

From the point of view of a stationary observer, the volume of the flood plain per unit length filled up by the lateral discharge in time is given by:

$$Vol = \int_0^t q_y dt \qquad [2.115]$$

and also, $dx = V_w dt$ [2.116]

Hence, $Vol = \int_0^L \frac{q_y}{V_w} dx = \frac{Q_o}{V_w}$ [2.117]

Therefore, equation [2.117] gives a very simple relationship between the volume of flood plain per unit length filled up by the lateral inflow, the wave velocity and the total steady state discharge across the flood plain as seen by a moving observer.

Assuming a constant longitudinal velocity across the flood plain at the final stage of a flood i.e., neglecting the momentum transfer phenomena, the total flood plain discharge can be calculated as:

$$Q_o = -(U_{pu} - V_w)(H_c - D)W_p \qquad [2.118]$$

Substituting equation [2.118] into equation [2.117], the volume per unit length filled up by lateral discharge can be expressed in the following non-dimensional form.

$$\frac{Q_o}{V_w H_c W_c} = \left(1 - \frac{U_{pu}}{V_w}\right)\left(\frac{H_c - D}{H_c}\right) W_r \qquad [2.119]$$

The percentage of the volume of the flood plain filled up by the lateral inflow can also be determined by the following:

$$Vol\% = \frac{Q_o}{V_w (H_c - D) W_p} = \left(1 - \frac{U_{pu}}{V_w}\right) * 100 \qquad [2.120]$$

Substituting the expressions for U_{pu} and V_w, the above expression can be simplified as:

$$Vol\% = \frac{1 - \frac{C_{pu}}{C_{cu}}\left(\frac{H_c - D}{H_c}\right)^{\frac{3}{2}} - \frac{C_{cd}}{C_{cu}}\left(\frac{D}{H_c}\right)^{\frac{3}{2}}}{1 + \frac{C_{pu}}{C_{cu}}\left(\frac{H_c - D}{H_c}\right)^{\frac{3}{2}} W_r - \frac{C_{cd}}{C_{cu}}\left(\frac{D}{H_c}\right)^{\frac{3}{2}}} * 100 \qquad [2.121]$$

From the above equation, it is seen that the percentage of volume is a function of the depth ratio of the final flood plain depth to the total main channel depth, the ratio of the initial depth to the final depth of the main channel, the width ratio, and the roughness ratio. For a depth ratio of $(H_c - D)/H_c = 1$, the compound channel becomes a single rectangular channel with an initially dry bed. The variation of the volume per unit length in non-dimensional form [equation 2.119] with the depth ratio for different width ratios and a particular roughness ratio of 1 is plotted in Figure 2.7. It is clearly noticed that the contribution increases from zero to a maximum at a certain depth ratio and then decreases again to zero. The variation of the percentage of volume filled up by the lateral discharge with depth ratio for different width ratios for a particular roughness ratio of 1 is also shown in Figure 2.8. It is revealed that the contribution of the lateral inflow in filling the flood plain decreases as the width ratio increases. It is also seen that at very low flood plain depth, the contribution is almost 100 %. This is because of the division by small flood plain depth as seen from equation [2.120]. Figure 2.9 shows the variation of the percentage of volume filled up with depth ratio for different roughness ratios (ratio = 1, 10, and 20) and a particular width ratio of 1. It can be inferred that the rougher the flood plain, the more the contribution of lateral flow in the filling process of the flood plain.

2.6 NON-DIMENSIONAL FORM OF THE GOVERNING FLOW EQUATIONS

Dimensional analysis of the governing equations leads to the non-dimensional forms of these equations with non-dimensional variables. As such, the number of the dimensional variables is reduced. The monoclinal wave approximation results in a further reduction in the number of non-dimensional variables as discussed herein. The obtained non-dimensional variables will be used in designing numerical experiments. Dimensional variables are defined as the product of a constant reference variable and a dimensionless ratio as follows:

$$x^* = \frac{x}{L_o}, y^* = \frac{y}{L_o}, H^* = \frac{H}{D}, U^* = \frac{U}{U_o}, V^* = \frac{V}{U_o}, q_x^* = \frac{q_x}{U_o D}, q_y^* = \frac{q_y}{U_o D}, t^* = \frac{t}{T_o} \qquad [2.122]$$

The reference variables can be defined as: U_o is the uniform flow velocity, D is the depth of the main channel below the flood plain level,
L_o is the natural length scale of the channel given by $L_o = \frac{D}{S_{ox}}$, (Ponce and Simons, 1977) [2.123]

and T_o is the response time of the channel given by

$$T_o = \frac{L_o}{U_o} \tag{2.124}$$

The governing equations are reproduced below:

$$\frac{\partial H}{\partial t} + \frac{\partial q_x}{\partial x} + \frac{\partial q_y}{\partial y} = 0 \tag{2.125}$$

$$\frac{\partial H}{\partial x} = S_{ox} - S_{fx} = S_{ox} - \frac{U^2}{gHC_*^2} \tag{2.126}$$

$$\frac{\partial H}{\partial y} = S_{oy} - S_{fy} = S_{oy} - \frac{UV}{gHC_*^2} = -\frac{UV}{gHC_*^2} \tag{2.127}$$

where S_{ox} and S_{fx} are the longitudinal bed slope and the friction slope respectively. S_{oy} and S_{fy} are the lateral bed slope and the lateral friction slope respectively. The value of the lateral bed slope is taken as zero for simplicity.

Substitution of the non-dimensional variables into equations [2.125] to [2.127] results in the following:

$$\frac{L_o}{U_o T_o}\frac{\partial H^*}{\partial t^*} + \frac{\partial q_x^*}{\partial x} + \frac{\partial q_y^*}{\partial y} = 0 \tag{2.128}$$

$$\frac{D}{L_o}\frac{\partial H^*}{\partial x^*} = S_{ox} - \frac{C_*^2 g D S_{ox} U^{*2}}{gDH^* C_*^2} = S_{ox} - \frac{S_{ox} U^{*2}}{H^*} \tag{2.129}$$

$$\frac{D}{L_o}\frac{\partial H^*}{\partial y^*} = -\frac{S_{ox} U^* V^*}{H^*} \tag{2.130}$$

Using [2.123] and [2.124], the above equations can be written in the following non-dimensional forms:

$$\frac{\partial H^*}{\partial t^*}+\frac{\partial q_x^*}{\partial x}+\frac{\partial q_y^*}{\partial y}=0 \qquad [2.131]$$

$$\frac{\partial H^*}{\partial x^*}=1-\frac{U^{*2}}{H^*} \qquad [2.132]$$

$$\frac{\partial H^*}{\partial y^*}=-\frac{U^*V^*}{H^*} \qquad [2.133]$$

The initial flow condition is given as the following non-dimensional form:

at $t^*=0$, $U^*=0$ in the flood plain.
$=1$ in the main channel. [2.134]
$V^*=0$.
$H^*=0$ in the flood plain.
$=1$ in the main channel.

The inflow boundary condition at $x^*=0$ is given as follows:

$$q_x^*=\frac{q_{xo}(t)}{U_oD} \qquad [2.135]$$

The peak flow condition can be expressed in the following non-dimensional form:

$$\text{at } t^*=\frac{T_p}{T_o},\ \frac{q_m}{U_oD}=\frac{Q_m}{W_cU_oD} \qquad [2.136]$$

where q_m is the peak longitudinal discharge per unit width, Q_m is the total peak longitudinal discharge, W_c is the half-width of the main channel, and T_p is the time to peak.

The outflow boundary condition at $x^*=\dfrac{\Lambda}{L_o}$ is given as follows:

$$q_x^* = H^{*\frac{3}{2}} \qquad [2.137]$$

where Λ is the length of the reach of interest.

The lateral side boundary conditions are given as follows:

at $y^* = \dfrac{W_p}{L_o}$, $q_y^* = 0$ and

at $y^* = \dfrac{W_c}{L_o}$, $q_y^* = 0$ [2.138]

Hence, from the above dimensional analysis, it is revealed that equations [2.131] to [2.133] are to be solved for q_x^*, q_y^*, H^*, U^*, and V^* as functions of x^*, y^*, t^* and W_p/L_o, W_c/L_o, $Q_m/(W_cU_oD)$, T_p/T_o, and C_{*p}/C_{*c},

where C_{*p} and C_{*c} are the dimensional Chezy roughness coefficients in the flood plain and the main channel, respectively.

The non-dimensional governing parameters can also be grouped as:

W_p/D, W_c/D or W_p/W_c, k_{sp}/D, k_{sc}/D or k_{sp}/k_{sc} and S_{ox}.

where k_{sp} and k_{sc} are the roughness height in the flood plain and the main channel respectively.

As the pseudo-steady state form of the monoclinal wave approximation is adopted in the present analysis, the non-dimensional time parameter is eliminated. Also, the non-dimensional peak discharge parameter can be replaced by the non-dimensional ratio of the flood plain depth to the total main channel depth at the peak level, $(H_c - D)/H_c$. Hence, in the present study, extensive numerical experiments will be carried out to investigate the characteristics of lateral flows by utilizing the following non-dimensional variables:

$(H_c - D)/H_c$, S_{ox}, W_p/D, W_c/D, k_{sp}/D and k_{sc}/D.

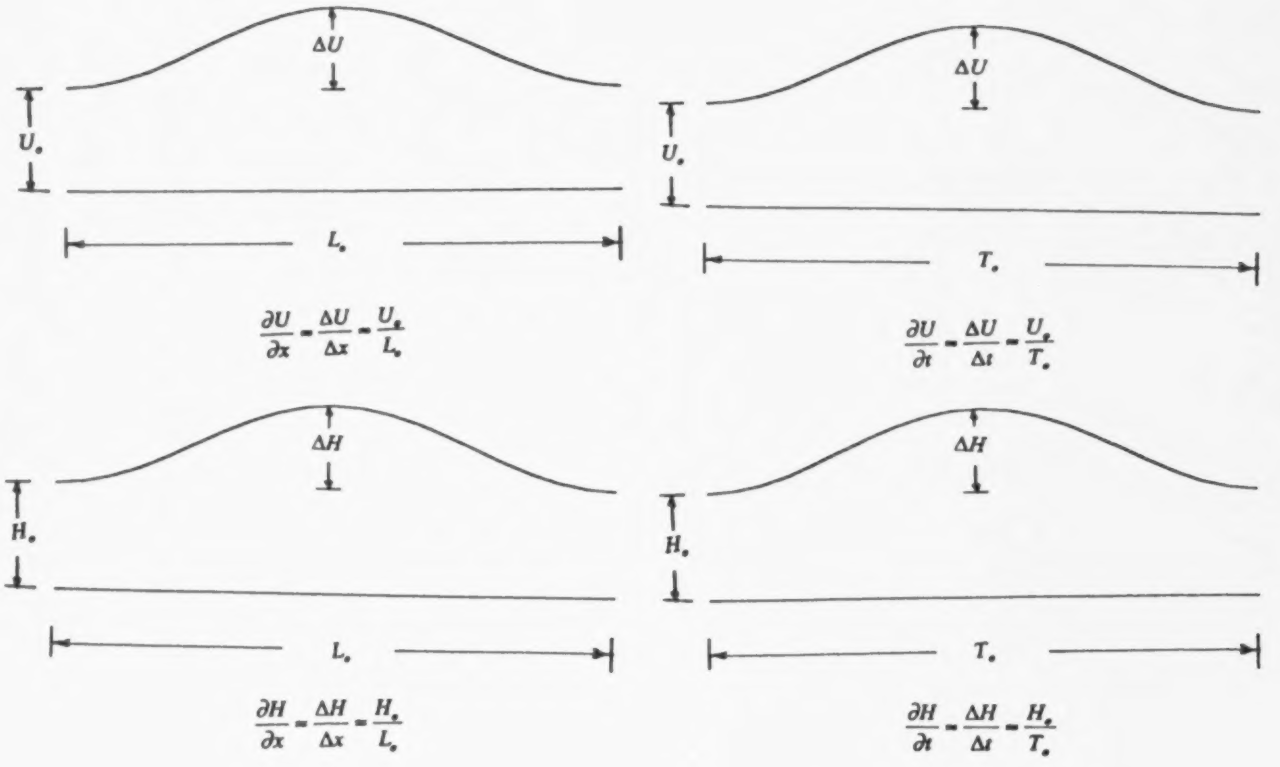
ΔU
U_*
L_*
$\frac{\partial U}{\partial x} = \frac{\Delta U}{\Delta x} = \frac{U_*}{L_*}$
ΔU
U_*
T_*
$\frac{\partial U}{\partial t} = \frac{\Delta U}{\Delta t} = \frac{U_*}{T_*}$
ΔH
H_*
L_*
$\frac{\partial H}{\partial x} = \frac{\Delta H}{\Delta x} = \frac{H_*}{L_*}$
ΔH
H_*
T_*
$\frac{\partial H}{\partial t} = \frac{\Delta H}{\Delta t} = \frac{H_*}{T_*}$

Figure 2.1 Schematic representation of the approximations of the various derivative terms for the Order of Magnitude Analysis

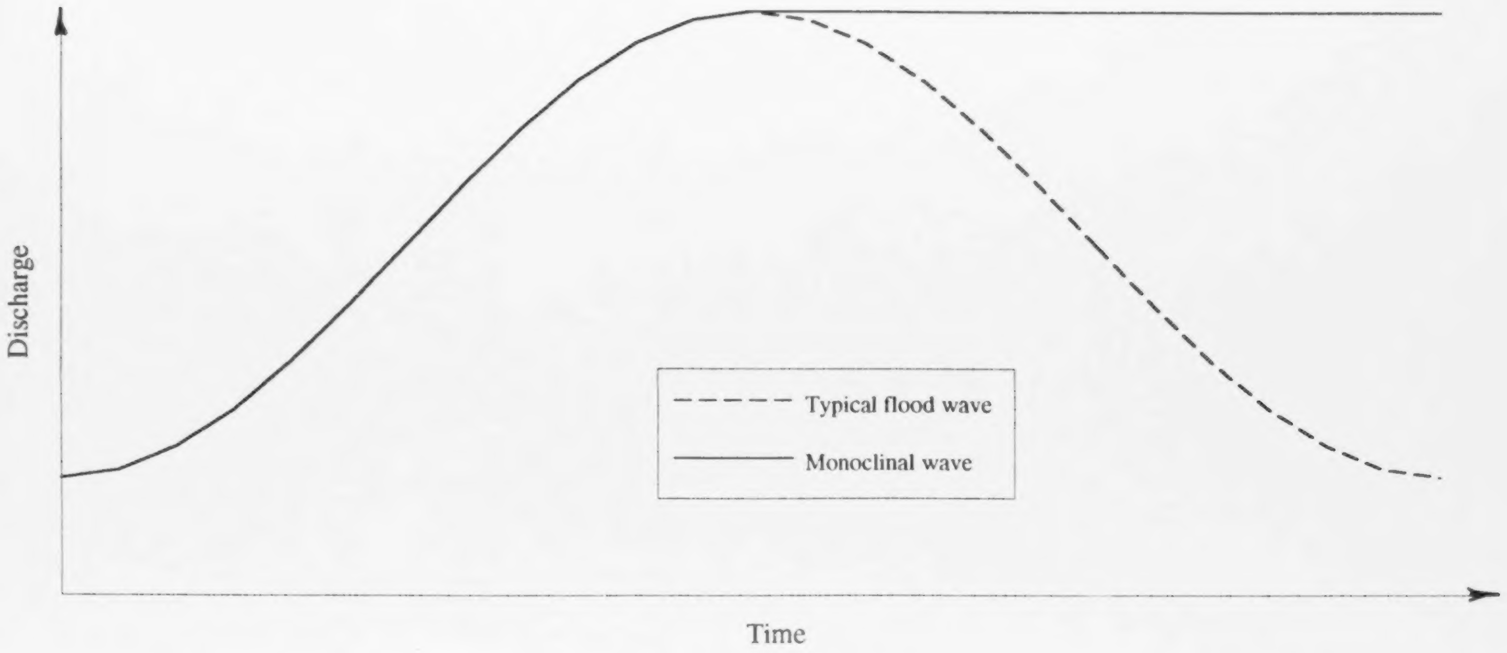

Figure 2.2 Monoclinal flood hydrograph.

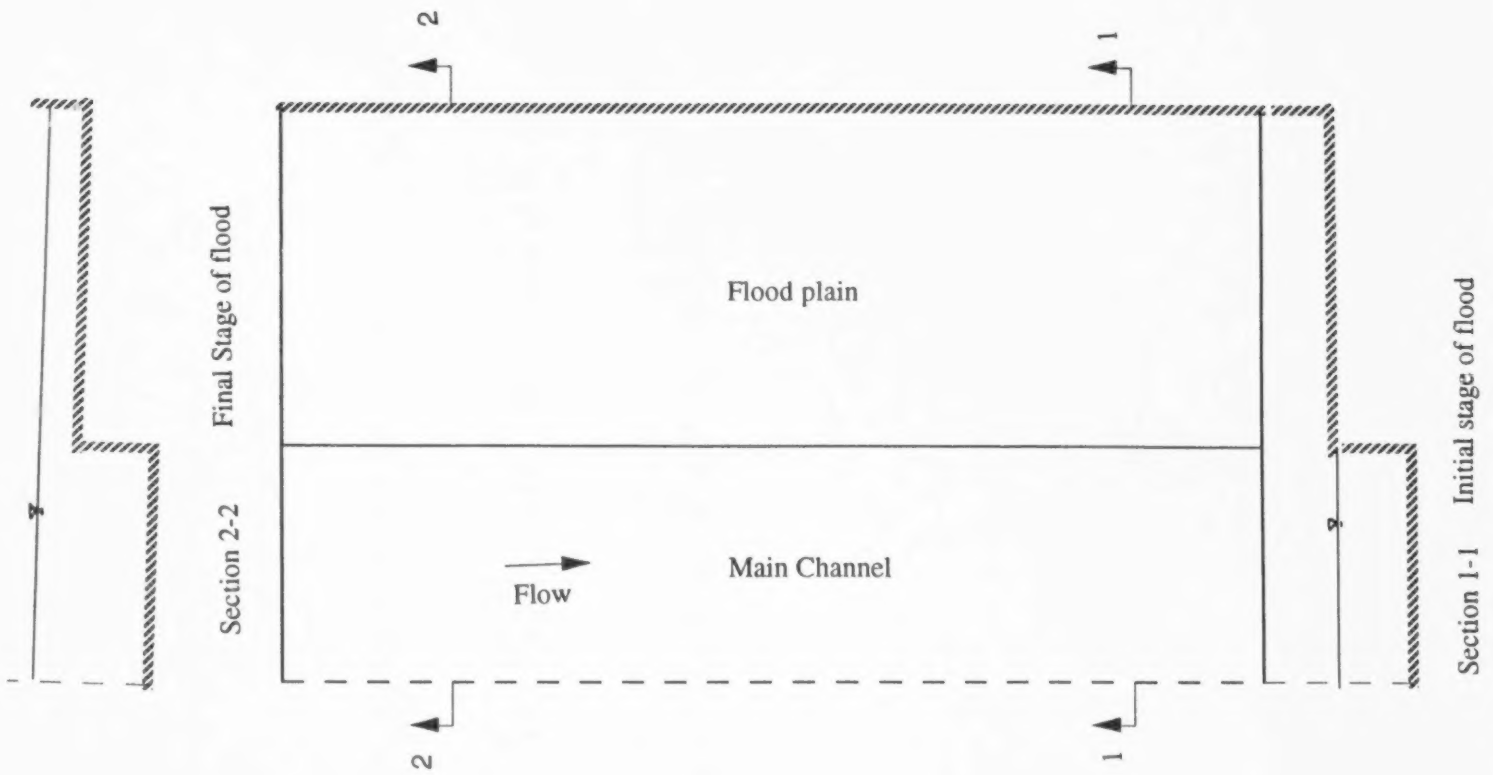
2
1
Final Stage of flood
Section 2-2
Flood plain
Main Channel
Flow
Initial stage of flood
Section 1-1
2
1

Figure 2.3 Half of the plan view of the compound channel.

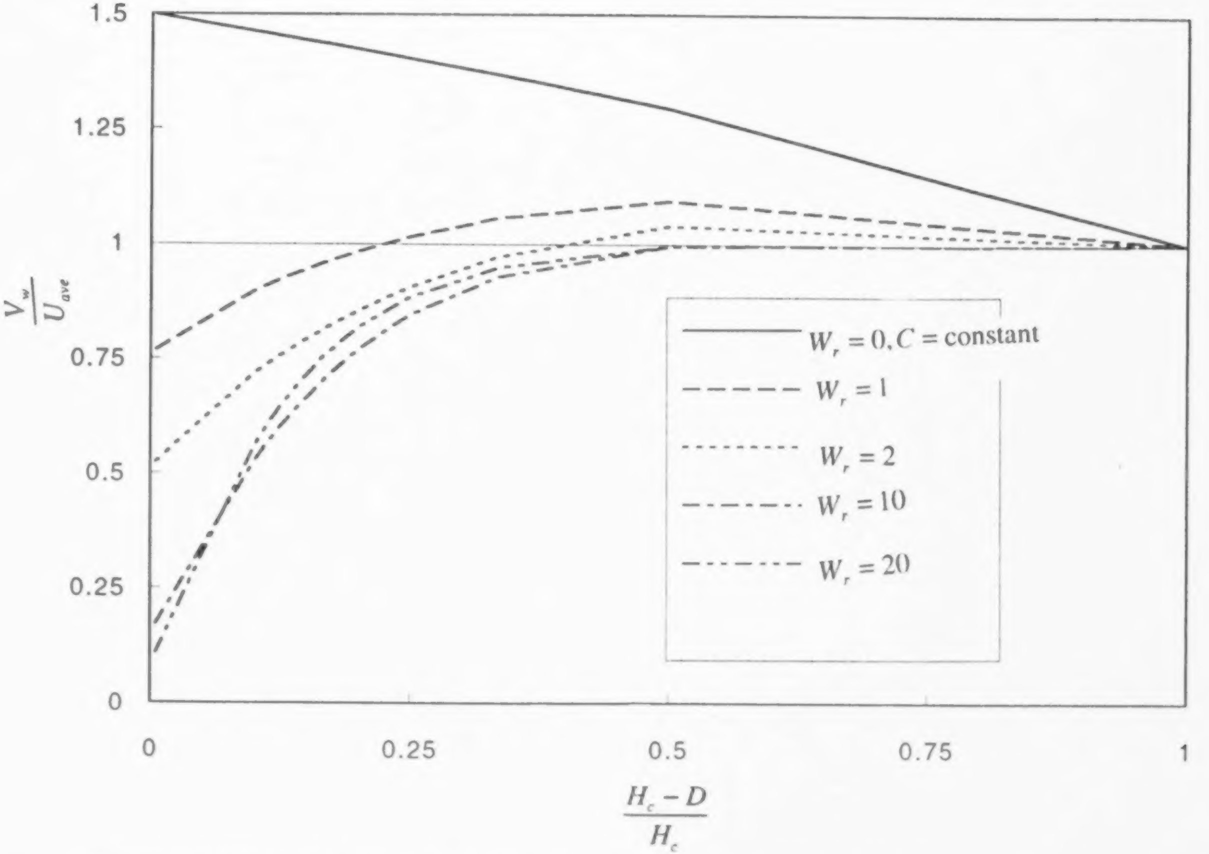

Figure 2.4 Effect of width ratio on the ratio of the average wave velocity to the average flow velocity.

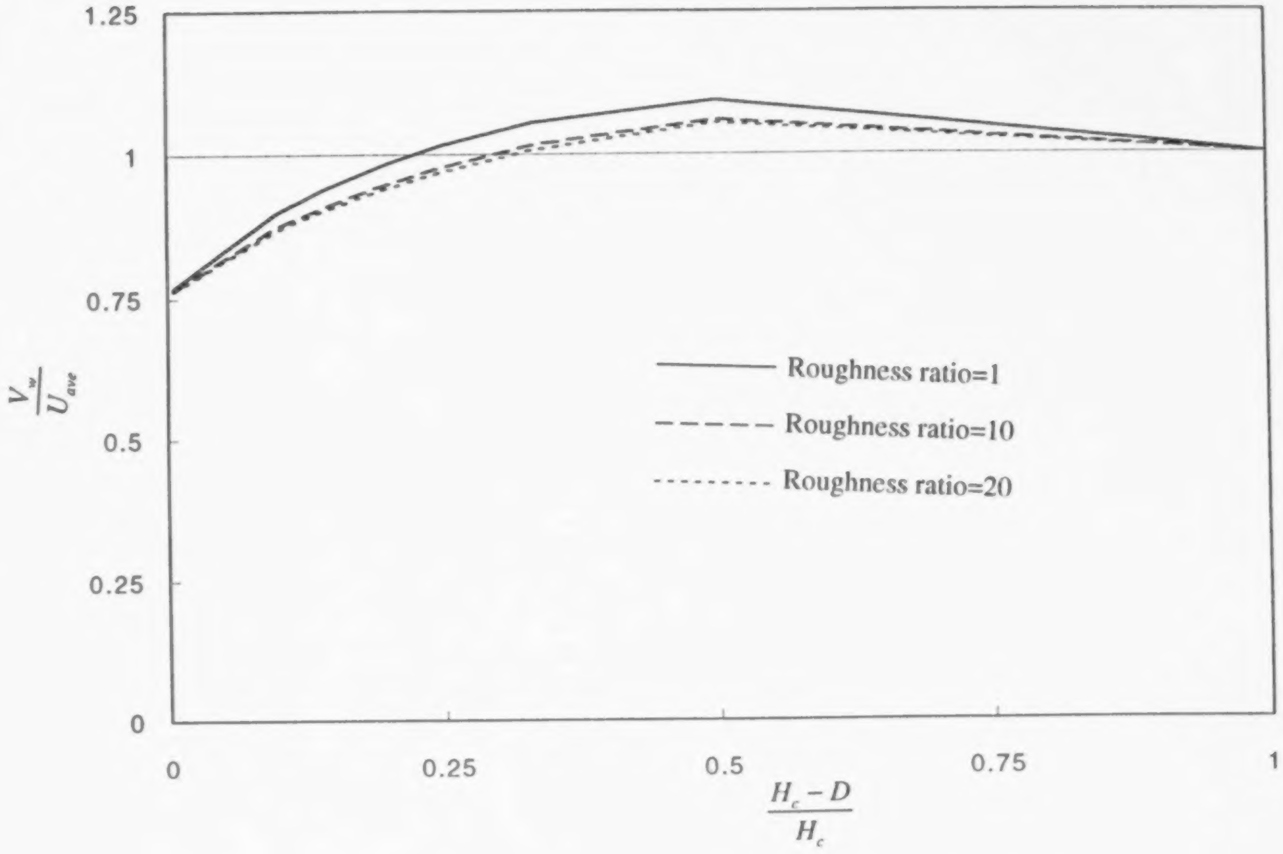

Figure 2.5 Effect of roughness ratio on the ratio of the average wave velocity to the average flow velocity.

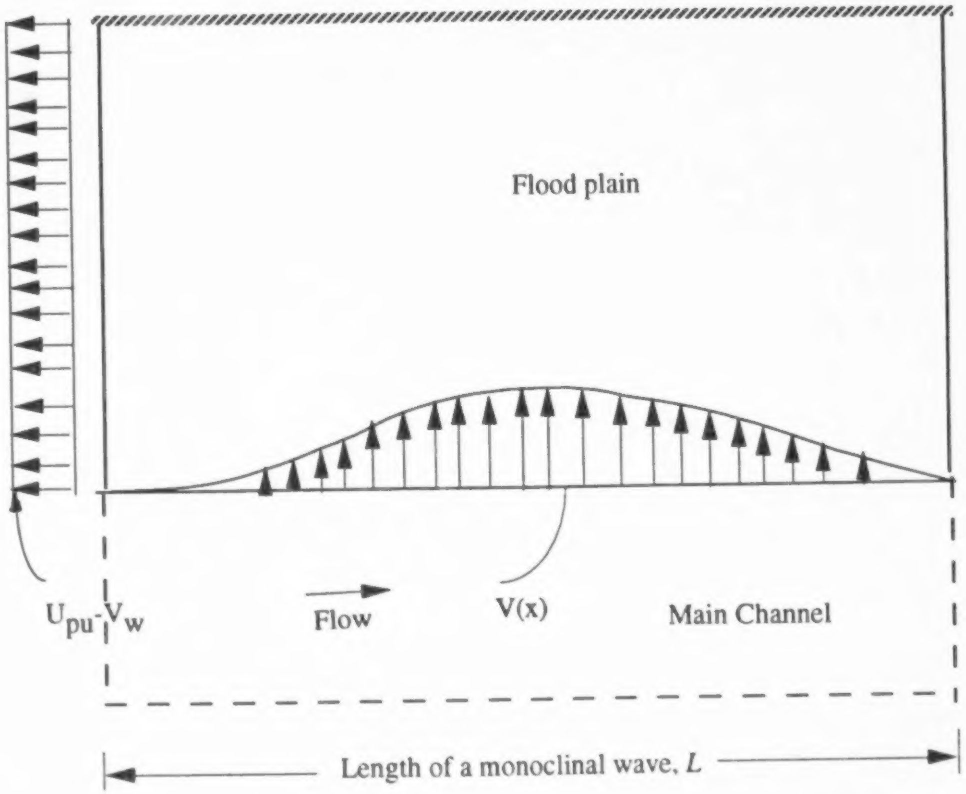
Flood plain
$U_{pu}-V_w$
Flow
V(x)
Main Channel
Length of a monoclinal wave, L

Figure 2.6 Distribution of pseudo-steady flow in the flood plain.

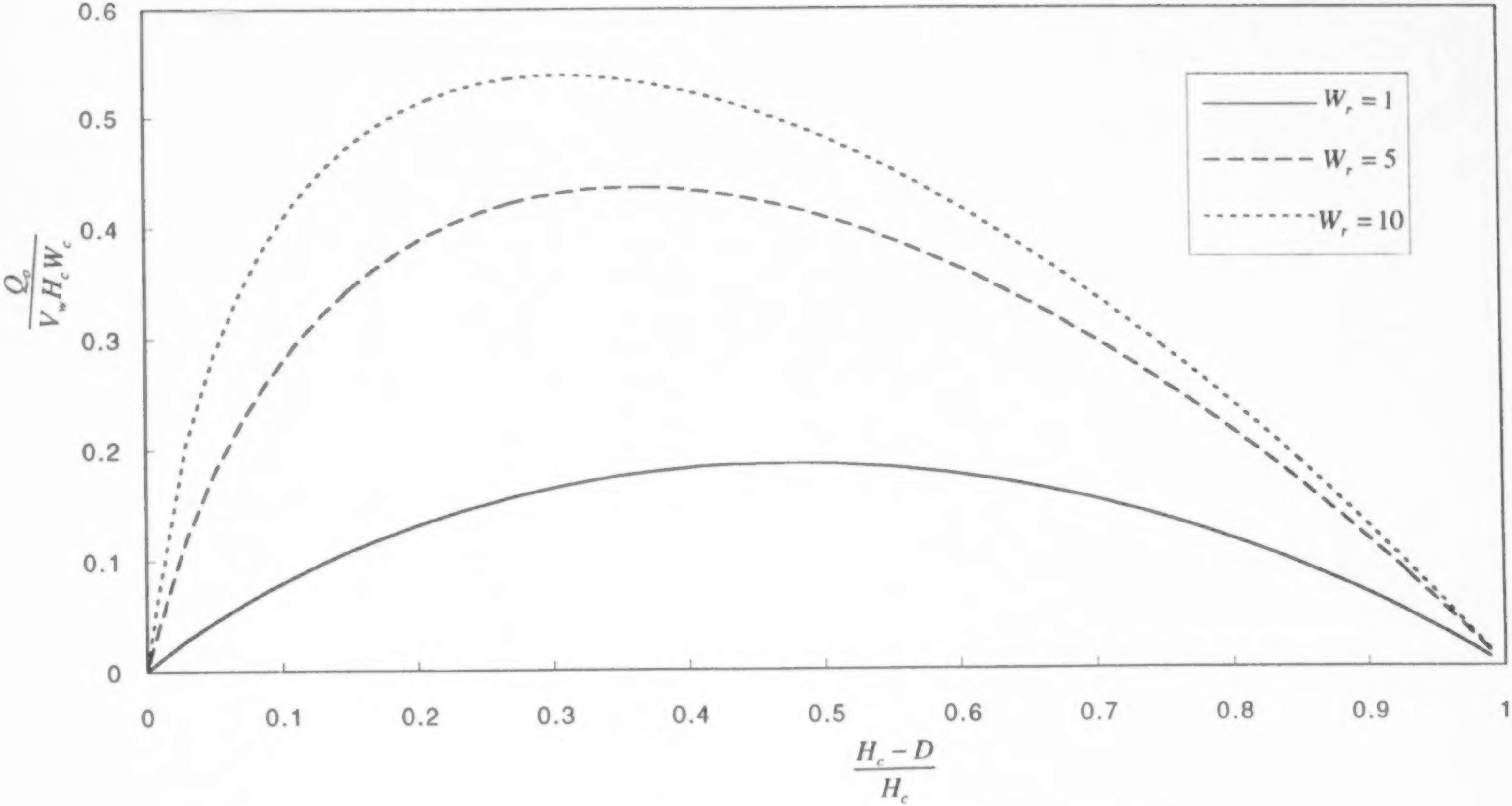

Figure 2.7 Variation of the non-dimensional volume per unit length filled by lateral discharge with depth ratios for different width ratios.

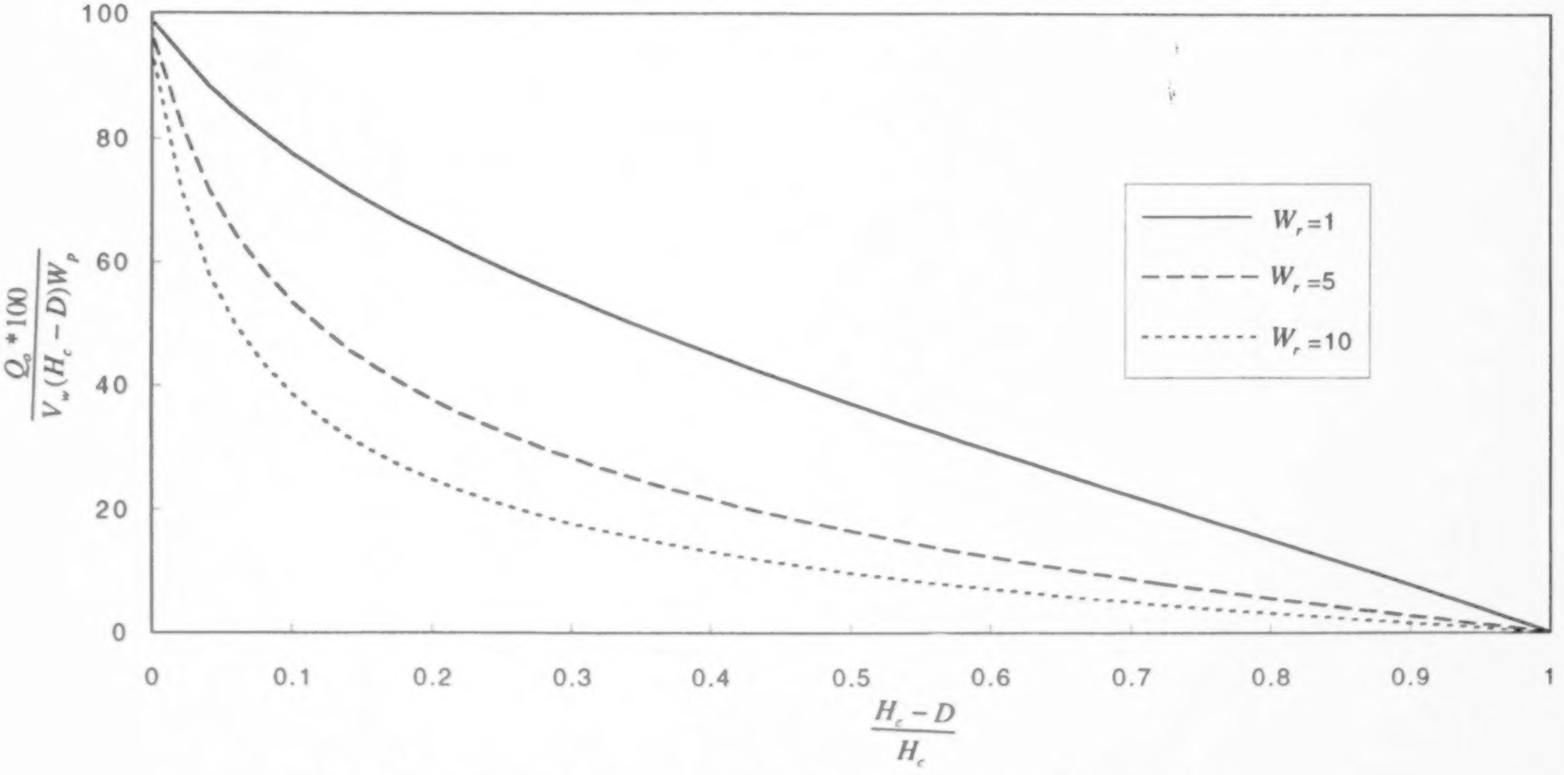

Figure 2.8 Variation of the percentage of flood plain volume per unit length filled by lateral discharge with depth ratios for different width ratios.

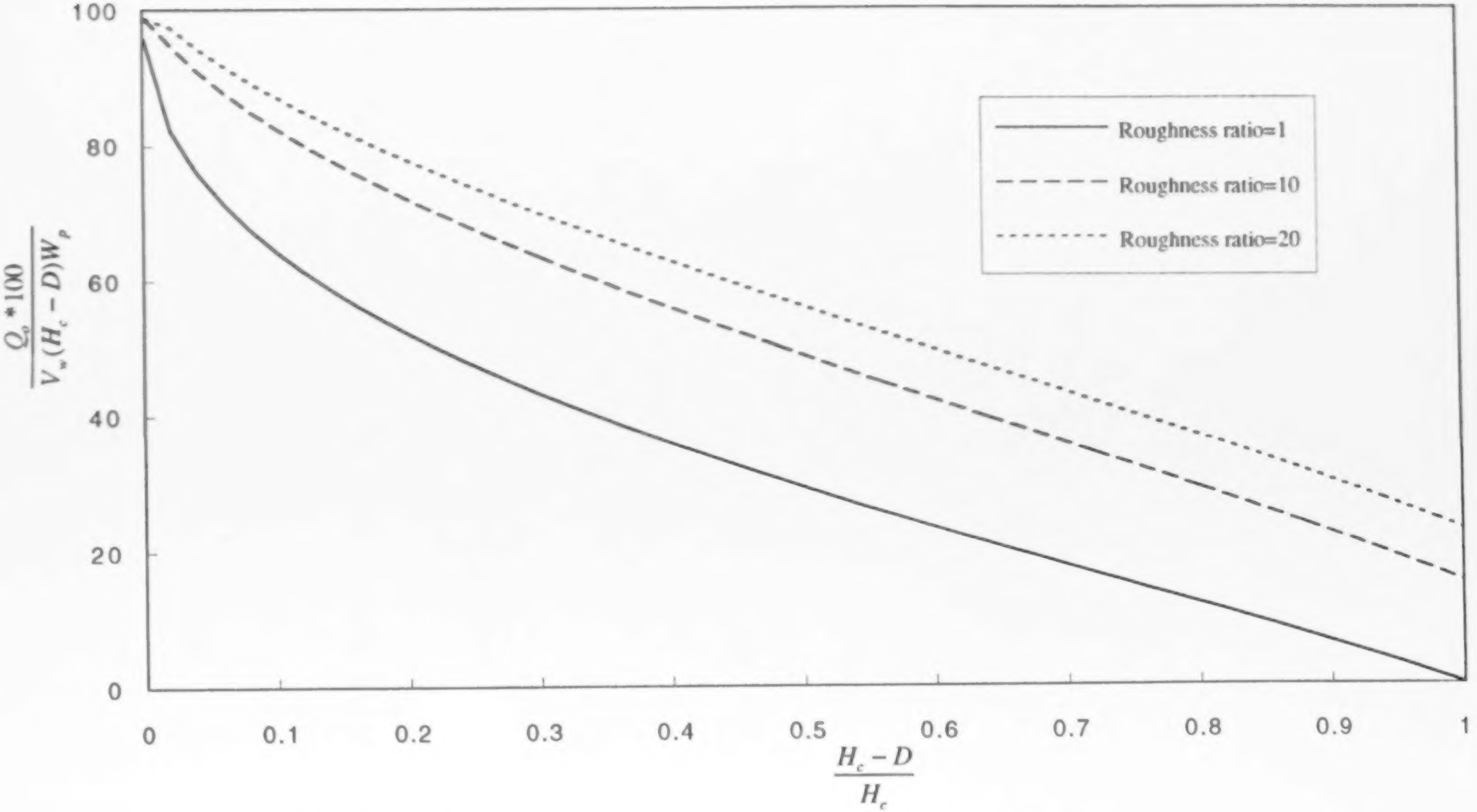

Figure 2.9 Variation of the percentage of flood plain volume per unit length filled by lateral discharge with depth ratios for different roughness ratios.

3 NUMERICAL MODEL

3.1 INTRODUCTION

The governing equations for open channel flow are nonlinear and it is not possible to solve them analytically for generalized boundary conditions. Therefore, numerical techniques are used to solve these equations. A number of numerical methods, namely, the method of characteristics, the finite difference method, the finite element method, and the control volume method have been developed and applied to solve unsteady open channel flow problems. Detailed descriptions of the various methods are available in many texts, such as Abbott (1979), Celia and Gray (1992), and Chaudhry (1993). In this chapter, a brief review of several models for compound channel flow will be presented in Section 3.2 with special emphasis on zero-inertia models. A brief review of several numerical models for overland flow will also be provided in Section 3.3. The development of the present zero-inertia scheme will be described in detail in Section 3.4.

3.2 REVIEW OF NUMERICAL MODELING OF COMPOUND CHANNEL FLOWS

A great deal of numerical modeling of compound channel flows has been reported in the literature. These models vary from estimating the distribution of steady uniform discharge to the movement of unsteady flood flows through a compound channel system. Applications of these models also range from one to three-dimensional. Some of the models take momentum transfer phenomena into account and some of them do not. A brief review of them is given below.

3.2.1 MODELING OF STEADY FLOW IN COMPOUND CHANNELS

Various one-dimensional models have been developed and applied to compute the velocity and discharge distribution in compound channels. Among the many other investigators, Ervine and Baird (1982), Prinos and Townsend (1984), Dracos and Hardegger (1987), Wark, Samuels, and Ervine (1990), Wormleaton and Merrett (1990), and Martin and Myers (1991) proposed various numerical models by taking the lateral momentum transfer process into account.

Keller and Rodi (1984, 1988), Pasche, Rouve, and Evers (1985), and Djordjevic (1993) developed several two-dimensional models for steady flow. All of them used boundary layer approximation in deriving the parabolic forms of the governing equations. As a result, the water surface is horizontal across the channel leading h to be a function of x only and the streamwise variation of the water surface elevation is normally obtained from one-dimensional backwater profile calculation. All these works included the effect of lateral momentum transfer phenomena.

Urban and Zielke (1985) presented a steady state two-dimensional finite element model for compound channel flows. The model did not consider the effect of momentum transfer phenomena. They applied the model to a river section of 1.5 km long with a water depth of 5 - 6 m in the main channel and 0-2 m in the flood plains. They compared the results obtained with and without considering convective acceleration terms and concluded that these terms can be neglected in friction-dominated flood plain flows.

Krishnappan and Lau (1986) and Tominaga, Nezu, and Kobatake (1989) studied the flow structure of steady flood plain flows by applying three-dimensional flow models on the basis of algebraic stress models, adopting the full three dimensional flow equations. Prinos (1989) studied the flow structure adopting the two-dimensional depth-averaged and three-dimensional models using experimental data. He concluded that both types of models overestimated the mean velocities and boundary shear stresses in the main channel while these are underestimated in the flood plain for low relative depths. For high relative depths, however, both types of models reproduce the flow characteristics properly. Recently, Pezzinga (1994) applied a three dimensional flow model along with a $\kappa - \varepsilon$ model to predict the distribution of the primary velocity component, the discharge distribution and the secondary circulation. He also used the numerical results to compare different subdivision methods for determining the discharge distribution. He concluded that the better subdivisions are the diagonal surface that leaves from the corner between the flood plain and the main channel to the free surface on the symmetry plane and the bisector surface of the corner between the main channel and the flood plain.

3.2. 2 MODELING OF UNSTEADY FLOW IN COMPOUND CHANNELS

One- and two-dimensional modeling of unsteady flows in compound channels has been carried out by many researchers. Investigations of the movement of flood waves in compound channels by applying the one-dimensional St. Venant equations include Fread (1976, 1988), Radojkovic(1976), Ervine and Ellis (1987), Tingsanchali and Kumar (1988), Stephensen and Kolovopoulos (1990), Rashid and Chaudhry (1993), and Abida and Townsend (1994). Recently, the CSCE Task Committee on River Models

(1993) reviewed the performance of a few one-dimensional full dynamic models by simulating experimental data on compound channels. Among all these models, only Stephensen et al. (1990) considered the momentum transfer phenomena. In these models, the whole cross-section of the channel is treated either as a single unit or divided into a main channel, left flood plain and right flood plain sections. At every time step, the water surface is assumed to be horizontal across the channel. These models give a reasonable estimate of the various features of flood waves but are unable to provide the distribution of flow patterns in a compound channel.

Quasi-2-D modeling or ' Cell Type ' modeling of compound channel flows have been carried out by many investigators. Included among these models are Cunge (1975), Grijsen and Meijer (1979), Cunge, Holly, and Verwey (1980), Lesleighter (1983), and Tingsanchali and Chaiwat (1984). In these models, the computational domain is divided into irregular grids or computational cells based on the physical boundaries. The cells are connected by one-dimensional links. Although, a good approximation of the flows can be achieved by these models, a detailed study of the flow patterns is not possible.

Two-dimensional modeling of compound channel flow, have also been carried out by many researchers. These models include either the full dynamic equations or simplified equations. Katopodes and Strelkoff (1978), as well as Schmitz, Seus, and Czirwitzky (1983) adopted the method of characteristics to solve the full dynamic equations. Samuels (1985), Katopodes (1987), Akanbi and Katopodes (1988), and Gee, Anderson, and Baird (1990) also used these equations but in a finite element method. Vreugdenhil and Wijbenga (1982) applied a finite difference method to model the flow. Jenkins and Keller (1990) also adopted a finite difference method but in curvilinear coordinate system. Popovska (1989), Soulis (1992) and Lai and Yen (1993) adopted a control volume method to study the propagation of flood waves. Among all these studies, only Vregdenhil and Wijbenga (1982), Gee et al. (1990) and Lai and Yen

(1993) took the effective shear stress or lateral momentum transfer into account. The major limitation of the full dynamic models is that they are not easily applicable to the dry bed situation. Special techniques have to be adopted to handle this situation (Cunge et al., 1980; Akanbi and Katopodes, 1988; and Meselhe and Holly, 1993). Moreover, all these models need significant amounts of computational time and effort to simulate the flood events. Also, it is worth mentioning that the finite element method requires more computational storage and time in solving the two-dimensional depth-averaged full dynamic equations than the finite difference method (Thaker, 1978). Recently, Naaim and Brugnot (1994) compared the performances of the two-dimensional finite element model based on Galerkin formulation and the control volume formulation. They concluded that the control volume method is much faster than the other while producing results of the same accuracy.

Apart from all of these full dynamic models, several investigators adopted simplified models. Xanthopoulos and Koutitas (1976) applied the zero-inertia wave model using an explicit finite difference scheme to compute the velocity components and water depth. Hromadka II, Berenbrock, and Freckleton (1985), Hromadka II and Durbin (1986) adopted such models to simulate the inundation of flood plains. De Vries, Hromadka II, and Nestlinger (1986) adopted a hybrid model to study such phenomena. They coupled the one-dimensional main channel model with the two-dimensional flood plain model through an interface model. Giammarco, Todini, Consuegra, Joerin, and Vitalini (1994) adopted a hybrid model by linking river and flood plain flows by weir type links. All these models adopted Nodal Domain Integration (NDI) method with an explicit scheme. Description of the NDI method is available in Hromadka II and Guymon (1982).

Gallati and Braschi (1989) applied a control volume method to simulate the flooding of urban areas due to a levee breach. They excluded the convective inertial terms and effective shear stress terms but included the local inertial terms in the momentum equations. They adopted a fully implicit scheme with a Gauss-Seidel iteration technique to solve the governing equations. However, Ponce (1990) has demonstrated that the complete non-inertial model is a better approximation to the full dynamic model than either the convective or the local inertial models.

3.3 REVIEW OF UNSTEADY FLOW MODELS IN OVERLAND FLOW

Some researchers have adopted zero-inertia wave models for overland flows. Chow and Ben-Zvi (1973) developed a two-dimensional explicit model for simulating overland flow in a watershed. Hromadka II, McCuen, and Yen (1985) applied their zero-inertia model for analyzing overland flows. Ponce (1986) applied diffusive, kinematic and full dynamic flow models for modeling catchment dynamics and demonstrated the advantage of the zero-inertia model over the kinematic models. He also showed that there was no significant difference in the results obtained by full dynamic and zero-inertia models for the case studied. Tayfur, Kavvas, Govindaraju, and Storm (1993) compared the performance of the two-dimensional kinematic and diffusive wave models with the full dynamic models for overland flow with rough infiltrating surfaces. They used an implicit centered finite difference method to solve these equations numerically. They compared the performance of the simplified models and the full dynamic models by simulating the experimental data and concluded that both types of models gave good agreement with the data. Recently, Giammarco and Todini (1994) developed a two-dimensional zero-inertia wave model using control volume finite element method with an implicit scheme.

3.4 DEVELOPMENT OF THE TWO-DIMENSIONAL ZERO-INERTIA MODEL

One of the objectives of the present research is to develop a numerical model for simulating compound channel flows. As such, attention is paid to the development of a numerical scheme which is simple, relatively easy to implement but produces results with reasonable accuracy under certain conditions. An order of magnitude analysis of the governing flow equations has shown that inertial terms can be neglected for most flood flows. As a result, the present work is concerned with the development and the application of a two-dimensional depth-averaged zero-inertia model. Among the many investigators, Akan and Yen (1981) and Sabur (1990) applied a one-dimensional zero-inertia model to simulate river flows. Sabur (1990) adopted a control volume method with a semi-implicit time discretization in his model.

The zero-inertia model has several advantages over the full dynamic models. It solves for one dependent variable instead of three as will be shown in the sequel. Naturally, it needs less computational time and effort. The salient features of the proposed model differ from the zero-inertia models presented in the literature review mainly on three distinctive points. Firstly, the proposed model includes the momentum transfer mechanism which plays a significant role in various hydraulic aspects of compound channel flows. Secondly, the approximation of the resultant bed shear stress yields an expression for lateral velocity (equation 2.93) which is different than the conventional one-dimensional Manning or Chezy equation. Thirdly, the proposed scheme employs the control volume formulation which is , simple, easy to understand, and it follows from a direct physical interpretation (Patankar,1980). Moreover, the model solution uses an alternating direction implicit (ADI) algorithm which is robust and computationally very efficient (Gerald and Wheatly, 1985).

3.4.1 MODEL EQUATIONS:

The model equations are based on the depth-averaged continuity and simplified forms of the momentum equations as presented in Chapter 2. The basic equations are reproduced here as follows:

$$\frac{\partial h}{\partial t}+\frac{\partial q_x}{\partial x}+\frac{\partial q_y}{\partial y}=0 \tag{3.1}$$

$$g\frac{\partial h}{\partial x}=-\frac{\tau_{bx}}{\rho H}+\frac{1}{\rho H}\frac{\partial}{\partial y}\left(\rho v_t H\frac{\partial U}{\partial y}\right) \tag{3.2}$$

$$g\frac{\partial h}{\partial y}=-\frac{\tau_{by}}{\rho H} \tag{3.3}$$

3.4.2 INITIAL AND BOUNDARY FLOW CONDITIONS:

In order to solve the governing equations, the problem must be well-defined with an appropriate specification of the initial and the boundary conditions. The boundary conditions at the upstream and the downstream ends of the computational flow field must be known.

I. INITIAL FLOW CONDITION

Initially, any realistic combination of flow distributions in the main channel and the flood plain can be used.

II UPSTREAM FLOW BOUNDARY

At the upstream section of the computational flow field, the boundary condition can be provided either by an inflow discharge hydrograph or by a stage hydrograph.

III DOWNSTREAM FLOW BOUNDARY

At the downstream section of the domain, a stage-discharge relationship, a stage hydrograph, or a fixed stage can be specified.

IV SOLID BOUNDARIES

At the flood plain side boundaries, the condition of no flow across each of the boundaries has to be specified. This condition implies that the velocity or the discharge component normal to the solid boundaries is zero.

3.4.3 CONTROL VOLUME FORMULATION AND NUMERICAL SCHEME

The flow equations are discretized using a control volume method, which is briefly discussed herein. Details of this method can be found in Patankar (1980). The computational domain is subdivided into a finite number of non-overlapping control volumes. The depth and all other scalar variables are defined in the center of each control volume. The velocity or the discharge components are defined at the interfaces of each control volume. Consistent flow approximations between control volumes lead to mass conservation at the discrete level.

Considering a typical control volume as shown in Figure 3.1, the continuity equation can be integrated over this volume and the following is obtained:

$$\frac{\Delta h}{\Delta t}\Delta x \Delta y = (q_{x_{in}} - q_{x_{out}})\Delta y + (q_{y_{in}} - q_{y_{out}})\Delta x \qquad [3.4]$$

where Δh is the change in stage in time Δt, $q_{x_{in}}$ is the inflow longitudinal discharge per unit width, $q_{y_{in}}$ is the inflow lateral discharge per unit length, $q_{x_{out}}$ is the outflow longitudinal discharge per unit width, $q_{y_{out}}$ is the outflow lateral discharge per unit length, Δx is the grid size in the longitudinal direction, and Δy is the grid size in the lateral direction.

Deriving expressions for q_x and q_y from equations [3.2] and [3.3], respectively, and substituting in equation [3.4] results in an equation which contains only one dependent variable, h.

In order to solve this equation numerically, either explicit or implicit schemes can be used. In the explicit schemes, the unknown variable at a computational node is expressed as function of other known variables obtained from an old time step. These methods are simple but the time step size is limited from stability point of view. In the fully implicit schemes, however, the value of an unknown variable at any instant depends on the unknown values of other variables at several other computational nodes, as well as known values from an old time step. Consequently, a system of algebraic equations has to be solved simultaneously. It implies that both large computer storage and computational time are needed to achieve the desired solution. The implicit methods have no restrictions on time step size from a stability point of view but accuracy criteria sets a limit on it (Fread, 1976).

In order to reduce the computational storage and time, a modified implicit method known as the Alternating Direction Implicit (ADI) scheme can be used. The ADI scheme divides each time step into two stages of equal half time step. In this method, a tridiagonal coefficient matrix is obtained by alternately writing the finite difference equations, first implicitly along columns and explicitly along rows and then vice versa. As a result, it significantly saves computational storage and time (Gerald and Wheatley, 1985). In the present study, the ADI scheme has been adopted. Ponce and Yabusaki (1981) also used an ADI scheme for solving the full dynamic depth-averaged equations in order to model circulation in depth-averaged flow.

For the first half time step, considering the $y-$ direction implicit and the $x-$ direction explicit, equation [3.4] can be written as follows:

$$\frac{h_{i,j}^{n+\frac{1}{2}} - h_{i,j}^{n}}{\frac{\Delta t}{2}} \Delta x \Delta y = \left(q_{x_{in}}^{n} - q_{x_{out}}^{n}\right)\Delta y + \left(q_{y_{in}}^{n+\frac{1}{2}} - q_{y_{out}}^{n+\frac{1}{2}}\right)\Delta x \qquad [3.5]$$

where n is the nth time step.

This can be written as:

$$h_{i,j}^{n+\frac{1}{2}} - h_{i,j}^{n} = \frac{\Delta t}{2\Delta x}\left(q_{x_{i-\frac{1}{2},j}}^{n} - q_{x_{i+\frac{1}{2},j}}^{n}\right) + \frac{\Delta t}{2\Delta y}\left(q_{y_{i,j-\frac{1}{2}}}^{n+\frac{1}{2}} - q_{y_{i,j+\frac{1}{2}}}^{n+\frac{1}{2}}\right) \qquad [3.6]$$

For the second half time step, the $x-$ direction becomes implicit and the $y-$direction becomes explicit and equation [3.4] can be written as follows:

$$h_{i,j}^{n+1} - h_{i,j}^{n+\frac{1}{2}} = \frac{\Delta t}{2\Delta x}\left(q_{x_{i-\frac{1}{2},j}}^{n+1} - q_{x_{i+\frac{1}{2},j}}^{n+1}\right) + \frac{\Delta t}{2\Delta y}\left({}_{y_{i,j-\frac{1}{2}}}^{n+\frac{1}{2}} - q_{y_{i,j+\frac{1}{2}}}^{n+\frac{1}{2}}\right) \qquad [3.7]$$

The grid sizes , Δx and Δy can be varied in the computational code. However, they are treated as constants here for simplicity.

In order to solve equations [3.6] and [3.7], expressions for q_x and q_y are required. The expression for a typical q_y can be obtained from equation [3.3] as:

$$q_y = K_y \frac{\Delta h}{\Delta y} \qquad [3.8]$$

where $K_y = \dfrac{C^2 H^2}{|U|}$ [3.9]

At the outflow face of the control volume, equation [3.8] can be written as:

$$q_{y_{i,j+\frac{1}{2}}} = -\frac{C^2_{i,j+\frac{1}{2}} H^2_{i,j+\frac{1}{2}}}{\left|U_{i,j+\frac{1}{2}}\right|}\left(\frac{h_{i,j+1} - h_{i,j}}{\Delta y}\right) \qquad [3.10]$$

where

$$H_{i,j+\frac{1}{2}} = 0.5\left(H_{i,j} + H_{i,j+1}\right) \qquad [3.11]$$

$$C_{i,j+\frac{1}{2}} = 0.5\left(C_{i,j} + C_{i,j+1}\right) \qquad [3.12]$$

and

$$U_{i,j+\frac{1}{2}} = 0.25\left(U_{i-\frac{1}{2},j} + U_{i-\frac{1}{2},j+1} + U_{i+\frac{1}{2},j} + U_{i+\frac{1}{2},j+1}\right) \qquad [3.13]$$

The expression for a typical q_x can be derived from equation [3.2] as follows:

$$gH\frac{\partial h}{\partial x} = -g\frac{U|U|}{C^2} + \frac{\partial}{\partial y}\left(Hv_t\frac{\partial U}{\partial y}\right) \qquad [3.14]$$

Solving this quadratic equation, treating the last term as a constant, an expression for U can be obtained as:

If $U_{i+\frac{1}{2},j} > 0$, then

$$U_{i+\frac{1}{2},j} = 0.5\left[-A_1 + \sqrt{(A_1^2 - 4A_2)}\right] \qquad [3.15]$$

If $U_{i+\frac{1}{2},j} < 0$, then

$$U_{i+\frac{1}{2},j} = 0.5\left[A_1 - \sqrt{(A_1^2 + 4A_2)}\right] \qquad [3.16]$$

where

$$A_1 = \frac{C^2_{i+\frac{1}{2},j}}{g\Delta y^2}\left(E_{i+\frac{1}{2},j+\frac{1}{2}} + E_{i+\frac{1}{2},j-\frac{1}{2}}\right) \qquad [3.17]$$

$$A_2 = C^2_{i+\frac{1}{2},j} H_{i+\frac{1}{2},j} \frac{h_{i+1,j} - h_{i,j}}{\Delta x} - A_3 - A_4 \qquad [3.18]$$

$$A_3 = \frac{C^2_{i+\frac{1}{2},j}}{g\Delta y^2} E_{i+\frac{1}{2},j+\frac{1}{2}} U_{i+\frac{1}{2},j+1} \qquad [3.19]$$

$$A_4 = \frac{C^2_{i+\frac{1}{2},j}}{g\Delta y^2} E_{i+\frac{1}{2},j-\frac{1}{2}} U_{i+\frac{1}{2},j-1} \qquad [3.20]$$

$$H_{i+\frac{1}{2},j} = 0.5(H_{i,j} + H_{i+1,j}) \qquad [3.21]$$

$$C_{i+\frac{1}{2},j} = 0.5(C_{i,j} + C_{i+1,j}) \qquad [3.22]$$

$$H_{i+\frac{1}{2},j+\frac{1}{2}} = 0.25\left(H_{i,j} + H_{i,j+1} + H_{i+1,j} + H_{i+1,j+1}\right) \qquad [3.23]$$

$$H_{i+\frac{1}{2},j-\frac{1}{2}} = 0.25\left(H_{i,j} + H_{i,j-1} + H_{i+1,j} + H_{i+1,j-1}\right) \qquad [3.24]$$

$$E_{i+\frac{1}{2},j+\frac{1}{2}} = c_v \frac{\sqrt{g}U_{i+\frac{1}{2},j+\frac{1}{2}} H^2_{i+\frac{1}{2},j+\frac{1}{2}}}{C_{i+\frac{1}{2},j+\frac{1}{2}}} \qquad [3.25]$$

$$E_{i+\frac{1}{2},j-\frac{1}{2}} = c_v \frac{\sqrt{g}U_{i+\frac{1}{2},j-\frac{1}{2}} H^2_{i+\frac{1}{2},j-\frac{1}{2}}}{C_{i+\frac{1}{2},j-\frac{1}{2}}} \qquad [3.26]$$

$$U_{i+\frac{1}{2},j+\frac{1}{2}} = 0.5\left(U_{i+\frac{1}{2},j} + U_{i+\frac{1}{2},j+1}\right) \qquad [3.27]$$

and

$$U_{i+\frac{1}{2},j-\frac{1}{2}} = 0.5\left(U_{i+\frac{1}{2},j} + U_{i+\frac{1}{2},j-1}\right) \qquad [3.28]$$

Hence, determining the longitudinal velocity at any face of the control volume, the corresponding discharge can be calculated as:

$$q_{x_{i+\frac{1}{2},j}} = U_{i+\frac{1}{2},j} H_{i+\frac{1}{2},j} \qquad [3.29]$$

Without considering the effective stress term in the longitudinal direction, the expression for a typical q_x can be written as:

$$q_x = K_x \sqrt{\frac{\Delta h}{\Delta x}} \qquad [3.30]$$

where $K_x = CH^{\frac{3}{2}}$ [3.31]

In order to solve the continuity equation for the first half time step, equation [3.6] is rewritten as follows:

$$F_{i,j} = h_{i,j}^{n+\frac{1}{2}} - h_{i,j}^{n} - \frac{\Delta t}{2\Delta x}\left(q_{x_{i-\frac{1}{2},j}}^{n} - q_{x_{i+\frac{1}{2},j}}^{n}\right) - \frac{\Delta t}{2\Delta y}\left(q_{y_{i,j-\frac{1}{2}}}^{n+\frac{1}{2}} - q_{y_{i,j+\frac{1}{2}}}^{n+\frac{1}{2}}\right) \qquad [3.32]$$

where, $F_{i,j}$ is the residual.

Substitution of the expressions for q_x's and q_y's in the equation [3.32] results in three unknowns and three known nodal values of water surface elevation at each control volume at one half time step. If N is the total number of control volumes along a particular column, then the application of the continuity equation and two boundary conditions for lateral discharge results in a system of N nonlinear equations with N unknowns. These equations are nonlinear as the coefficients in equation [3.32] are functions of the unknown h's. In the present study, the generalized Newton-Raphson technique is used to solve these equations.

In the Newton-Raphson method, at a new time step, the unknown nodal values are estimated and substituted in equation [3.32]. This substitution results in N residuals. New values are calculated in the next iteration so that the residuals approach zero. These new values can be obtained by solving the following functional relationship:

$$\frac{\partial F_{i,j}}{\partial h_{i,j-1}^{n+\frac{1}{2}}}\Delta h_{i,j-1}^{n+\frac{1}{2}}+\frac{\partial F_{i,j}}{\partial h_{i,j}^{n+\frac{1}{2}}}\Delta h_{i,j}^{n+\frac{1}{2}}+\frac{\partial F_{i,j}}{\partial h_{i,j+1}^{n+\frac{1}{2}}}\Delta h_{i,j+1}^{n+\frac{1}{2}}=-F_{i,j},\ j=1,2,3,\ldots\ldots\ldots\ldots,N \qquad [3.33]$$

In matrix notation, this system of linear algebraic equations can be expressed as:

$$[\mathbf{A}]\{\Delta\mathbf{h}\}^{n+\frac{1}{2}}=-\{\mathbf{F}_{i,j}\} \qquad [3.34]$$

where $[\mathbf{A}]$ is the Jacobian matrix, $\{\Delta\mathbf{h}\}$ is the stage correction vector, and $\{\mathbf{F}_{i,j}\}$ is the residual vector.

The coefficients of this tridiagonal matrix are comprised of partial derivatives which have to be evaluated. This can be accomplished either analytically or numerically. The analytical approach has been adopted herein and such that:

$$\frac{\partial F_{i,j}}{\partial h_{i,j-1}}=-\frac{\Delta t}{2\Delta y}\frac{\partial q_{y_{i,j-\frac{1}{2}}}^{n+\frac{1}{2}}}{\partial h_{i,j-1}} \qquad [3.35]$$

$$\frac{\partial F_{i,j}}{\partial h_{i,j}}=1-\frac{\Delta t}{2\Delta y}\frac{\partial q_{y_{i,j-\frac{1}{2}}}^{n+\frac{1}{2}}}{\partial h_{i,j}}+\frac{\Delta t}{2\Delta y}\frac{\partial q_{y_{i,j+\frac{1}{2}}}^{n+\frac{1}{2}}}{\partial h_{i,j}} \qquad [3.36]$$

$$\frac{\partial F_{i,j}}{\partial h_{i,j+1}}=\frac{\Delta t}{2\Delta y}\frac{\partial q_{y_{i,j+\frac{1}{2}}}^{n+\frac{1}{2}}}{\partial h_{i,j+1}} \qquad [3.37]$$

The typical derivatives of q_y's with respect to h's are given as follows:

$$\frac{\partial q_{y_{i,j+\frac{1}{2}}}^{n+\frac{1}{2}}}{\partial h_{i,j}} = \frac{C^2_{i,j+\frac{1}{2}} H_{i,j+\frac{1}{2}}}{|U|_{i,j+\frac{1}{2}}} \frac{h_{i,j} - h_{i,j+1}}{\Delta y} + \frac{C^2_{i,j+\frac{1}{2}} H^2_{i,j+\frac{1}{2}}}{|U|_{i,j+\frac{1}{2}} \Delta y} \qquad [3.38]$$

$$\frac{\partial q_{y_{i,j+\frac{1}{2}}}^{n+\frac{1}{2}}}{\partial h_{i,j+1}} = \frac{C^2_{i,j+\frac{1}{2}} H_{i,j+\frac{1}{2}}}{|U|_{i,j+\frac{1}{2}}} \frac{h_{i,j} - h_{i,j+1}}{\Delta y} - \frac{C^2_{i,j+\frac{1}{2}} H^2_{i,j+\frac{1}{2}}}{|U|_{i,j+\frac{1}{2}} \Delta y} \qquad [3.39]$$

Having obtained the corrections, $\Delta h_{i,j}$, by solving equation [3.34] using the Thomas Algorithm (Wang and Anderson, 1982), the unknown nodal values are corrected in the next iteration by the following:

$$h_{i,j}^{n+\frac{1}{2},m+1} = h_{i,j}^{n+\frac{1}{2},m} + \Delta h_{i,j}^{n+\frac{1}{2}} \qquad [3.40]$$

where m is the number of iterations.

Following this procedure, the corrections, $\Delta h_{i,j}$ are obtained for all the columns ($i = 1,2,3,\dots\dots\dots,M$) in the computational domain in each iteration. Here, M is the total number of control volumes in a particular row. The iteration is then terminated when the maximum nodal changes in h, i.e., $\Delta h_{i,j}$ between two consecutive iterations is less than some tolerance limit (ξ) which can be given as:

$$\left|\Delta h_{i,j}^{n+\frac{1}{2}}\right|_{\max} \leq \xi \qquad [3.41]$$

When this convergence criteria is satisfied for the first half time step, the computational procedure proceeds to the second half time step and solves equation [3.7].The equation [3.7] can be expressed as:

$$G_{i,j} = h_{i,j}^{n+1} - h_{i,j}^{n+\frac{1}{2}} - \frac{\Delta t}{2\Delta x}\left(q_{x_{i-\frac{1}{2},j}}^{n+1} - q_{x_{i+\frac{1}{2},j}}^{n+1}\right) - \frac{\Delta t}{2\Delta y}\left(q_{y_{i,j-\frac{1}{2}}}^{n+\frac{1}{2}} - q_{y_{i,j+\frac{1}{2}}}^{n+\frac{1}{2}}\right) \qquad [3.42]$$

where, $G_{i,j}$ is the residual.

In a similar fashion, applying the Newton-Raphson technique, the corrections for the nodal values of h's for all the M control volumes along a particular row can be obtained by solving the following equation:

$$\frac{\partial G_{i,j}}{\partial h_{i-1,j}^{n+1}}\Delta h_{i,j-1}^{n+1} + \frac{\partial G_{i,j}}{\partial h_{i,j}^{n+1}}\Delta h_{i,j}^{n+1} + \frac{\partial G_{i,j}}{\partial h_{i+1,j}^{n+1}}\Delta h_{i+1,j}^{n+1} = -G_{i,j},\ i = 1,2,3,\ldots\ldots\ldots\ldots, M \qquad [3.43]$$

In matrix notation, this system of linear algebraic equations can be expressed as:

$$[\mathbf{B}]\{\Delta \mathbf{h}\}^{n+1} = -\{\mathbf{G}_{i,j}\} \qquad [3.44]$$

where $[\mathbf{B}]$ is the Jacobian matrix, $\{\Delta \mathbf{h}\}$ is the stage correction vector and $\{\mathbf{G}_{i,j}\}$ is the residual vector and

$$\frac{\partial G_{i,j}}{\partial h_{i-1,j}} = -\frac{\Delta t}{2\Delta x}\frac{\partial q_{x_{i-\frac{1}{2},j}}^{n+1}}{\partial h_{i-1,j}} \qquad [3.45]$$

$$\frac{\partial G_{i,j}}{\partial h_{i,j}} = 1 - \frac{\Delta t}{2\Delta x}\frac{\partial q_{x_{i-\frac{1}{2},j}}^{n+1}}{\partial h_{i,j}} + \frac{\Delta t}{2\Delta x}\frac{\partial q_{x_{i+\frac{1}{2},j}}^{n+1}}{\partial h_{i,j}} \qquad [3.46]$$

$$\frac{\partial G_{i,j}}{\partial h_{i+1,j}} = \frac{\Delta t}{2\Delta x}\frac{\partial q_{x_{i+\frac{1}{2},j}}^{n+1}}{\partial h_{i+1,j}} \qquad [3.47]$$

The typical derivatives of q_x's with respect to h's are given as follows:

If $U_{i+\frac{1}{2},j} > 0$

$$\frac{\partial q_{x_{i+\frac{1}{2},j}}}{\partial h_{i,j}} = 0.5U_{i+\frac{1}{2},j} - \frac{H_{i+\frac{1}{2},j}}{\sqrt{\left(A_1^2 - 4A_2\right)}}\left(\frac{C^2_{i+\frac{1}{2},j}}{2}\frac{h_{i+1,j} - h_{i,j}}{\Delta x} - \frac{C^2_{i+\frac{1}{2},j} H_{i+\frac{1}{2},j}}{\Delta x}\right) \qquad [3.48]$$

$$\frac{\partial q_{x_{i+\frac{1}{2},j}}}{\partial h_{i+1,j}} = 0.5U_{i+\frac{1}{2},j} - \frac{H_{i+\frac{1}{2},j}}{\sqrt{\left(A_1^2 - 4A_2\right)}}\left(\frac{C^2_{i+\frac{1}{2},j}}{2}\frac{h_{i+1,j} - h_{i,j}}{\Delta x} + \frac{C^2_{i+\frac{1}{2},j} H_{i+\frac{1}{2},j}}{\Delta x}\right) \qquad [3.49]$$

If $U_{i+\frac{1}{2},j} < 0$

$$\frac{\partial q_{x_{i+\frac{1}{2},j}}}{\partial h_{i,j}} = 0.5U_{i+\frac{1}{2},j} - \frac{H_{i+\frac{1}{2},j}}{\sqrt{\left(A_1^2 + 4A_2\right)}}\left(\frac{C^2_{i+\frac{1}{2},j}}{2}\frac{h_{i+1,j} - h_{i,j}}{\Delta x} - \frac{C^2_{i+\frac{1}{2},j} H_{i+\frac{1}{2},j}}{\Delta x}\right) \qquad [3.50]$$

$$\frac{\partial q_{x_{i+\frac{1}{2},j}}}{\partial h_{i+1,j}} = 0.5U_{i+\frac{1}{2},j} - \frac{H_{i+\frac{1}{2},j}}{\sqrt{\left(A_1^2 + 4A_2\right)}}\left(\frac{C^2_{i+\frac{1}{2},j}}{2}\frac{h_{i+1,j} - h_{i,j}}{\Delta x} + \frac{C^2_{i+\frac{1}{2},j} H_{i+\frac{1}{2},j}}{\Delta x}\right) \qquad [3.51]$$

Applying similar procedures as described in the first half time step, all the nodal unknown values are obtained at the second half time step along the rows of the computational domain. The computations are then repeated for subsequent time steps until the desired level of time is achieved.

3.4.4 SMALL DEPTH PROBLEMS

In certain numerical computations, computational difficulties are encountered when the depth of flow in the computational domain is small. Cunge, et al. (1975, 1980) and Meselhe et al. (1993) discussed this problem in detail. The numerical problem associated with the small depth or dry bed situation can be explained in the following way. The simplified x- momentum equation can be rewritten as:

$$q_{x_{i+\frac{1}{2},j}} = \phi\left(h_{i+\frac{1}{2},j}\right)\sqrt{\left|h_{i,j} - h_{i+1,j}\right|} \qquad [3.52]$$

where

$$\phi\left(h_{i+\frac{1}{2},j}\right) = \frac{C_{i+\frac{1}{2},j}}{\sqrt{\Delta x}}\left(h_{i+\frac{1}{2},j} - z_{b_{i+\frac{1}{2},j}}\right)^{\frac{3}{2}} \qquad [3.53]$$

$$\left(h_{i+\frac{1}{2},j} - z_{b_{i+\frac{1}{2},j}}\right) = \omega\left(h_{i,j} - z_{b_{i,j}}\right) + (1-\omega)\left(h_{i+1,j} - z_{b_{i+1,j}}\right) \qquad [3.54]$$

where, $0 \le \omega \le 1$ and $h_{i+1,j} \le h \le h_{i,j}$

Taking the derivative of the equation [3.52] with respect to the downstream water surface elevation, $h_{i+1,j}$,

$$\frac{\partial q_{x_{i+\frac{1}{2},j}}}{\partial h_{i+1,j}} = (1-\omega)\sqrt{\left|h_{i,j} - h_{i+1,j}\right|}\,\frac{\partial \phi}{\partial h_{i+1,j}} - \frac{\phi}{2\sqrt{\left|h_{i,j} - h_{i+1,j}\right|}} \qquad [3.55]$$

The sign of this derivative is normally negative ensuring that the discharge increases as the downstream water surface elevation decreases. A downstream water surface elevation exists for which the derivative is zero and the discharge is maximum. If this elevation falls further, discharge starts decreasing and the sign of the derivative becomes positive. This relationship is shown in Figure 3.2. As a non unique solution exists (two water surface elevations for a particular discharge), the computation becomes unstable. To avoid this problem, a test is required to check the sign of the derivative. If the sign is positive, the value of ω is to be estimated such that the derivative is zero. Equation [3.55] can be solved iteratively by putting the left hand side equal to zero for the estimation of ω. Another way of ensuring that the derivative is always negative is to use a fully upstream weighted coefficient, i.e., $\omega = 1$. This latter approach was used by Meselhe et al. (1993) for simulating unsteady flow in an irrigation canal with a dry bed and is used in the present study.

In addition to the above mentioned difficulty, negative depths are sometimes encountered in the numerical computation. To overcome these difficulties, the following discharge flux limiter is adopted in the present study. At any instant of time, the maximum outflow from a control volume is such that the control volume is completely emptied. An expression for the maximum longitudinal outflow discharge from a control volume can be computed using equation [3.7] and that for the lateral direction can be computed using equation [3.6]. These are written as follows:

$$q_{x_{i+\frac{1}{2},j}}^{n+1} = \frac{\frac{\Delta t}{2\Delta y}\left(q_{y_{i,j-\frac{1}{2}}}^{n+\frac{1}{2}} - q_{y_{i,j+\frac{1}{2}}}^{n+\frac{1}{2}}\right) + h_{i,j}^{n+\frac{1}{2}} - z_{b_{i,j}}}{\frac{\Delta t}{2\Delta x}} + q_{x_{i-\frac{1}{2},j}}^{n+1} \qquad [3.56]$$

$$q_{y_{i,j+\frac{1}{2}}}^{n+\frac{1}{2}} = \frac{\frac{\Delta t}{2\Delta x}\left(q_{x_{i-\frac{1}{2},j}}^{n} - q_{x_{i+\frac{1}{2},j}}^{n}\right) + h_{i,j}^{n} - z_{b_{i,j}}}{\frac{\Delta t}{2\Delta y}} + q_{y_{i,j-\frac{1}{2}}}^{n+\frac{1}{2}} \qquad [3.57]$$

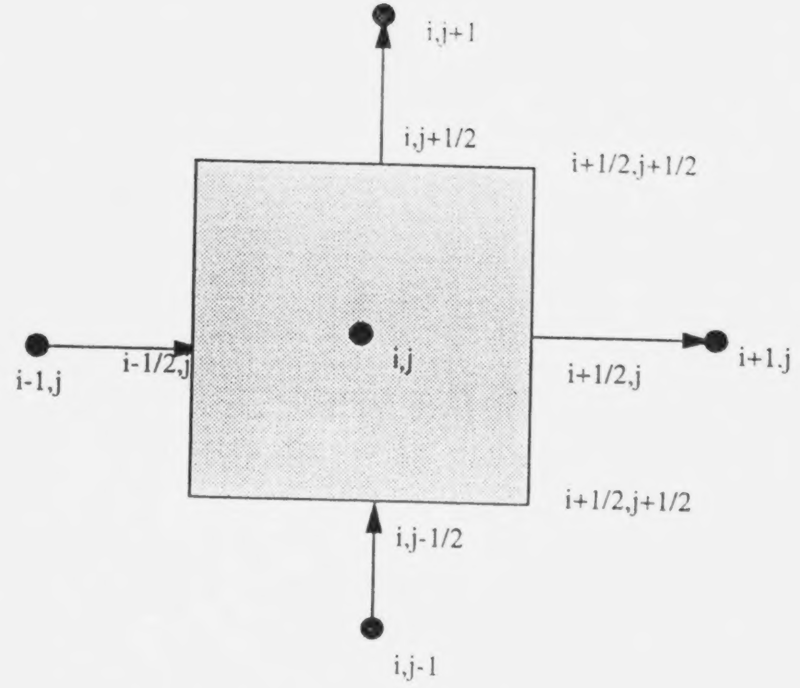
i,j+1
i,j+1/2
i+1/2,j+1/2
i-1,j
i-1/2,j
i,j
i+1/2,j
i+1,j
i+1/2,j+1/2
i,j-1/2
i,j-1

Figure 3.1 Typical Control Volume

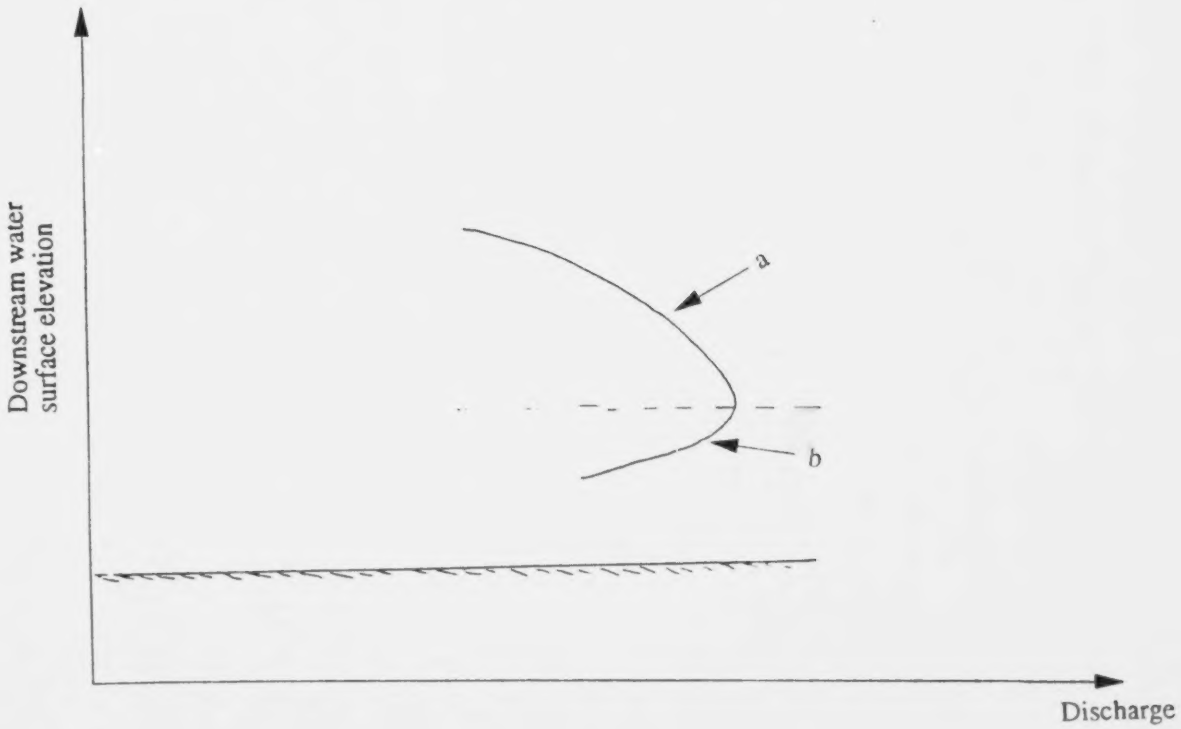

Figure 3.2 Relationship between discharge and downstream water surface elevation in small depth situation; a, Increasing slope dominates; b. Decreasing cross sectional area dominates (Meselhe et. al., 1993)

4 THE LINEAR STABILITY AND ACCURACY ANALYSES OF THE NUMERICAL MODEL

4.1 INTRODUCTION

A large number of numerical methods and schemes have been developed and applied for solving unsteady open channel flow. In order to assess the adequacy of the computed results obtained through these numerical models, knowledge of the properties of the numerical scheme is essential. In doing so, consistency, convergence and stability of the scheme are normally investigated. Sabur(1990) performed detailed stability and accuracy analyses for a one dimensional zero-inertia model. As the present study employs a two-dimensional zero-inertia model, the linear stability and accuracy analyses of this type of flow model are carried out. A brief description of consistency and convergence is given in Section 4.2 and the detailed discussion on the stability and the accuracy analyses is presented in Section 4.3.

4.2 CONSISTENCY AND CONVERGENCE

A finite difference scheme is said to be consistent when this approximation approaches the original partial differential equation in the limit that each of the grid sizes approaches zero. The consistency of a numerical scheme can be determined by evaluating the functional form of the truncation error. This error is found by applying a Taylor Series expansion to each term of the difference equation about the point at which the differential equation is computed. Detailed procedures are found in several books such as Jansen et al. (1979) and Cunge et al. (1980).

If the sequence of solutions approaches the true solution as each of the grid sizes tends to zero, then the solution of the difference scheme is said to be convergent. No analytical tools are readily available to directly analyze the convergence of a numerical scheme (Celia and Gray, 1992). Consistency and stability analyses, however, determine the convergence of a scheme as stated in the Lax Equivalence Theorem (Richtmyer and Morton, 1967):

"Given a properly posed initial value problem and a finite difference approximation to it that satisfies the consistency condition, stability is the necessary and sufficient condition for convergence." The stability of a numerical scheme does not depend on the nature of the governing differential equation to be solved but does depend on the difference equations. Consistency deals with equations whereas convergence deals with the solutions (Richtmyer and Morton, 1967).

4.3 STABILITY AND ACCURACY

The solution of a numerical scheme requires that the numerical errors introduced in the computational method not be amplified in an unlimited manner as time advances. This can be investigated by numerical experiments (Fread, 1973) or by detailed analysis of the numerical properties of the scheme (Katopodes, 1984). In the present study, the latter approach is adopted as this gives a clear picture how error grows with time.

One of the most commonly used techniques for stability analysis is the Fourier Series method (Roache, 1972). This method is, however, only applicable to linear equations with constant coefficients with periodic boundary conditions. Hence, the nonlinear partial differential equations used in the present study are linearized in order to apply this method. Although, the results obtained through this process are valid for linear equations, the information obtained can be used to gain valuable insights about the accuracy of the scheme. This information can also be used to compare different numerical methods as well as to determine appropriate temporal and spatial discretization sizes of a problem for a particular scheme.

4.3.1 LINEARIZATION OF THE GOVERNING EQUATION

Linearization procedure of the present non-linear difference equation can be explained in the following way. At instants of time $n\Delta t$ and $(n+1)\Delta t$, the following can be defined:

$$h_{i,j}^{n} = z_{b_{i,j}} + H_o + \hat{h}_{i,j}^{n} \qquad [4.1]$$

$$h_{i,j}^{n+1} = z_{b_{i,j}} + H_o + \hat{h}_{i,j}^{n+1} \qquad [4.2]$$

where H_o is the normal depth, $\hat{h}_{i,j}^{n}$ is the perturbation at time, t^n, and $\hat{h}_{i,j}^{n+1}$ is the perturbation at time, t^{n+1}.

Considering the y-direction implicit and the x-direction explicit, the mass balance in a control volume is,

$$\frac{h_{i,j}^{n+\frac{1}{2}} - h_{i,j}^{n}}{\frac{\Delta t}{2}} \Delta x \Delta y = \left(q_{x_{in}}^{n} - q_{x_{out}}^{n}\right)\Delta y + \left(q_{y_{in}}^{n+\frac{1}{2}} - q_{y_{out}}^{n+\frac{1}{2}}\right)\Delta x \qquad [4.3]$$

Substituting the expressions for q_x and q_y, the following is obtained:

$$\frac{h_{i,j}^{n+\frac{1}{2}} - h_{i,j}^{n}}{\frac{\Delta t}{2}} \Delta x \Delta y = K_{y_{i,j-\frac{1}{2}}}^{n+\frac{1}{2}} \left(\frac{h_{i,j-1}^{n+\frac{1}{2}} - h_{i,j}^{n+\frac{1}{2}}}{\Delta y}\right)\Delta x - K_{y_{i,j+\frac{1}{2}}}^{n+\frac{1}{2}} \left(\frac{h_{i,j}^{n+\frac{1}{2}} - h_{i,j+1}^{n+\frac{1}{2}}}{\Delta y}\right)\Delta x$$

$$+ K_{x_{i-\frac{1}{2},j}}^{n} \sqrt{\frac{h_{i-1,j}^{n} - h_{i,j}^{n}}{\Delta x}}\,\Delta y - K_{x_{i+\frac{1}{2},j}}^{n} \sqrt{\frac{h_{i,j}^{n} - h_{i+1,j}^{n}}{\Delta x}}\,\Delta y \qquad [4.4]$$

The effect of lateral momentum transfer is neglected from the expressions for longitudinal discharges for simplicity.

By applying Taylor series expansion , the followings can be obtained:

$$K_{x_{i-\frac{1}{2},j}}^{n} = K_{ox} + 0.5a\left(\hat{h}_{i-1,j}^{n} + \hat{h}_{i,j}^{n}\right) \qquad [4.5]$$

$$K_{x_{i+\frac{1}{2},j}}^{n} = K_{ox} + 0.5a\left(\hat{h}_{i,j}^{n} + \hat{h}_{i+1,j}^{n}\right) \qquad [4.6]$$

where

$$K_{ox} = CH_o^{\frac{3}{2}} \qquad [4.7]$$

$$a = \left.\frac{\partial K_x}{\partial H}\right|_{H=H_o} = \frac{3}{2}C\sqrt{H_o} \qquad [4.8]$$

$$K_{y_{i,j-\frac{1}{2}}}^{n+\frac{1}{2}} = K_{oy} + 0.5b\left(\hat{h}_{i,j-1}^{n+\frac{1}{2}} + \hat{h}_{i,j}^{n+\frac{1}{2}}\right) \qquad [4.9]$$

$$K_{y_{i,j+\frac{1}{2}}}^{n+\frac{1}{2}} = K_{oy} + 0.5b\left(\hat{h}_{i,j}^{n+\frac{1}{2}} + \hat{h}_{i,j+1}^{n+\frac{1}{2}}\right) \qquad [4.10]$$

where

$$K_{oy} = \frac{C^2 H_o^2}{U_o} \qquad [4.11]$$

$$b = \left.\frac{\partial K_y}{\partial H}\right|_{H=H_o} = \frac{\partial}{\partial H_o}\left(\frac{C^2 H_o^2}{U_o}\right) \qquad [4.12]$$

This can be written as:

$$b = C^2\left[\frac{2H_o}{U_o} + H_o^2\left(-\frac{1}{U_o^2}\frac{\partial U_o}{\partial H_o}\right)\right] \qquad [4.13]$$

Now, $\dfrac{\partial U_o}{\partial H_o} = 0.5C\sqrt{\dfrac{S_{ox}}{H_o}}$ [4.14]

After some manipulation the following is obtained:

$$b = \frac{3}{2}\frac{C^2 H_o}{U_o} \qquad [4.15]$$

To illustrate the linearization process, the first term and third term on the right hand side of equation [4.4] are considered. The first term can be written as:

$$\left[K_{oy} + 0.5b\left(\hat{h}_{i,j-1}^{n+\frac{1}{2}} + \hat{h}_{i,j}^{n+\frac{1}{2}}\right)\right]\left(\frac{z_{b_{i,j-1}} + H_o + \hat{h}_{i,j-1}^{n+\frac{1}{2}} - z_{b_{i,j}} - H_o - \hat{h}_{i,j}^{n+\frac{1}{2}}}{\Delta y}\right)\Delta x$$

$$= \left[K_{oy} + .5b\left(\hat{h}_{i,j-1}^{n+\frac{1}{2}} + \hat{h}_{i,j}^{n+\frac{1}{2}}\right)\right]\left(\frac{z_{b_{i,j-1}} - z_{b_{i,j}}}{\Delta y}\right)\left(1 + \frac{\hat{h}_{i,j-1}^{n+\frac{1}{2}} + \hat{h}_{i,j}^{n+\frac{1}{2}}}{z_{b_{i,j-1}} - z_{b_{i,j}}}\right)\Delta x$$

This expression can be simplified by neglecting the product of smaller terms as:

$$= \left[K_{oy}S_{oy} + 0.5bS_{oy}\left(\hat{h}_{i,j-1}^{n+\frac{1}{2}} + \hat{h}_{i,j}^{n+\frac{1}{2}}\right)\right] + \frac{K_{oy}}{\Delta y}\left(\hat{h}_{i,j-1}^{n+\frac{1}{2}} + \hat{h}_{i,j}^{n+\frac{1}{2}}\right)\Delta x$$

Similarly, the second term becomes

$$= \left[K_{oy}S_{oy} + 0.5bS_{oy}\left(\hat{h}_{i,j}^{n+\frac{1}{2}} + \hat{h}_{i,j+1}^{n+\frac{1}{2}}\right)\right] + \frac{K_{oy}}{\Delta y}\left(\hat{h}_{i,j}^{n+\frac{1}{2}} + \hat{h}_{i,j+1}^{n+\frac{1}{2}}\right)\Delta x$$

Now, considering the third term, it can be written as:

$$\left[K_{ox} + 0.5a\left(\hat{h}_{i-1,j}^{n} + \hat{h}_{i,j}^{n}\right)\right]\sqrt{\left(\frac{z_{b_{i-1,j}} + H_o + \hat{h}_{i-1,j}^{n} - z_{b_{i,j}} + H_o + \hat{h}_{i,j}^{n}}{\Delta x}\right)}\Delta y$$

$$= \left[K_{ox} + 0.5a\left(\hat{h}_{i-1,j}^{n} + \hat{h}_{i,j}^{n}\right)\right]\sqrt{\frac{z_{b_{i-1,j}} - z_{b_{i,j}}}{\Delta x}}\sqrt{\left(1 + \frac{\hat{h}_{i-1,j}^{n} - \hat{h}_{i,j}^{n}}{z_{b_{i-1,j}} - z_{b_{i,j}}}\right)}\Delta y$$

Evidently , the term $\left(\frac{z_{b_{i-1,j}} - z_{b_{i,j}}}{\Delta x}\right)$ in the above expression is the longitudinal slope of the channel. Assuming that absolute value of $\left(\frac{\hat{h}^n_{i-1,j} - \hat{h}^n_{i,j}}{z_{b_{i-1,j}} - z_{b_{i,j}}}\right)$is less than 1, then, the exponentiation can be expanded binomially. After multiplying and neglecting the terms containing higher powers of $\hat{h}$, the first term takes the following form:

$$\left[K_{ox}\sqrt{S_{ox}} + \frac{a\sqrt{S_{ox}}}{2}\left(\hat{h}^n_{i-1,j} + \hat{h}^n_{i,j}\right) + \frac{K_{ox}}{2\Delta x\sqrt{S_{ox}}}\left(\hat{h}^n_{i-1,j} - \hat{h}^n_{i,j}\right)\right]\Delta y$$

Similarly, the 4th term becomes

$$\left[K_{ox}\sqrt{S_{ox}} + \frac{a\sqrt{S_{ox}}}{2}\left(\hat{h}^n_{i,j} + \hat{h}^n_{i+1,j}\right) + \frac{K_{ox}}{2\Delta x\sqrt{S_{ox}}}\left(\hat{h}^n_{i,j} - \hat{h}^n_{i+1,j}\right)\right]\Delta y$$

Substituting in equation [4.4] and simplifying, the following linear form of the difference equation is obtained:

$$\begin{aligned}
\frac{\hat{h}^{n+\frac{1}{2}}_{i,j} - \hat{h}^n_{i,j}}{\frac{\Delta t}{2}} = &\left[\frac{K_{oy}S_{oy}}{\Delta y} + \frac{bS_{oy}}{2\Delta y}\left(\hat{h}^{n+\frac{1}{2}}_{i,j-1} + \hat{h}^{n+\frac{1}{2}}_{i,j}\right) + \frac{K_{oy}}{\Delta y^2}\left(\hat{h}^{n+\frac{1}{2}}_{i,j-1} - \hat{h}^{n+\frac{1}{2}}_{i,j}\right)\right] \\
&-\left[\frac{K_{oy}S_{oy}}{\Delta y} + \frac{bS_{oy}}{2\Delta y}\left(\hat{h}^{n+\frac{1}{2}}_{i,j} + \hat{h}^{n+\frac{1}{2}}_{i,j+1}\right) + \frac{K_{oy}}{\Delta y^2}\left(\hat{h}^{n+\frac{1}{2}}_{i,j} - \hat{h}^{n+\frac{1}{2}}_{i,j+1}\right)\right] \qquad [4.16] \\
&+\left[\frac{K_{ox}\sqrt{S_{ox}}}{\Delta x} + \frac{a\sqrt{S_{ox}}}{2\Delta x}\left(\hat{h}^n_{i-1,j} + \hat{h}^n_{i,j}\right) + \frac{K_{ox}}{2\Delta x^2\sqrt{S_{ox}}}\left(\hat{h}^n_{i-1,j} - \hat{h}^n_{i,j}\right)\right] \\
&-\left[\frac{K_{ox}\sqrt{S_{ox}}}{\Delta x} + \frac{a\sqrt{S_{ox}}}{2\Delta x}\left(\hat{h}^n_{i,j} + \hat{h}^n_{i+1,j}\right) + \frac{K_{ox}}{2\Delta x^2\sqrt{S_{ox}}}\left(\hat{h}^n_{i,j} - \hat{h}^n_{i+1,j}\right)\right]
\end{aligned}$$

Equation [4.16] can be further simplified as:

$$\frac{\hat{h}_{i,j}^{n+\frac{1}{2}} - \hat{h}_{i,j}^{n}}{\frac{\Delta t}{2}} = \frac{3}{2}U_o \frac{\hat{h}_{i-1,j}^{n} - \hat{h}_{i+1,j}^{n}}{2\Delta x} + \frac{3}{2}V_o \frac{\hat{h}_{i,j-1}^{n+\frac{1}{2}} - \hat{h}_{i,j+1}^{n+\frac{1}{2}}}{2\Delta x} + \frac{K_{ox}}{2\sqrt{S_{ox}}}\left(\frac{\hat{h}_{i-1,j}^{n} - 2\hat{h}_{i,j}^{n} + \hat{h}_{i+1,j}^{n}}{\Delta x^2}\right)$$

$$+K_{oy}\left(\frac{\hat{h}_{i,j-1}^{n+\frac{1}{2}} - 2\hat{h}_{i,j}^{n+\frac{1}{2}} + \hat{h}_{i,j+1}^{n+\frac{1}{2}}}{\Delta y^2}\right) \qquad [4.17]$$

Finally the linearized difference equation for the first half time step takes the following form:

$$\frac{\hat{h}_{i,j}^{n+\frac{1}{2}} - \hat{h}_{i,j}^{n}}{\frac{\Delta t}{2}} + U'\frac{\hat{h}_{i+1,j}^{n} - \hat{h}_{i-1,j}^{n}}{2\Delta x} + V'\frac{\hat{h}_{i,j+1}^{n+\frac{1}{2}} - \hat{h}_{i,j-1}^{n+\frac{1}{2}}}{2\Delta x} = D_x\left(\frac{\hat{h}_{i-1,j}^{n} - 2\hat{h}_{i,j}^{n} + \hat{h}_{i+1,j}^{n}}{\Delta x^2}\right)$$

$$+D_y\left(\frac{\hat{h}_{i,j-1}^{n+\frac{1}{2}} - 2\hat{h}_{i,j}^{n+\frac{1}{2}} + \hat{h}_{i,j+1}^{n+\frac{1}{2}}}{\Delta y^2}\right) \qquad [4.18]$$

where

$$U' = \frac{3}{2}U_o \qquad [4.19]$$

$$V' = \frac{3}{2}V_o \qquad [4.20]$$

$$D_x = \frac{K_{ox}}{2\sqrt{S_{ox}}} = \frac{C^2 H_o^{\ 2}}{2U_o} \qquad [4.21]$$

and

$$D_y = K_{oy} = \frac{C^2 H_o^{\ 2}}{U_o} \qquad [4.22]$$

Following a similar procedure, the linearized difference equation for the second half time step can be derived as:

$$\frac{\hat{h}_{i,j}^{n+1}-\hat{h}_{i,j}^{n+\frac{1}{2}}}{\frac{\Delta t}{2}}+U'\frac{\hat{h}_{i+1,j}^{n+1}-\hat{h}_{i-1,j}^{n+1}}{2\Delta x}+V'\frac{\hat{h}_{i,j+1}^{n+\frac{1}{2}}-\hat{h}_{i,j-1}^{n+\frac{1}{2}}}{2\Delta x}=D_x\left(\frac{\hat{h}_{i-1,j}^{n+1}-2\hat{h}_{i,j}^{n+1}+\hat{h}_{i+1,j}^{n+1}}{\Delta x^2}\right)$$
$$+D_y\left(\frac{\hat{h}_{i,j-1}^{n+\frac{1}{2}}-2\hat{h}_{i,j}^{n+\frac{1}{2}}+\hat{h}_{i,j+1}^{n+\frac{1}{2}}}{\Delta y^2}\right)$$

[4.23]

From equations [4.18] and [4.23], it can be concluded that the control volume formulation leads to a discrete form of convection-diffusion equation with a centered difference in space. Each equation is forward difference in time with respect to one space direction and backward with respect to the other. The overall effect is a centered (Crank-Nicolson) time discretization. It is also revealed that the apparent diffusion coefficient in the lateral direction is twice as that in the longitudinal direction. This relationship has also been derived in Chapter 2 by applying an ' Order of Magnitude Analysis' .

4.3.2 NUMERICAL AMPLIFICATION FACTOR

In this subsection, the Fourier method is applied to obtain an expression for the amplification factor for an error growth or decay as time progresses. Equation [4.18] can be written as:

$$\hat{h}_{i,j}^{n+\frac{1}{2}}-\hat{h}_{i,j}^{n}+\frac{U'\Delta t}{4\Delta x}\left(\hat{h}_{i+1,j}^{n}-\hat{h}_{i-1,j}^{n}\right)+\frac{V'\Delta t}{4\Delta x}\left(\hat{h}_{i,j+1}^{n+\frac{1}{2}}-\hat{h}_{i,j-1}^{n+\frac{1}{2}}\right)=D_x\left(\frac{\hat{h}_{i-1,j}^{n}-2\hat{h}_{i,j}^{n}+\hat{h}_{i+1,j}^{n}}{2\Delta x^2}\right)$$

$$+D_y\left(\frac{\hat{h}_{i,j-1}^{n+\frac{1}{2}}-2\hat{h}_{i,j}^{n+\frac{1}{2}}+\hat{h}_{i,j+1}^{n+\frac{1}{2}}}{2\Delta y^2}\right) \quad [4.24]$$

This equation can be simplified as:

$$-\left(\frac{C_{ry}}{4}+\frac{r_y}{2}\right)\hat{h}_{i,j-1}^{n+\frac{1}{2}}+\left(1+r_y\right)\hat{h}_{i,j}^{n+\frac{1}{2}}+\left(\frac{C_{ry}}{4}-\frac{r_y}{2}\right)\hat{h}_{i,j+1}^{n+\frac{1}{2}}$$

$$=\left(\frac{C_{rx}}{4}+\frac{r_x}{2}\right)\hat{h}_{i-1,j}^{n}+\left(1-r_x\right)\hat{h}_{i,j}^{n}-\left(\frac{C_{rx}}{4}-\frac{r_x}{2}\right)\hat{h}_{i+1,j}^{n} \qquad [4.25]$$

where

$C_{rx}=\dfrac{U'\Delta t}{\Delta x}$ is the Courant number in the x direction, [4.26]

$C_{ry}=\dfrac{V'\Delta t}{\Delta y}$ is the Courant number in the y direction, [4.27]

$r_x=\dfrac{D_x\Delta t}{\Delta x^2}$ is the non- dimensional diffusion coefficient in the x direction, [4.28]

and

$r_y=\dfrac{D_y\Delta t}{\Delta y^2}$ is the non-dimensional diffusion coefficient in the y direction. [4.29]

Applying the Fourier technique to the linearized equation and considering one Fourier component and defining the following:

$$\hat{h}_{i,j}^{n}=Ae^{Ik_1 i\Delta x k_2 j\Delta y} \qquad [4.30]$$

where $\mathrm{I}=\sqrt{-1}$ and A is a Fourier coefficient and a function of time,

$k_1=\dfrac{2\pi}{L_x}$ is the wave number in the x direction,

$k_2=\dfrac{2\pi}{L_y}$ is the wave number in the y direction,

L_x is the wave length in the x direction, and

L_y is the wave length in the y direction.

Then

$$\hat{h}_{i,j}^{n+\frac{1}{2}} = \gamma_y{}^n \hat{h}_{i,j}^n \qquad [4.31]$$

where $\gamma_y{}^n$ is the amplification factor for first half time step.

Similarly,

$$\hat{h}_{i,j+1}^n = Ae^{Ik_1 i\Delta x k_2 (j+1)\Delta y} \qquad [4.32]$$

$$\hat{h}_{i,j+1}^{n+\frac{1}{2}} = \gamma_y{}^n \hat{h}_{i,j+1}^n \qquad [4.33]$$

$$\hat{h}_{i,j-1}^n = Ae^{Ik_1 i\Delta x k_2 (j-1)\Delta y} \qquad [4.34]$$

$$\hat{h}_{i,j-1}^{n+\frac{1}{2}} = \gamma_y{}^n \hat{h}_{i,j-1}^n \qquad [4.35]$$

$$\hat{h}_{i-1,j}^n = Ae^{Ik_1 (i-1)\Delta x k_2 j\Delta y} \qquad [4.36]$$

$$\hat{h}_{i+1,j}^n = Ae^{Ik_1 (i+1)\Delta x k_2 j\Delta y} \qquad [4.37]$$

Substituting the above expressions in [4.25], and simplifying, the following is obtained:

$$\gamma_y{}^n = \left[\frac{1 - r_x(1-\cos k_1\Delta x) - \frac{1}{2} IC_{rx} \sin k_1 \Delta x}{1 + r_y(1-\cos k_2\Delta y) + \frac{1}{2} IC_{ry} \sin k_2 \Delta y} \right] \qquad [4.38]$$

Following a similar procedure, the amplification factor for the linearized difference equation for the second half time step can be obtained as:

$$\gamma_x^{\,n} = \left[\frac{1 - r_y(1 - \cos k_2\Delta y) - \frac{1}{2} IC_{ry}\sin k_2\Delta y}{1 + r_x(1 - \cos k_1\Delta x) + \frac{1}{2} IC_{rx}\sin k_1\Delta x}\right] \tag{4.39}$$

Hence, the combined amplification factor for one complete time step is given by

$$\gamma^n = \gamma_y^{\,n}\gamma_x^{\,n} \tag{4.40}$$

This can be expressed as:

$$\gamma^n = \left[\frac{1 - r_x(1 - \cos k_1\Delta x) - \frac{1}{2} IC_{rx}\sin k_1\Delta x}{1 + r_y(1 - \cos k_2\Delta y) + \frac{1}{2} IC_{ry}\sin k_2\Delta y}\right] * \left[\frac{1 - r_y(1 - \cos k_2\Delta y) - \frac{1}{2} IC_{ry}\sin k_2\Delta y}{1 + r_x(1 - \cos k_1\Delta x) + \frac{1}{2} IC_{rx}\sin k_1\Delta x}\right] \tag{4.41}$$

Let

Wave length ratio, $L_r = \dfrac{L_y}{L_x}$ [4.42]

Grid aspect ratio, $a_r = \dfrac{\Delta x}{\Delta y}$ [4.43]

$$r_y = 2r_x a_r^{\,2} \tag{4.44}$$

$$\frac{L_y}{\Delta y} = L_r a_r \frac{L_x}{\Delta x} \tag{4.45}$$

$$R_1 = 1 - r_y(1 - \cos k_2 \Delta y) = 1 - 2r_x a_r^2 \left[1 - \cos\left(\frac{2\pi}{L_r a_r \dfrac{L_x}{\Delta x}} \right) \right] \qquad [4.46]$$

$$R_2 = 1 + r_x(1 - \cos k_1 \Delta x) = 1 + r_x \left[1 - \cos\left(\frac{2\pi}{\dfrac{L_x}{\Delta x}} \right) \right] \qquad [4.47]$$

$$R_3 = 1 - r_x(1 - \cos k_1 \Delta x) = 1 - r_x \left[1 - \cos\left(\frac{2\pi}{\dfrac{L_x}{\Delta x}} \right) \right] \qquad [4.48]$$

$$R_4 = 1 + r_y(1 - \cos k_2 \Delta y) = 1 + 2r_x a_r^2 \left[1 - \cos\left(\frac{2\pi}{L_r a_r \dfrac{L_x}{\Delta x}} \right) \right] \qquad [4.49]$$

$$I_1 = \frac{1}{2} C_{ry} \sin k_2 \Delta y = \frac{1}{2} C_{ry} \sin\left(\frac{2\pi}{L_r a_r \dfrac{L_x}{\Delta x}} \right) \qquad [4.50]$$

$$I_2 = \frac{1}{2} C_{rx} \sin k_1 \Delta x = \frac{1}{2} C_{rx} \sin\left(\frac{2\pi}{\dfrac{L_x}{\Delta x}} \right) \qquad [4.51]$$

Substitution of all the above expressions in the equation [4.41] yields the following:

$$\gamma^n = \frac{(R_1 - I_1 I)(R_3 - I_2 I)}{(R_2 + I_2 I)(R_4 + I_1 I)} \qquad [4.52]$$

Here , $I = \sqrt{-1}$

$$\gamma^n = \frac{[R_1R_3 - I_1I_2 - I(I_1R_3 + I_2R_1)]}{[R_2R_4 - I_1I_2 + I(I_1R_2 + I_2R_4)]} \qquad [4.53]$$

After simplifying, the following can be obtained:

$$\gamma^n = \alpha_1 + I\beta_1 \qquad [4.54]$$

where

$$\alpha_1 = \frac{(R_1R_3 - I_1I_2)(R_2R_4 - I_1I_2) - (I_1R_3 + I_2R_1)(I_1R_2 + I_2R_4)}{(R_2R_4)^2 + (I_1I_2)^2 + (I_1R_2)^2 + (I_2R_4)^2} \qquad [4.55]$$

$$\beta_1 = \frac{(I_1I_2 - R_1R_3)(I_1R_2 + I_2R_4) + (I_1I_2 - R_2R_4)(I_1R_3 + I_2R_1)}{(R_2R_4)^2 + (I_1I_2)^2 + (I_1R_2)^2 + (I_2R_4)^2} \qquad [4.56]$$

As the amplification factor is a complex variable, its magnitude can be determined by

$$\left|\gamma^n\right| = \pm\sqrt{(\alpha_1{}^2 + \beta_1{}^2)} \qquad [4.57]$$

and the numerical celerity can be determined by

$$\theta^n = \tan^{-1}(\frac{\beta_1}{\alpha_1}) \qquad [4.58]$$

In order to get a stable numerical scheme, the amplification factor derived above must satisfy the following condition:

$$\left|\gamma^n\right| \le 1 \qquad [4.59]$$

The L.H.S. of [4.59] is too complicated to simplify in order to show that the magnitude of the amplification factor is always less than 1 for the present scheme. Hence, the magnitude of this factor has been studied graphically. The amplification factor is a function of the wave length ratio, L_r, grid size ratio, a_r, non-dimensional diffusion coefficient, r_x and non-dimensional wave length (number of nodes per wave length), $\frac{L_x}{\Delta x}$. Figures 4.1 to 4.8 show the variation of its magnitude for different C_{rx}, r_x and a_r. For all these cases, the magnitude is always less than 1. Therefore, it can be concluded that the present numerical scheme is unconditionally stable.

4.3.3 ANALYTICAL AMPLIFICATION FACTOR

The comparison of the ratio of the magnitude of the numerical and analytical amplification factors and the ratio of the numerical wave celerity to the analytical wave celerity provides a measure of how closely a numerical solution approximates the analytical solution. The model equation is linear, an analytical solution to such equation can be obtained in the following way:

$$\frac{\partial \hat{h}}{\partial t} + U' \frac{\partial \hat{h}}{\partial x} + V' \frac{\partial \hat{h}}{\partial y} = D_x \frac{\partial^2 \hat{h}}{\partial x^2} + D_y \frac{\partial^2 \hat{h}}{\partial y^2} \qquad [4.60]$$

Let, $\hat{h}(x, y, n\Delta t) = Ae^{Ik_1xk_2y}$ [4.61]

$$\frac{\partial \hat{h}}{\partial x} = AIk_1e^{Ik_1xk_2y} \qquad [4.62]$$

$$\frac{\partial \hat{h}}{\partial y} = AIk_2e^{Ik_1xk_2y} \qquad [4.63]$$

$$\frac{\partial^2 \hat{h}}{\partial x^2} = -Ak_1^2e^{Ik_1xk_2y} \qquad [4.64]$$

$$\frac{\partial^2 \hat{h}}{\partial y^2} = -Ak_2{}^2 e^{Ik_1xk_2y} \qquad [4.65]$$

$$\frac{\partial \hat{h}}{\partial t} = \frac{dA}{dt} e^{Ik_1xk_2y} \qquad [4.66]$$

Substituting in the Convection-Diffusion equation, [4.58], the following is obtained:

$$\frac{dA}{dt} e^{Ik_1xk_2y} + U'AIk_1 e^{Ik_1xk_2y} + V'AIk_2 e^{Ik_1xk_2y} = -D_x Ak_1{}^2 e^{Ik_1xk_2y} - D_y Ak_2{}^2 e^{Ik_1xk_2y} \qquad [4.67]$$

This can be simplified as:

$$\frac{dA}{dt} + U'AIk_1 + V'AIk_2 = -D_x Ak_1{}^2 - D_y Ak_2{}^2 \qquad [4.68]$$

This equation can be written as:

$$\frac{dA}{A} = \left[-I\left(U'k_1 + V'k_2\right) - \left(D_x k_1{}^2 + D_y k_2{}^2\right)\right] dt \qquad [4.69]$$

Integrating,

$$A = e^{-[I(U'k_1 + V'k_2) + (D_x k_1{}^2 + D_y k_2{}^2)]t} \qquad [4.70]$$

Hence, the general solution is

$$\hat{h}(x,y,t) = A_o e^{-[I(U'k_1 + V'k_2) + (D_x k_1{}^2 + D_y k_2{}^2)]t} e^{Ik_1xk_2y} \qquad [4.71]$$

where A_o is a coefficient.

Now, the analytical solution at time level $n\Delta t$ is given by

$$\hat{h}(x,y,n\Delta t) = A_o e^{-[I(U'k_1+V'k_2)+(D_x k_1{}^2+D_y k_2{}^2)]n\Delta t} e^{Ik_1 x k_2 y} \qquad [4.72]$$

and the analytical solution at time level $(n+1)\Delta t$ is given by

$$\hat{h}(x,y,(n+1)\Delta t) = A_o e^{-[I(U'k_1+V'k_2)+(D_x k_1{}^2+D_y k_2{}^2)](n+1)\Delta t} e^{Ik_1 x k_2 y} \qquad [4.73]$$

Hence, the analytical amplification factor is given by

$$\gamma^a = \frac{\hat{h}(x,y,(n+1)\Delta t)}{\hat{h}(x,y,n\Delta t)}) = e^{-[I(U'k_1+V'k_2)+(D_x k_1{}^2+D_y k_2{}^2)]\Delta t} \qquad [4.74]$$

Using the previously used notations, equation [4.74] can be written as:

$$\gamma^a = e^{-I\left(C_{rx}\frac{2\pi}{\frac{L_x}{\Delta x}}+C_{ry}\frac{2\pi}{L_r a_r\frac{L_x}{\Delta x}}\right)} e^{-\left[r_x\left(\frac{2\pi}{\frac{L_x}{\Delta x}}\right)^2+2r_x a_r{}^2\left(\frac{2\pi}{L_r a_r\frac{L_x}{\Delta x}}\right)\right]} \qquad [4.75]$$

Hence, the magnitude of the analytical factor can be given as:

$$|\gamma^a| = e^{-\left[r_x\left(\frac{2\pi}{\frac{L_x}{\Delta x}}\right)^2+2r_x a_r{}^2\left(\frac{2\pi}{L_r a_r\frac{L_x}{\Delta x}}\right)^2\right]} \qquad [4.76]$$

and the analytical celerity can be expressed by the following:

$$\theta^a = -\left(C_{rx}\frac{2\pi}{\frac{L_x}{\Delta x}}+C_{ry}\frac{2\pi}{L_r a_r\frac{L_x}{\Delta x}}\right) \qquad [4.77]$$

4.3.4 AMPLITUDE AND PHASE PORTRAITS ANALYSIS

Having obtained the expressions for numerical and analytical amplification factors and the celerities, the amplification ratio and the celerity ratio, respectively, can be obtained as follows:

$$R_d = \frac{\gamma^n}{\gamma^a} \qquad [4.78]$$

$$R_\theta = \frac{\theta^n}{\theta^a} \qquad [4.79]$$

These expressions show that these two ratios are functions of the wave length ratio, L_r, grid size ratio, a_r, non-dimensional diffusion coefficient, r_x, and non-dimensional wave length (number of nodes per wave length), $L_x/\Delta x$. When R_d and R_θ are equal to unity, the numerical representation of the amplitude and celerity of a wave component are identical to the analytical behavior. The plots of R_d and R_θ as functions of $L_x/\Delta x$ are known as amplitude and phase portraits respectively. These portraits provide a valuable indication of the accuracy of the numerical scheme employed (Fread, 1976). Several portraits are presented in the figures that follow for wave length ratio, L_r, of 1 and the reference Courant number in the lateral direction, C_{ry}, of zero. Figures 4.9 to 4.14 show the effects of grid size ratio on the amplitude and phase errors for certain C_{rx} and r_x. It is evident that grid size ratio has no effect on the phase errors but it has influence on the amplitude errors. For a particular C_{rx} and r_x, as the a_r increases, the value of $L_x/\Delta x$ required for the same level of accuracy increases. However, for higher values of a_r, for example, a_r= 10 and 100 in the present case, no change in behavior is observed.

It is worth mentioning that the parameter, a_r has a significant role in the present study. The present study considers a compound channel where the length of the reach is many times greater than the width of the channel. Consequently, in order to get a better resolution in the lateral direction, a very fine discretization size in the lateral direction and a relatively large discretization size in the longitudinal direction are economically and computationally feasible. Hence a higher aspect ratio is usually desirable. The present analysis clearly shows that a reasonable accuracy can be obtained even for very large values of a_r such as 100. This finding will be utilized in numerical experiments conducted for the present study.

Figures 4.15a and 4.15b represent the effects of r_x on the accuracy for a particular grid size ratio, a_r of 100. In general, it is noticed that for a desired accuracy level, phase error portraits require more nodes per wave length than the amplitude portraits do. From all these plots, it appears that for an accuracy level of 1% or better, $L_x/\Delta x \geq 20$ should be used. Utilizing these plots, the computational grid sizes, Δt, Δx, and Δy can be determined as described below. For a desired accuracy level, the $L_x/\Delta x$, C_{rx}, and r_x are chosen from the Figures 4.9 to 4.14. When L_x, a_r, and $L_x/\Delta x$ are known, Δx and Δy can easily be determined. Then two values of time step can be calculated from the reference Courant number, C_{rx} and the non-dimensional diffusion coefficient, r_x. The smaller of these two values will provide the time step increment, Δt for the desired accuracy level.

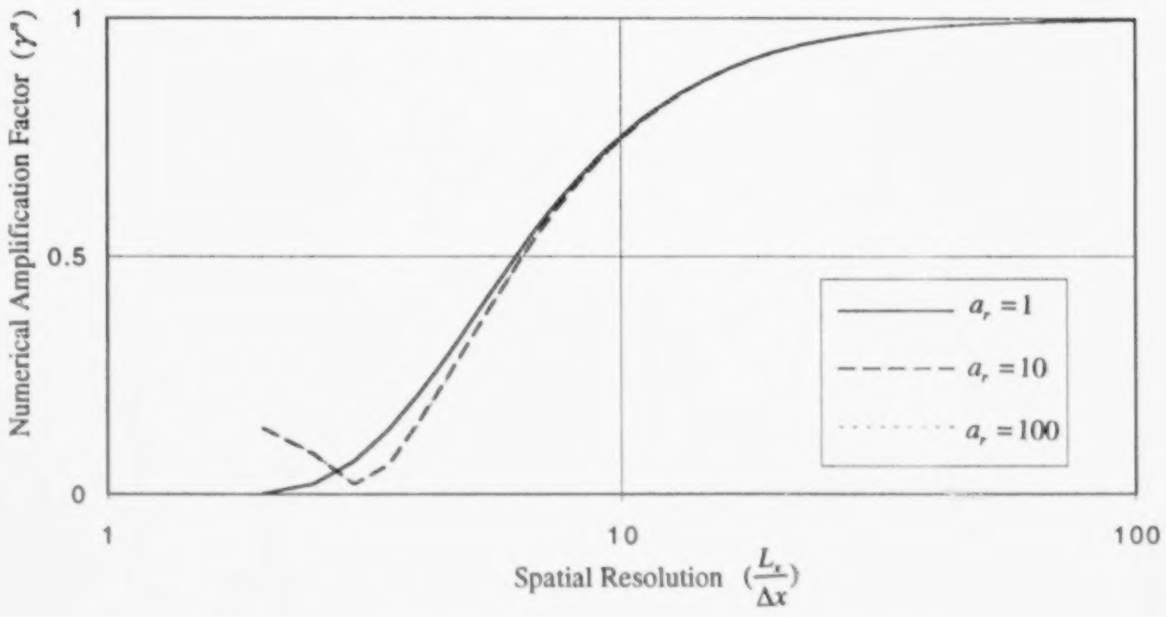

Figure 4.1 Numerical Amplification factor for C_{rx}=0.5, and r_x=0.25.

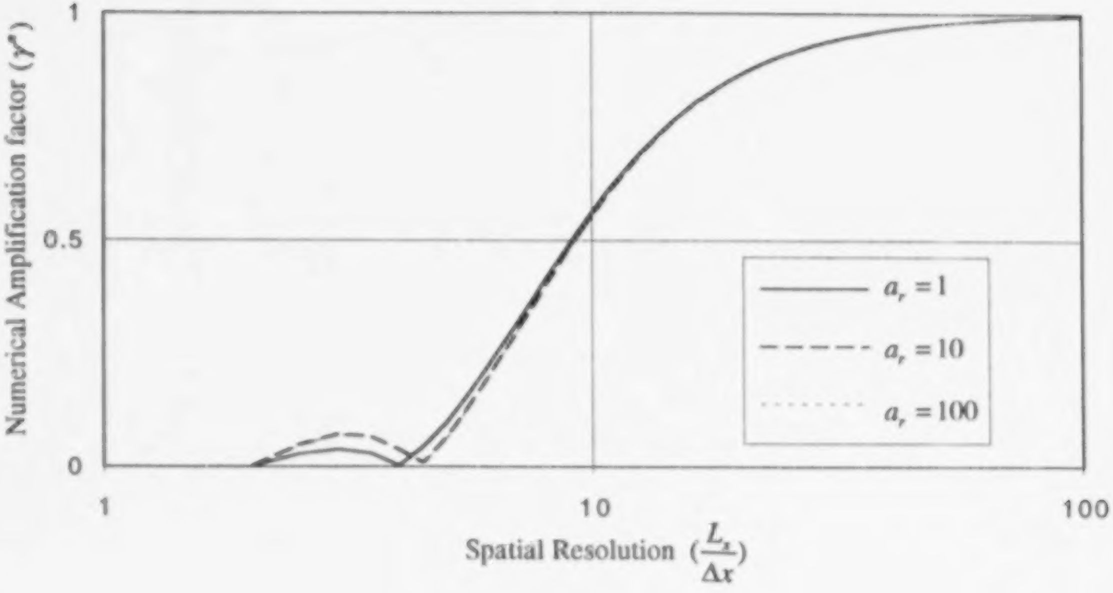

Figure 4.2 Numerical Amplification factor for C_{rx}=0.5, and r_x=0.5.

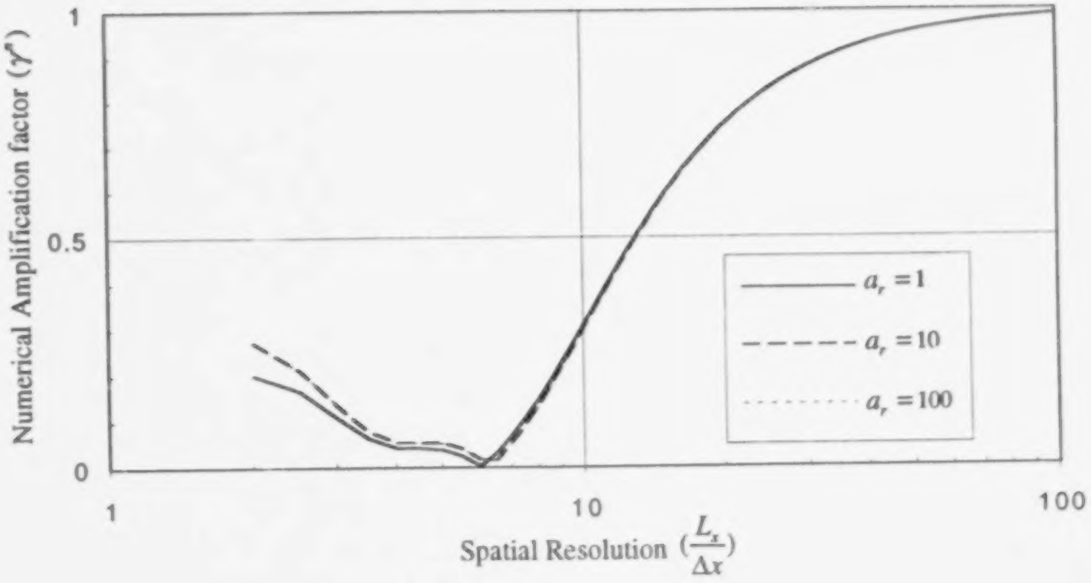

Figure 4.3 Numerical Amplification factor for C_{rx}=0.5, and r_x=1.0.

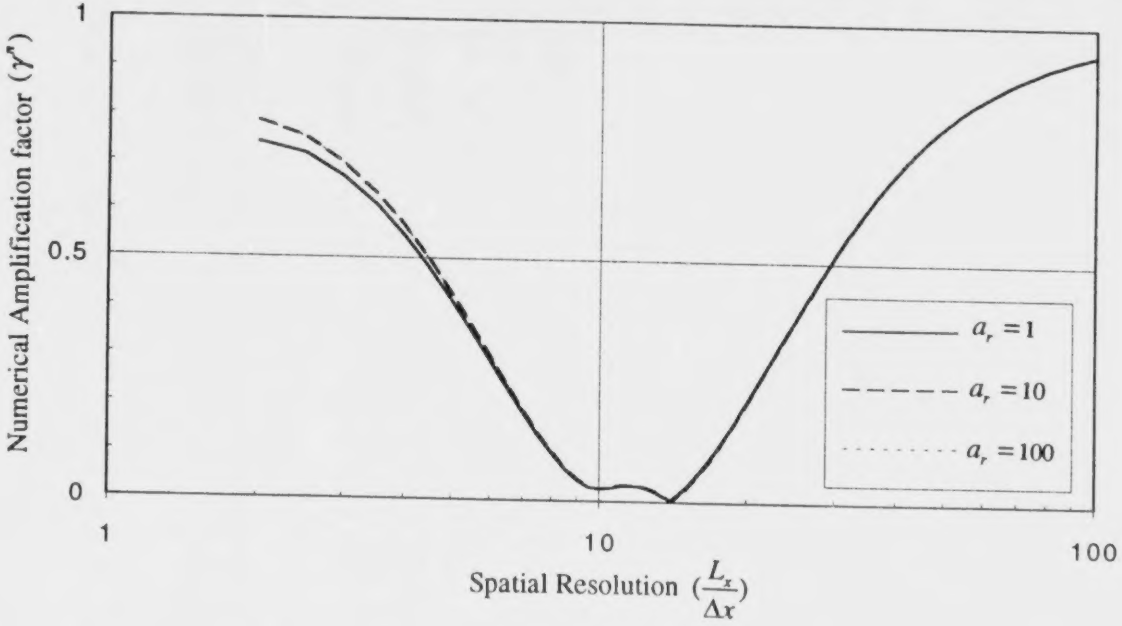

Figure 4.4 Numerical Amplification factor for C_{rx}=0.5, and r_x=5.0.

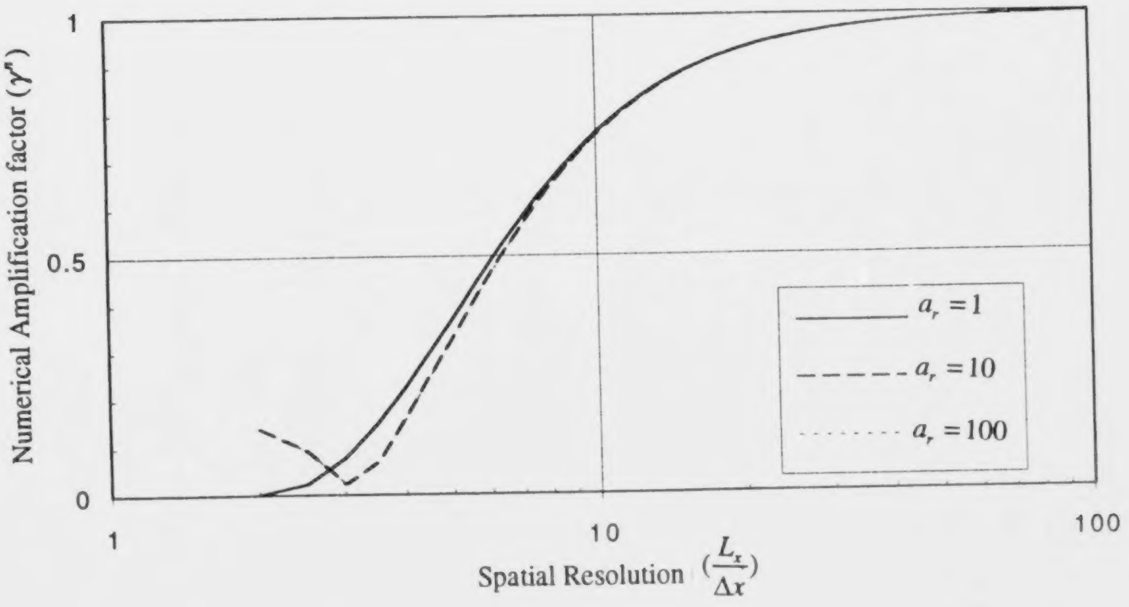

Figure 4.5 Numerical Amplification factor for C_{rx}=1.0, and r_x=0.25.

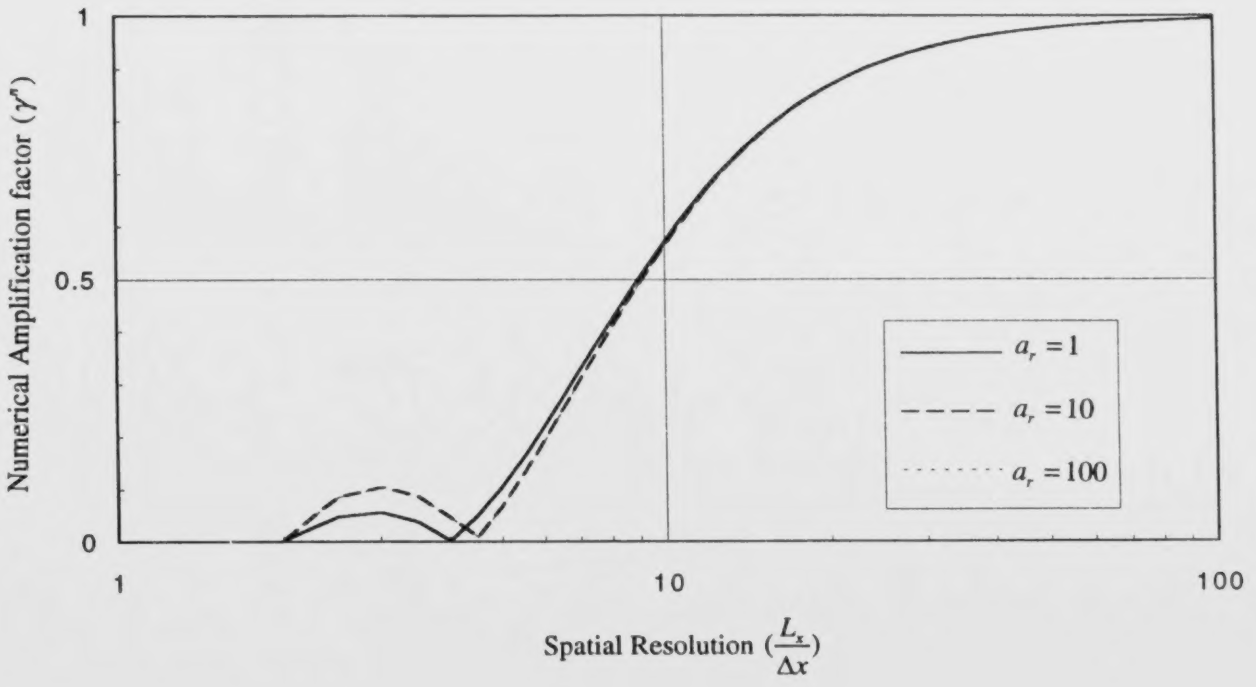

Figure 4.6 Numerical Amplification factor for C_{rx}=1.0, and r_x=0.5.

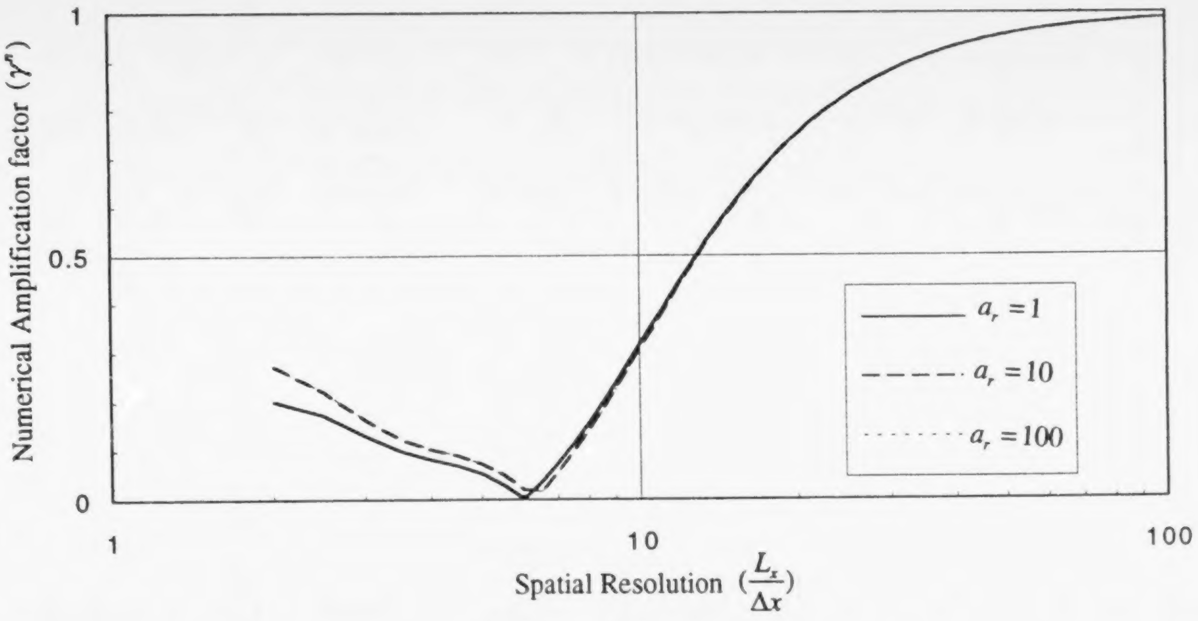

Figure 4.7 Numerical Amplification factor for C_{rx}=1.0, and r_x=1.0.

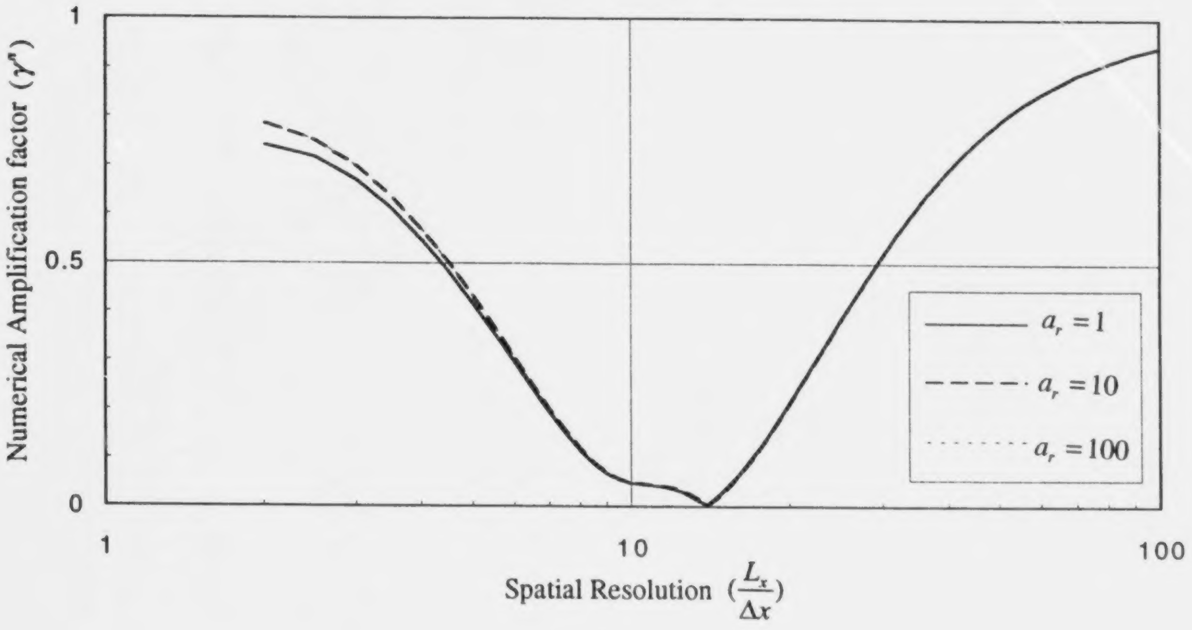

Figure 4.8 Numerical Amplification factor for C_{rx}=1.0, and r_x=5.0.

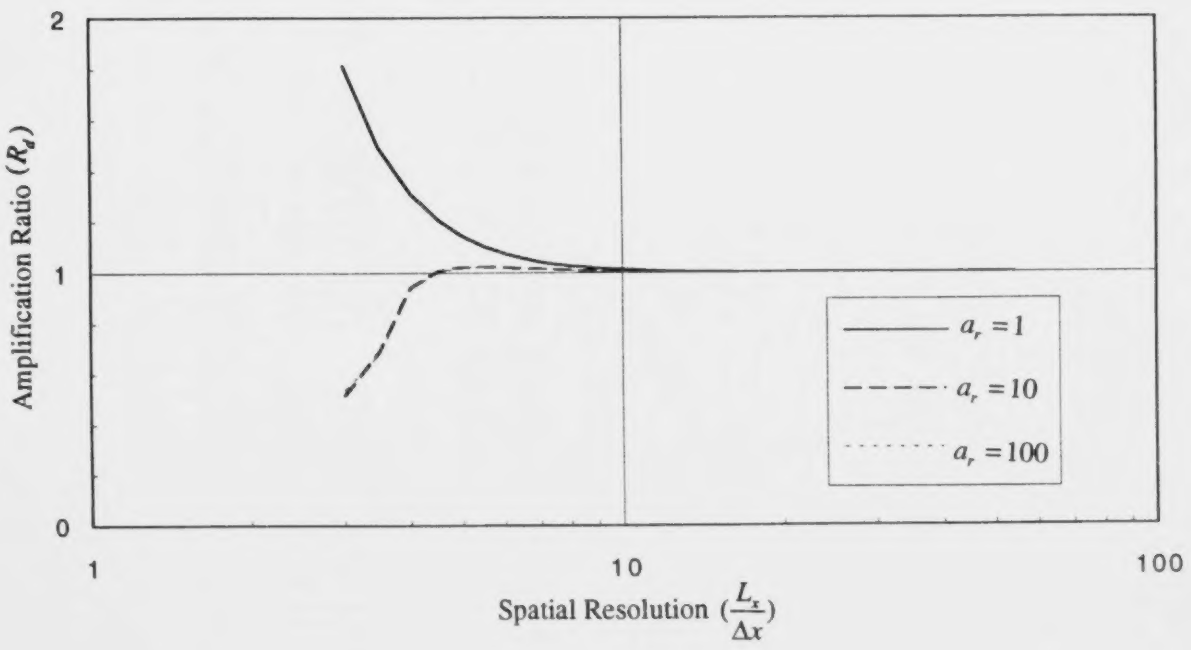

Figure 4.9a Amplitude Portraits for C_{rx}=0.5, and $r_x = 0.25$.

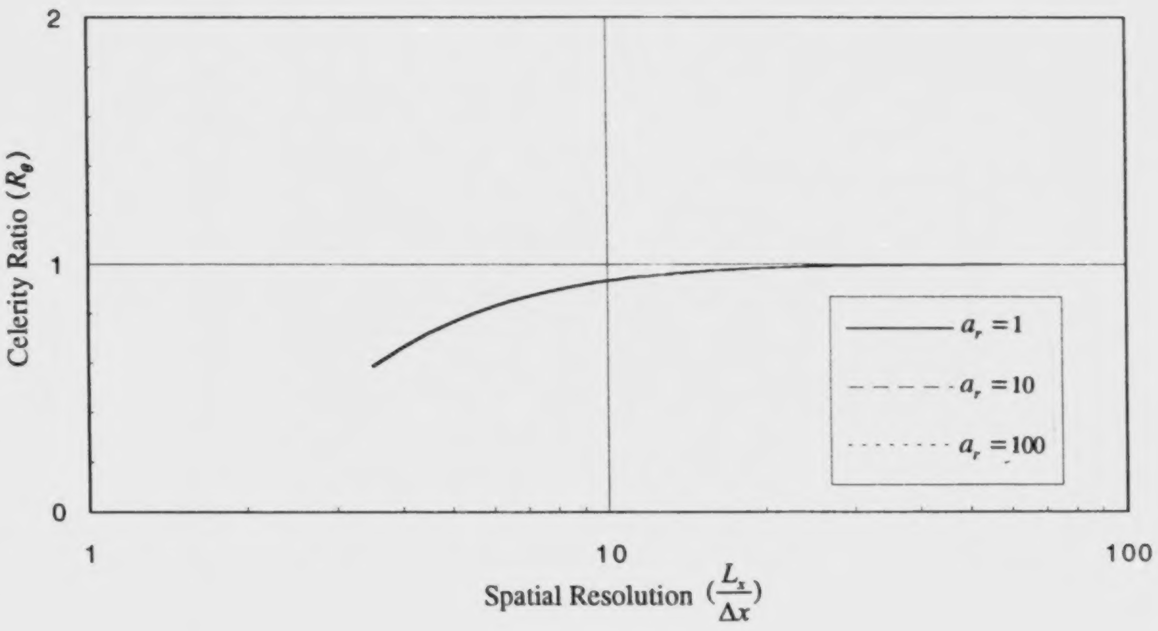

Figure 4.9b Phase Portraits for C_{rx}=0.5, and r_x= 0.25.

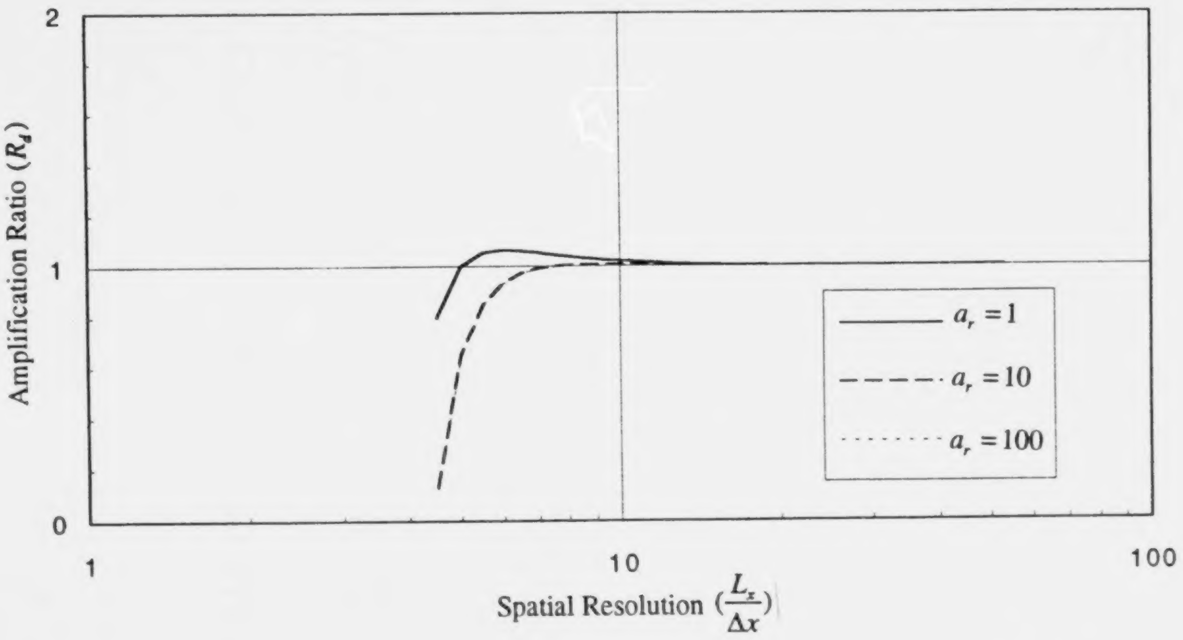

Figure 4.10a Amplitude Portraits for C_{rx}=0.5, and r_x=0.5.

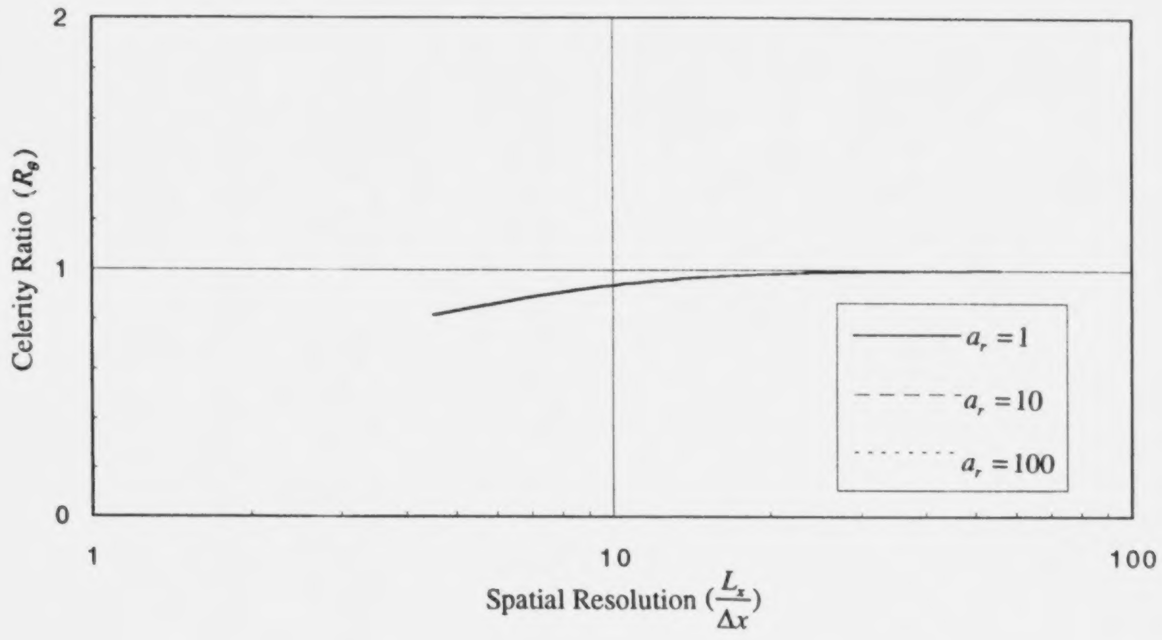

Figure 4.10b Phase Portraits for C_{rx}=0.5, and r_x=0.5.

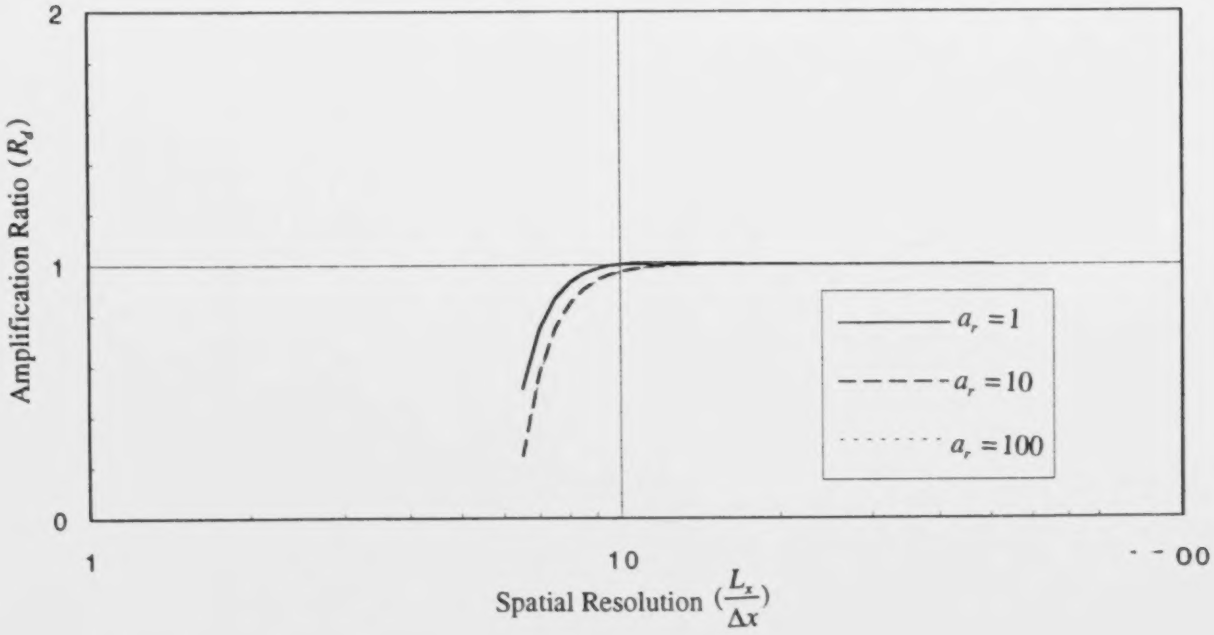

Figure 4.11a Amplitude Portraits for C_{rx}=0.5, and r_x=1.0.

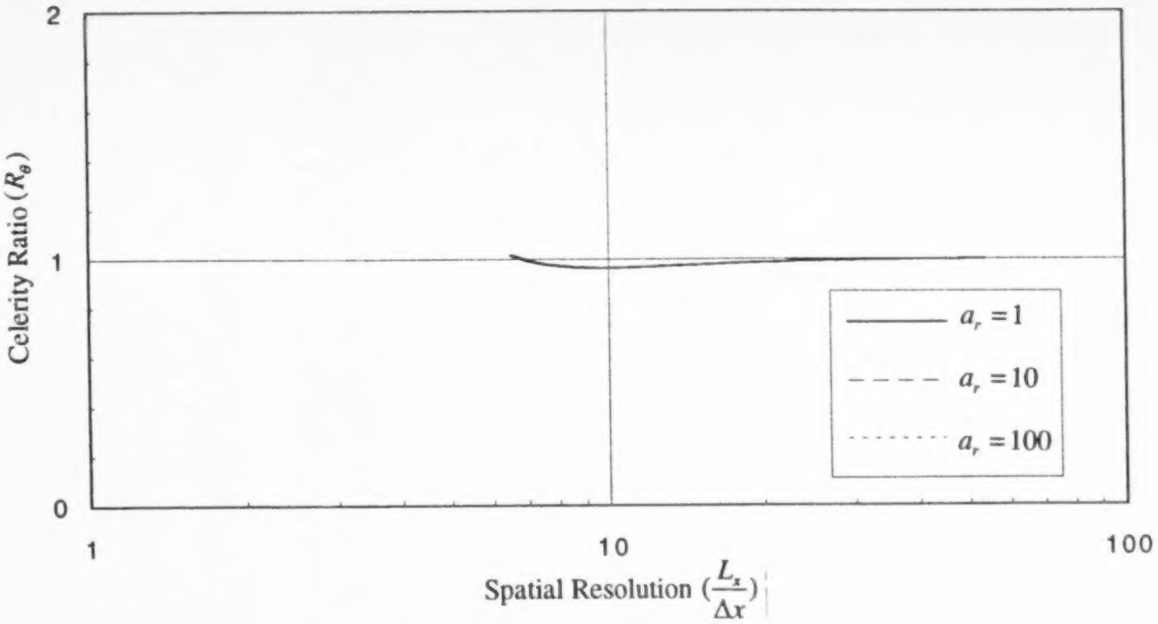

Figure 4.11b Phase Portraits for C_{rx}=0.5, and r_x=1.0

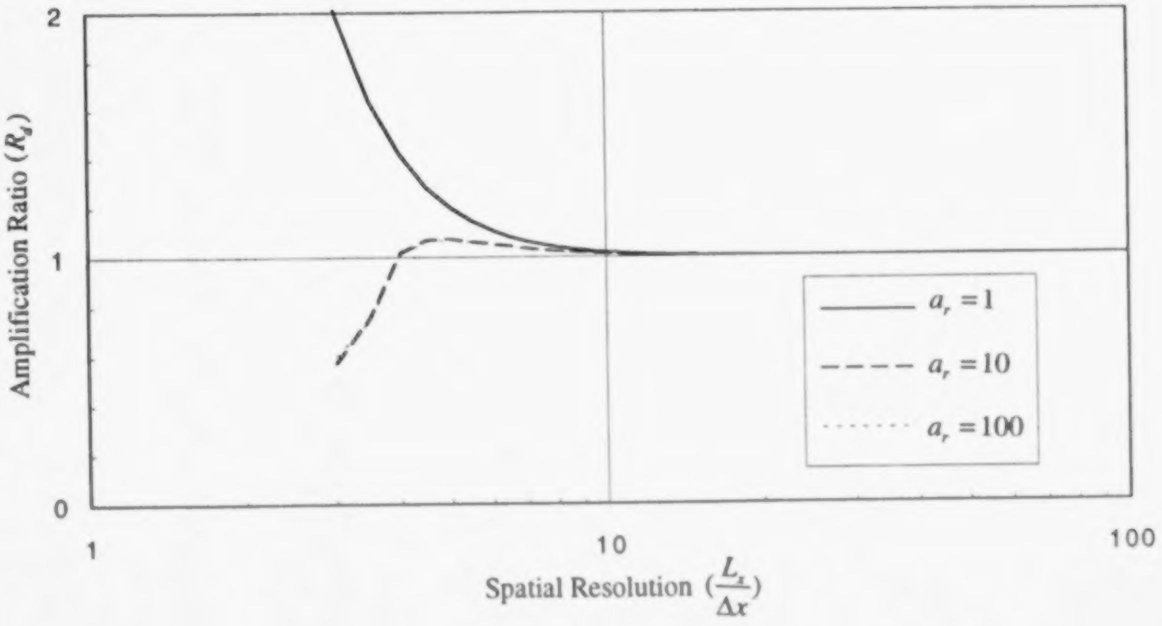

Figure 4.12a Amplitude Portraits for $C_{rx} = 1.0$ and $r_x = 0.25$.

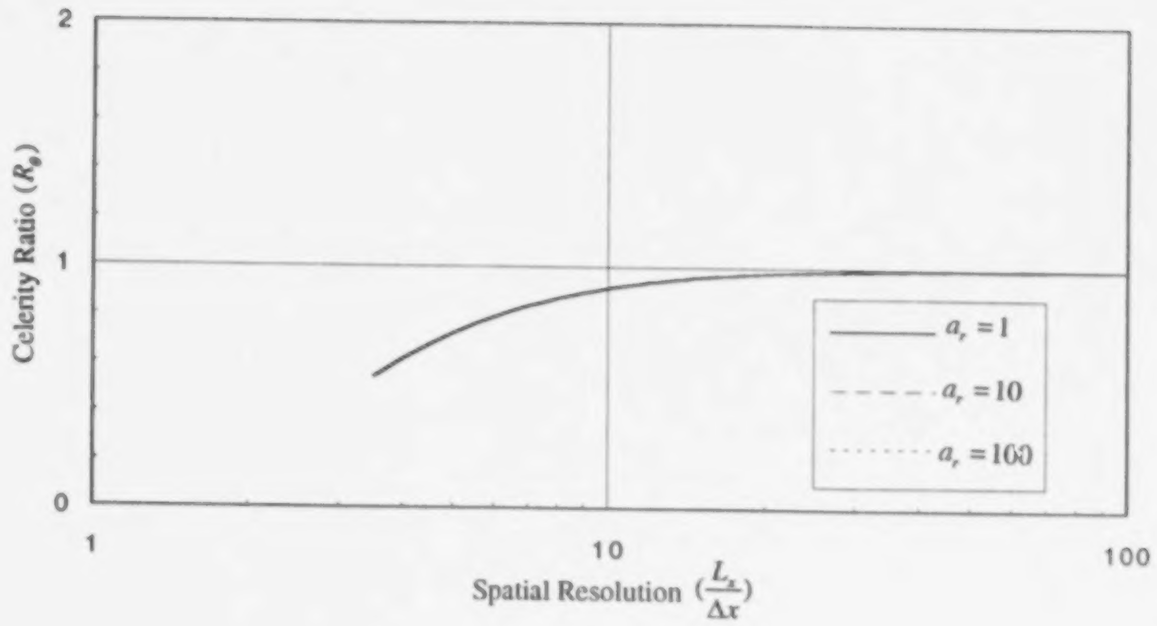

Figure 4.12b Phase Portraits for C_{rx}=1.0, and r_s = 0.25.

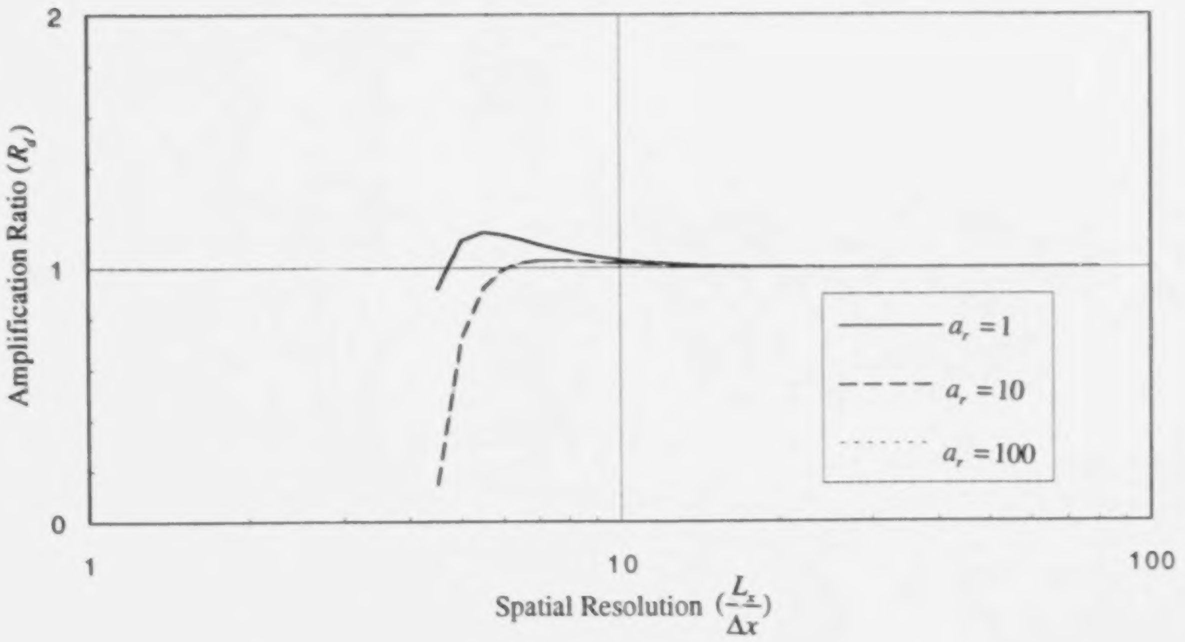

Figure 4.13a Amplitude Portraits for $C_{rx} = 1.0$, and $r_x = 0.5$.

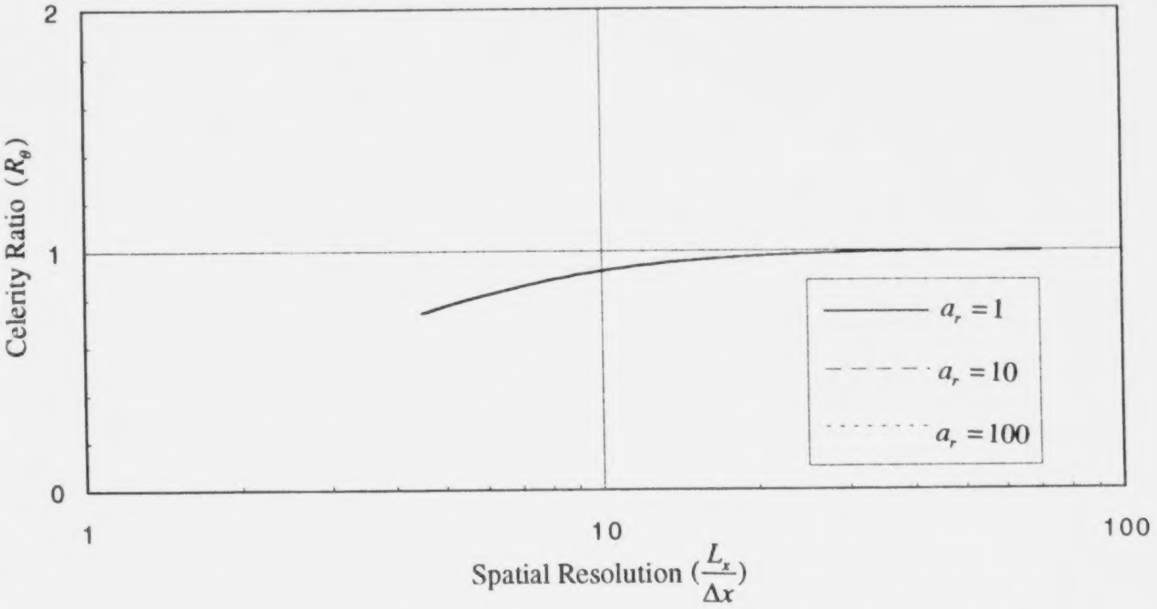

Figure 4.13b Phase Portraits for C_{rx}=1.0, and r_x=0.5.

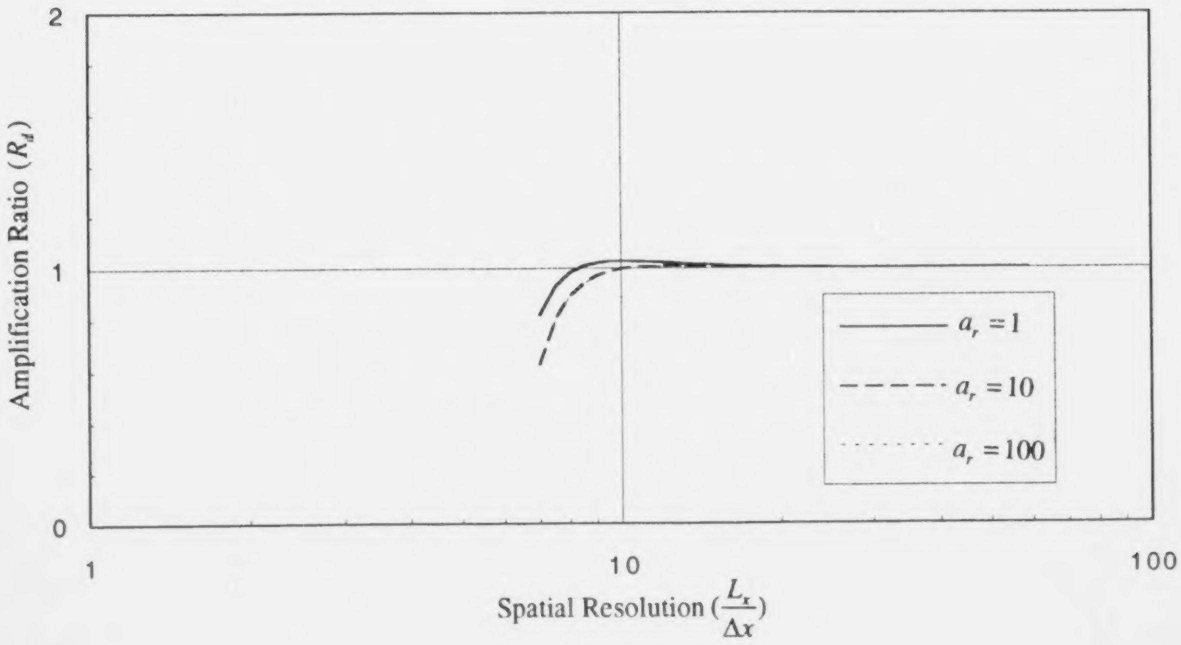

Figure 4.14a Amplitude for Portraits for C_{rx}=1.0, and r_x=1.0.

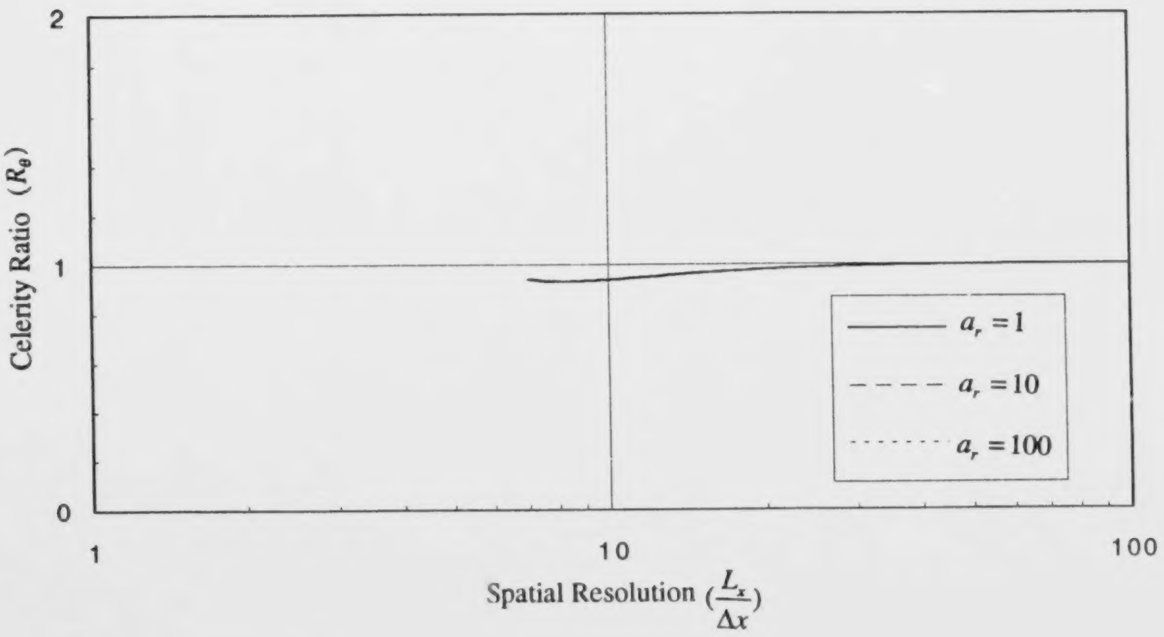

Figure 4.14b Phase Portraits for C_{rx}=1.0, and r_x=1.0.

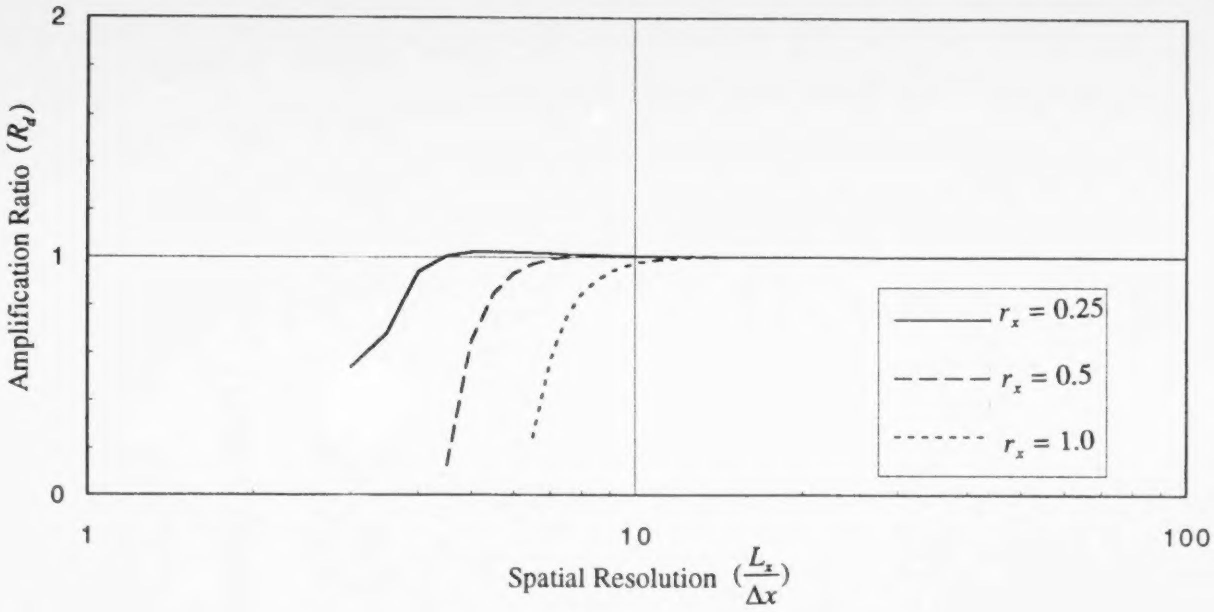

Figure 4.15a Amplitude for Portraits for C_{rx}=.5 and a_r=100.

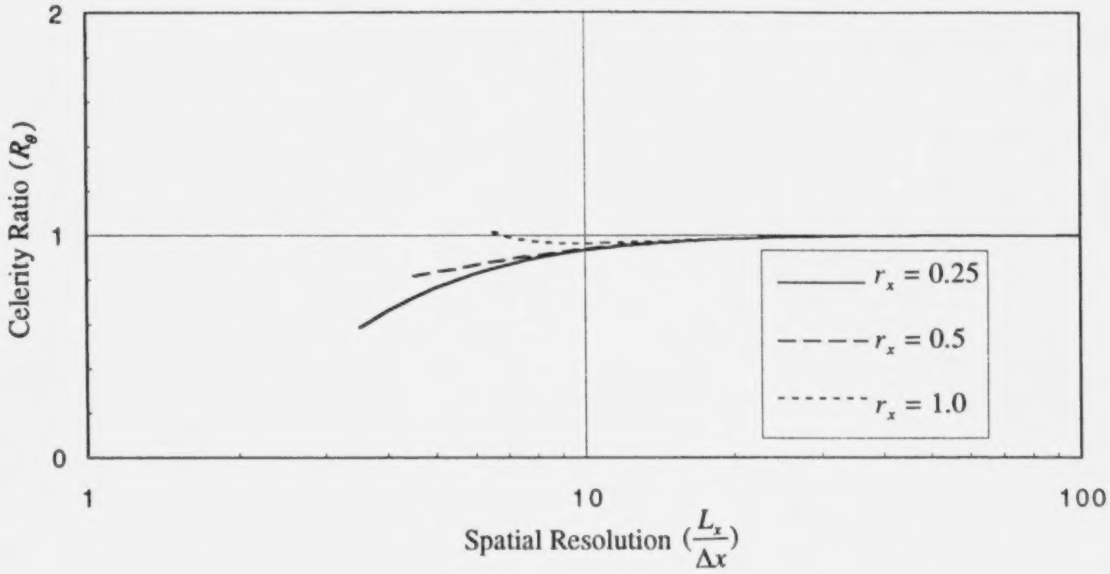

Figure 4.15b Phase Portraits for C_{rx}=1.0 and a_r=100.

5 VALIDATION OF THE NUMERICAL MODEL

5.1 INTRODUCTION

Validation of any numerical model is a vital part of the development of the numerical code. As little experimental data on unsteady flow in compound channels is available in the literature, the relative performance of the zero-inertia model is validated and critically examined by performing numerical experiments. Two experimental data sets are available in the literature, Treske (1980), and Rashid and Chaudhry (1993). In both experiments, longitudinal total discharges and stages were measured. The present model is, however, tested only against Treske's data. The model is also applied to simulate hypothetical floods and the data are compared with those obtained by a full dynamic numerical model, FESWMS-2DH (Finite Element Surface Water Modeling System) developed and applied by U.S. Federal Highway Administration (1989) as described in the sequel.

5.2 NUMERICAL SIMULATION OF FLOODS

In this section, four cases of hypothetical floods and one experimental flood are simulated by the zero-inertia model. Hypothetical floods belonging to Cases 4 and 5 are also simulated by FESWMS-2DH for the purpose of comparison. As the zero-inertia model is only applicable for flows with low Froude number, experiments are carried out for sub-critical flow only. The analysis of the simulated results for various cases are described below.

Case1 One -dimensional problem

This case demonstrates the ability of the zero-inertia model to handle the dry bed situation for a one-dimensional unsteady flow. This problem considers a rectangular canal 1 km long and 5 m wide with a gate structure at the upstream end and a weir with a free overfall at the downstream end. The slope of the bed is 0.003 and the roughness height is 0.2 m. The weir crest is 0.3 m above the canal invert. Meselhe et al. (1993) used a similar hypothetical problem to validate their one-dimensional model for simulating flow in a dry canal. The computational domain is discretized into 50 control volumes with each control volume of size 100 m by 1 m. The key parameters are approximately as follows: ${}^{L_x}\!/_{\Delta x} = 90$, $\beta = 135$, and $F_o = 0.5$. A variable time step is computed by satisfying the criteria, $r_x = 0.5$ which gives approximately C_{rx} =0.6. During the simulation of the dry period, a constant time step increment of 10 seconds is used. The total discharge hydrograph as shown in Figure 5.1 is given as the inflow boundary condition and the downstream boundary condition is given as critical flow over the weir. Figure 5.2 shows the simulated variation of water surface elevation with time at the upstream boundary of the computational reach. It is noticed that a dry period is involved in this simulation. The simulated longitudinal water surface profiles at the various stages of the unsteady flow are shown in Figure 5.3. It can be inferred from these figures that the zero-inertia model handles a dry bed situation without any computational difficulty.

Case 2 Simulation of the Experimental Data

This case is studied to test the performance of the zero-inertia model in simulating unsteady flow against available experimental data. Treske's experimental data (1980), reported by the CSCE task committee on river models (1993) obtained for a straight compound channel are used in this case study. The cross-section and the longitudinal profile of the experimental set up are shown in Figure 5.4. The length of the experimental reach was 210 m. The depth and the width of the main channel were 0.39 m and 1.25 m respectively. The width of the left flood plain was 3.0 m and that of the right flood plain was 1.5 m. The bed slope of the main channel and the two flood plains was 0.019% and the Manning roughness coefficient for the compound channel was 0.012. Both the discharge and stage hydrographs were measured at the upstream and the downstream ends of the experimental reach. Figures 5.5 and 5.6 show the measured discharge hydrograph at the upstream end and the stage hydrograph at the downstream end, respectively. In order to simulate the experimental result numerically, the measured discharge hydrograph at the upstream end is taken as the inflow boundary condition and the measured stage hydrograph at the downstream end is taken as the downstream boundary condition. Moreover, the rectangular cross-section of the experimental setup is approximated as a trapezoidal section for numerical simulation. The simulated stage hydrograph at the upstream end and the discharge hydrograph at the downstream end are compared with the corresponding experimental data. The experimental domain is discretized into 483 control volumes with each of size 10 m by 0.25 m. The key parameters are approximately as follows: ${}^{L_x}\!/\!{}_{\Delta x} = 625$, $\beta = 75$, and $F_o = 0.28$. A constant time step of 1 second which gives approximately $r_x = 2.0$ and $C_{rx} = 0.03$ is used for the numerical simulation. From the given initial condition, the equivalent roughness height is estimated as 0.001 m. The non-dimensional eddy viscosity coefficients of 0.15 and 0.23 are used but no significant difference is observed. Figure 5.7 compares the measured and the simulated downstream discharge hydrographs along with the percentage of relative error. It is clearly noticeable that the zero-inertia model produces the comparable results with reasonable accuracy. Figure 5.8 compares the measured and the simulated upstream depth hydrographs along with the percentage of relative error. It is noticed that the computational model produces almost identical results for the in-bank flow but slightly underestimates the out of bank flow. This discrepancy can be attributed to the fact that the accurate estimation of the roughness height is not possible. Nonetheless, it is worth mentioning that the zero-inertia model produces comparable results with similar trends as observed in the experiment.

Case 3 Hypothetical flood routing in a river with and without flood plain

This case study is carried out to route a hypothetical flood wave through a river with and without flood plains. This will demonstrate the effects of the flood plains on the various hydraulic features of a flood wave. The length of a hypothetical compound channel reach is taken as 100 km and the width of the main channel is 100 m. The half of the cross-section of the symmetric and prismatic compound channel is shown in Figure 5.9. For modeling the case of a river without flood plains, imaginary walls are introduced at the main channel boundaries and the same flood wave is routed. The flood plain level is 5 m above the bed of the main channel. The slope of the compound channel is 0.0005. The initial depth of flow in the main channel is 1m and the flood plain is dry. The roughness height is 0.52 m for both the channel and the flood plain. The computational domain is divided into 500 control volumes with a size of 2000 m by 20 m each for the case of river with flood plain and 250 control volumes for the case of river without flood plain. The following inflow discharge hydrograph is introduced as the upstream boundary condition:

$$Q_{inflow} = 55.0 + 1500(1 - \cos\frac{2\pi t}{T}) \qquad (m^3 / \sec) \qquad [5.1]$$

where T = duration of flood = 48 hours, and t = time.

A uniform flow rating curve is provided as the downstream boundary condition. The flow perpendicular to the each of the side boundaries is zero and a perfect slip condition along each of the side boundaries is assumed to prevail. The key parameters are approximately as follows: $L_x/\Delta x = 240$, $\beta = 700$, $W/L_x = 0.0002$, and $F_o = 0.26$. A variable time step increment is calculated by satisfying the criteria, $r_x = 1.0$ which gives approximately $C_{rx} = 0.6$ for the numerical simulation.

Figure 5.10 shows several discharge hydrographs simulated at 50 km downstream from the upstream boundary along with the inflow discharge hydrograph. For the case of a river with a flood plain, as the flood wave moves with different speeds as it goes to the over bank area, two kinks are easily noticeable at the time of flow entering and exiting the flood plain. In comparison to the case of a river without a flood plain, it is seen that main channel discharge decreases significantly. Figure 5.11 shows the depth hydrographs at 50 km downstream from the upstream end and 50 m off the center line for river with and without flood plains. The effect of the flood plain in reducing the stage of a flood wave at a location is clearly noticed. The depth-discharge relationship at the same computational node is also shown in Figure 5.12. It is seen that the loop rating curve is different for the two cases which is expected.

Cases 4 and 5 Comparison with FESWMS-2DH

These two cases are carried out to compare the relative performance of the zero-inertia model with a full dynamic finite element model. Numerical experiments are performed with the zero-inertia model. The computed results are compared with the results obtained by a well-recognized hydraulic model, FESWMS-2DH (Finite Element Surface Water Modeling System) developed and applied by U.S. Federal Highway Administration (1989). This model utilizes the depth-averaged continuity and full dynamic momentum equations to simulate surface-water flows. The comparative performance of these two models is examined for two hypothetical flood events.

Different bed slopes, roughness, length of the reach, and flood duration are considered in these two cases. Since the FESWMS model cannot handle a dry bed situation easily, only numerical tests considering an initially wet bed are investigated. This means that the flood plain is initially flooded.

Depth and discharge comparisons are carried out for these cases. Figure 5.13 shows the cross-sectional geometry of the half of the symmetric and prismatic compound channel along with the initial flow condition used for the numerical experiments. The flow in the compound channel is assumed initially uniform with a main channel depth of 6m and flood plain depth of 1 m for both cases. The total inflow discharge hydrograph is used as an upstream boundary condition. The constant main channel depth of 6 m and flood plain depth of 1 m is used as the downstream boundary condition. The flow perpendicular to the each of the side boundaries is zero and a perfect slip condition along each of the side boundaries is assumed.

Case4

This case describes the simulation of an unsteady flow phenomena by the two models. The following physical parameters are used: Length of the Compound Channel, $\Lambda = 30$ km, Slope, $S_{ox} = 0.0005$, Manning roughness coefficient, $n = 0.035$. The inflow hydrograph is given by the following equation:

$$Q_{\text{inflow}} = 4375 + 2500(1 - \cos\frac{2\pi t}{T}) \qquad (m^3 / \text{sec}) \qquad [5.2]$$

where T = duration of flood = 14 hours.

The following discretization sizes are used: $\Delta x = 2\text{km}$, $\Delta t = 180$ seconds, and Δy = variable

To apply the finite element model, the computational domain is discretized into 135 elements with 8 - node quadrilaterals resulting in total 454 nodes. For the application of the zero-inertia model, the domain is discretized into 135 control volumes. The key parameters are approximately as follows: ${L_s}/{\Delta x} = 70$, $\beta = 200$, ${W}/{L_s} = 0.002$, and $F_o = 0.28$. A constant time step increment of 180 seconds gives approximately $r_x = 0.4$ and $C_{rx} = 0.25$ for the numerical simulation.

The simulated hydrographs of longitudinal discharge per unit width at a computational node located at 16 km downstream from the inflow section and 150 m off-center (as shown in Figure 5.14, point a) are compared at Figure 5.15. The hydrographs of longitudinal discharge per unit width for a computational node in the flood plain located at 16 km downstream from the inflow section and 500 m off-center (as shown in Figure 5.14, point c) are compared in Figure 5.16. The variations of the depths with time for the nodes a and c of Figure 5.14 are compared in Figures 5.17 and 5.18 respectively. In all these figures, the percentage of relative differences with respect to FESWMS are also provided. Also, the hydrographs of the lateral discharge per unit length at 350 m and 550 m off the center line and 15 km from the inflow section (points b and d in Figure 5.14) are compared in Figures 5.19 and 5.20 respectively. It is clearly evident that the two models produce almost identical depths. However, a little difference in discharge hydrographs can be observed. In the case of lateral discharge hydrographs, significant differences can be noticed. This can also be attributed to the fact that the discharge is very sensitive to the difference in water levels and a little difference produces a large difference in discharge. Besides this, as the FESWMS uses the full dynamic equations, the inertial terms may have some contributions to these discrepancies.

Case 5

This case simulates the hypothetical flood event with the following parameters: The following physical parameters are used: Length of the Channel, $\Lambda = 120$ km, Slope, $S_{ox} = 0.00005$, Manning roughness coefficient, $n = 0.03$. The inflow hydrograph is given by the following equation:

$$Q_{inflow} = 1600 + 1000(1 - \cos\frac{2\pi t}{T}) \qquad (m^3 / \sec) \qquad [5.3]$$

where T = Duration of flood = 24 hours.

The following discretization sizes are used: $\Delta x = 4\text{km}$, $\Delta t = 270$ seconds, and $\Delta y =$ variable.

Figure 5.21 shows the half of the cross-section of the symmetric and prismatic compound channel along with the initial flow condition. For this case, the computational domain has been discretized into 270 elements with 8 - node quadrilaterals resulting in total 889 nodes for the finite element model. For the application of the zero-inertia model, the domain has been discretized into 270 control volumes. The key parameters are approximately as follows: $L_x/\Delta x = 23$, $\beta = 90$, $W/L_x = 0.0045$, and $F_o = 0.1$. A constant time step of 270 seconds gives approximately $r_x = 0.6$ and $C_{rx} = 0.07$ for the numerical simulation.

The simulated hydrographs of longitudinal discharge per unit width at a computational node located at 60 km downstream from the inflow section and 150 m off-center (as shown in Figure 5.22, point a) are compared at Figure 5.23. The hydrographs of longitudinal discharge per unit width for a computational node in the flood plain located at 60 km downstream from the inflow section and 500 m off-center (as shown point c in Figure 5.22) are compared in Figure 5.24. The variations of the depths with time for the nodes a and c as shown in Figure 5.22 are compared in Figures 5.25 and 5.26 respectively. In all these figures, the percentage of relative differences with respect to FESWMS are also provided. The comparisons of the lateral variation of water depth and longitudinal flow velocity at 60 km downstream from the inflow boundary at 24 hours are shown in Figures 5.27 and 5.28 respectively. Also, the hydrographs of the lateral discharge per unit length at 350 m and 550 m off the center line and 60 km from the inflow section (points b and d in Figure 5.22) are compared in Figures 5.29 and 5.30 respectively. These figures clearly show a very good agreement in results obtained by two models with little discrepancy in lateral discharges.

5.3 CONCLUSION

From the above case studies, it is revealed that the proposed two-dimensional zero-inertia wave model predicts discharge and stage for non-dynamic flood events with reasonable accuracy both for data from laboratory experiments as well as in a comparison to a fully dynamic wave model. The zero-inertia model is simple, straightforward and relatively easy to implement. While the more sophisticated numerical models such as FESWMS requires several hours (about 24 hours for the case 4) to run on IBM PC-486 DX with 50 MHz, comparable results are obtained by the present zero-inertia model in about 20 minutes. Within the applicable range of its use, the zero-inertia model may replace the complicated fully dynamic model for some flood predictions.

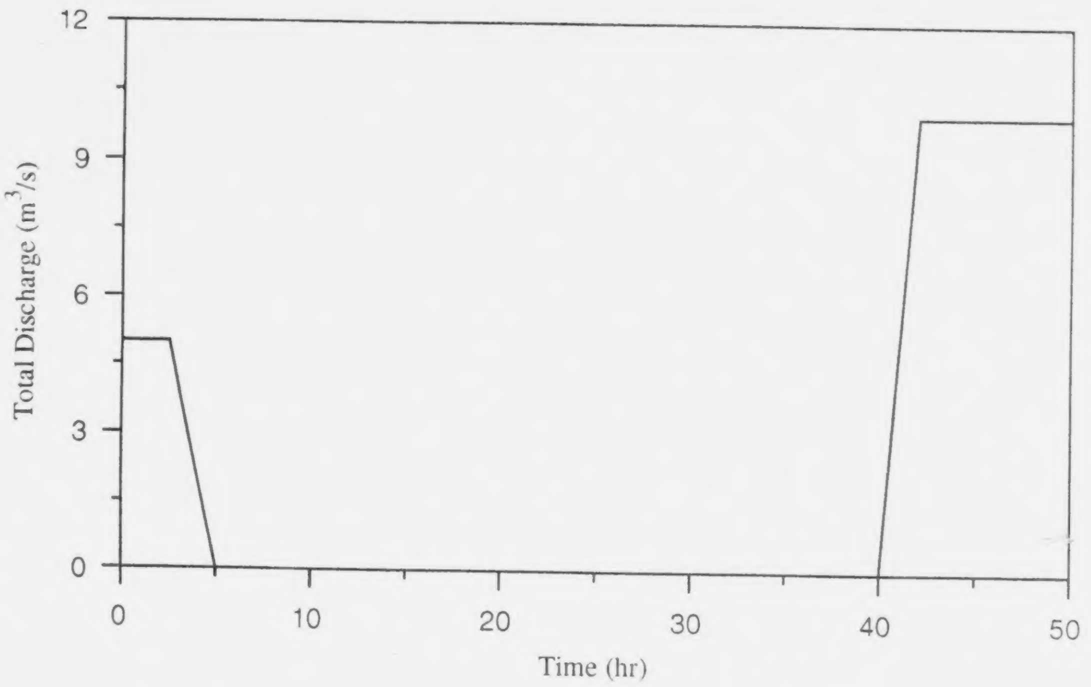

Figure 5.1 Inflow discharge hydrograph for Case 1.

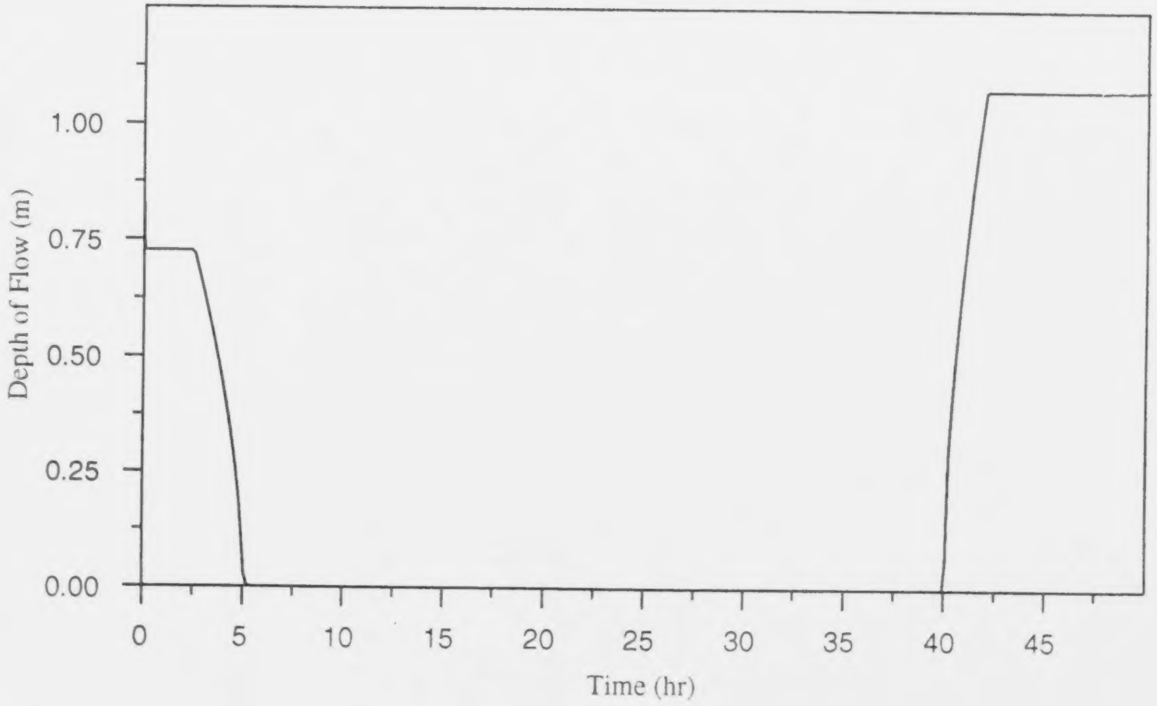

Figure 5.2 Simulated variation of the depth of flow with time at the inflow boundary for Case 1.

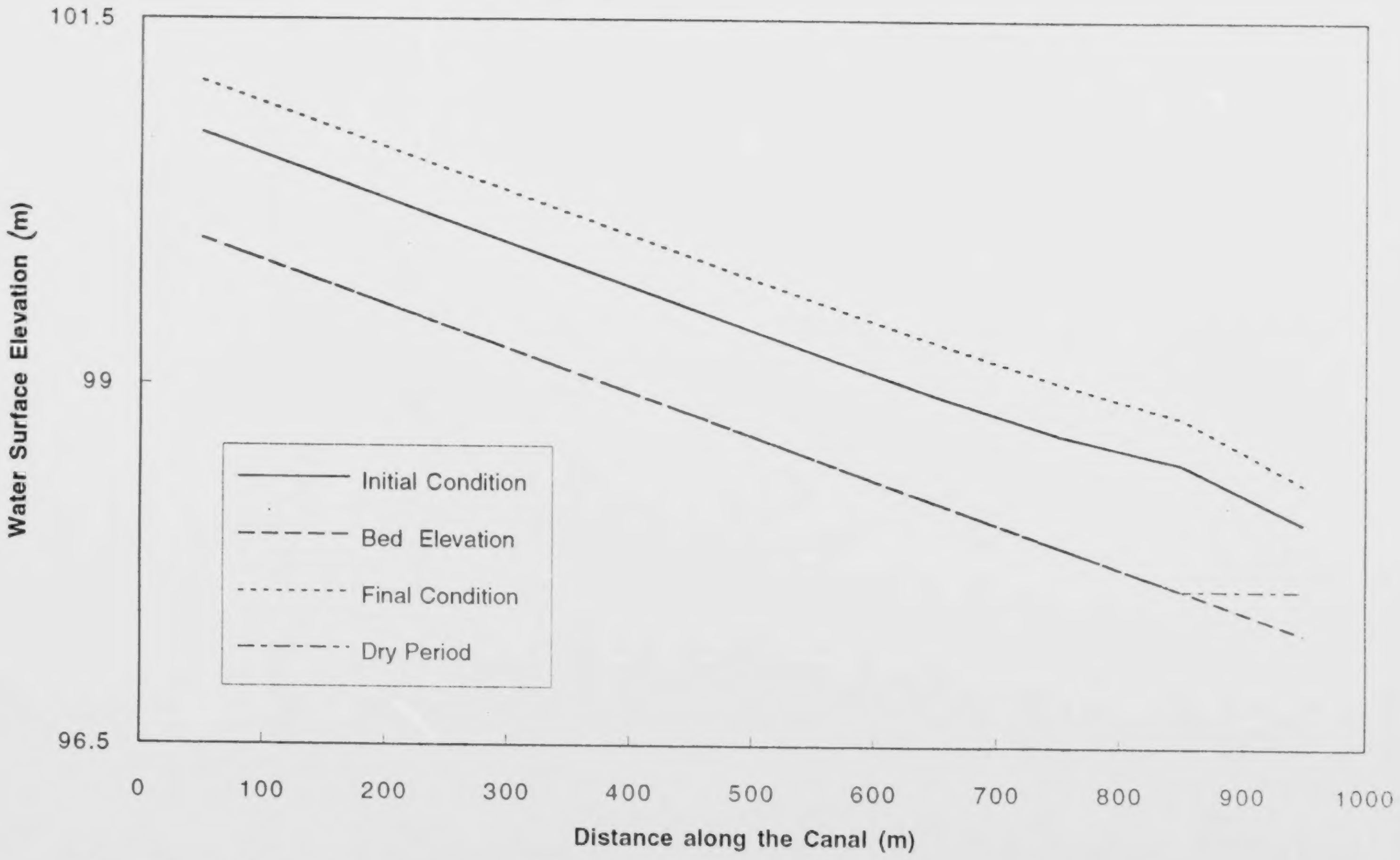

Figure 5.3 Simulated longitudinal water surface profiles at the various stages of the unsteady flow for Case 1.

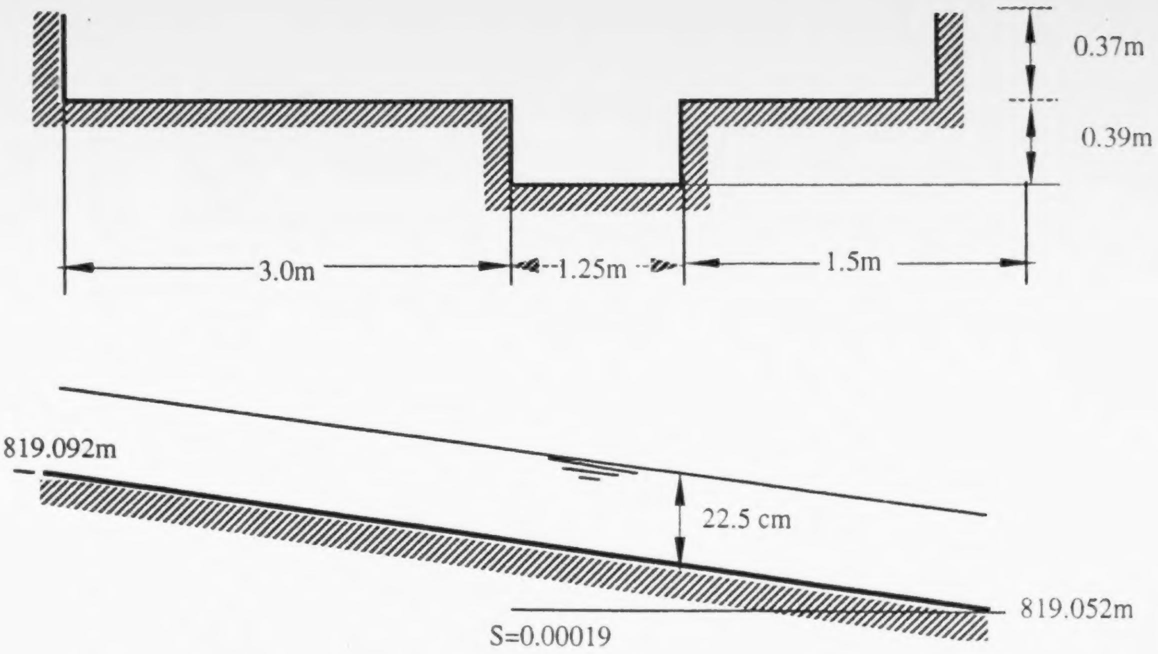
0.37m
0.39m
3.0m
1.25m
1.5m
819.092m
22.5 cm
819.052m
S=0.00019

Figure 5.4 Cross section and longitudinal profile of the Treske's prismatic compound channel (1980).

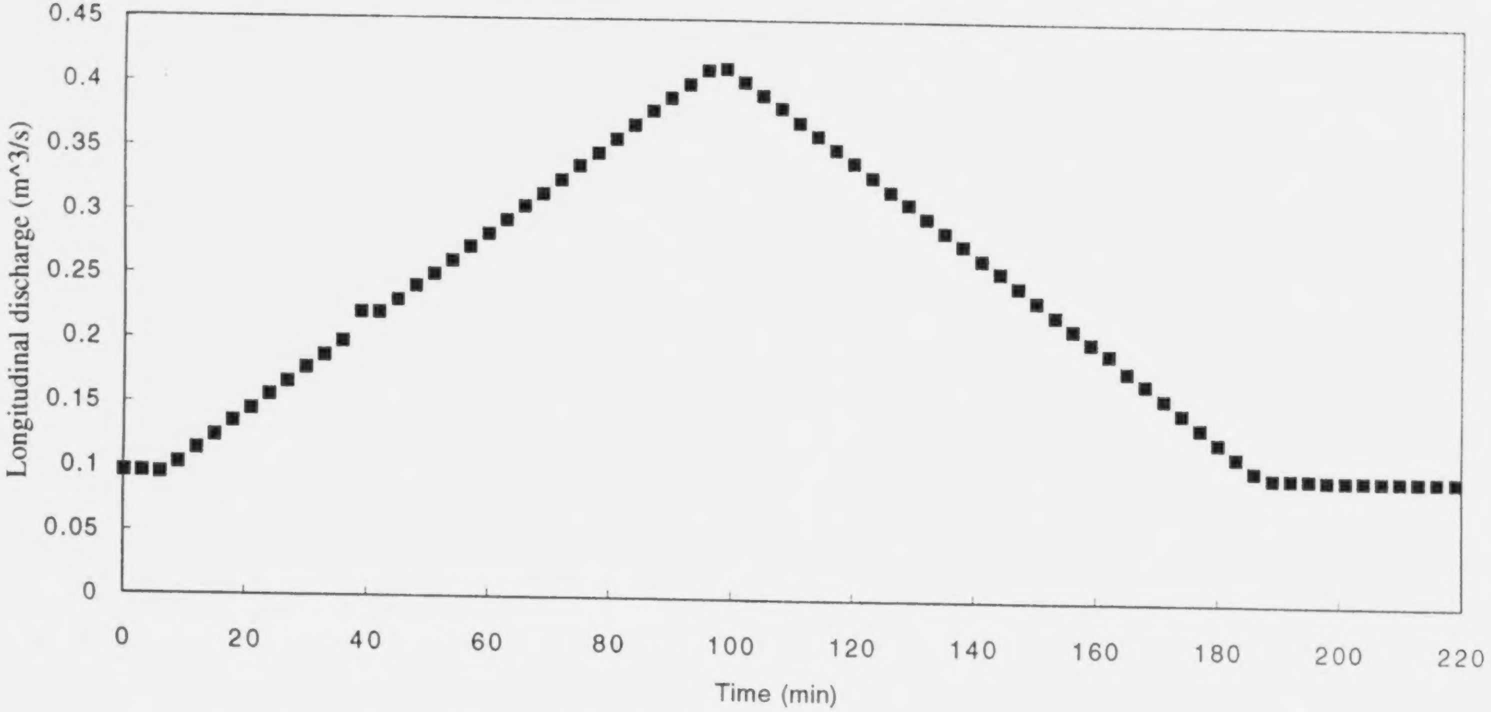

Figure 5.5 Measured discharge hydrograph at the inflow boundary of Treske's experiment (1980).

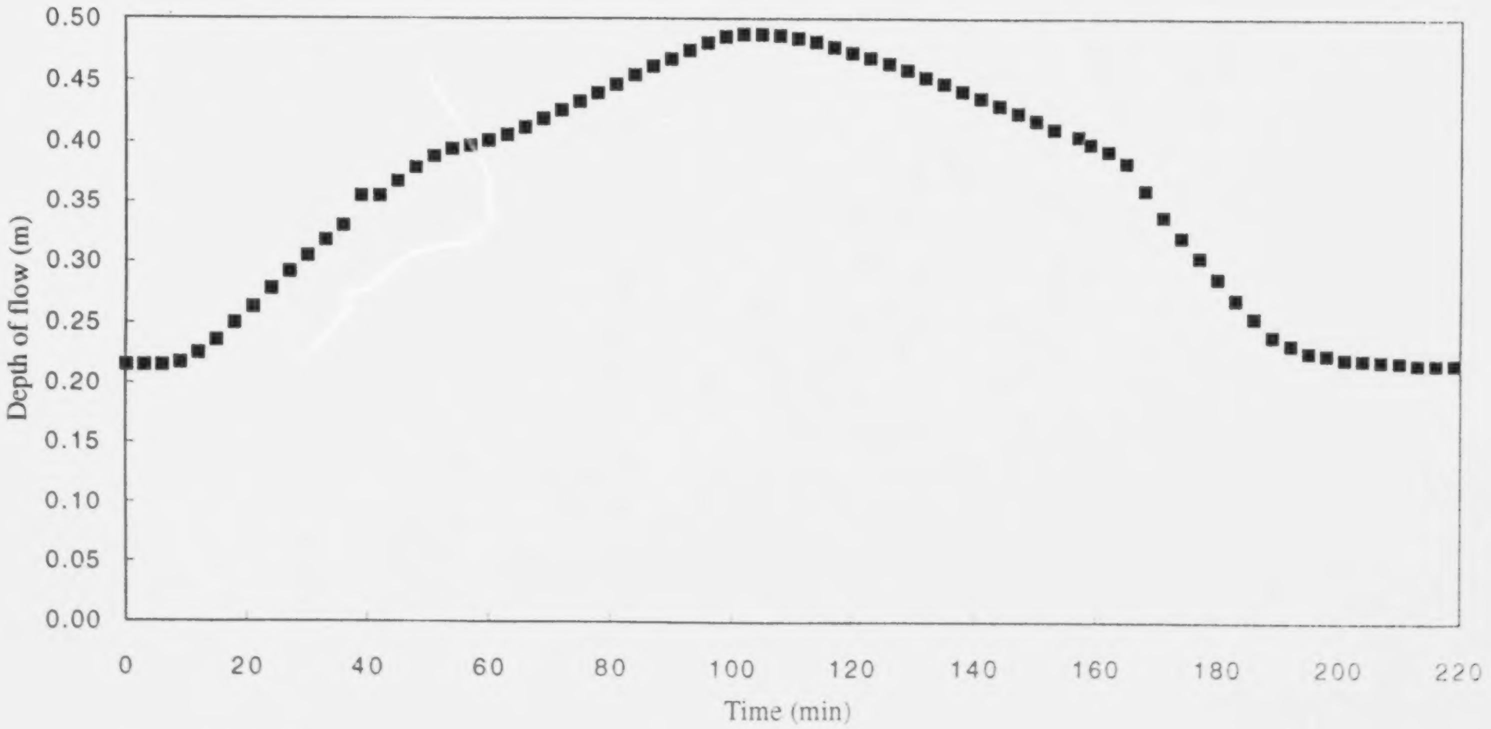

Figure 5.6 Measured depth hydrograph at the downstream end of the Treske's experiment (1980).

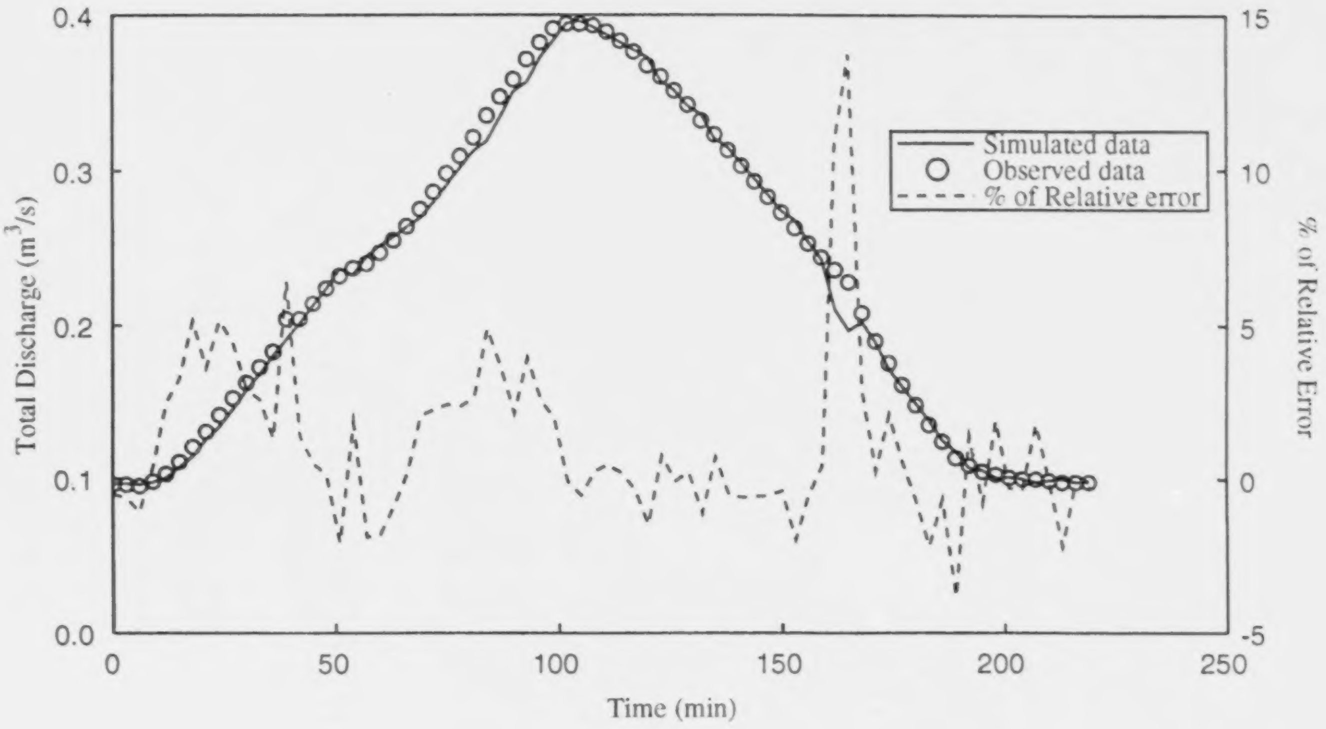

Figure 5.7 Comparison of the downstream discharge hydrograph simulated by zero-inertia model with Treske's data

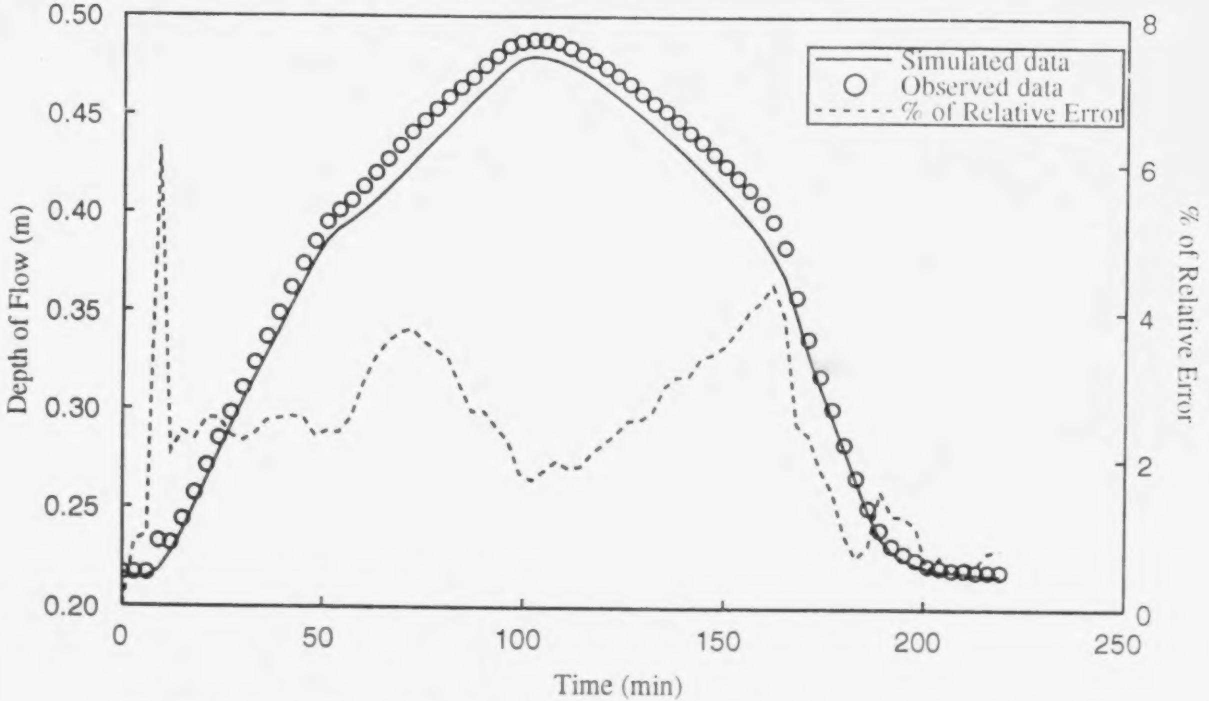

Figure 5.8 Comparison of the upstream depth hydrograph simulated by zero-inertia model with Treske's data.

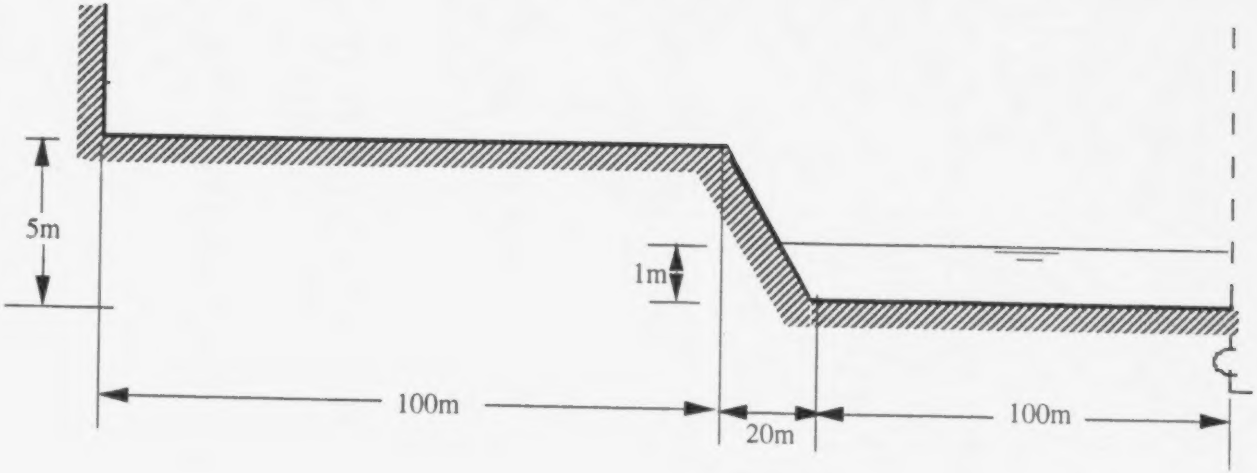
5m
1m
100m
20m
100m

Figure 5.9 Cross section of the prismatic compound channel for Case 3.

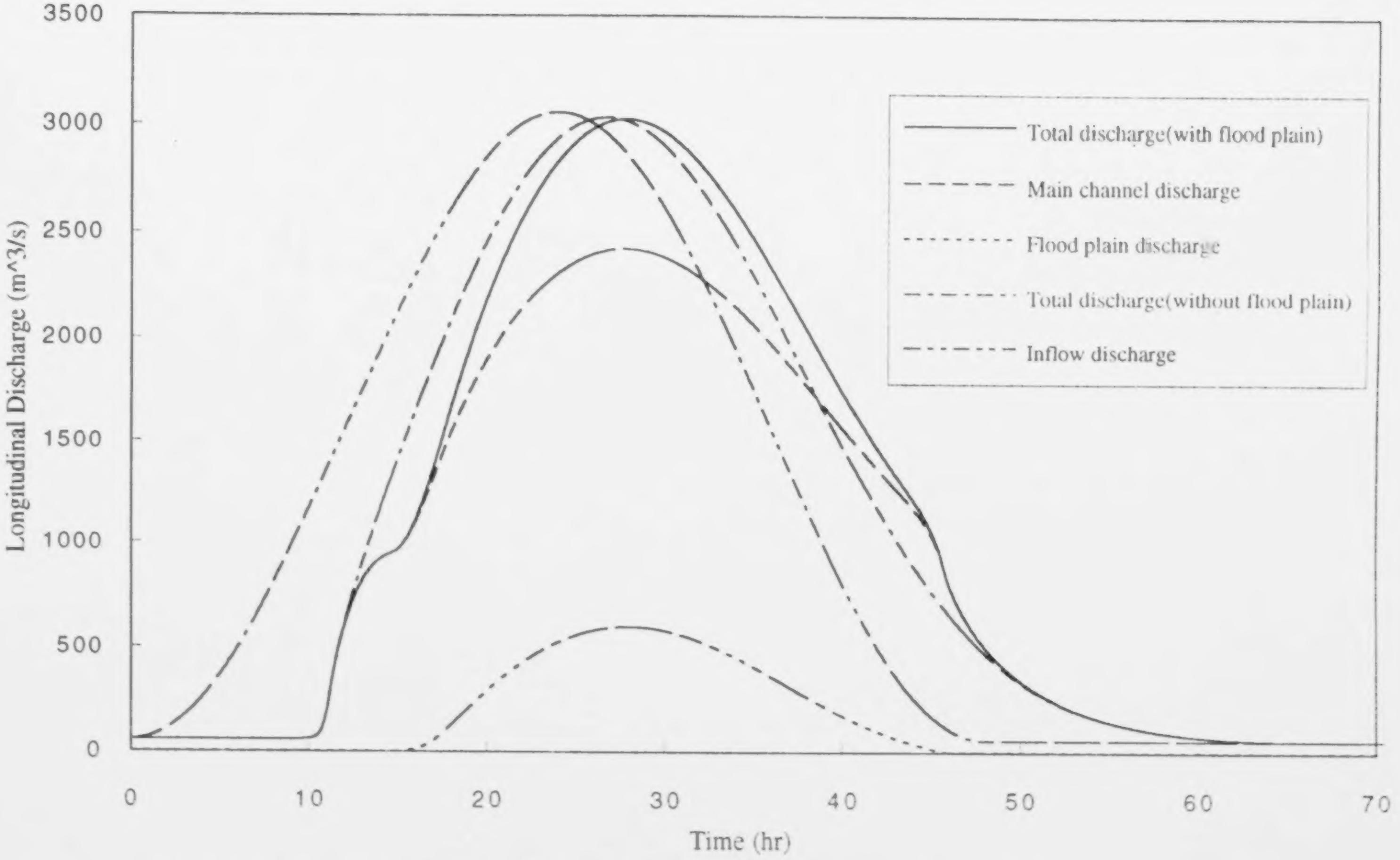

Figure 5.10 Various longitudinal discharge hydrographs at 50 km downstream from the inflow boundary along with inflow discharge hydrograph for Case 3.

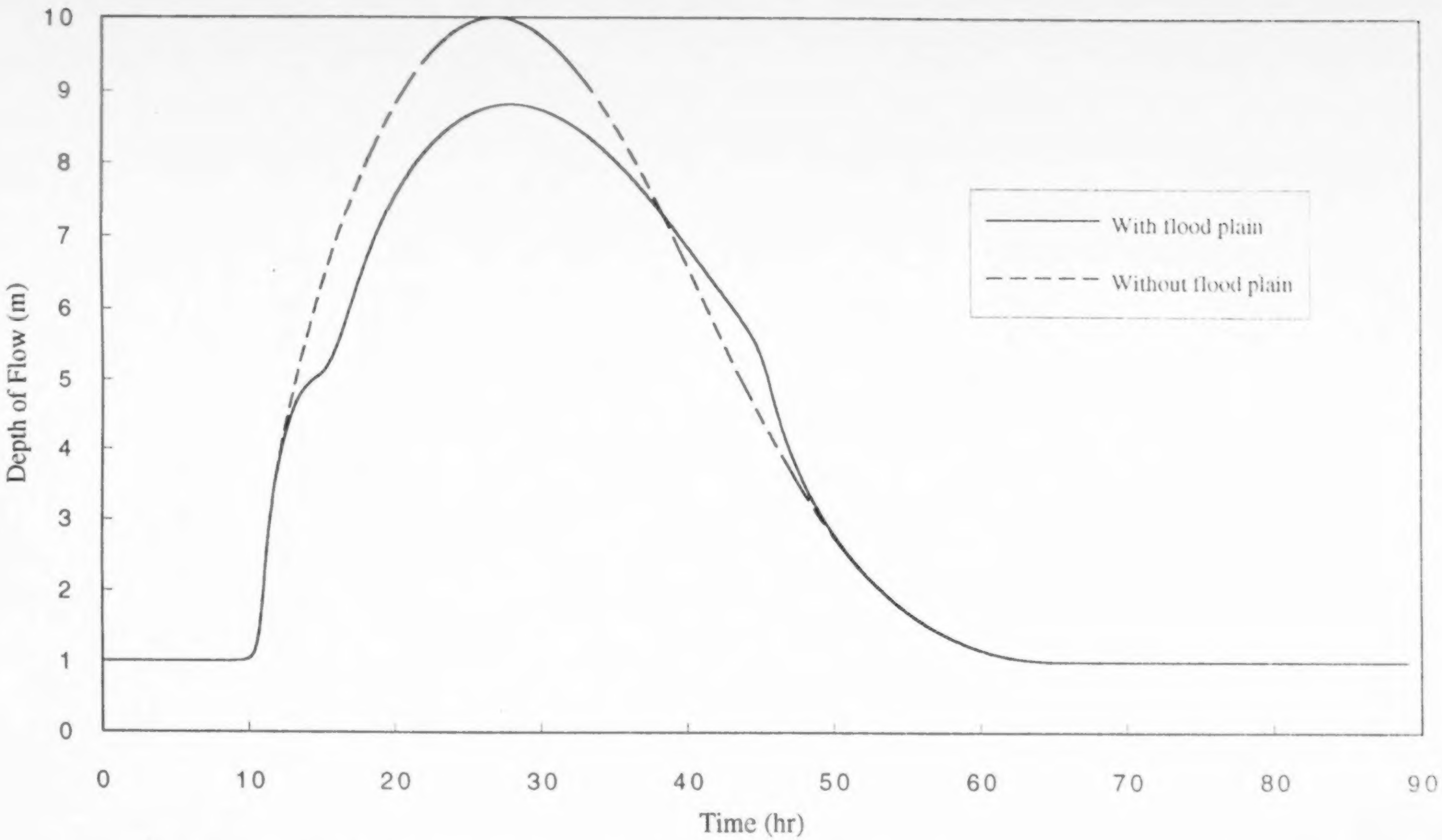

Figure 5.11 Simulated depth hydrographs at 50 km downstream from the inflow boundary for Case 3.

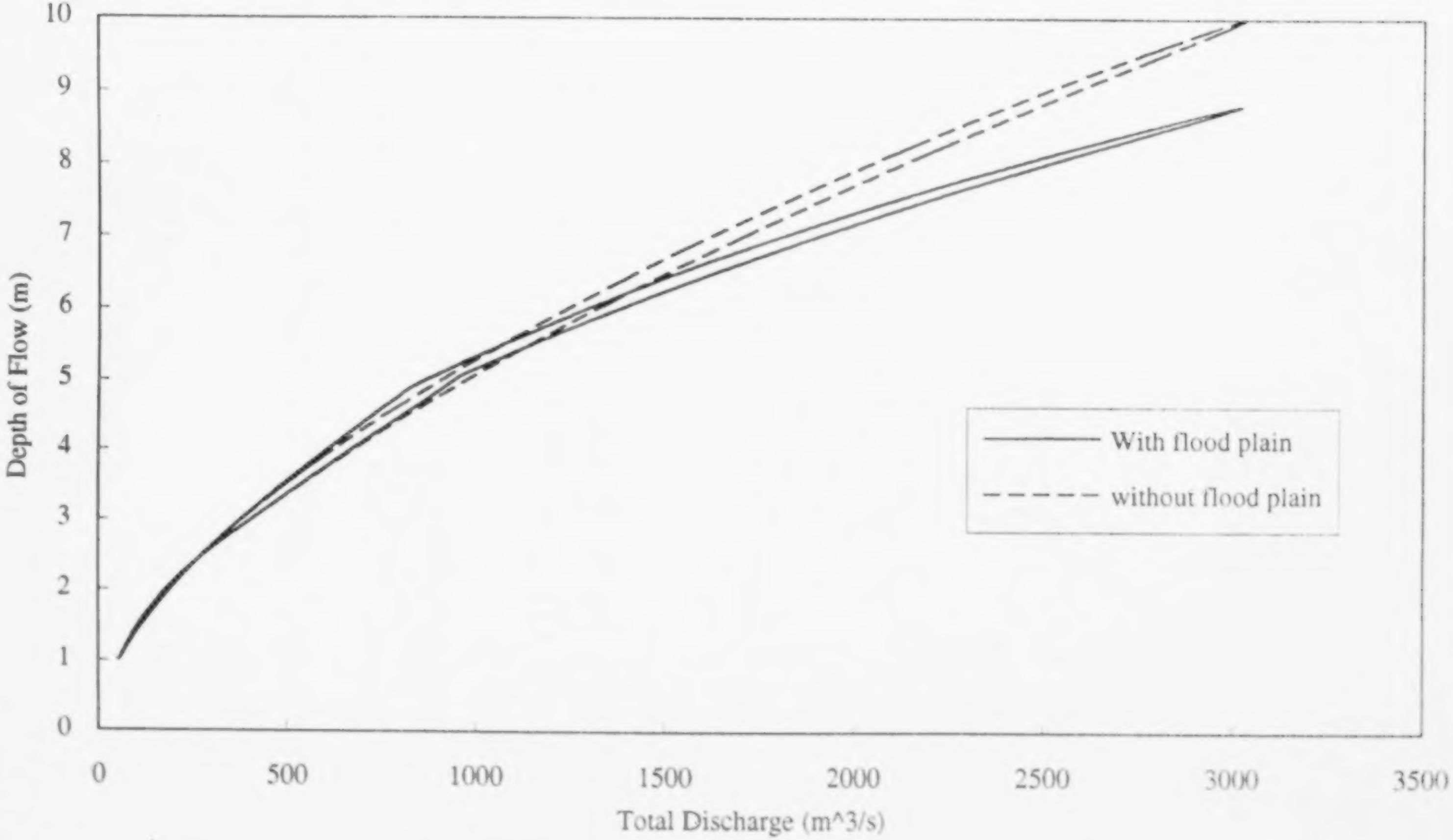

Figure 5.12 Stage-discharge relationship at 50 km downstream from the inflow boundary for Case 3.

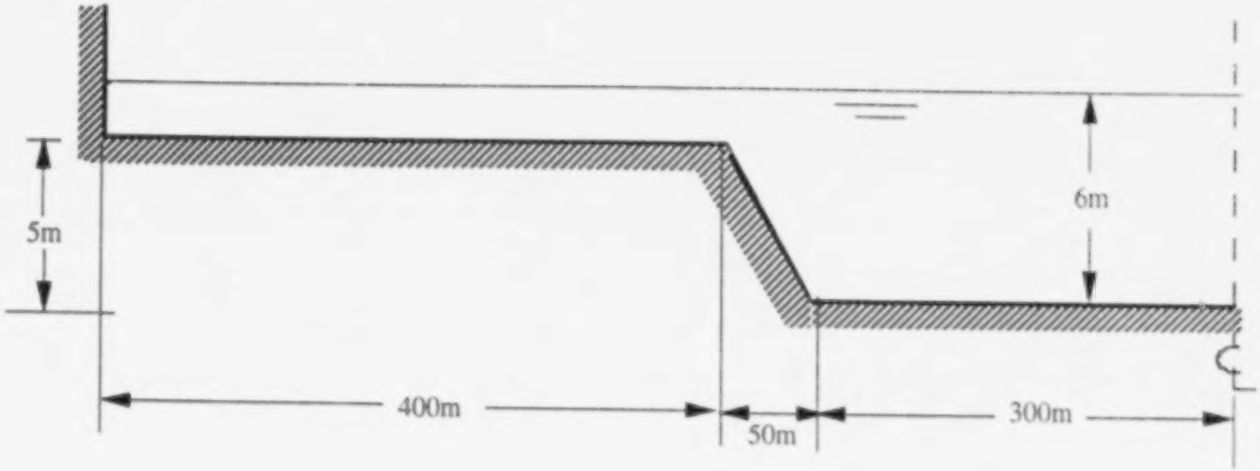
5m
6m
400m
50m
300m

Figure 5.13 Cross-section of the prismatic compound channel for Case 4.

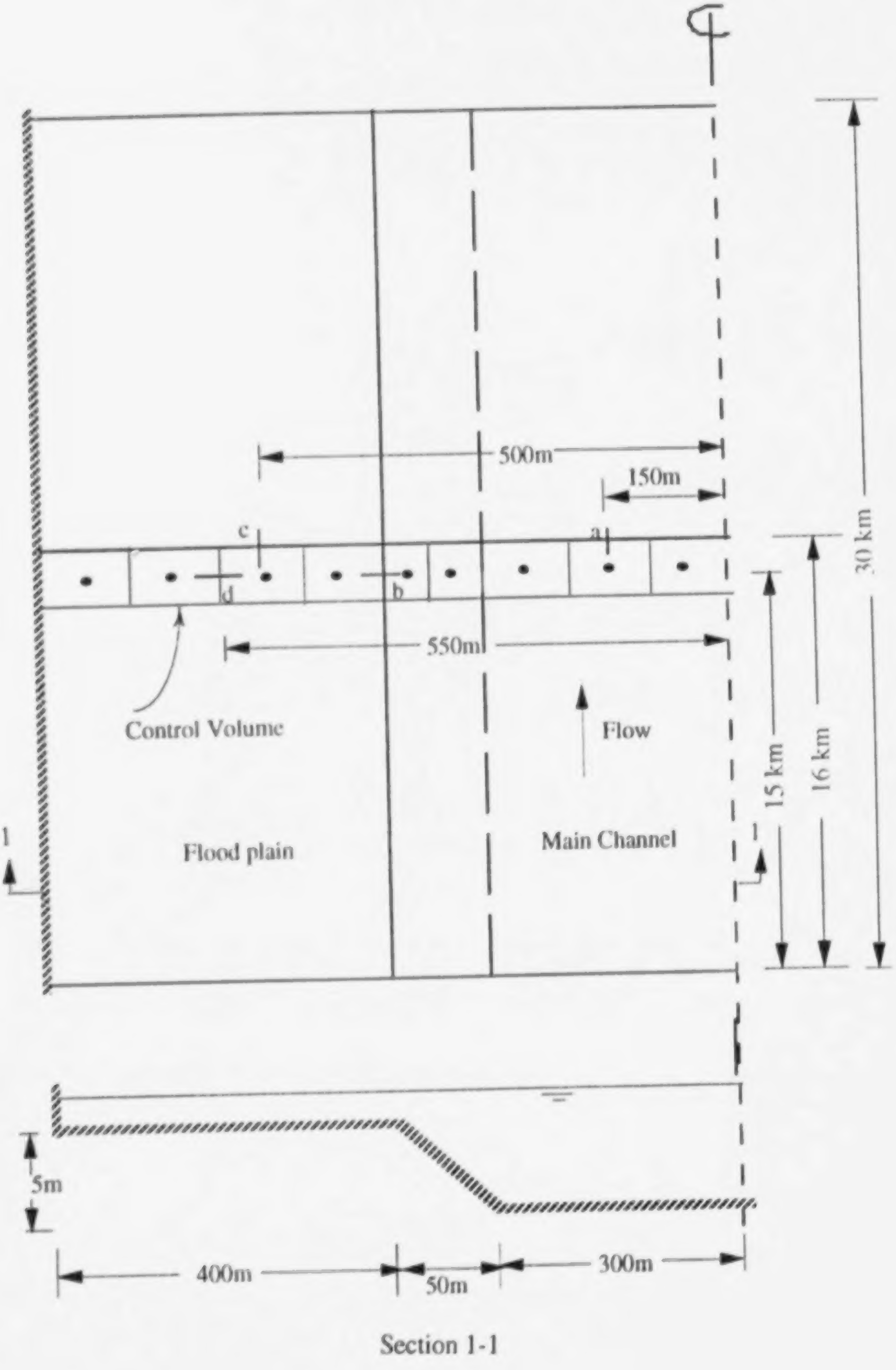
500m
150m
c
a
d
b
550m
30 km
16 km
15 km
Control Volume
Flow
Flood plain
Main Channel
1
5m
400m
50m
300m
Section 1-1

Figure 5.14 Plan view of the half of the symmetric and prismatic compound channel for Case 4.

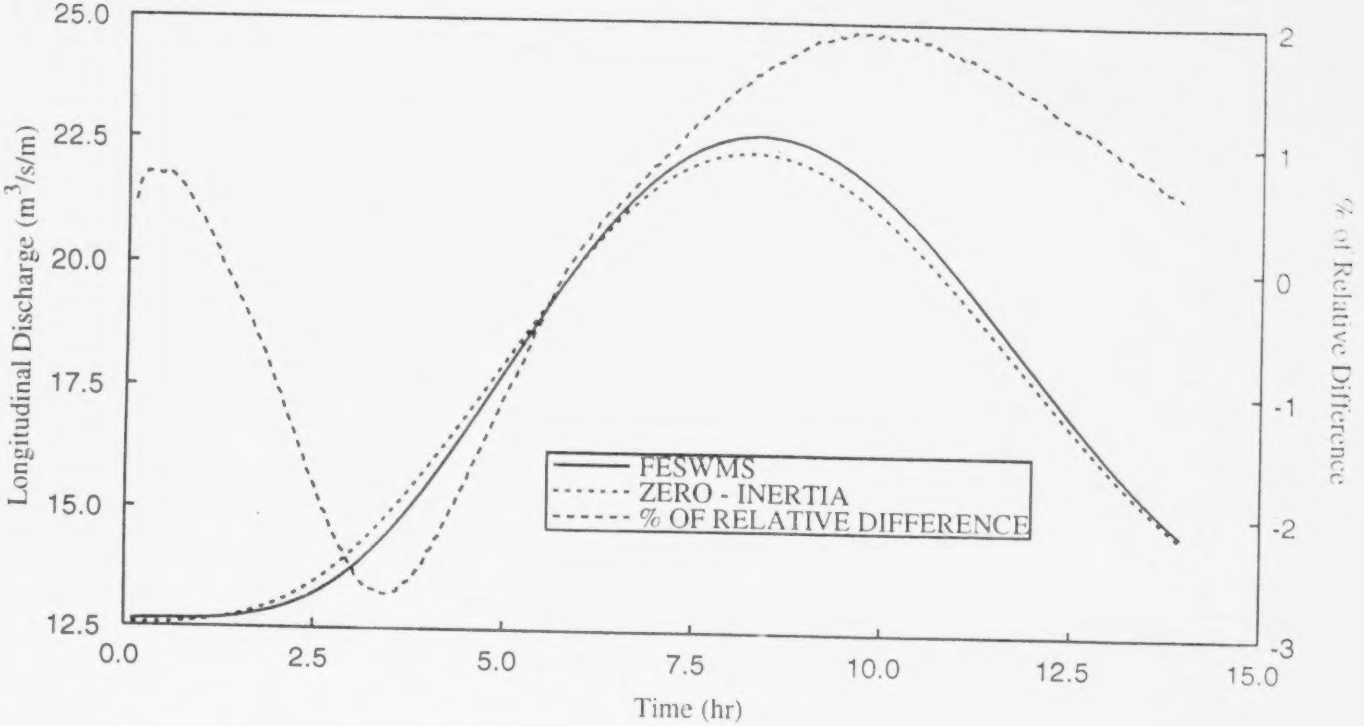

Figure 5.15 Comparison of the main channel longitudinal discharge hydrographs per unit width at 16 km downstream from the inflow boundary and 150 m off the center line for Case 4.

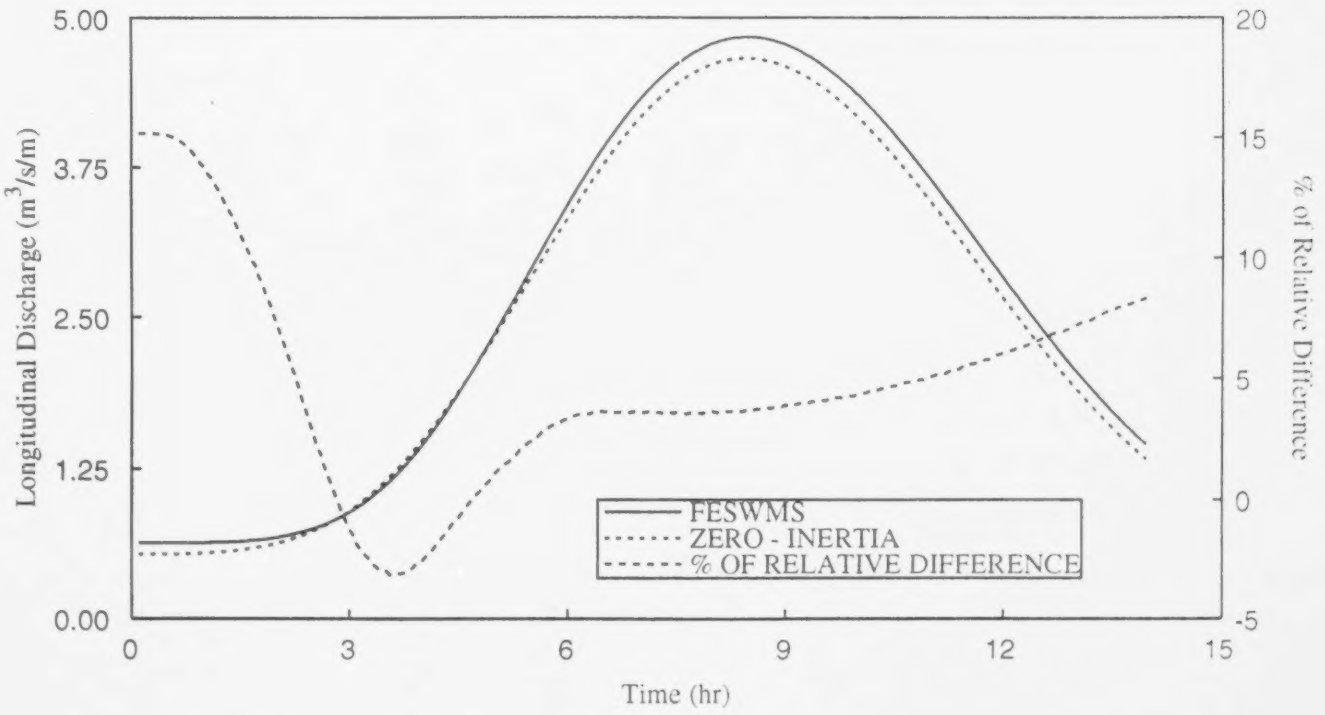

Figure 5.16 Comparison of the flood plain longitudinal discharge hydrographs per unit width at 16 km downstream from the inflow boundary and 500 m off the center line for Case 4.

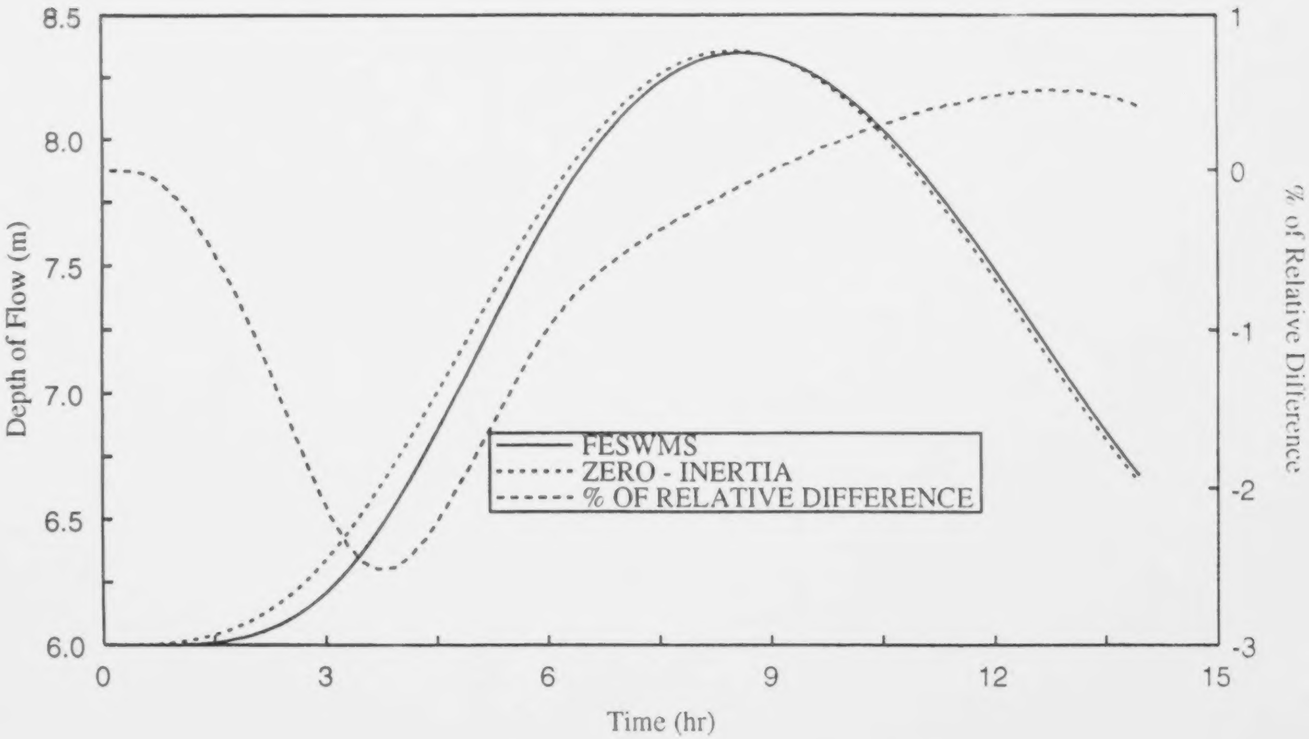

Figure 5.17 Comparison of the main channel depth hydrographs at 16 km downstream from the inflow boundary and 150 m off the center line for Case 4.

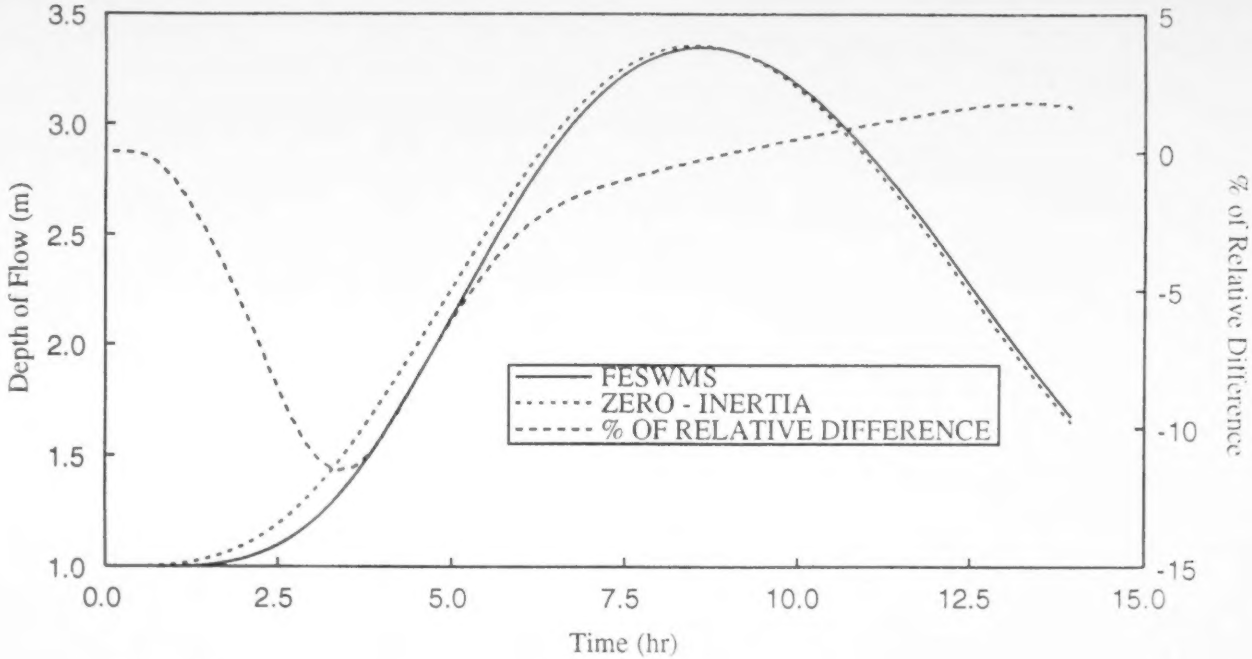

Figure 5.18 Comparison of the flood plain depth hydrographs at 16 km downstream from the inflow boundary and 500 m off the center line for Case 4.

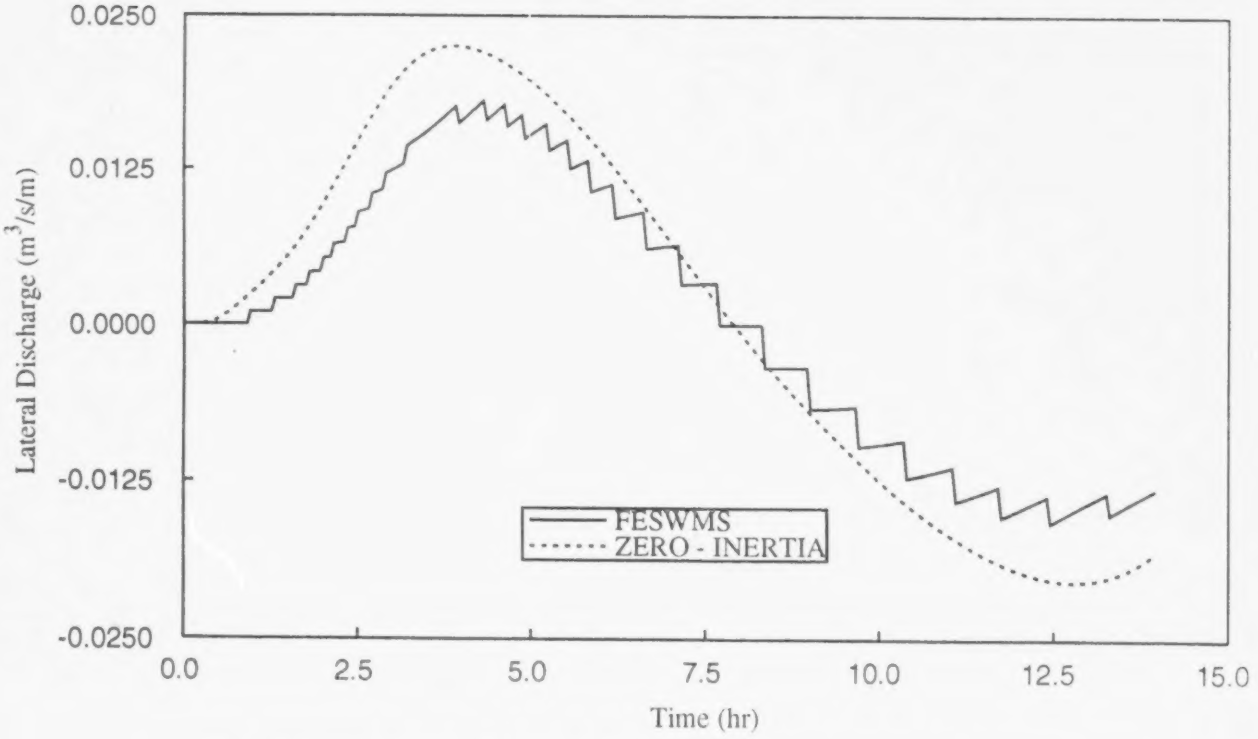

Figure 5.19 Comparison of the lateral discharge hydrographs per unit length at 15 km downstream from the inflow boundary and 350 m off the center line for Case 4.

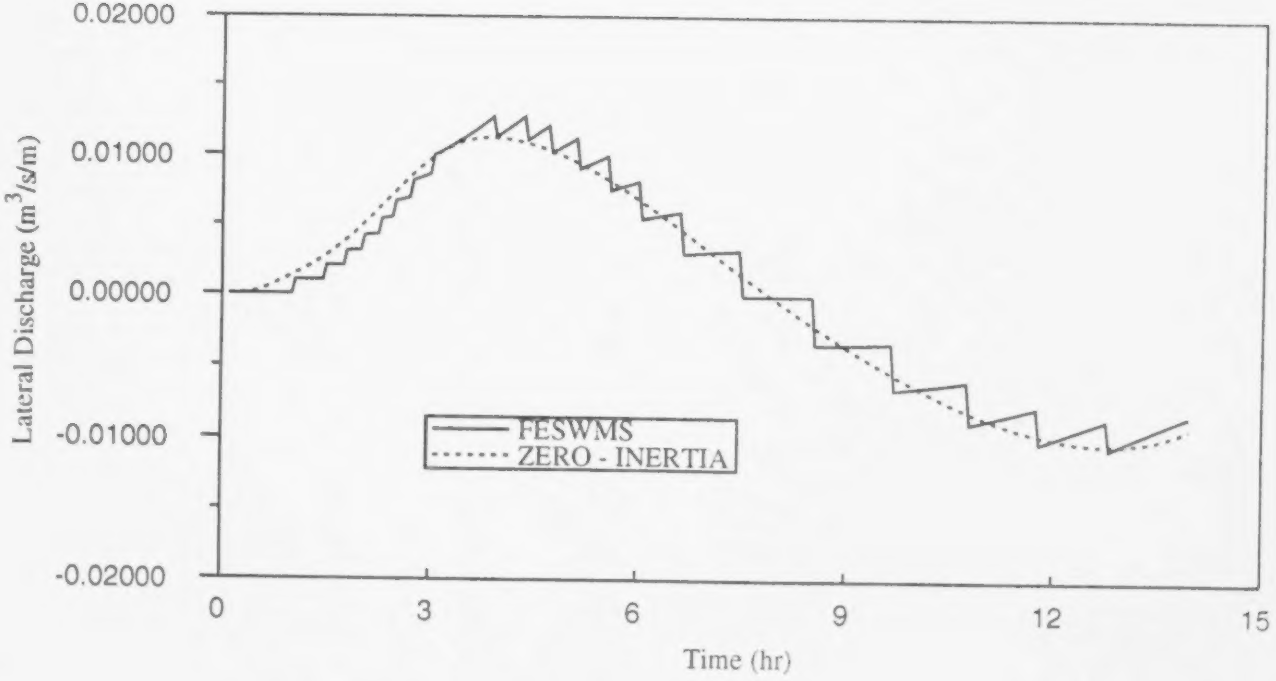

Figure 5.20 Comparison of the lateral discharge hydrographs at 15 km downstream from the inflow boundary and 550 m off the center line for Case 4.

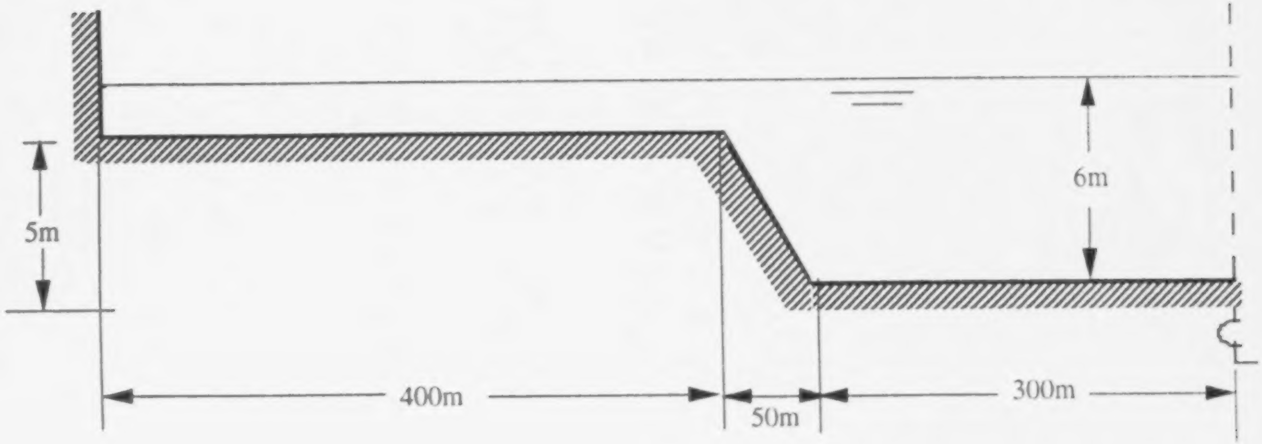
6m
5m
400m
50m
300m

Figure 5.21 Cross-section of the prismatic compound channel for Case 5.

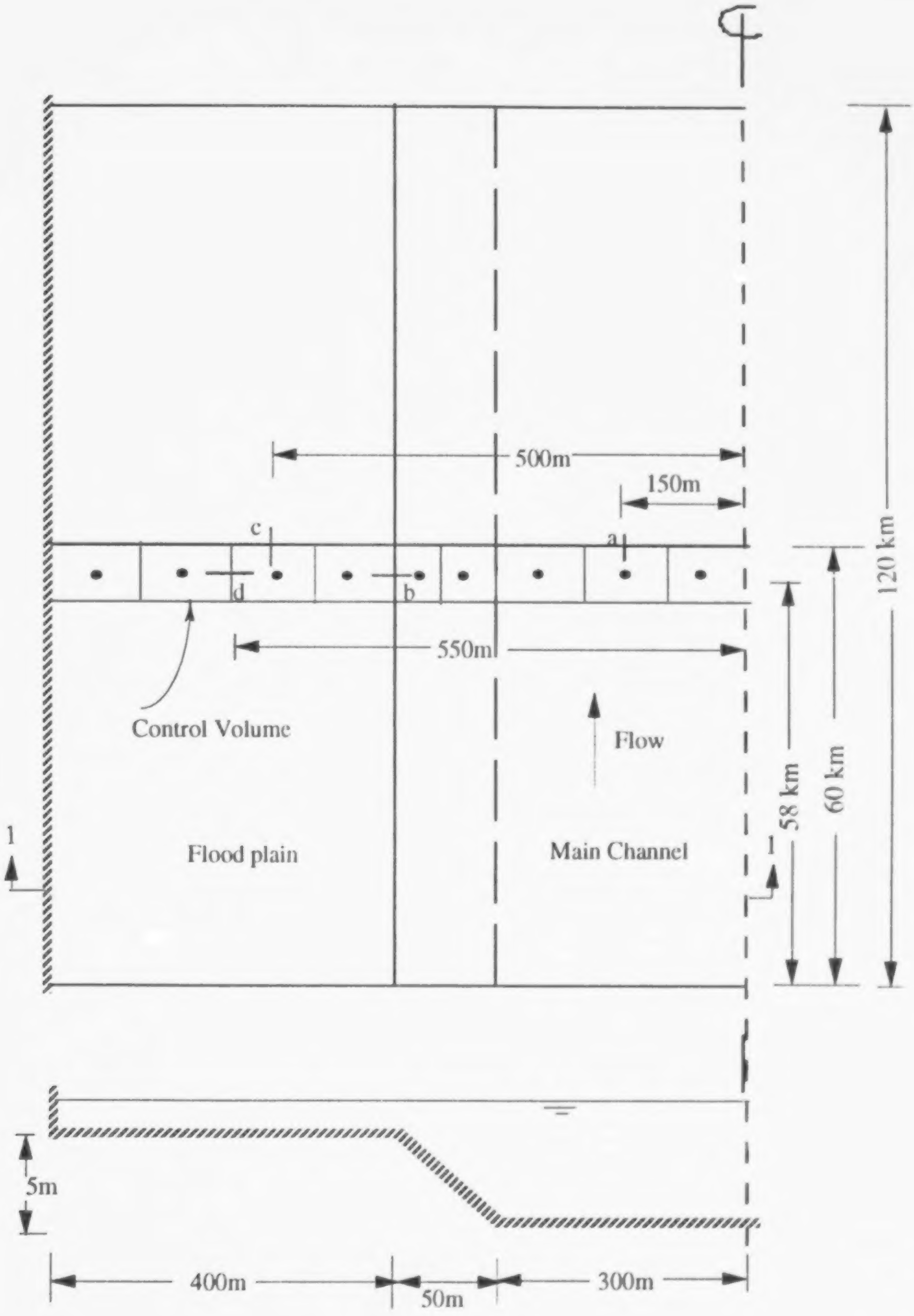
500m
150m
c
a
d
b
550m
Control Volume
Flow
Flood plain
Main Channel
1
1
58 km
60 km
120 km
5m
400m
50m
300m

Section 1-1

Figure 5.22 Plan view of the half of the symmetric and prismatic compound channel for Case 5.

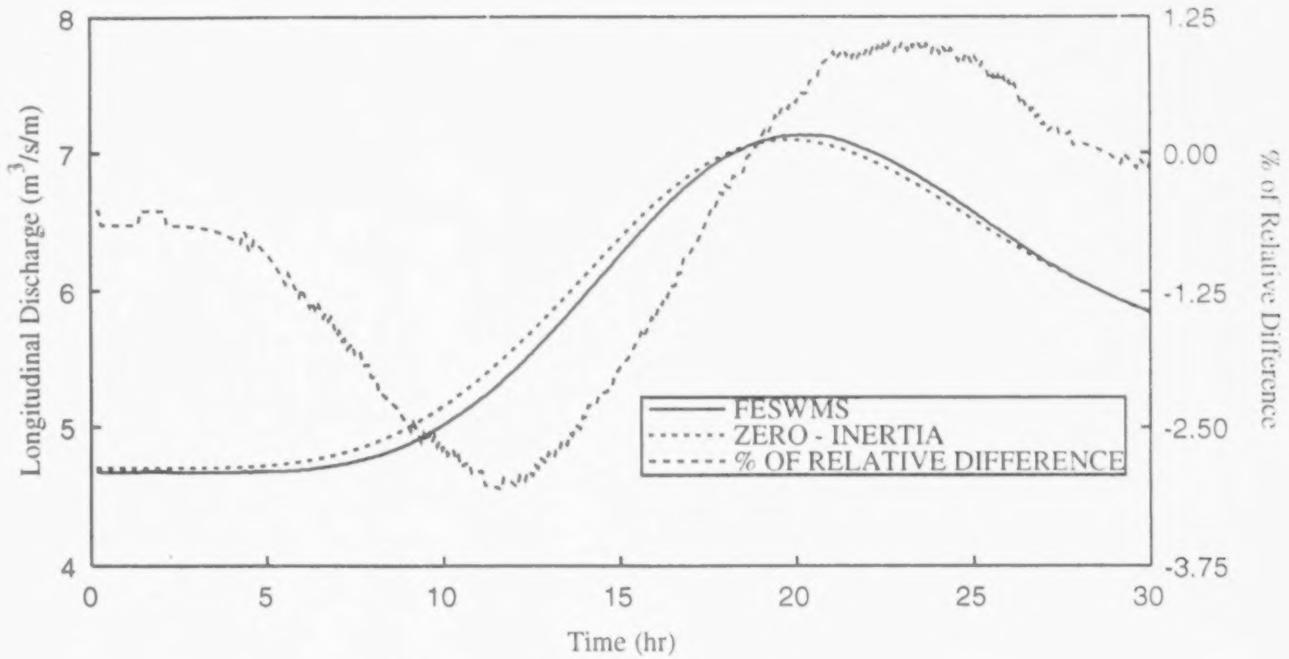

Figure 5.23 Comparison of the main channel longitudinal discharge hydrographs per unit width at 60 km downstream from the inflow boundary and 150 m off the center line for Case 5.

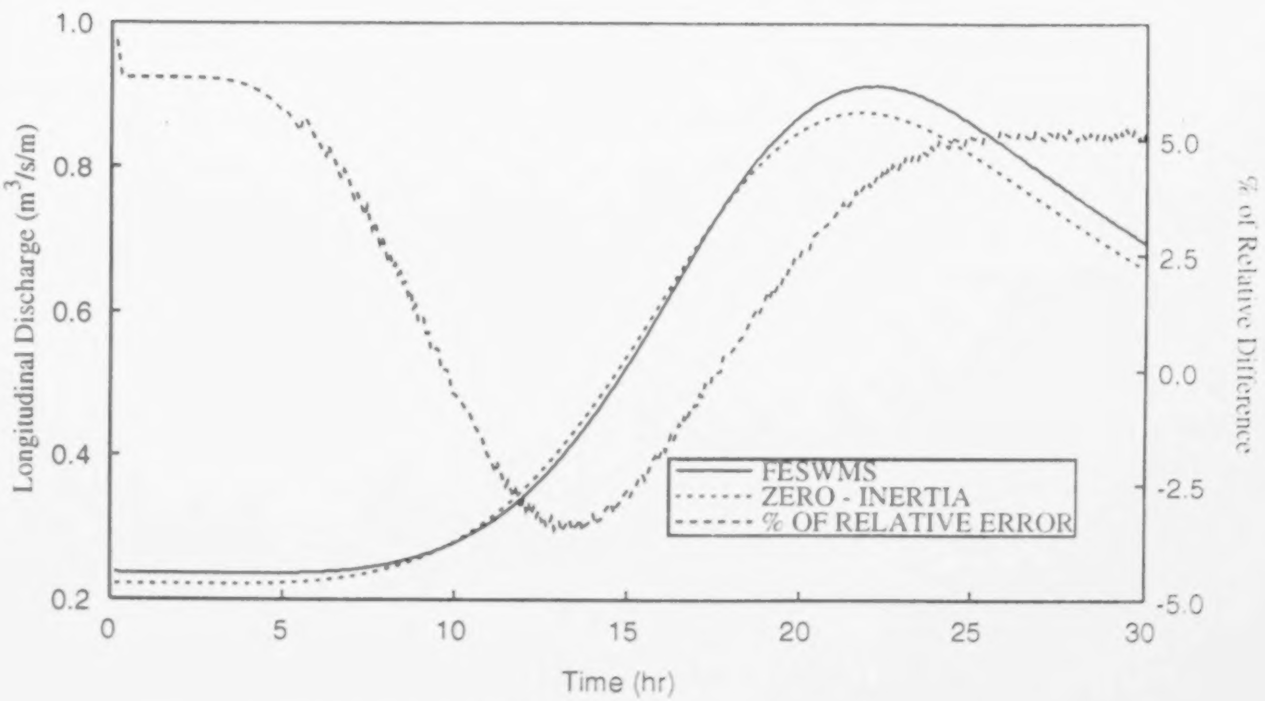

Figure 5.24 Comparison of the flood plain longitudinal discharge hydrographs per unit width at 60 km downstream from the inflow boundary and 500 m off the center line for Case 5.

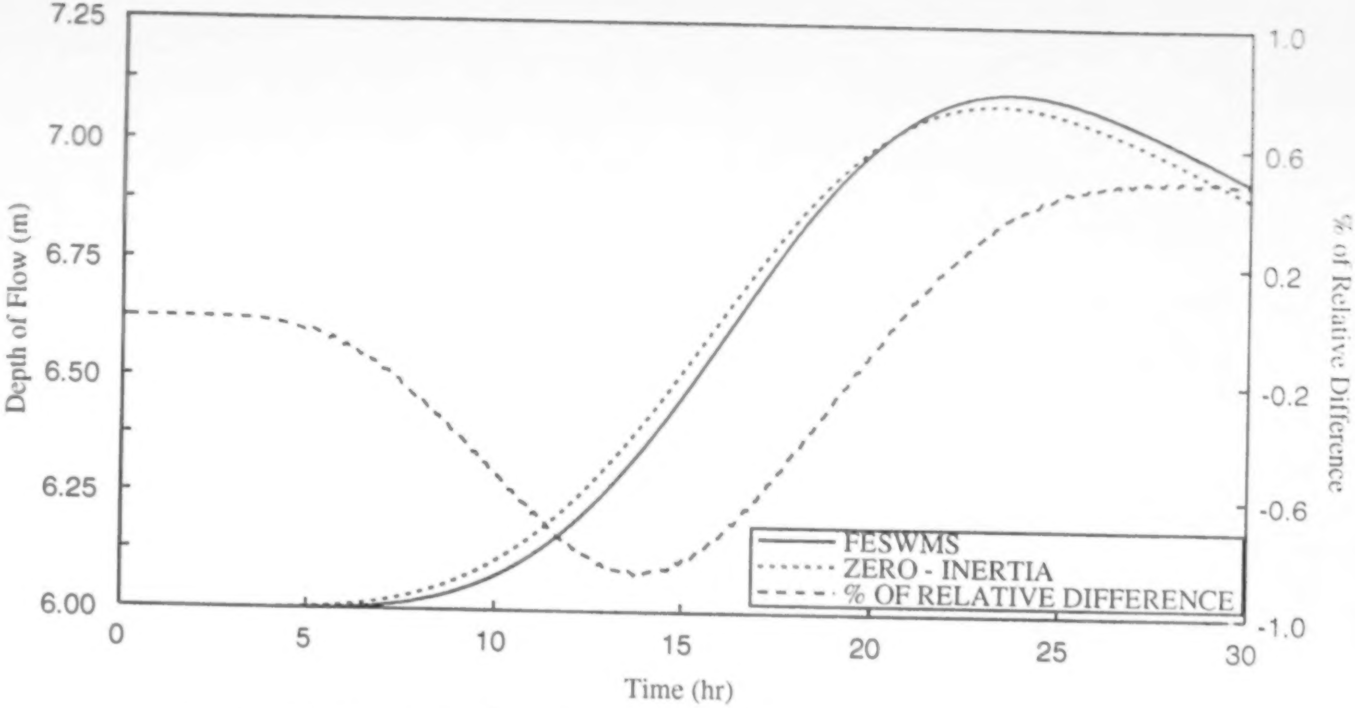

Figure 5.25 Comparison of the main channel depth hydrographs at 60 km downstream from the inflow boundary and 150 m off the center line for Case 5.

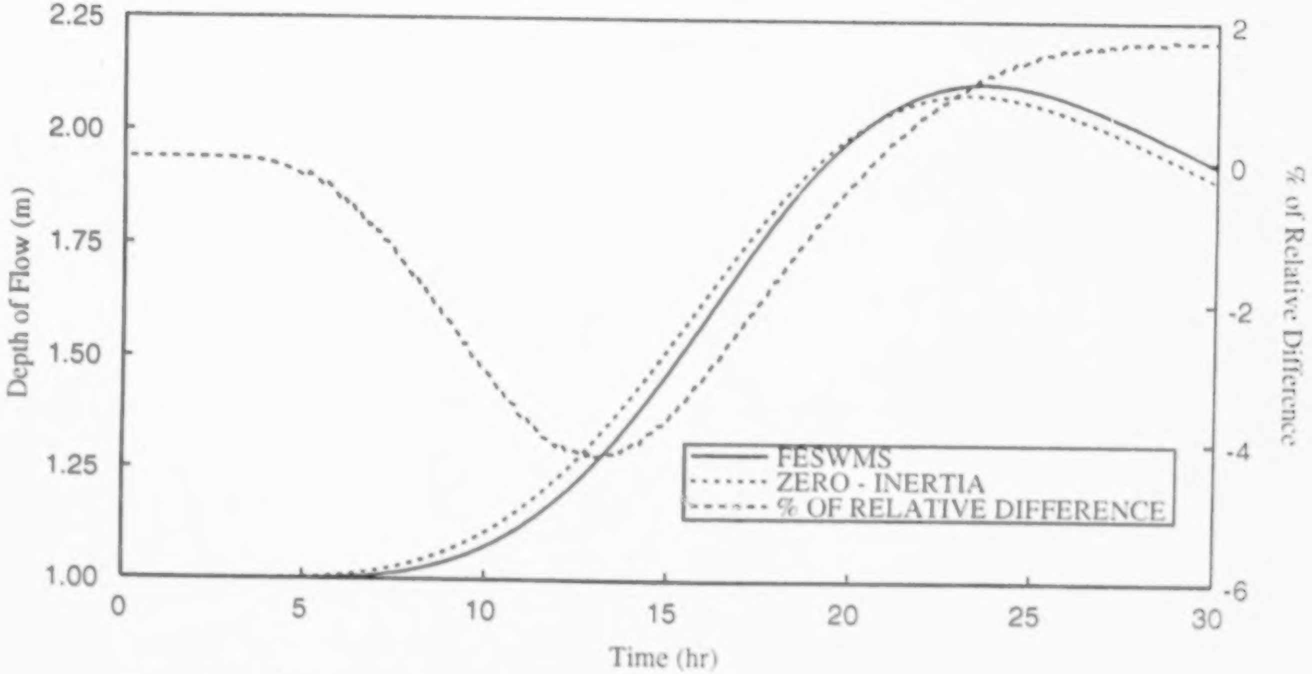

Figure 5.26 Comparison of the flood plain depth hydrographs at 60 km downstream from the inflow boundary and 500 m off the center line for Case 5.

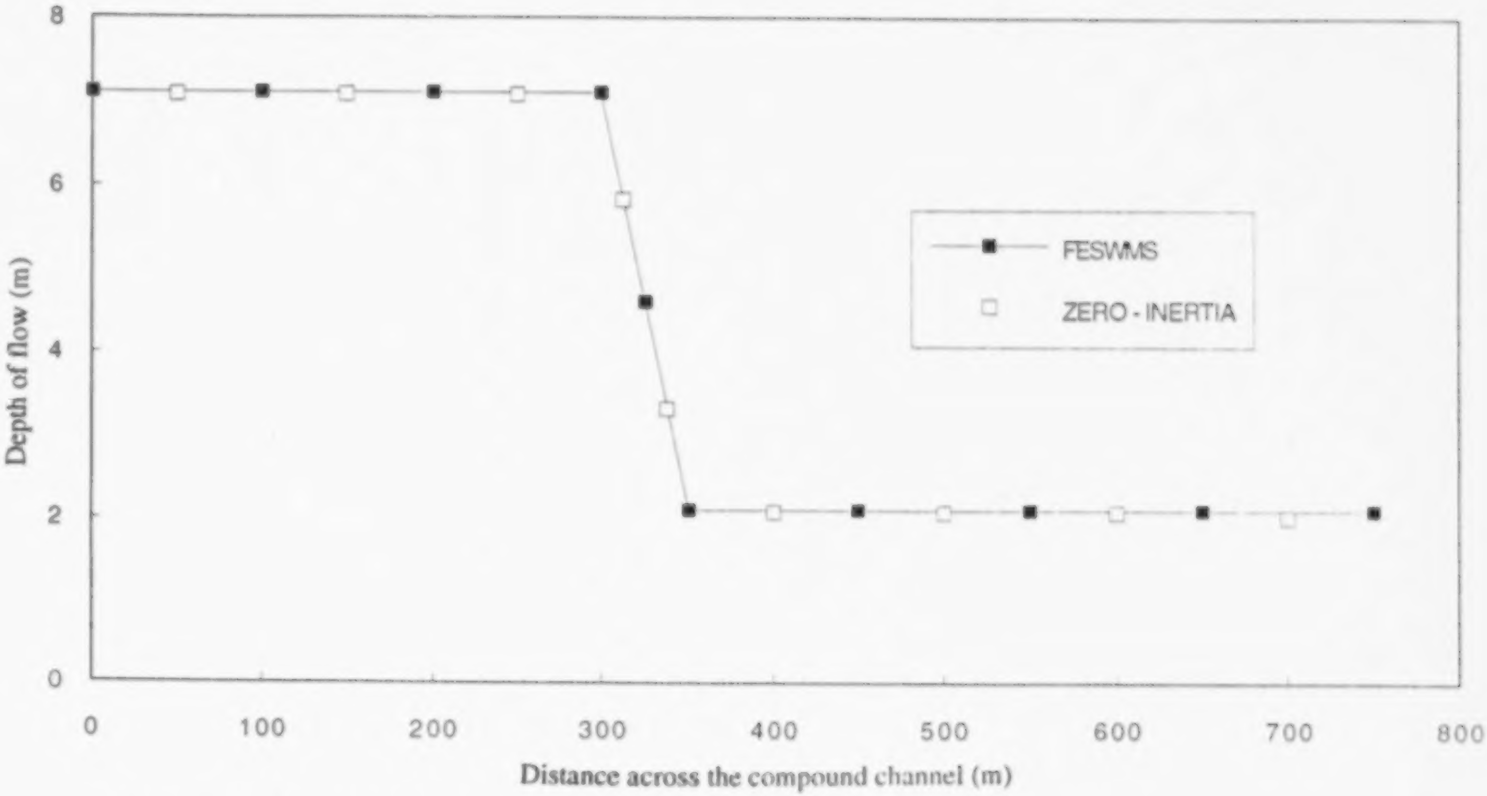

Figure 5.27 Comparison of the depth of flow across the compound channel section at 60 km downstream from the inflow boundary at 24 hours for Case 5.

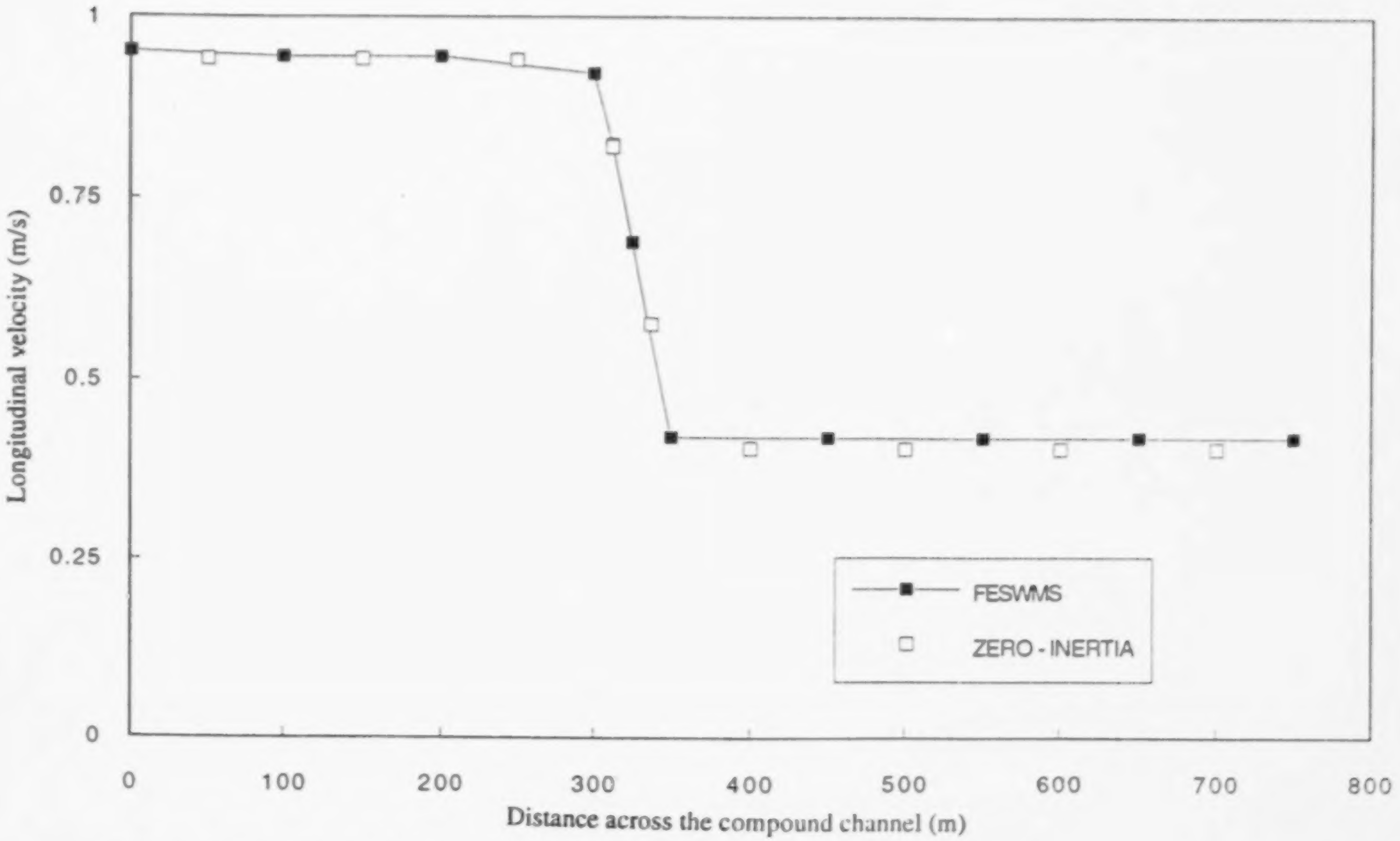

Figure 5.28 Comparison of the lateral distribution of the longitudinal velocity across the compound channel section at 60 km downstream from the inflow boundary at 24 hours for Case 5.

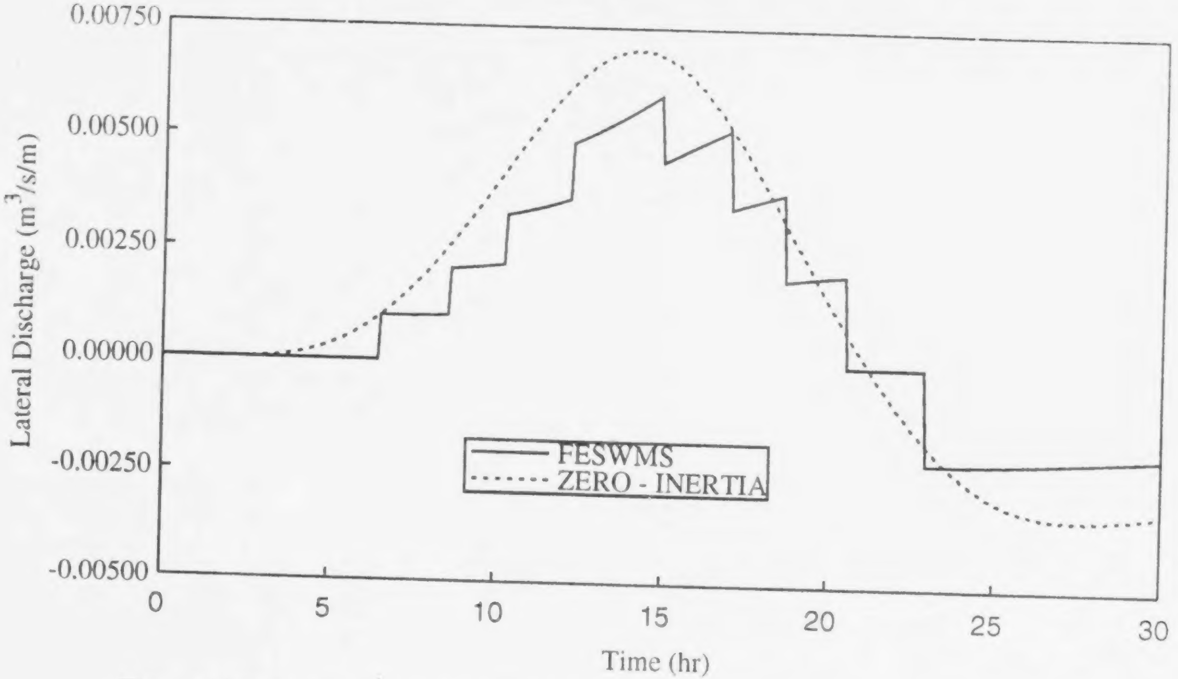

Figure 5.29 Comparison of the lateral discharge hydrographs per unit length at 58 km downstream from the inflow boundary and 350 m off the center line for Case 5.

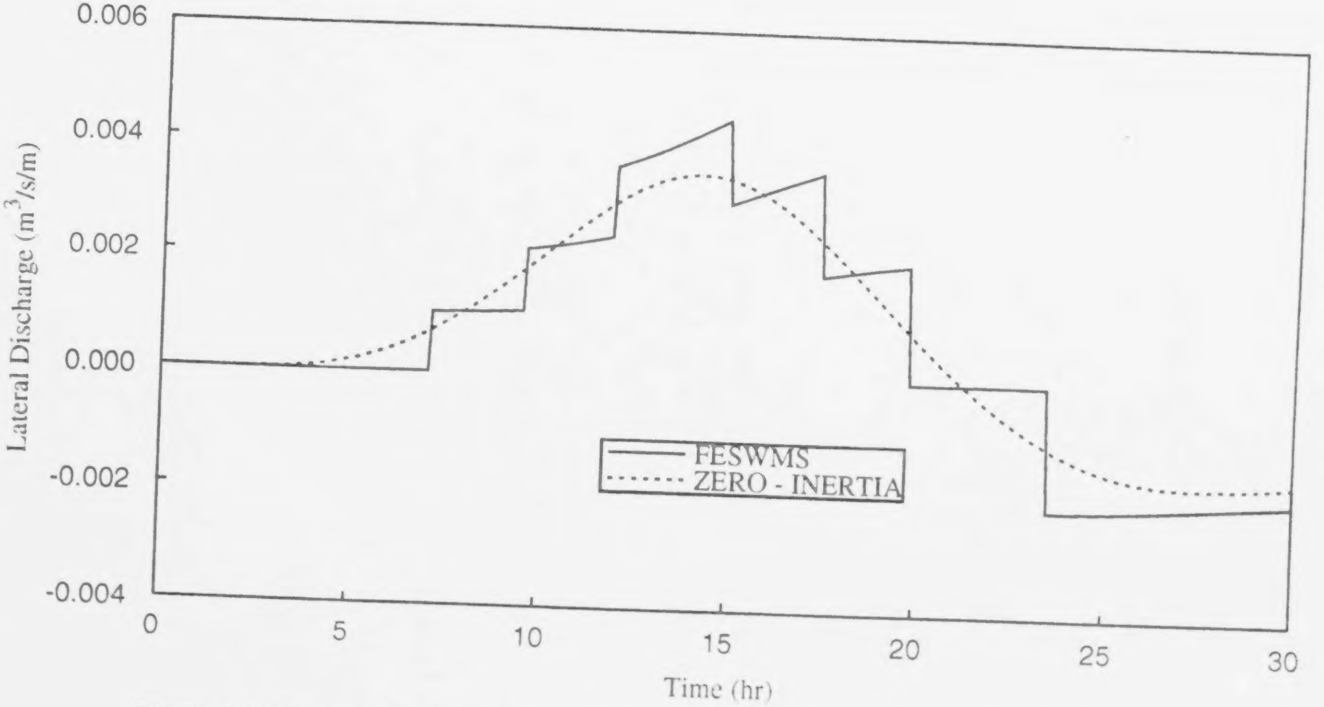

Figure 5.30 Comparison of the lateral discharge hydrographs at 58 km downstream from the inflow boundary and 550 m off the center line for Case 5.

6 APPLICATION OF THE MONOCLINAL WAVE MODEL

6.1 INTRODUCTION

In this chapter, an effort is made to examine and analyze the hydraulic characteristics of the lateral flows that take place between the main channel and the flood plain during the propagation of a monoclinal flood wave in a straight, symmetric, and prismatic compound channel. A pseudo-steady state form of the zero-inertia model is applied for this purpose. This modified model will be referred to as the two-dimensional monoclinal wave model hereafter. Accordingly, the rising part of a natural flood wave is emphasized in the present analysis. Application of the monoclonal wave approximation from the point of view of a moving observer makes it possible to analyze the characteristics of the lateral discharge within the flood wave instead of investigating through the whole length of the channel. It is also possible to use large time steps for numerical experiments. A brief description of the monoclinal wave model and various boundary conditions and the range of non-dimensional variables used in the numerical experiments are presented in Section 6.2. Extensive numerical experiments are then carried out and the characteristics of the lateral discharges are discussed in Section 6.3. Finally, a theoretical analysis is carried out to derive relationship(s) for lateral flow exchange between the main channel and the flood plain in terms of the local depths of the main channel and the flood plain. The numerical experimental data are then used to verify the simplified analyses. The theoretical and the numerical analyses are presented in Section 6.4.

6.2 MODEL EQUATIONS

In order to study the characteristics of the lateral inflows in the compound channel, the unsteady two-dimensional zero-inertia model developed in the present study is adopted. However, as the pseudo-steady state form of the monoclinal wave is considered in this study, the continuity equation has been modified from the point of view of a moving observer and written as follows:

$$\frac{\partial h}{\partial t}+\frac{\partial(q_x-V_wH)}{\partial x}+\frac{\partial q_y}{\partial y}=0 \qquad [6.1]$$

The simplified x- and y- momentum equations remain as presented in Chapter 2. No modification to these equations is necessary as the inertial terms are neglected in the zero-inertia model.

6.2.1 INITIAL AND BOUNDARY FLOW CONDITIONS

As the unsteady zero-inertia flow model is applied to get the pseudo-steady state profile of the monoclinal wave, the flow depth at the final stage of flood event was given as the upstream flow boundary and the depth of the main channel below the flood plain level was given as the downstream flow boundary. A linear longitudinal variation of water surface profile was assumed as the initial condition.

6.2.2 NUMERICAL EXPERIMENTS

Several numerical experiments were conducted for different flood events. In all the experiments, the main channel was initially full and the flood plain was dry. The numerical runs were terminated when the flow became steady. Numerical experiments were conducted for the following conditions:

1. Depth ratio, $\frac{H_c - D}{H_c}$ varies from 0.1 to 0.8.
2. Relative flood plain roughness, $\frac{k_{sp}}{D}$ varies from 0.0001 to 0.3
3. Relative main channel roughness $\frac{k_{sc}}{D}$ varies from 0.0001 to 0.1
4. S_{ox} varies from 0.0001 to 0.001.

6.3 ANALYSIS OF RESULTS

An extensive analysis of the data obtained from the numerical experiments was carried out in this study. The effects of various physical parameters on the movement of the flood waves are discussed and the characteristics of the lateral discharge in particular are examined in detail.

6.3.1 GENERAL DISCUSSION

Figure 6.1 shows a final water surface profile of a monoclinal wave along the center line of the main channel along with the initially assumed water surface profile. The effects of the ratio of the flood plain roughness and the main channel roughness on the water surface profile along the center line of the main channel are graphically shown in Figure 6.2. The corresponding depth hydrographs as seen by a stationary observer are plotted in Figure 6.3. It is seen that as the flood plain roughness increases, main channel flow depths arrive sooner at a particular location. Similar effects on the flood plain flow depths are noticed as shown in Figure 6.4. The spatial distribution of the longitudinal main channel and flood plain flow velocities along the wave are shown in Figures 6.5 and 6.6, respectively. Also shown in each of these figures is the distribution of the longitudinal velocity calculated using uniform flow formula. It is inferred that the use of uniform flow formula results in erroneous results for the initial stage of the flood for the case of main channel but less error is introduced for the flood plain velocity. For all the cases discussed above, the main channel was full.

In order to examine the shape of the total longitudinal discharge hydrograph of a monoclinal wave, a numerical experiment was conducted for the condition that the main channel was not full. The physical parameters were as follows: $H_c = 6\text{m}$, $D = 3$ m, $k_{sp} = k_{sc} = 0.2$ m, and S_{ox}=0.0005. Also, the initial flow depth in the main channel was 1 m. The spatial distribution of the total longitudinal discharge along the wave is shown in Figure 6.7. This distribution is transferred to a discharge hydrograph as seen by a stationary observer and is shown in Figure 6.8. The feature that the in-bank and out of bank flows move with different velocities is clearly noticed in these figures.

The distributions of lateral discharge along the flood wave at various locations across the flood plain are shown in Figure 6.9. It is seen that the lateral discharge profile at the interface envelops all other profiles. An interesting feature can be seen in Figure 6.10 which shows the variation of peak lateral discharge across the flood plain. It is found that the peak discharge varies linearly across the flood plain. Figure 6.11 shows the effect of the ratio of the flood plain roughness to the main channel roughness on the spatial distribution of the lateral discharge at the interface. These distributions are also transferred to the lateral discharge hydrographs as shown in Figure 6.12. It is seen that as the flood plain roughness increases, the contribution from the lateral inflow increases with a reduction in the peak. This is attributed to the fact that as the flood plain roughness increases, longitudinal flow in the flood plain slows down and consequently, the faster moving main channel flow has to make up the deficit. The effects of the longitudinal bed slopes on the spatial distribution of the lateral discharge are plotted in Figure 6.13. It is noticed that as the slope increases, the peak lateral discharge and the overall volume of lateral flow increase. Similar effects are observed for the effects of the width ratio on the spatial distribution of the lateral discharge at the interface as shown in Figure 6.14.

6.3.2 NON-DIMENSIONAL ANALYSIS OF LATERAL DISCHARGE DISTRIBUTIONS

As similar results are obtained from all the experiments, a non-dimensional plot of the distribution of lateral discharge could be possible. With this point of view, each of the lateral discharge is non-dimensionalized by the peak value of the corresponding lateral discharge profile and two length scales are chosen such that they represent the distances from the peak where the discharge is half of the peak value. Figure 6.15 shows the obtained distribution and it is obvious that the lateral discharge profiles are similar. In order to make use of this universal graph, the estimations of the peak values of all the lateral discharge profiles and the magnitudes of the two length scales are required. Hence, a relationship between all the peaks and the maximum lateral discharge which corresponds to the peak value of the interface , denoted by q_{yedge}, is required. In doing so, the peak values of all the discharge profiles across the flood plain are non-dimensionalized by q_{yedge}, and the distance across the flood plain is non-dimensionalized by the width of the flood plain. This linear non-dimensional plot is shown in Figure 6.16. This linear distribution can be expressed by the following equation:

$$\frac{q_{ypeak}}{q_{yedge}} = 1 - \frac{y}{W_p} \qquad [6.2]$$

where y is an arbitrary lateral distance across the flood plain.

The next task is to determine each of the length scales. The variation of the non-dimensional left and right length scales with the depth ratios are shown in Figures 6.17 and 6.18 respectively. By performing multiple regression analysis, the distributions shown in these figures can also be approximated by the following two equations:

For the left scale, $$\frac{L_{ls}S_{ox}}{H_c - D} = 0.18_{\pm 0.075}\left(\frac{H_c - D}{H_c}\right)^{-2.33_{\pm 0.17}} \quad ; R^2=0.80 \qquad [6.3]$$

For the right scale, $\dfrac{R_{ls}S_{ox}}{H_c - D} = 0.15_{\pm 0.07}\left(\dfrac{H_c - D}{H_c}\right)^{-2.33_{\pm 0.17}}$; R^2=0.81 [6.4]

where R^2 is the coefficient of determination and the values specified as subscripts are the tolerance limits of the coefficients.

Hence , knowing the depth ratio for a particular flood event and the slope of the channel, length scales can be determined from these equations. The final step is to find an expression for q_{yedge} . It can be shown that q_{yedge} is a function of the following variables:

$$q_{yedge} = f\left(W_p, W_c, \frac{H_c - D}{H_c}, S_{ox}, k_{sp}, k_{sc}, g\right) \qquad [6.5]$$

In non-dimensional form, it can be written as:

$$\frac{q_{yedge}}{\sqrt{g}D^{\frac{3}{2}}} = ff\left(\frac{H_c - D}{H_c}, S_{ox}, \frac{W_p}{D}, \frac{W_c}{D}, \frac{k_{sp}}{D}, \frac{k_{sc}}{D}\right) \qquad [6.6]$$

By performing a multiple regression analysis on the numerical experimental data, the following equation is obtained for practical purposes:

$$\frac{q_{yedge}}{\sqrt{g}D^{\frac{3}{2}}} =$$

$$13.18_{\pm 0.23} * \left(\frac{H_c - D}{H_c}\right)^{2.47_{\pm 0.095}} S_{ox}{}^{1.35_{\pm 0.045}} \left(\frac{W_p}{D}\right)^{0.97_{\pm 0.07}} \left(\frac{W_c}{D}\right)^{-0.24_{\pm 0.11}} \left(\frac{k_{sc}}{D}\right)^{-0.03_{\pm 0.03}} \left(\frac{k_{sp}}{D}\right)^{-0.04_{\pm 0.03}}$$

[6.7]

The coefficient of determination is 0.97 and the relationship is shown in Figure 6.19. Hence, by knowing the channel and flood properties, the maximum lateral discharge can be determined by the above regression equation.

It should be mentioned that the determination of the location of the peak lateral discharge within the wave is not required. This is because of the fact that in the similarity profile, the position of the peak is used as a reference point. However, an attempt is made in this study to examine the position of the peak and it is found that it occurs in the vicinity of the point of inflection of the longitudinal water surface profile where the maximum longitudinal friction slope occurs.

Therefore, Figures 6.15 to 6.19 may be applied to determine the distribution and the volume of the lateral discharge for a flood event keeping their limitations in mind. This finding can then be used to quantify the distribution of transferred material by knowing its concentration in the flood flows.

6.4 EXPRESSIONS FOR LATERAL FLOW EXCHANGE

During the propagation of flood wave in a compound channel, flow exchange takes place between the main channel and the flood plain. To quantify this lateral flow exchange in the application of one-dimensional models, weir type equations are normally used (Cunge et al., 1980; Tuitoek, 1995). In the present study, however, an effort is made to derive a theoretical expression for the lateral flow exchange in terms of the local main channel and flood plain flow depths based on the physical processes involved. Two different flood plain flow situations, namely, fully flooded (entire flood plain width inundated) and partially flooded plains are considered as described herein. The numerical experimental results are then used to verify the simplified theoretical analyses.

6.4.1 FLOW INTO FULLY FLOODED PLAINS

In order to derive an expression to estimate the lateral flow exchange for the fully inundated flood plains, a control volume per unit length as shown in Figure 6.20 is considered. This control volume extends from the interface of the main channel and the flood plain to the outer wall of the flood plain. Balancing the lateral forces acting on this control volume results in:

$$P_1 - P_2 + M_l = F_\tau \qquad [6.8]$$

where P_1 is the hydrostatic pressure force acting at the interface between the main channel and the flood plain, P_2 is the hydrostatic pressure force acting at the outer edge of the flood plain, M_l is the convective momentum transfer, and F_τ is the boundary shear force on the flood plain.

Neglecting convective momentum, equation [6.8] can be rewritten as:

$$P_1 - P_2 = F_\tau \qquad [6.9]$$

Assuming the water surface varies linearly across the flood plain, then the average depth in the flood plain can be expressed as:

$$H_f = \frac{H_1 + H_2}{2} \qquad [6.10]$$

where H_f is the average depth of flow in the flood plain, H_1 is the average depth of flow in the main channel above the flood plain level, and H_2 is the depth of flow at the outer edge of the flood plain.

The above equation can be rearranged as:

$$H_2 = 2H_f - H_1 \qquad [6.11]$$

Now,

$$P_1 = \frac{\gamma H_1^2}{2} \qquad [6.12]$$

$$P_2 = \frac{\gamma H_2^2}{2} \qquad [6.13]$$

Therefore,

$$P_1 - P_2 = \frac{\gamma}{2}\left(H_1^2 - H_2^2\right) \qquad [6.14]$$

This equation can be further simplified by using equation [6.10] as:

$$P_1 - P_2 = 2\gamma H_f (H_1 - H_f) \qquad [6.15]$$

Bed shear stress can be defined as:

$$\tau_f = \frac{\rho U V}{C_*^2} \qquad [6.16]$$

where τ_f is the boundary shear stress on the flood plain, U and V are the longitudinal and the lateral velocities, respectively.

Assuming a linear variation of the lateral discharge across the flood plain, as discussed earlier in this chapter, and uniform flow conditions in the longitudinal direction [6.16] can be expressed as:

$$\tau_f = \frac{\rho \sqrt{g S_{ox}}\, q_o}{C_* H_f}\left(1 - \frac{y}{W_p}\right) \qquad [6.17]$$

where ρ is the density of fluid, C_* is the non-dimensional Chezy coefficient, H_f is the average depth of flow in the flood plain, q_o is the lateral flow exchange, W_p is the width of the flood plain and y is an arbitrary lateral distance from the interface between the flood plain and the main channel.

Hence, the total boundary shear force can be calculated as:

$$F_\tau = \int_o^{W_p} \tau_f dy \qquad [6.18]$$

Substituting equation [6.17] into equation [6.18] and integrating, the following is obtained:

$$F_\tau = \frac{\rho\sqrt{gS_{ox}}q_o}{C_*\sqrt{H_f}}\frac{W_p}{2} \qquad [6.19]$$

Substitution of the equations [6.15] and [6.19] into equation [6.9] yields:

$$2H_f(H_1 - H_f) = \frac{\rho\sqrt{gS_{ox}}q_o}{C_*\sqrt{H_f}}\frac{W_p}{2} \qquad [6.20]$$

Equation [6.20] can be rearranged in a non-dimensional form as follows:

$$\frac{q_o W_p\sqrt{S_{ox}}}{C_*\sqrt{g}H_1^{\frac{5}{2}}} = 4\left(\frac{H_1 - H_f}{H_1}\right)\left(\frac{H_f}{H_1}\right)^{\frac{3}{2}} \qquad [6.21]$$

The above equation can be further simplified as:

$$\frac{q_o W_p\sqrt{S_{ox}}}{C_*\sqrt{g}H_1^{\frac{5}{2}}} = 4\left(\frac{H_1 - H_f}{H_1}\right)\left(1 - \frac{H_1 - H_f}{H_1}\right)^{\frac{3}{2}} \qquad [6.22a]$$

Therefore, by knowing the width, the slope, and the local depth in the main channel above the flood plain level as well as the local depth in the flood plain, equation [6.22a] can be used to quantify the lateral flow exchange between the main channel and the flood plain for the ranges $0 \le \frac{H_1 - H_f}{H_1} \le 0.5$. In order to use equation [6.22a] for flows leaving the flood plain to the main channel, this equation is modified as follows:

$$\frac{q_o W_p \sqrt{S_{ox}}}{C_* \sqrt{g} H_1^{\frac{5}{2}}} = 4\left(\frac{H_1 - H_f}{H_1}\right)\left(1 - \left|\frac{H_1 - H_f}{H_1}\right|\right)^{\frac{3}{2}} \qquad [6.22b]$$

6.4.2 FLOW INTO PARTIALLY FLOODED PLAINS

In the preceding subsection, 6.4.1, a theoretical equation is derived for the lateral flow exchange between the main channel and the flood plain for the ranges $0 \le \frac{H_1 - H_f}{H_1} \le 0.5$. In this subsection another theoretical equation is derived for the partially flooded flood plain valid for the ranges $0.5 \le \frac{H_1 - H_f}{H_1} \le 1.0$. Balancing the lateral forces acting on the control volume per unit length as shown in Figure 6.21 by neglecting the convective momentum yields:

$$P_1 = F_\tau \qquad [6.23]$$

where P_1 and F_τ are defined as before.

Boundary shear force is defined as:

$$F_\tau = \int_o^{W_e} \tau_f \, dy \qquad [6.24]$$

where W_e is the effective lateral distance flooded by flow.

Using the equation [6.15], an expression for boundary shear stress can be written as:

$$\tau_f = \frac{\rho\sqrt{gS_{ox}}}{C_{*}\sqrt{H}} q_o \left(1 - \frac{y}{W_e}\right) \qquad [6.25]$$

where H is the depth in the flood plain at any lateral distance from the interface.

Assuming a linear variation of depth across the inundated flood plain i.e.,

$$H = H_1\left(1 - \frac{y}{W_e}\right) \qquad [6.26]$$

Equation [6.25] can be simplified as:

$$\tau_f = \frac{\rho\sqrt{gS_{ox}}}{C_{*}\sqrt{H_1}} q_o \left(1 - \frac{y}{W_e}\right)^{\frac{1}{2}} \qquad [6.27]$$

Substituting equation [6.27] into equation [6.24] results in:

$$F_\tau = \int_0^{W_e} \frac{\rho\sqrt{gS_{ox}}\,q_o}{C_{*}\sqrt{H_1}} \left(1 - \frac{y}{W_e}\right)^{\frac{1}{2}} dy \qquad [6.28]$$

Define, $\eta = 1 - \dfrac{y}{W_e}$ [6.29]

Then

$$dy = -W_e d\eta \qquad [6.30]$$

Substituting equations [6.29] and [6.30] into equation [6.28]yields:

$$F_\tau = \frac{\rho\sqrt{gS_{ox}}\,q_o}{C_{*}\sqrt{H_1}} \int_0^1 \eta^{\frac{1}{2}} W_e d\eta = \frac{\rho\sqrt{gS_{ox}}\,q_o}{C_{*}\sqrt{H_1}} W_e \left[\frac{2}{3}\eta^{\frac{3}{2}}\right]_0^1 \qquad [6.31]$$

The above equation can be further simplified as:

$$F_{\tau} = \frac{2}{3}\frac{\rho\sqrt{gS_{ox}}\,q_o}{C.\sqrt{H_1}}W_e \qquad [6.32]$$

Now, in order to estimate the inundated width of the flood plain, W_e, an equivalent average depth which gives the same water volume is used:

$$\frac{1}{2}W_e H_1 = W_p H_f \qquad [6.33]$$

where H_f is the average depth of flow in the flood plain.

Then, the following relationship can be obtained:

$$W_e = 2\frac{H_f}{H_1}W_p \qquad [6.34]$$

Substituting equations [6.12] and [6.32] into equation [6.23] and using equation [6.34], and simplifying, the following non-dimensional form can be obtained:

$$\frac{q_o W_p\sqrt{S_{ox}}}{C.\sqrt{g}H_1^{\frac{5}{2}}} = \frac{3}{8}\frac{H_1}{H_f} \qquad [6.35]$$

The above equation can be further simplified as the following:

$$\frac{q_o W_p\sqrt{S_{ox}}}{C.\sqrt{g}H_1^{\frac{5}{2}}} = \frac{3}{8}\left(\frac{1}{1-\dfrac{H_1 - H_f}{H_1}}\right) \qquad [6.36]$$

Hence, by knowing the width, the slope, the local average depth in the main channel as well as in the flood plain, the equation [6.36] can be used to quantify the lateral flow exchange between the main channel and the flood plain for the ranges $0.5 \le \frac{H_1 - H_f}{H_1} \le 1.0$. This equation is only applicable for flow leaving the main channel to the partially dry flood plain.

6.4.3 REGRESSION EQUATIONS FOR LATERAL FLOW EXCHANGE

Having derived the theoretical equations for different flood plain flow situations, namely, fully and partially inundated flood plains, these equations were verified by numerically simulated data. Data obtained by the monoclinal wave model were used for lateral flows from the main channel to the flood plain and data obtained by the unsteady zero-inertia model were used for flows leaving and entering the flood plain. The theoretical variation of the non-dimensional variable $\frac{q_o W_p \sqrt{S_{ox}}}{C.\sqrt{g} H_1^{\frac{5}{2}}}$ with the other non-dimensional variable $\frac{H_1 - H_f}{H_1}$ is shown in Figure 6.22. The relationship between these two variables for numerically simulated data are also shown in the same figure. It is clearly noticed that these data support the trend of the theoretical relationships reasonably well. By performing a regression analysis on the numerical experimental data, the following equation is obtained:

$$\frac{q_o W_p \sqrt{S_{ox}}}{C.\sqrt{g} H_1^{\frac{5}{2}}} = 3.58_{\pm 0.2}\left(\frac{H_1 - H_f}{H_1}\right) - 6.84_{\pm 0.7}\left(\frac{H_1 - H_f}{H_1}\right)^2 + 8.0_{\pm .61}\left(\frac{H_1 - H_f}{H_1}\right)^3$$

[6.37a]

In order to be applicable to both flow leaving and entering the main channel, the above equation is modified as follows:

$$\frac{q_o W_p \sqrt{S_{ox}}}{C.\sqrt{g} H_1^{\frac{5}{2}}} = \frac{H_1 - H_f}{\left|H_1 - H_f\right|}\left[3.58_{\pm 0.2}\left|\frac{H_1 - H_f}{H_1}\right| - 6.84_{\pm 0.7}\left(\frac{H_1 - H_f}{H_1}\right)^2 + 8.0_{\pm .61}\left|\left(\frac{H_1 - H_f}{H_1}\right)^3\right|\right]$$

[6.37b]

The coefficient of determination is 0.97 and the tolerance limit of each of the coefficients is given as subscript in the above equation. This relationship along with the simulated data is shown in Figure 6.23. It is also found from the numerical experiments that most of the lateral flow exchange data lie in the range of $0 \leq \frac{H_1 - H_f}{H_1} \leq 0.5$ and a linear relationship between the two non-dimensional variables is noticed in Figure 6.31. Hence, the following linear regression equation is proposed for practical purposes:

$$\frac{q_o W_p \sqrt{S_{ox}}}{C.\sqrt{g} H_1^{\frac{5}{2}}} = 2.21_{\pm 0.012}\left(\frac{H_1 - H_f}{H_1}\right) \qquad [6.38]$$

The coefficient of determination is 0.97 and the tolerance limit of the coefficient is shown as subscript in the above equation and the relationship is provided in Figure 6.32.

Equation [6.37] or [6.38] may be useful for specifying the lateral flow exchange between the main channel and the flood plain flows presently handled by weir type equations in one-dimensional compound channel flow models.

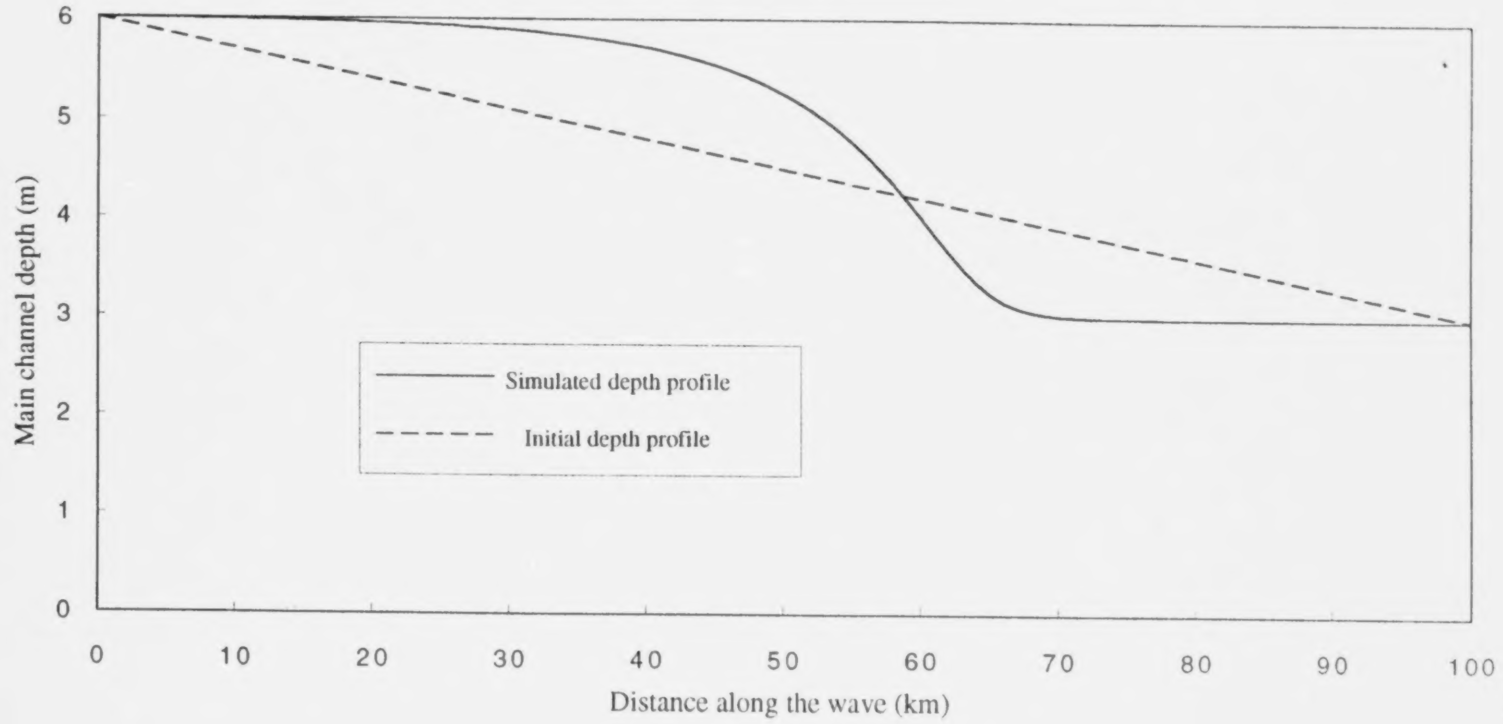

Figure 6.1 Steady water surface profile along the center line of the channel and the initial assumed water surface profile.

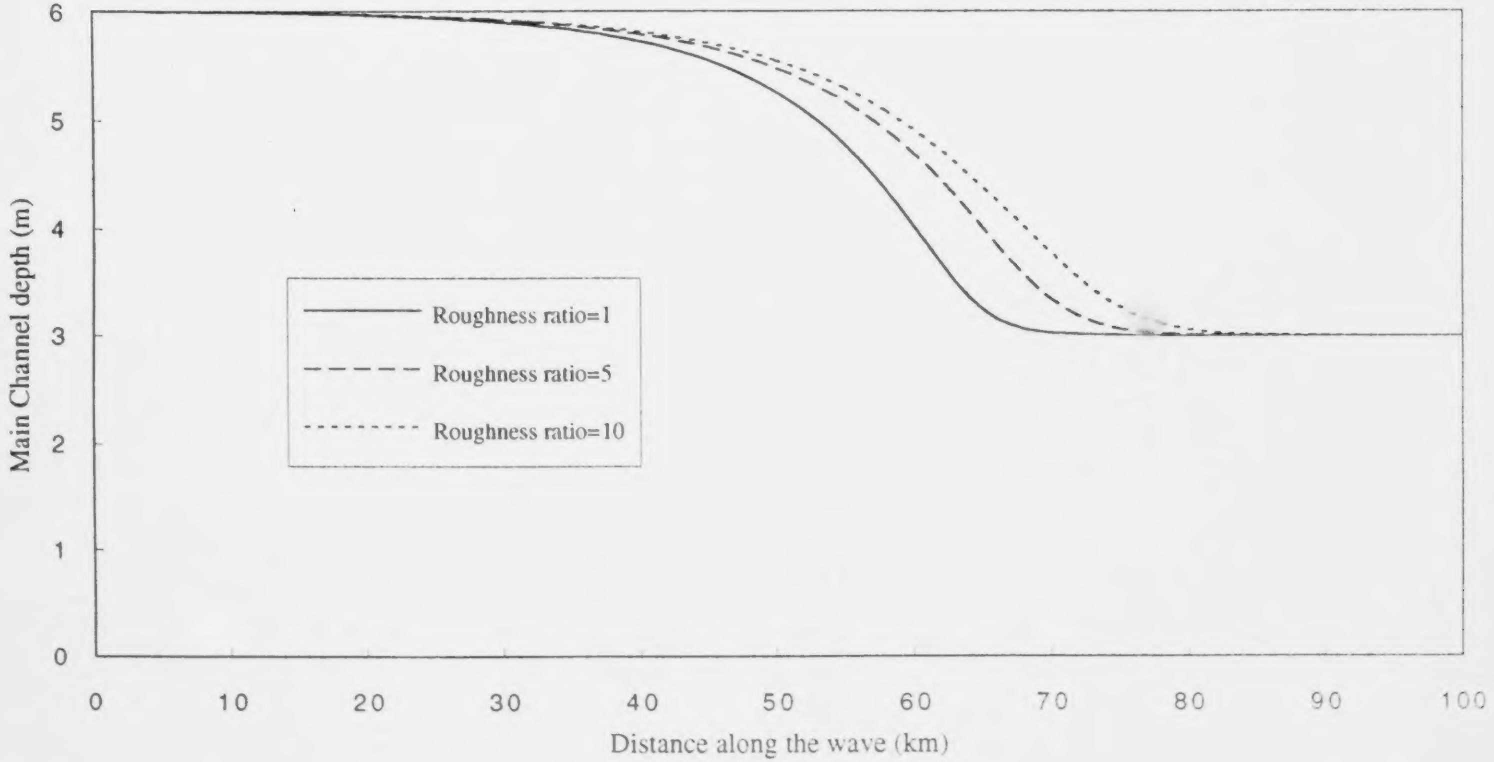

Figure (6.2) Effects of roughness ratio on the main channel water surface profiles.

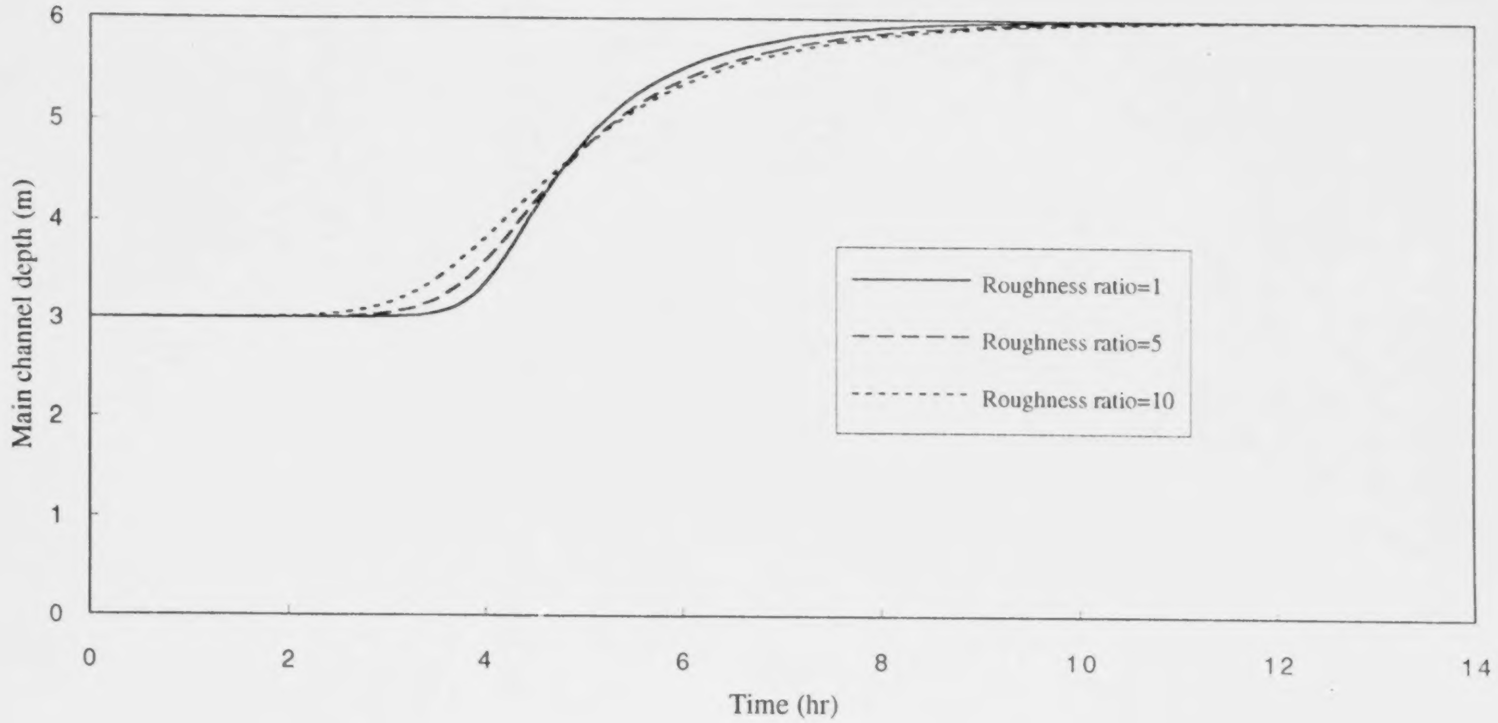

Figure 6.3 Effects of roughness ratio on the main channel depth hydrographs.

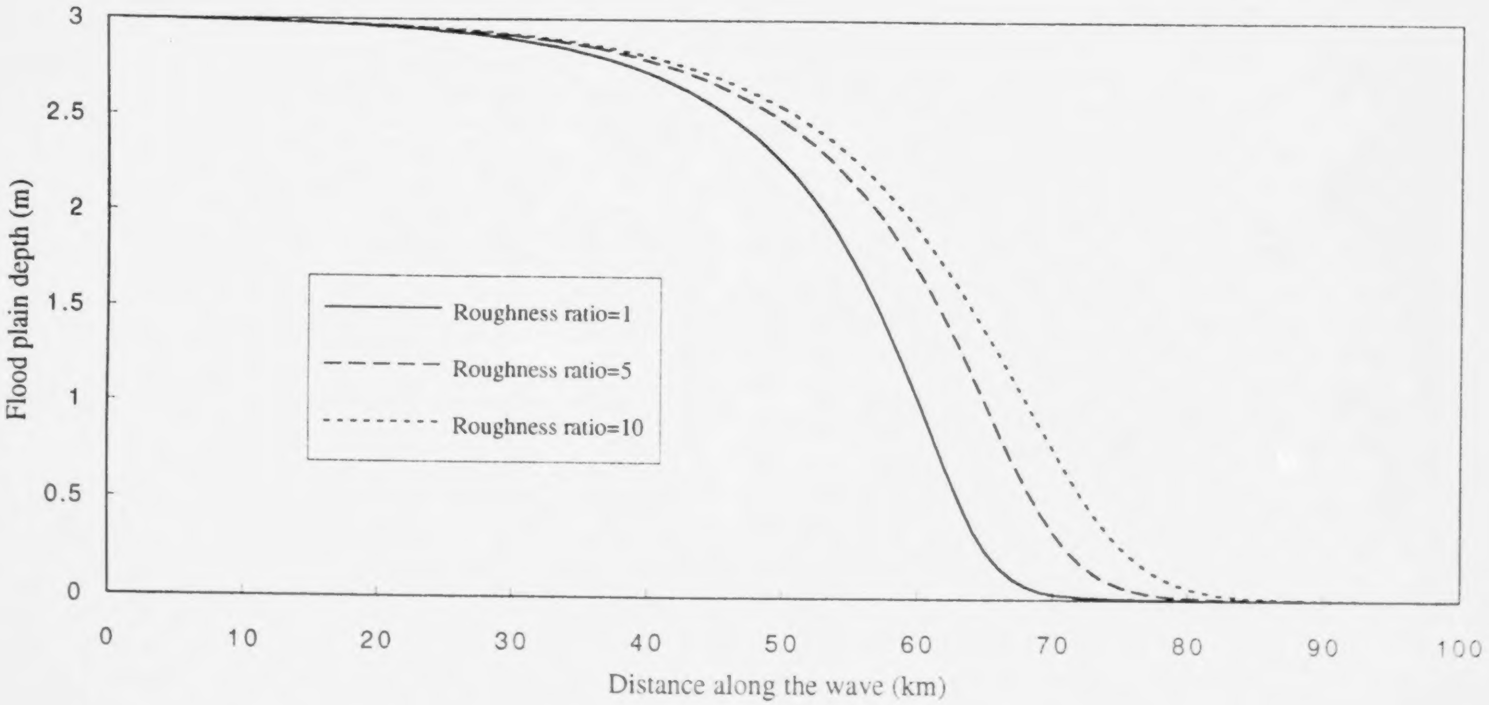

Figure 6.4: Effects of roughness ratio on the flood plain water surface profiles.

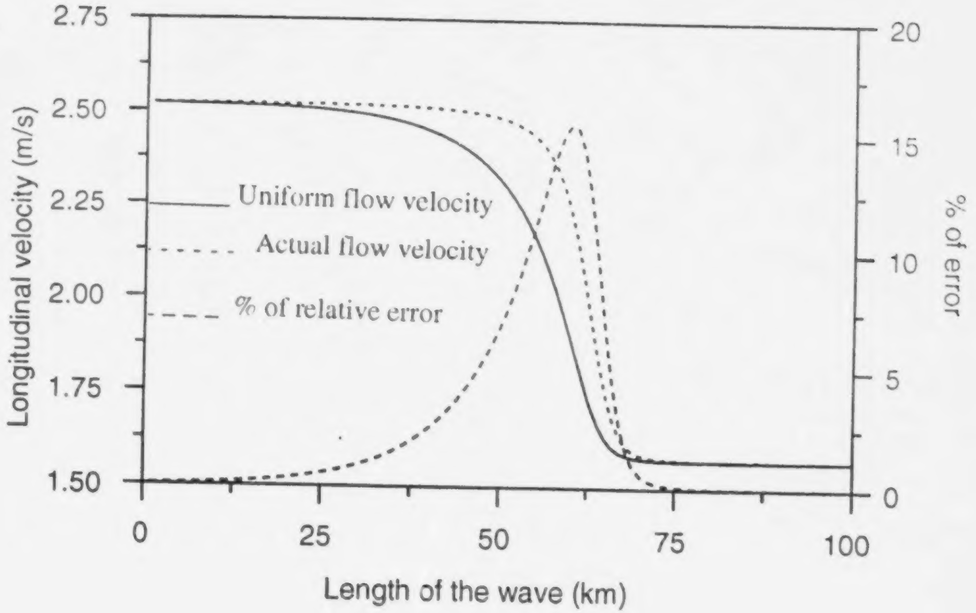

Figure 6.5 . Spatial distribution of the longitudinal main channel velocity along the wave.

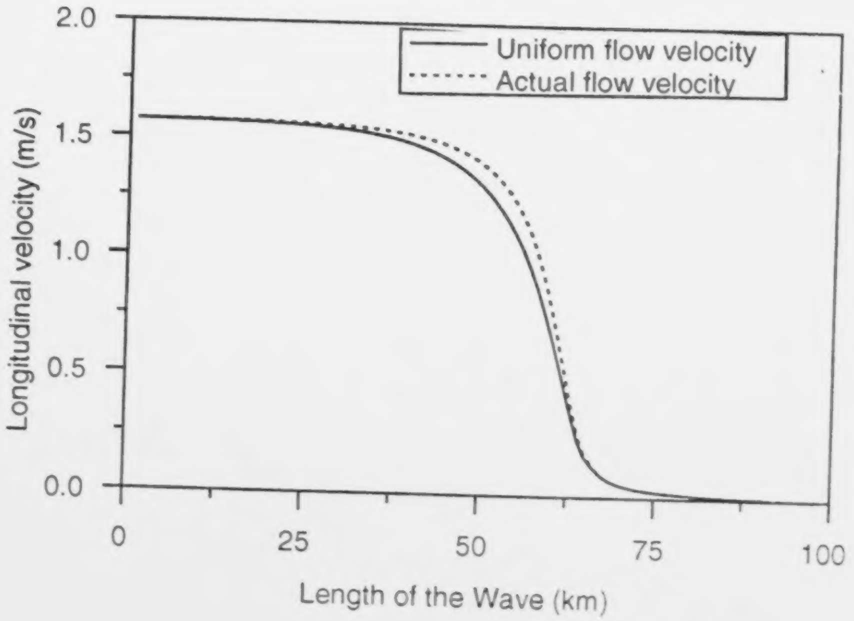

Figure 6.6 Spatial distribution of the longitudinal flood plain velocity along the wave.

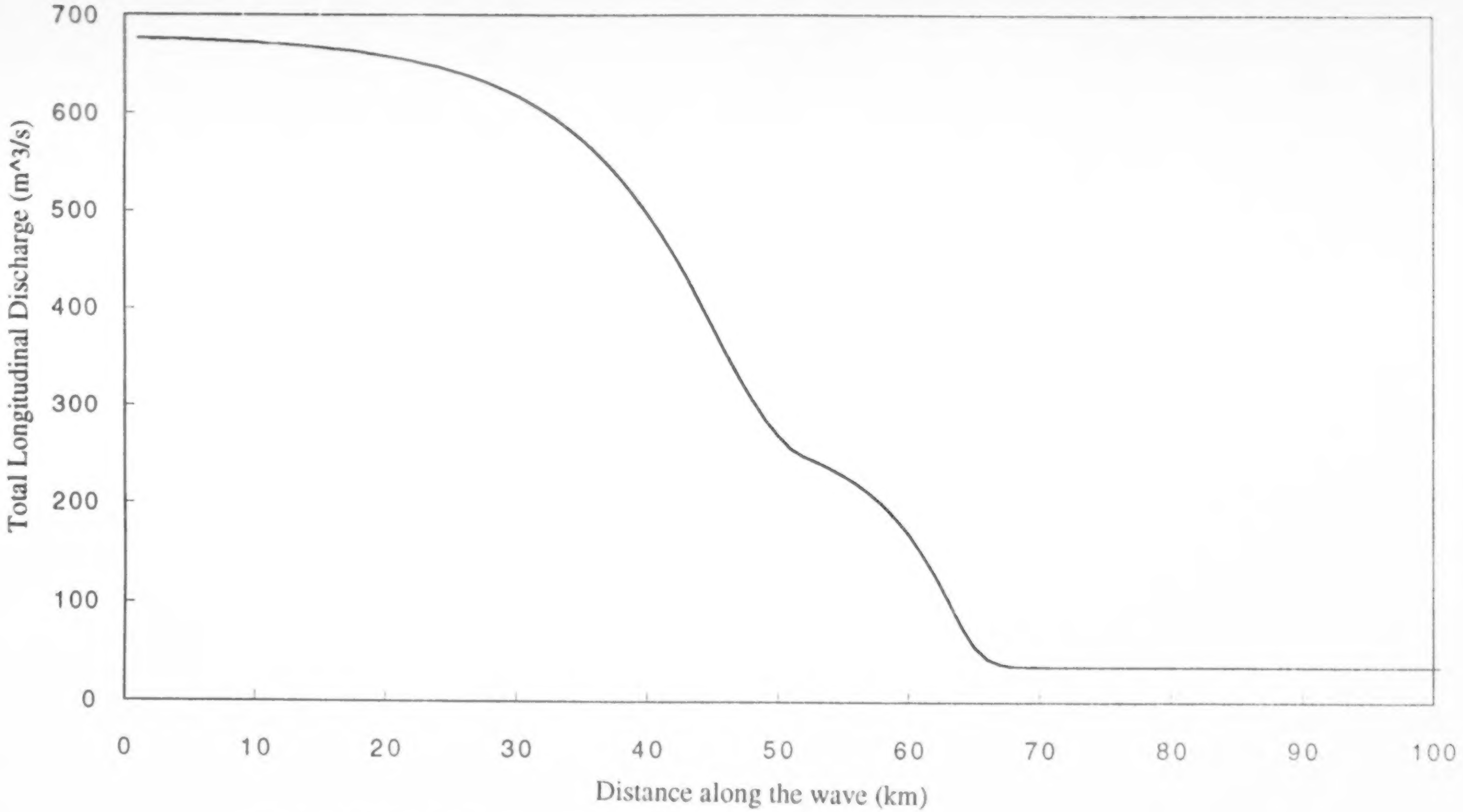

Figure 6.7 Spatial distribution of the total discharge along the wave.

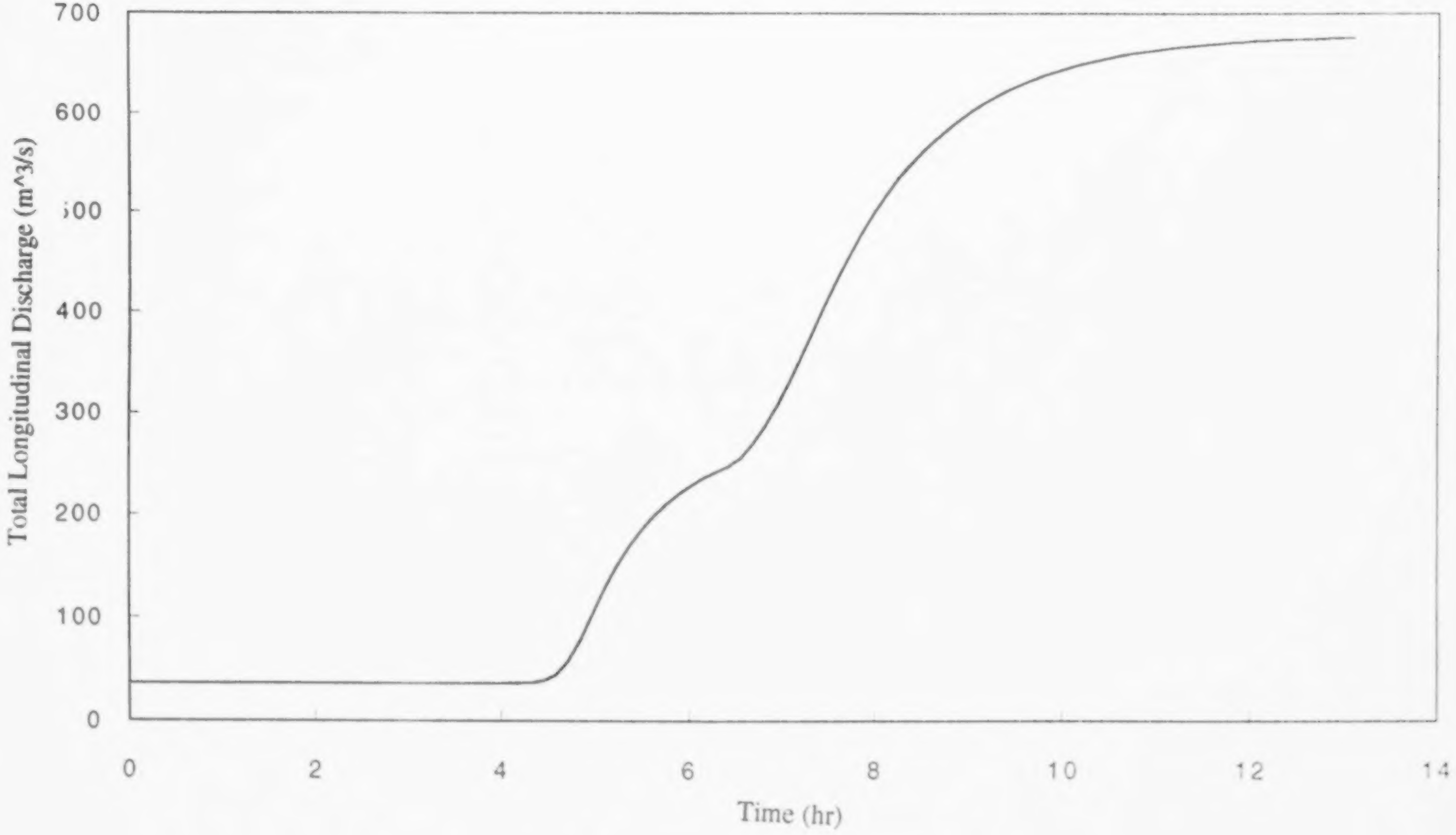

Figure 6.8 Monoclinal discharge hydrograph.

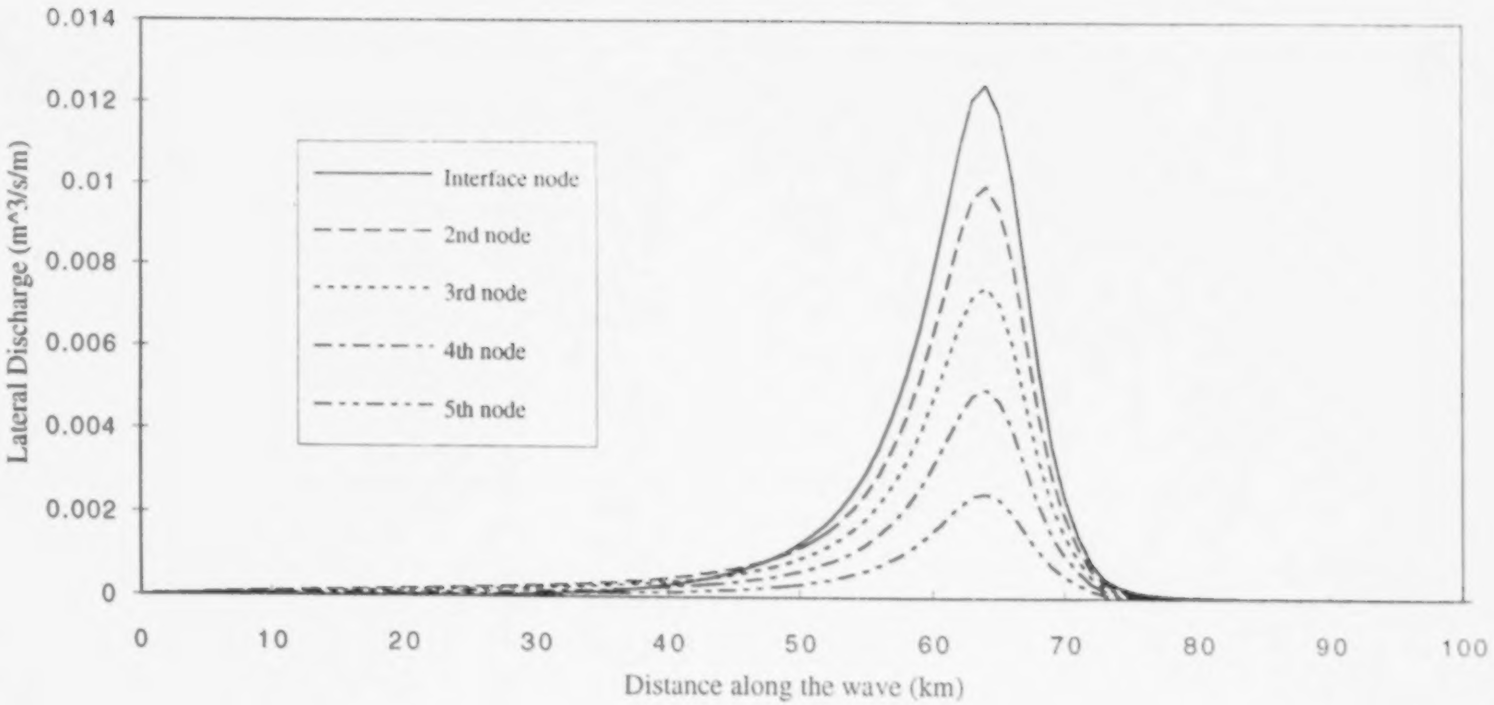

Figure 6.9 Profiles of lateral discharges at various locations across the flood plain.

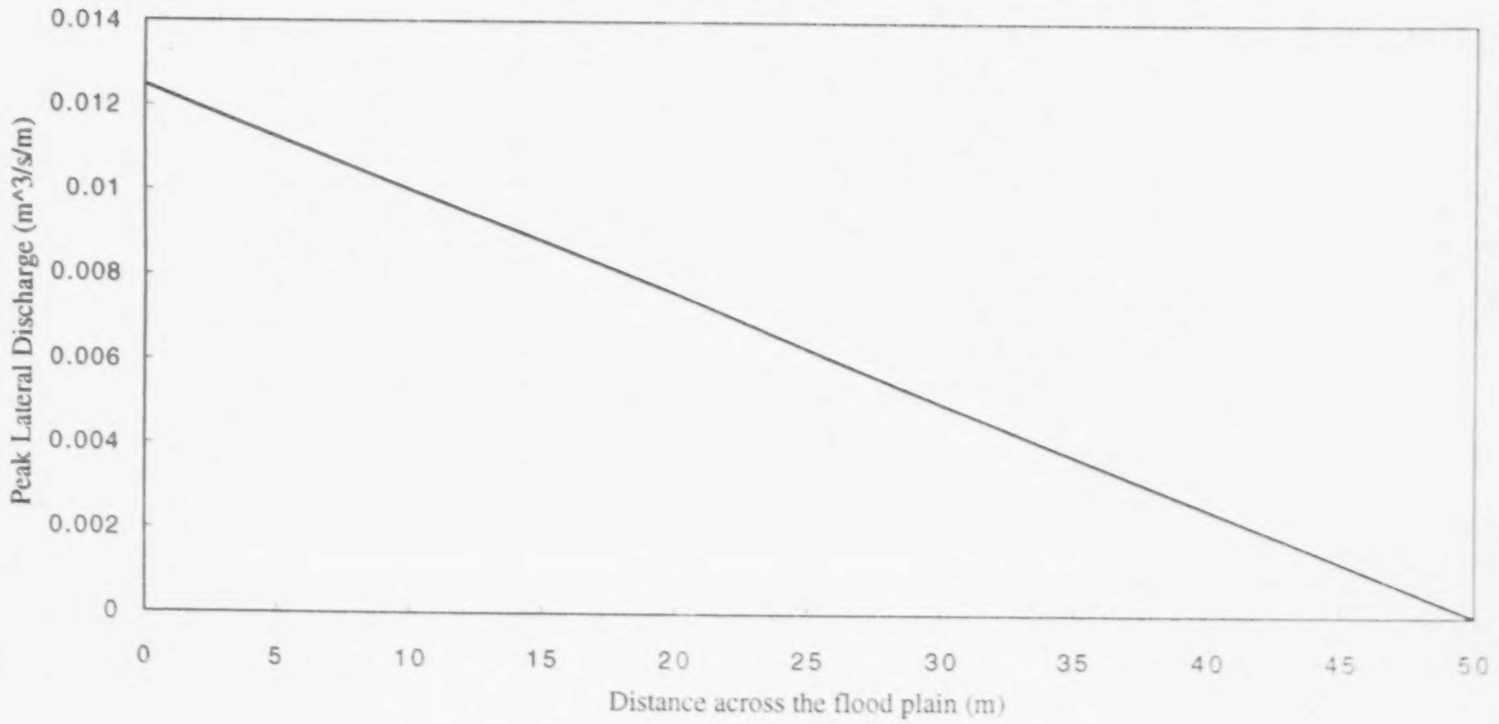

Figure 6.10 Variation of peak lateral discharge across the flood plain.

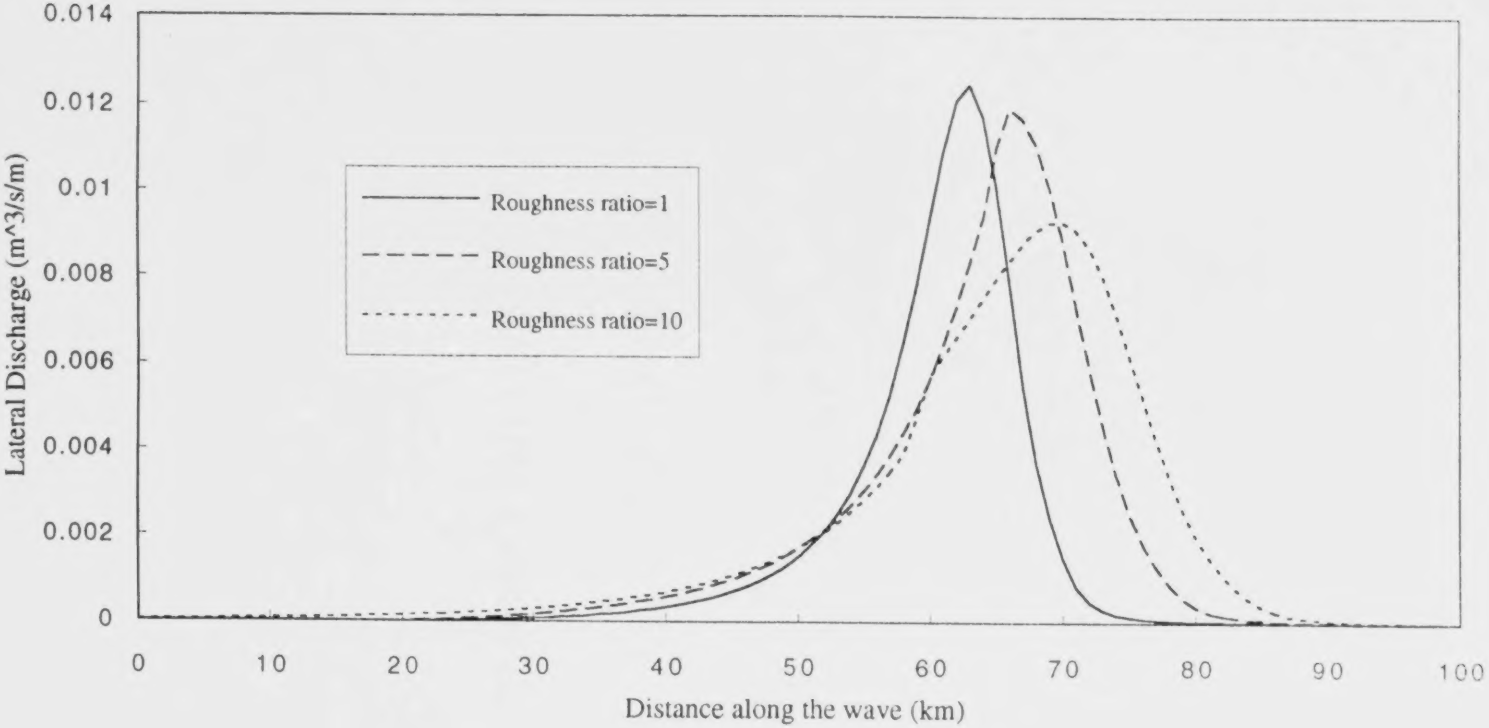

Figure 6.11 Effect of roughness ratio on the spatial distribution of lateral discharge profile at the interface.

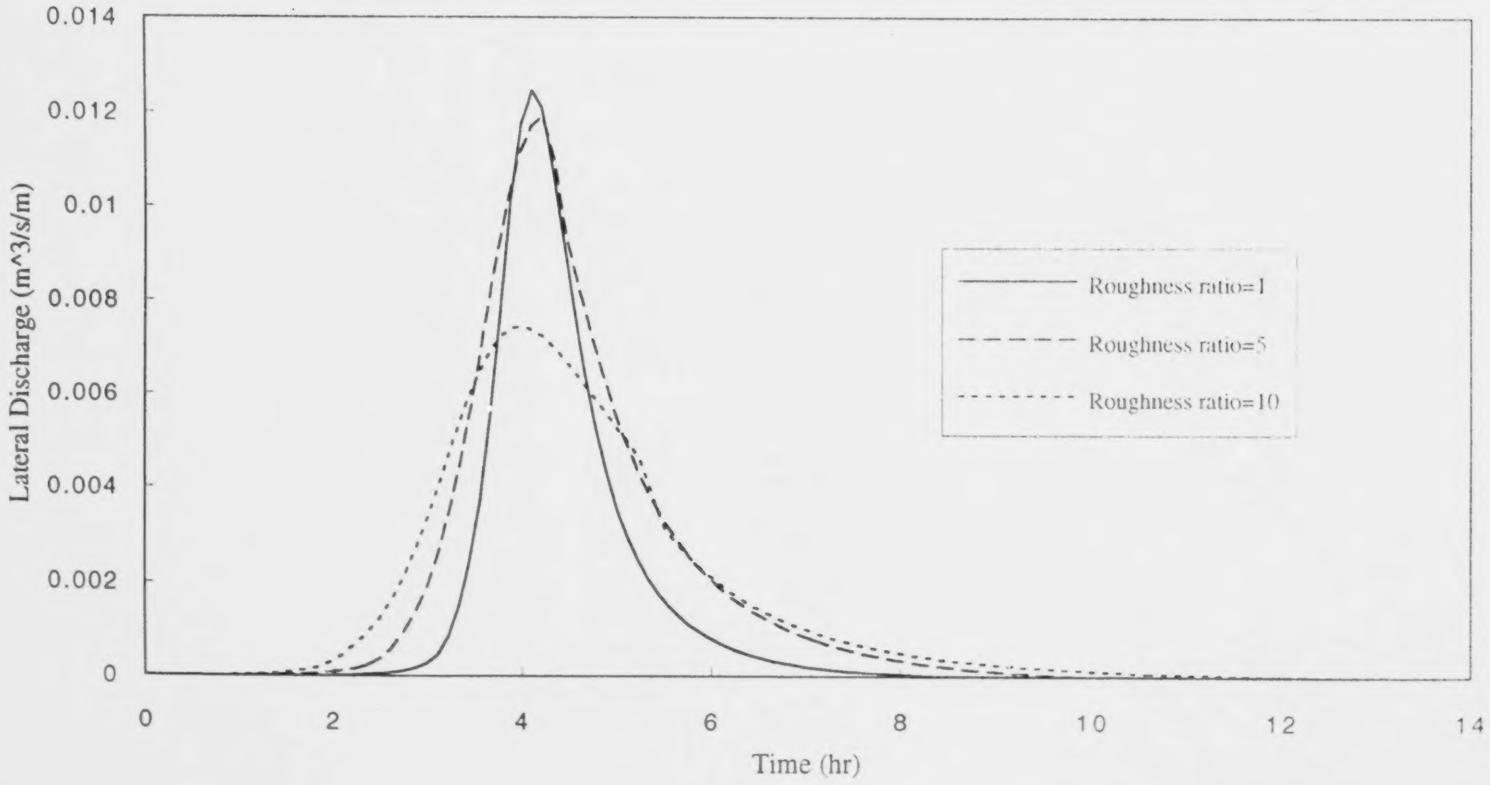

Figure 6.12 Effect of roughness ratio on the lateral discharge hydrographs at the interface.

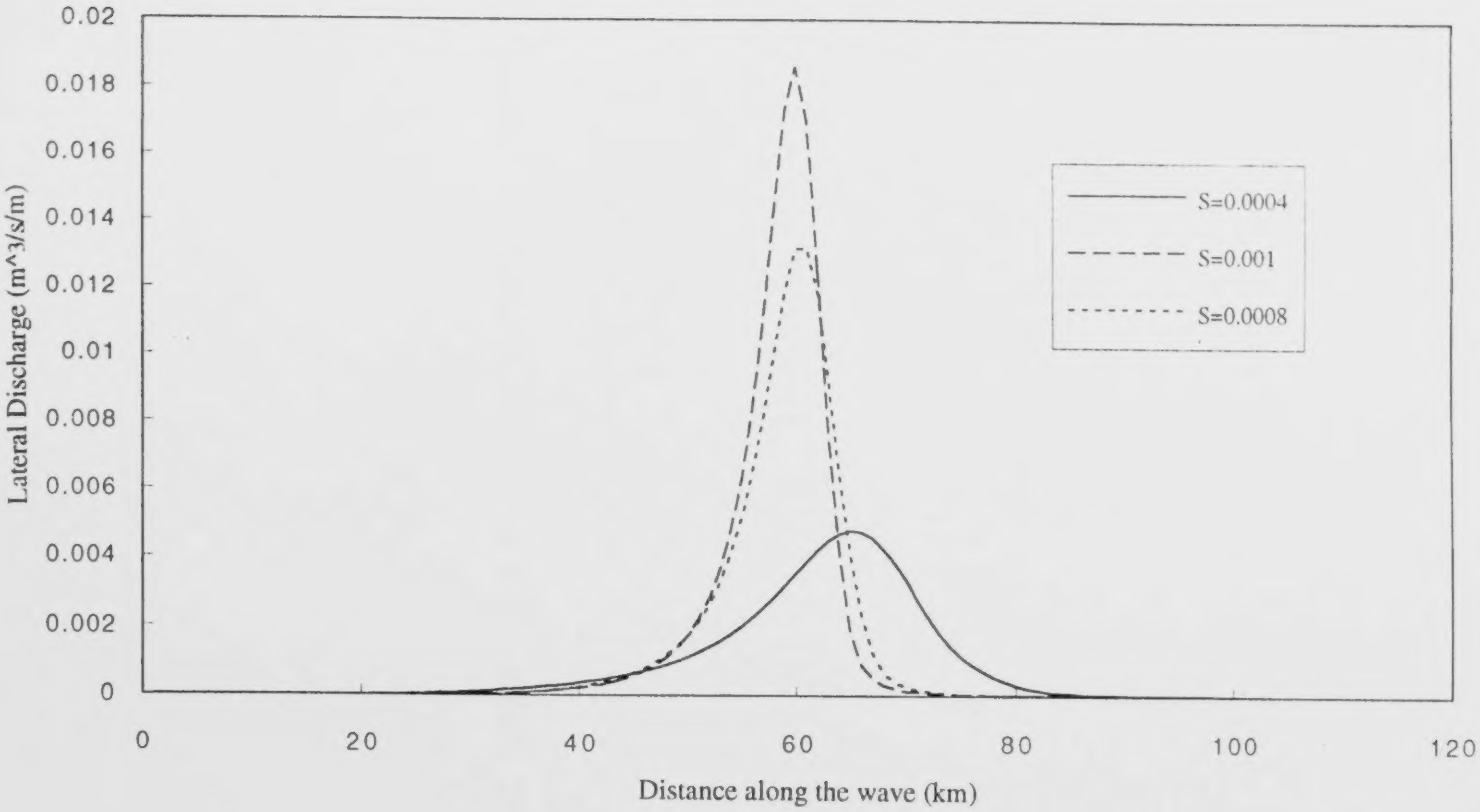

Figure 6.13 Effect of the longitudinal bed slope on the lateral discharge profile at the interface.

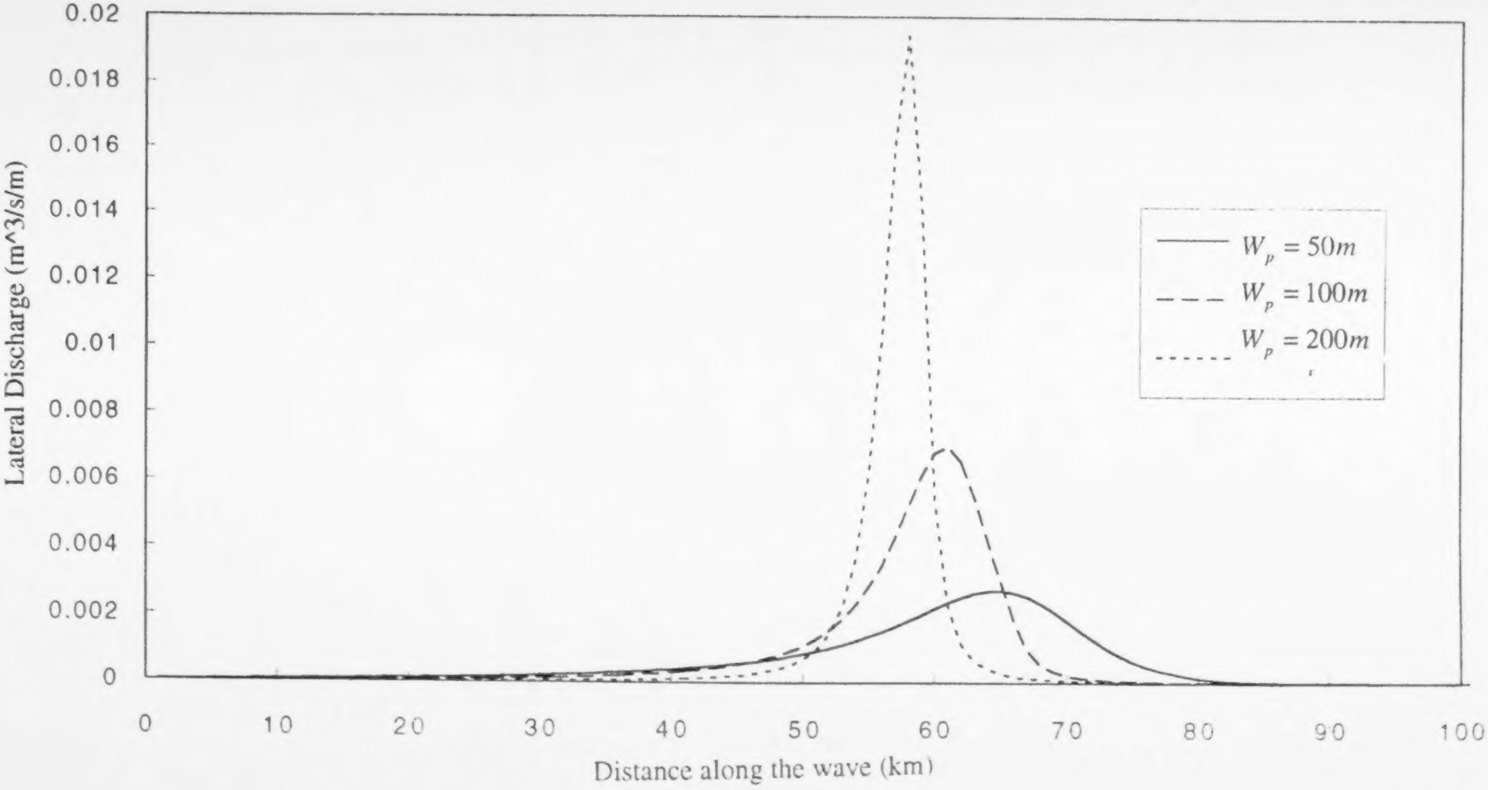

Figure 6.14 Effect of the flood plain width on the lateral discharge profile at the interface.

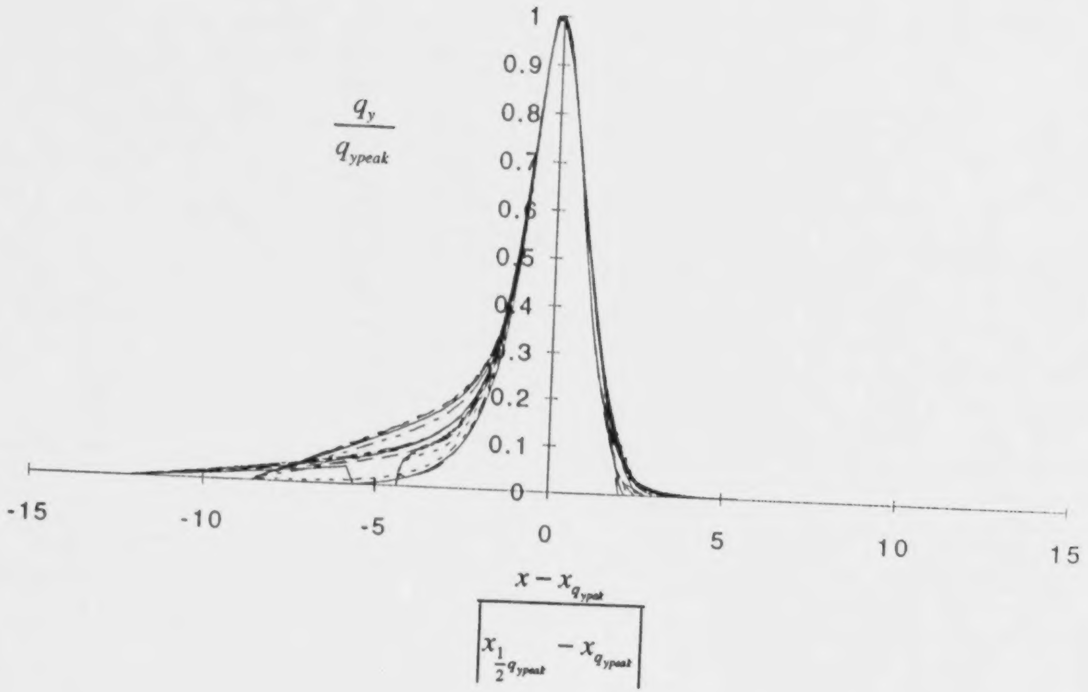

Figure 6.15 Similarity profiles of the lateral discharge.

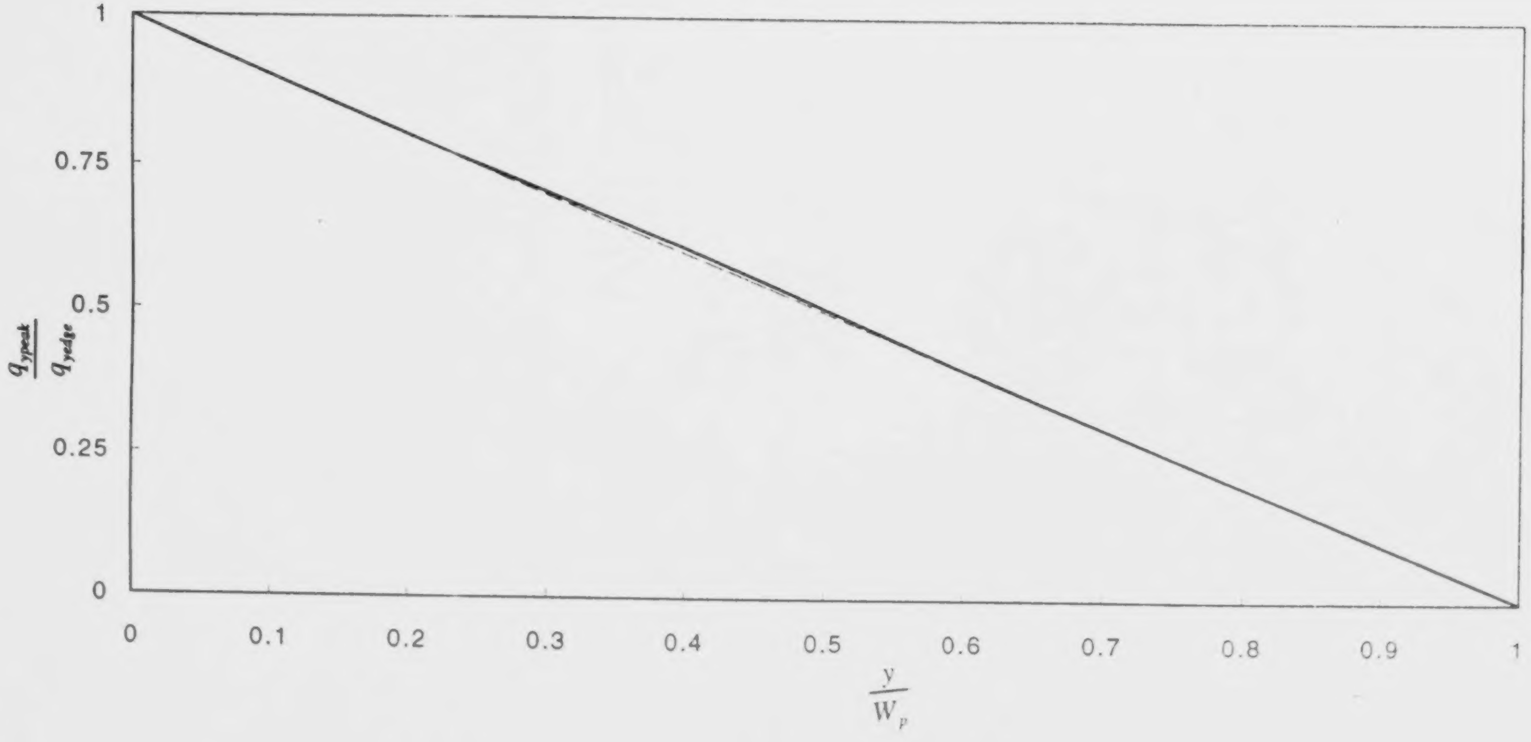

Figure 6.16 Non-dimensional plot of the peak lateral discharge across the flood plain.

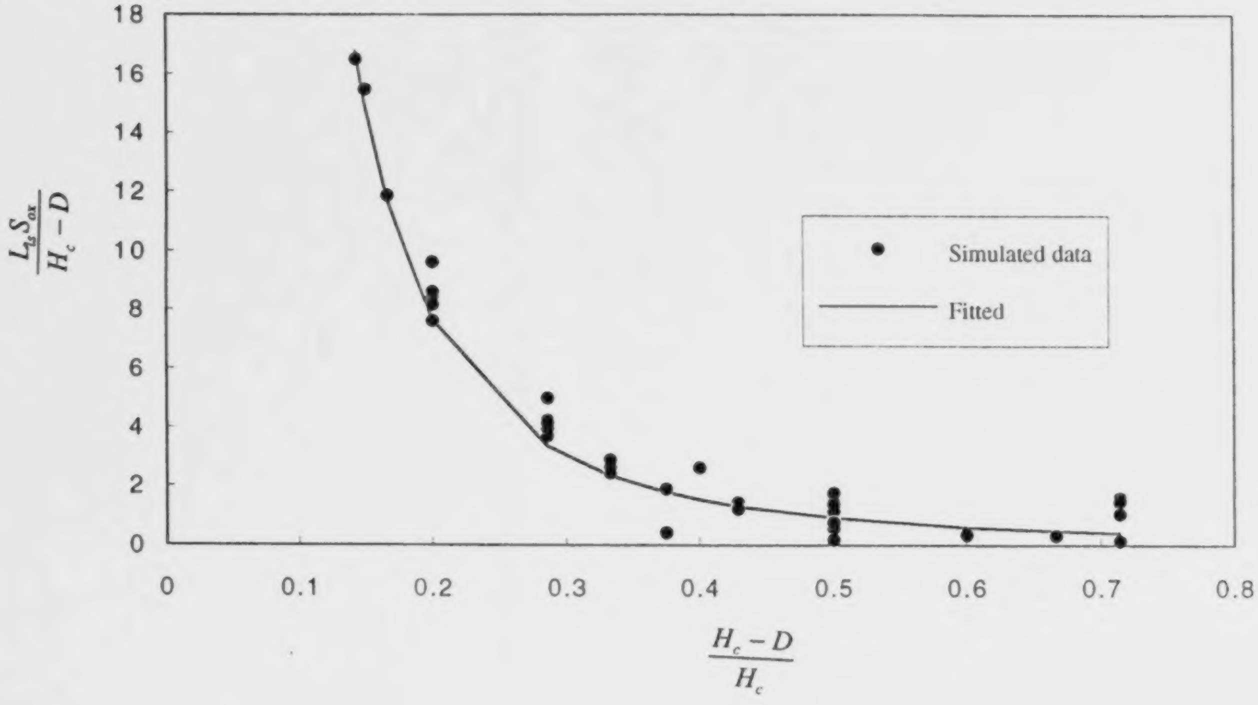

Figure 6.17 Non-dimensional plot of the left length scale.

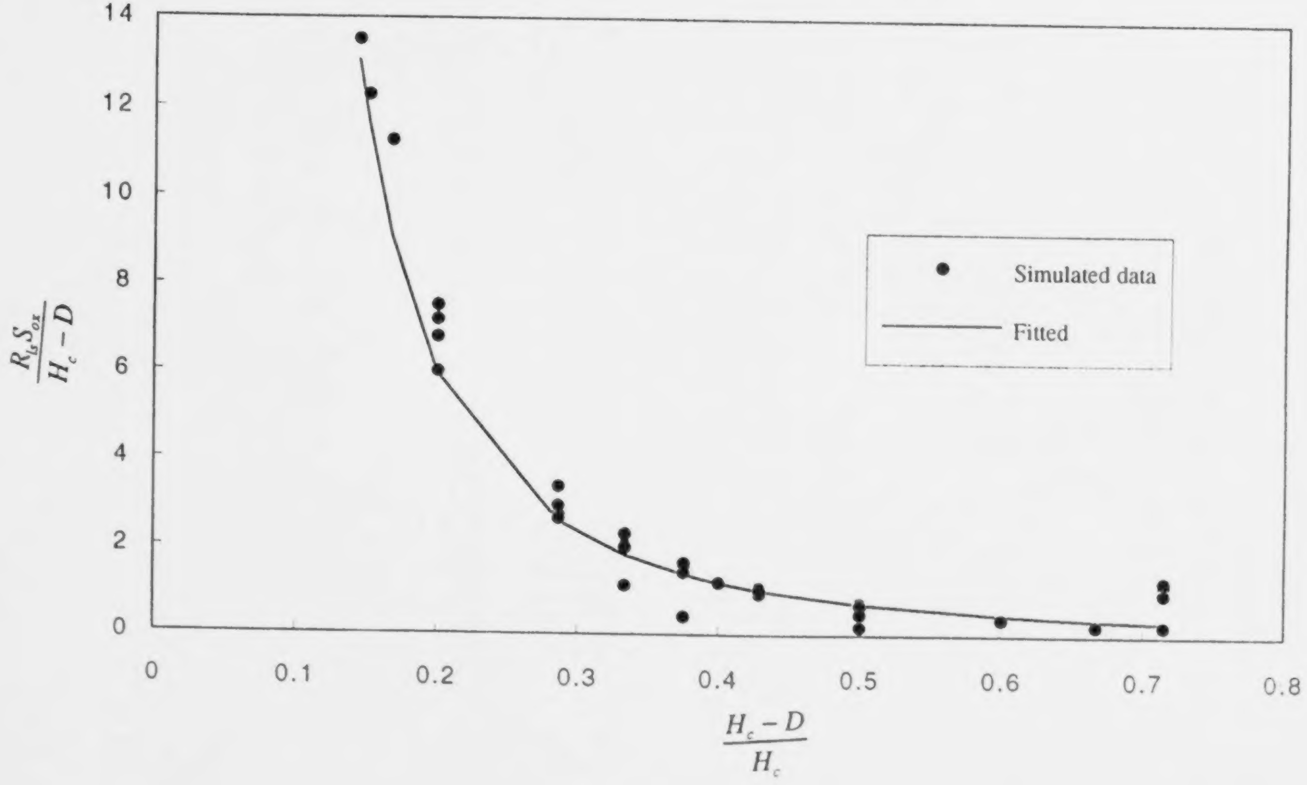

Figure 6.18 Non-dimensional plot of the right length scale.

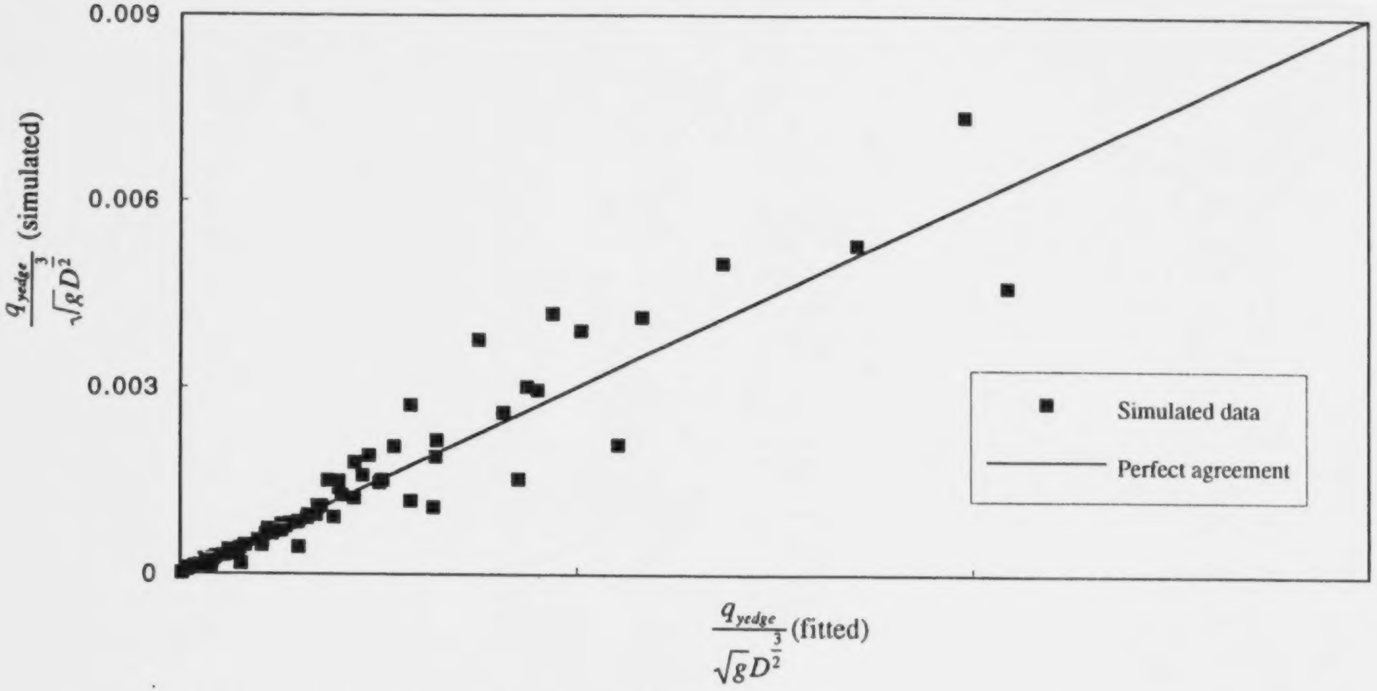

Figure 6.19 Comparison of the fitted and the numerical experimental lateral discharge at the interface of the main channel and the flood plain.

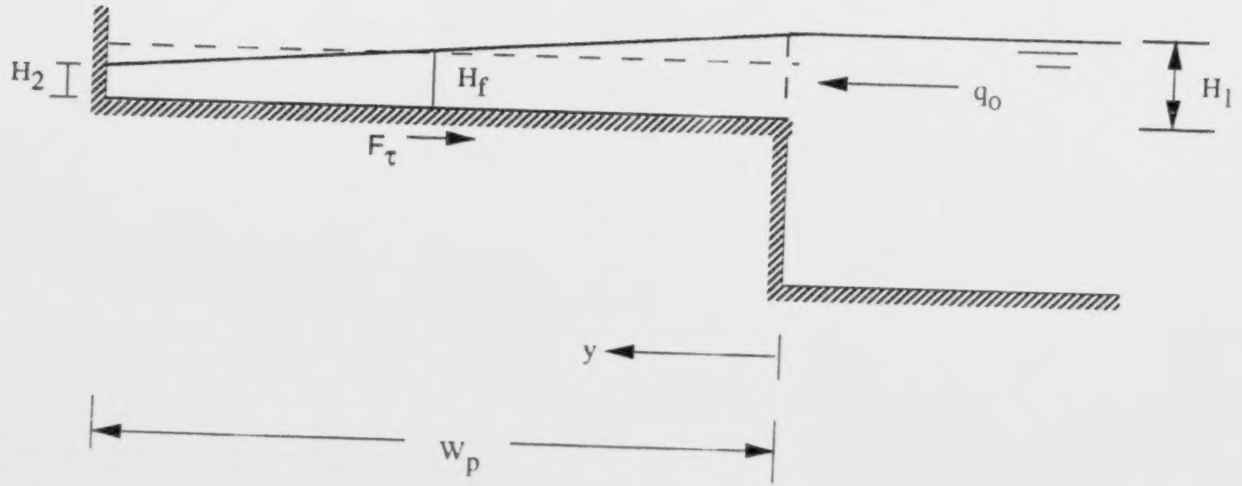
H_2
H_f
F_τ
q_o
H_1
y
W_p

Figure 6.20 Control volume of a fully flooded flood plain.

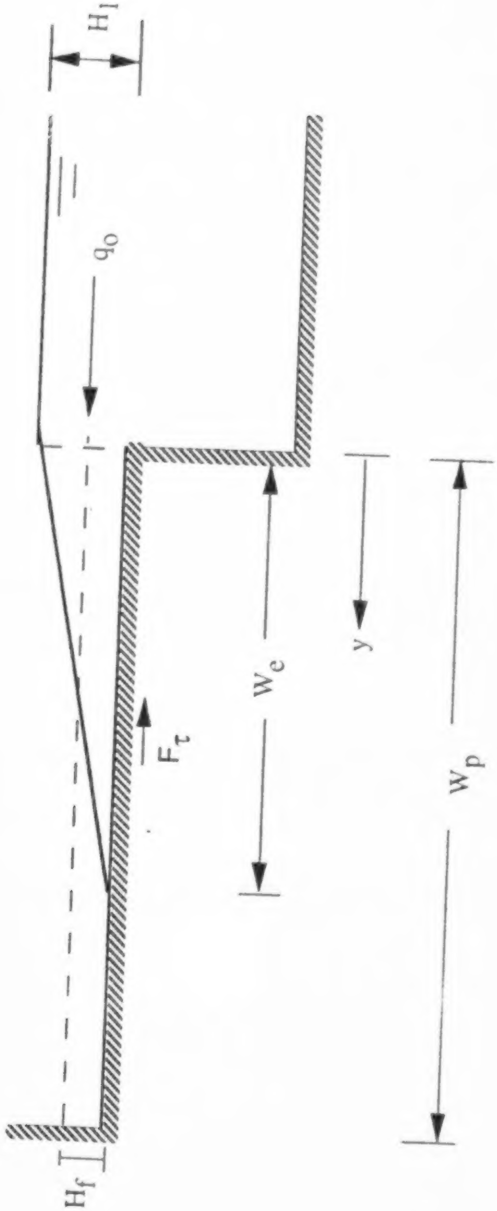
H_l
q_o
F_τ
W_e
y
W_p
H_f

Figure 6.21 Control volume of a partially flooded flood plain.

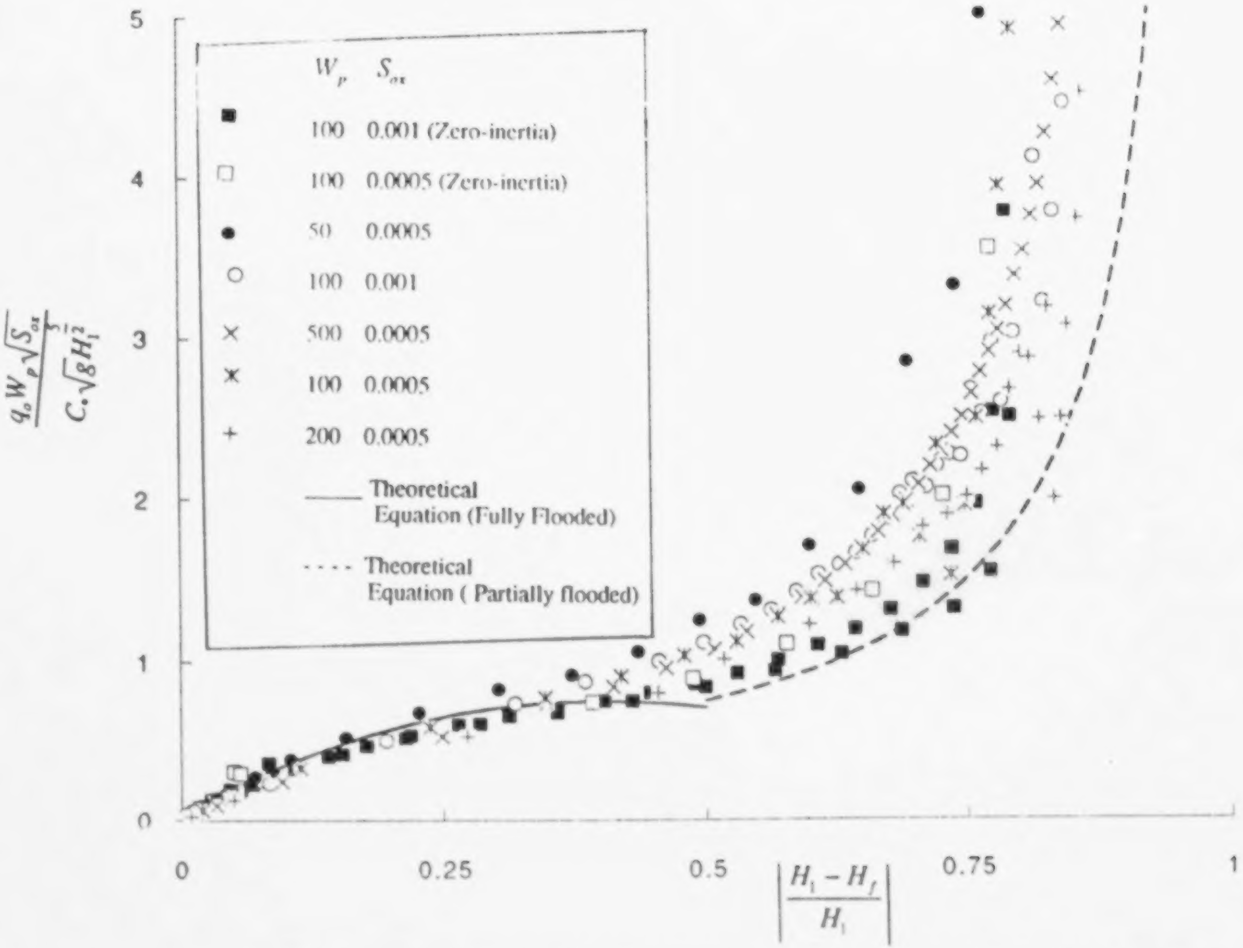

Figure 6.22 Comparison of the data obtained through the theoretical equations with the simulated data for lateral flow exchange.

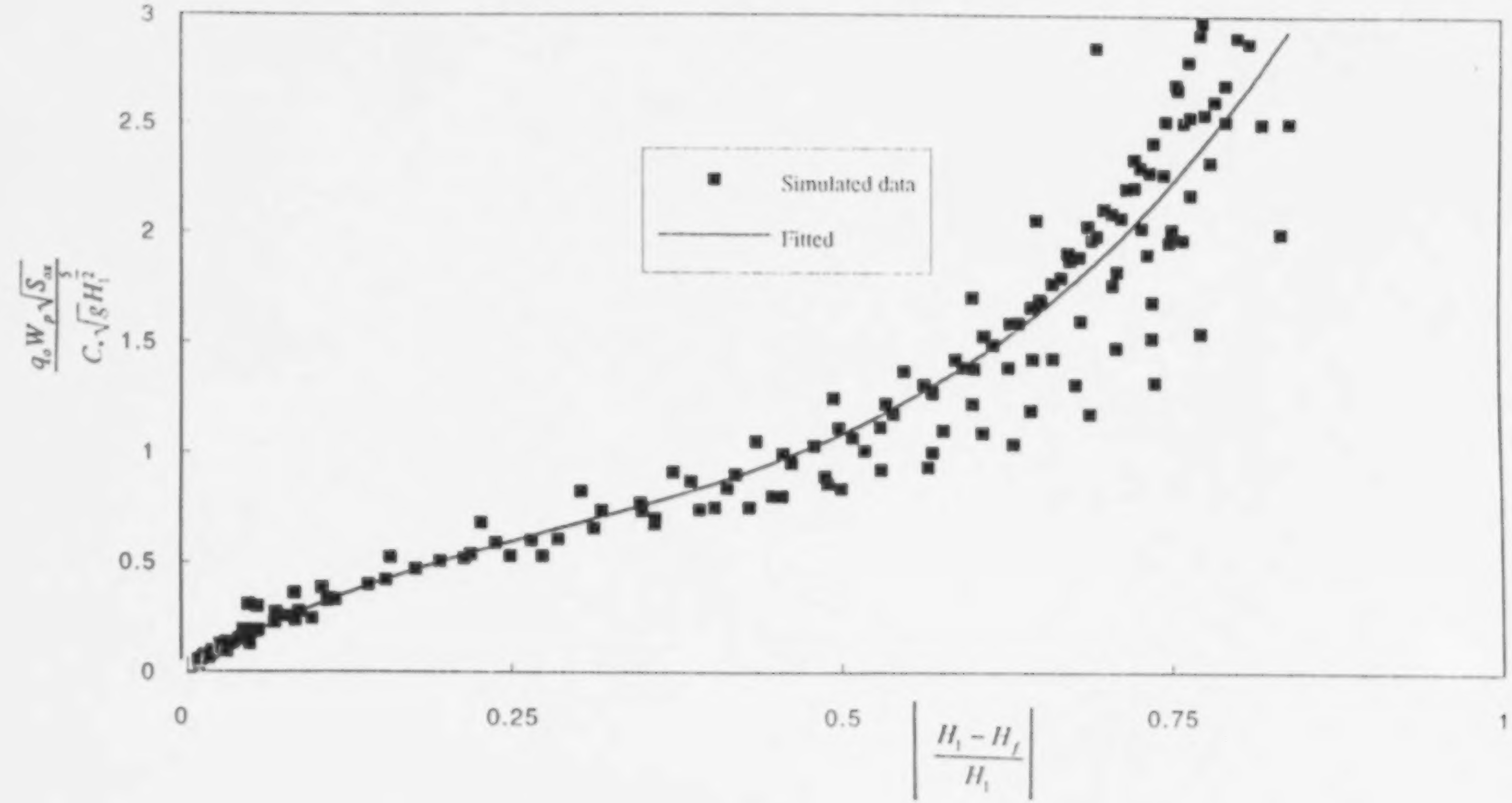

Figure 6.23 Comparison of the data obtained through the regression equation with the simulated data for lateral flow exchange.

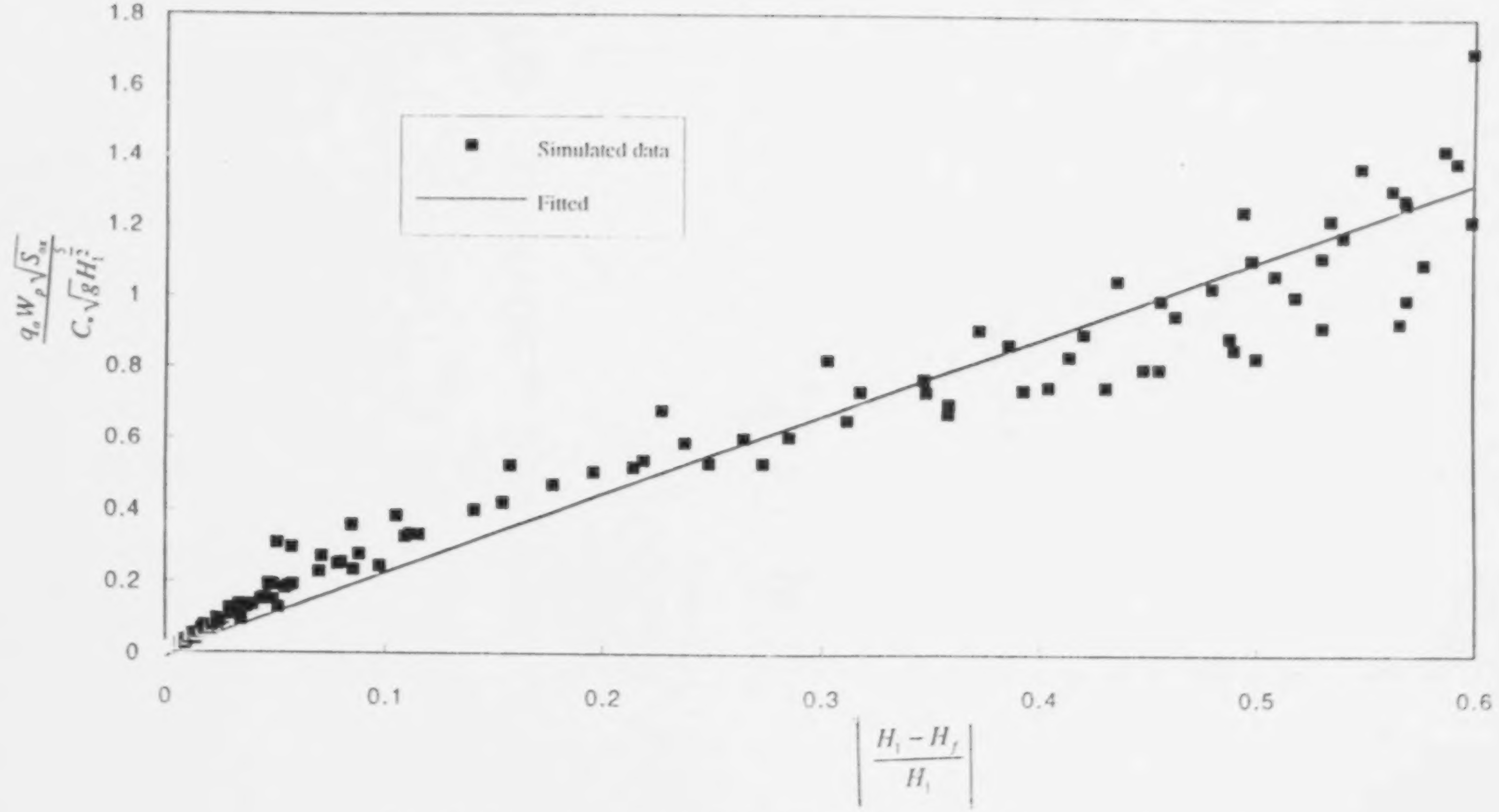

Figure 6.24 Comparison of the data obtained through the linear regression equation with the simulated data for lateral flow exchange.

7 CONCLUSIONS AND RECOMMENDATIONS

7.1 SUMMARY

The purpose of the present work was to perform a computational study of the hydraulic characteristics of the lateral discharges that take place between the main channel and the flood plain of a compound channel system during floods. This kind of study has many practical applications. As floods occur in the river-flood plain areas, the volume of a flood plain reach is filled up by the lateral flows from the main channel and by the longitudinal flows from the upstream end of the flood plain. An effort was made to investigate and analyze the characteristics of this lateral discharge in detail which might enable some simple estimates of the lateral transfer of materials and their distribution on the flood plains. These transferred materials could be the suspended sediments or the contaminants which normally remain confined in the river channel. Contaminants, in particular, may cause environmental and ecological hazards to the flood plain areas. Therefore, an adequate knowledge of the quantity and the distribution of these substances may provide some guidelines for preventive measures. As it is almost impossible to study this aspect by laboratory experiments, numerical experiments were conducted.

A two-dimensional zero-inertia computational model for simulating unsteady compound channel flows was developed to undertake these numerical experiments. A pseudo-steady state form of the model was then used to develop a methodology to quantify the volume of lateral flows from the main channel to the flood plain and their distribution along the flood wave as well as across the flood plain. The present study was also concerned with the theoretical analysis of flow exchange between the main channel and the flood plain and to derive relationships for flow exchange in terms of the local main channel and flood plain depths. The conclusions drawn from the studies discussed in the preceding chapters in detail are presented in Section 7.2 and the specific recommendations for further research are provided in Section 7.3.

7.2 CONCLUSIONS

The following conclusions are drawn from the present research:

1) An order of magnitude analysis of the governing flow equations provides three non-dimensional parameters. These are diffusion flow number, β, scale Froude number, F_o, and aspect ratio, W/L_o. Depending on the relative magnitudes of these variables for different floods, inertial terms can be neglected for some flood predictions.

2) The zero-inertia model developed in the present study is simple, robust and relatively easy to execute. It can simulate a dry bed situation without any computational difficulty, whereas special techniques are needed for full dynamic models to simulate such a case. The model was tested against the experimental data of Treske (1980) and reasonable agreement was found. Applications of this model to hypothetical cases showed that it is capable of simulating various features of floods which are normally observed in the field.

3) Comparison of the relative performance of the present model and a full dynamic model FESWMS-2DH for non-dynamic situations showed that the proposed model produced comparable results with much less computational time and effort. As an example, approximately 24 hours were required for FESWMS-2DH to simulate a hypothetical flood in IBM PC 486 DX with 50 MHz, whereas the present model needed

only about 20 minutes. Within the applicable range of its use, the zero-inertia model may replace the complicated full dynamic model for most flood predictions.

4) The theoretical analysis of a two-dimensional monoclinal wave provided a valuable insight into the effects of the various parameters of a compound channel and a flood on the ratio of average flood wave velocity to average flow velocity and on the filling process of the flood plain by lateral flows. These parameters are the width ratio, the roughness ratio, and the depth ratio. It was found that the ratio of velocities decreases as the width or the roughness ratio increases. A simple equation was derived to quantify the volume of lateral flow. It was found that the rougher or the shallower the flood plain, the more the volume of flow leaving the main channel and filling up the flood plain.

5) An analysis of lateral discharge data of monoclinal waves obtained through numerical experiments supported the theoretical analysis and also explored the hydraulic characteristics of such flows. It was found that the maximum lateral discharge per unit length varies linearly across the flood plain. The effects of the width ratio, the roughness ratio, and the bed slope on the water surface and the lateral discharge profiles of the monoclinal waves were also critically examined. As the roughness of the flood plain increases, the maximum lateral discharge per unit length decreases; however, the total volume of lateral flow increases. Moreover, the maximum lateral discharge and the total volume of flow from the main channel increase as the slope or the width of the flood plain increases.

6) Further analysis of data produced a similarity profile of the distribution of lateral flows. The scales are the peak lateral discharge and the two length scales chosen such that the magnitude of the lateral discharge on each side of the profile is half of the peak discharge. An analysis of the various scales is presented and empirical regression equations are proposed for practical purposes. The spatial distribution of the lateral discharge along the flood wave could be transferred to the lateral discharge hydrographs using the average flood wave velocity as seen by a stationary observer.

7) The methodology developed in this study provides detailed information on the volume and the distribution of the lateral discharge along the wave as well as across the flood plain. This may provide useful guidelines for the investigation and the analysis of the volume and the distribution of the transferred materials.

8) Two theoretical equations were derived for different flood plain flow situations, namely, for fully flooded and partially flooded plains to obtain a relationship for flow exchange between the main channel and the flood plain in terms of the local channel and flood plain flow depths. Data obtained through numerical experiments supported the trend of these theoretical equations reasonably well. Empirical equations are proposed for practical purposes. These equations may be useful for specifying the lateral flow exchange between the main channel and the flood plain flows presently handled by weir type equations in one-dimensional compound channel flow models.

7.3 RECOMMENDATIONS

The present research work demonstrates the development and the application of a simple two-dimensional zero-inertia model for simulating unsteady compound channel flow. It also represents the first step in developing a simple methodology to quantify the volume and the distribution of lateral flows and to obtain an approximate estimate of the quantity and the distribution of laterally transferred materials. The limitations of this work must also be recognized. The following recommendations for further research are suggested with a view to improving the ultimate utility of the present research.

1) The proposed regression equations should be applied only within the range of the non-dimensional variables used in the study. Hence, more numerical experiments may be undertaken for a wider range of variables which may be useful for field conditions.

2) Quantitative results obtained through the proposed methodology need to be verified. A computational model for lateral transport and deposition of suspended sediment needs to be developed and applied. Then the obtained results can initially be verified by undertaking laboratory experiments for floods in a compound channel. After performing several experiments, the quantity and the depositional pattern of suspended sediments on the flood plain will then be examined and quantified after the passage of each flood. The results obtained through the proposed methodology will then be compared with experimental data. If reasonable agreement is obtained, then this methodology may be applied to the field data. Having gained enough confidence about the accuracy and the reliability of this simple methodology, further analysis may be carried out for the natural rivers.

3) The proposed model is presently limited to straight prismatic channels. This model may be modified by probably adopting body fitted coordinates so that it can easily be applied to natural meandering rivers. The model is also only applicable to a fixed bed. This model may be modified to incorporate the mobile bed condition.

REFERENCES

Abbott, M. B., 1979, "*Computational Hydraulics; Elements of the Theory of Free Surface Flows.*" Pitman Publishing Company, London, England, 324 pp.

Abida, H. and Townsend, R. D., 1994, "A Model for Routing Unsteady Flows in Compound Channels." *IAHR Journal of Hydraulic Research.* Vol. 32, No. 1, pp. 145 - 153.

Adeff, S. E., 1988, "*A Sediment -laden Three -Dimensional -Flow Numerical Model.*" Thesis presented to the University of Iowa, USA in partial fulfillment of the requirements for the degree of Doctor of Philosophy.

Ahmadi R., 1979, "*An Experimental Study of the Interaction Between Main Channel and Flood plain Flows.*" Thesis presented to the University of Alberta, Edmonton, Alberta, Canada in partial fulfillment of the requirement for the degree of Doctor of Philosophy.

Akan, A. O. and Yen, B. C., 1981, "Diffusive-Wave Flood Routing in Channel Networks." *ASCE Journal of Hydraulic Engineering.* Vol. 107, (HY 6), pp. 719-732.

Akanbi, A. A. and Katopodes, N. D., 1988, "Model for Flood Propagation on Initially Dry Land." *ASCE Journal of Hydraulic Engineering.* Vol. 114, (HY7), pp. 689 - 706.

ASCE Task Committee on Turbulence Models in Hydraulic Computations, 1988, "Turbulence Modeling of Surface Water Flow and Transport." Parts 1 to 5. *ASCE Journal of Hydraulic Division.* Vol. 114, (HY9), pp. 970 - 1073.

REFERENCES (continued)

Barnes, H. H., 1987, "*Roughness characteristics of Natural Channels.*" U.S. Geological Survey Water Supply Paper, No. 1849. 213 pp.

Bhowmik, N. G. and Demissie, M., 1982, "Carrying Capacity of Flood Plains." *ASCE Journal of Hydraulic Engineering*. Vol. 108, (HY3), pp. 443 - 452.

Celia, M. A. and Gray, W. G., 1992, "*Numerical Methods for Differential Equations: Fundamental Concepts for Scientific and Engineering Applications.*" Prentice Hall Publishing Company. New Jersey. 436 pp.

Chaudhry, M. H., 1993, "*Open Channel Flow.*" Prentice Hall, New Jersey. 483 pp.

Chow, V. T., 1959, "*Open Channel Hydraulics.*" McGraw- Hill Book Company, New York, N. Y., pp. 680.

Chow, Ven Te and Zvi, Arie, Ben , 1973, "Hydrodynamic Modeling of Two Dimensional Watershed Flow." *ASCE Journal of Hydraulic Engineering.* Vol. 99, (HY11), pp. 2023 - 2040.

CSCE Task Committee on River Models, 1993, "Evaluation of Dynamic Models for Rivers with Flood plains." *CSCE annual conference,* 11th Canadian Hydrotechnical conference, June, 8-11, 1993, Fredericton, N. B., pp. 389-398.

Cunge, J. A., 1975, "Two Dimensional Modeling of Flood Plains." Chapter 17, of *Unsteady Flow in Open Channels,* K. Mahmood and V. Yevjevich, Eds., Vol. 2, Water Resources Publications, Fort Collins, Colorado, pp. 705 - 762.

REFERENCES (continued)

Cunge, J. A. , Holly, F. M. and Verwey, A., 1980, "*Practical Aspects of Computational River Hydraulics.*" Pitman Publishing Company, London, England, 420 pp.

DeVries, J. D., Hromadka, T. V., and Nestlinger, A. J., 1986, "Applications of a Two Dimensional Diffusion Hydrodynamic Model." *International Conference, Hydrosoft 86*, pp. 393-411.

Dingman, S. L., 1984, "Fluvial Hydrology." Freeman Publishing Company, Newyork. 383 pp.

Djordjevic, S., 1993, "Mathematical Model of Unsteady Transport and its Experimental Verification in a Compound Channel Flow." *IAHR Journal of Hydraulic Research*. Vol. 31, No. 2, pp. 229 - 248.

Dracos, T. and Hardegger, P., 1987, "Steady Uniform Flow in Prismatic Channels with Flood plains." *IAHR Journal of Hydraulic Research*. Vol. 25, No. 2, pp. 169-185.

Ervine, D. A. and Baird, J. I., 1982, "Rating Curves for Rivers with Overbank Flow." *Proceedings of Institute of Civil Engineers*, London, England, Pt.2. Vol. 73, pp. 465 - 472.

Ervine, D. A. and Ellis, J., 1987, "Experimental and Computational Aspects of Overbank Flood plain Flow." *Transactions of the Royal Society of Edinburgh, Earth Sciences*. Vol. 78, pp. 315 - 325.

Federal Highway Administration, 1989, "Finite Element Surface Water Modeling System: Two-Dimensional Flow in a Horizontal Plan (FESWMS-2DH)." Publication No. FHWA - Rd - 88 - 177.

REFERENCES (continued)

Fischer, H. B., List, E. J., Koh, R. C. Y., Imberger, J. and Brooks, N, H., 1979, *"Mixing in Inland and Coastal Waters."* Academic Press, 483 pp.

Flokstra, C., 1977, "The Closure Problem for Depth-Averaged 2D-Horizontal Flow." *Proceedings of the 17th IAHR Congress.* Baden - Baden, Germany, Vol. 2, pp. 247- 256.

Fread, D. L., 1973, "Effects of Time Step Size in Implicit Dynamic Routing." *Water Resources Bulletin.* Vol. 9, No. 2, pp. 338 - 351.

Fread, D. L., 1976, "Flood Routing in Meandering Rivers With Flood Plains." *Proceedings of the Symposium on Inland Waterways for Navigation, Flood Control, and Water Diversions, Waterways Harbors and Coastal Engineering Div., ASCE.* pp. 16-35.

Fread, D. L., 1988, *The NWS DAMBRK Model*: Theoretical Background / User Documentation." Office of Hydrology, National Weather Service (NWS), Maryland, USA.

Gallati, M. and Braschi, G., 1989, "Simulation of a Levee - Breaking Submersion of Planes and Urban areas." *Computational Modeling and Experimental methods in Hydraulics (Hydrocomp ' 89).* C. Maksimovic, and the late M. Radojkovic. Eds., pp. 117 - 126.

Gee, D. M. , Anderson, M. G. and Baird, L., 1990, " Large Scale Flood Plain Modeling." *Earth Surface Processes and Land forms.* Vol. 15, pp. 513 - 523.

Gerald, F. C., and Wheatley, P. O., 1985, *"Applied Numerical Analysis."* 3rd edition, Addison-Wesley Publishing Company, 579pp.

REFERENCES (continued)

Giammarco, P. D. and Todini, E., 1994, "A Control Volume Finite Element Method for the Solution of 2-D Overland Flow Problems." *In Modeling of Flood Propagation Over Initially Dry Areas*. Proceedings of the Specialty conference Co -sponsored by ASCE - CNR / GNDCI - ENEL spa. Paolo Molinaro and Luigi Natale Eds. pp. 82 - 101.

Giammarco, P. D. and Todini, E., Consuegra, D., Joerin. F., and Vitalini, F., 1994, "Combining a 2-D Flood Plain Model with GIS for Flood Delineation and Damage Assessment." *In Modeling of Flood Propagation Over Initially Dry Areas*. Proceedings of the Specialty conference co -sponsored by ASCE - CNR / GNDCI - ENEL spa. Paolo Molinaro and Luigi Natale Eds. pp. 171 - 185.

Grijsen, J. G. and Meijer, Th. J. G. P. , 1979, "On the Modeling of Flood Plain Flow in Large River Systems with Flood Plains." *Proceedings of the 18th IAHR Congress,* Paper No. D.d.8, pp. 227 - 235.

Hayami, S., 1951, "On the Propagation of Flood Waves." , *Bulletin 1, Disaster Prevention Research Institute*, Kyoto University, Japan.

Henderson, F. M., 1963, "Flood Wave in Prismatic Channels." ASCE *Journal of Hydraulic Engineering*. Vol. 89, (HY4), pp. 39 - 67.

Henderson, F. M. , 1966, "*Open Channel Flow*." Mcgraw Hill Publishing, Newyork, 522 pp.

Hicks, F., 1990, "*Finite Element Modeling of Open Channel Flow*." Thesis presented to the University of Alberta, Edmonton, Alberta, Canada in partial fulfillment of the requirements for the degree of Doctor of Philosophy.

REFERENCES (continued)

Hromadka II, T. V. and Guymon, G. L., 1982, "Nodal Domain Integration model of one-dimensional advection-diffusion." *Advances in Water Resources.* Vol. 5, pp. 9-16.

Hromadka II, T. V., Berenbrock, C. E., and Freckleton, J. R., 1985, "A Two-Dimensional Dam-Break Flood Plain Model." *Advances in Water Resources.* Vol. 8, pp. 7 - 14.

Hromadka II, T. V. and Durbin, T. J., 1986. "Two-Ddimensional Dam-Break Flood Flow Analysis for Orange County Reservoir." *Water Resources Bulletin,* American Water Resources Association. Vol. 22, No. 2, pp. 249 - 254.

Hromadka II, T. V., McCuen, R. H., and Yen, C. C., 1987, "Comparison of Overland Flow Hydrograph Models." *ASCE Journal of Hydraulic Engineering.* Vol. 113, (HY11), pp. 1422 - 1440.

James, C. S., 1985, "Sediment Transfer to Overbank Sections." *IAHR Journal of Hydraulic Research.* Vol. 23, pp. 435 - 452.

James, C. S., 1987, "The Distribution of Fine Sediment Deposits in Compound systems." *Water SA.* Vol. 13, No. 1, pp. 7 - 14.

Jansen, P. P., van Bendegom, L., van den Berg, J., deVries, M., and Zanen, A., 1979, "*Principles of River Engineering - The Non-Tidal Alluvial River.*" Pitman Publishing Company, London, England. 509 pp.

REFERENCES (continued)

Jenkins, G. A. and Keller, R. J., 1990, "Numerical Modeling of Flows in Natural Rivers." *Preprints of the conference on Hydraulics in Civil Engineering.* Sponsored by the National Committee on Water Engineering of the College of Civil Engineers, The Institute of Engineers, Australia and co-sponsored by IAHR, Sydney, Australia. pp. 22-27.

Katopodes, N. D. and Strelkoff, T., 1978, "Computing Two-Dimensional Dam-Break Flood Waves." *ASCE Journal of Hydraulic Engineering.* Vol. 104, (HY9), pp. 1269 - 1288.

Katopodes, N. D., 1984, "Fourier Analysis of Dissipative Finite Element Method Channel Flow Model." *ASCE Journal of Hydraulic Engineering.* Vol. 110, (HY7), pp. 927 - 944.

Katopodes, N. D., 1987, "Analysis of Transient Flow Through Broken Levees." *Turbulence Measurements and Flow Modeling.* C. J. Chen, L. D. Chen and F. M. Holly Jr. Eds. pp. 301 - 310.

Keller, R. J. and Rodi, W., 1984, "Prediction of Two-Dimensional Flow Characteristics in Complex Channel Cross-Sections." *Hydrosoft'84, Hydraulic Engineering Software. Proceedings of the Int. Conf.* Portoroz, Yugoslavia. pp.3-3-3-14.

Keller, R. J. and Rodi, W., 1988, "Prediction of Flow Characteristics in Main Channel / Flood Plain Flows." *IAHR Journal of Hydraulic Research.* Vol. 26, No. 4, pp. 425- 441.

REFERENCES (continued)

Kesel, R. H., Dunne, K. C., Mcdonald, R. C., Allison, K. R., and Spicer, B. E., 1974, "Lateral Erosion and Over bank Deposition on the Mississippi River in Louisiana Caused by 1973 Flooding." *Geology*. Vol. 1, pp. 461-464.

Kiely, G. K., Javan, M., McKeogh, E. J., 1990, "Prediction of Flow in Compound Channels." *Preprints of the Conference on Hydraulics in Civil Engineering*. Sponsored by the National Committee on Water Engineering of the College of Civil Engineers, The Institute of Engineers, Australia and co-sponsored by IAHR, Sydney, Australia, pp. 16 - 21.

Knight, D.W. and Demetriou, J. D., 1983, "Flood Plain and Main Channel Flow Interaction." *ASCE Journal of Hydraulic Engineering*. Vol. 109, (HY8), pp. 1073 - 1091.

Krishnappan, B. G. and Lau, Y. L., 1986, "Turbulence Modeling of Flood Plain Flows." *ASCE Journal of Hydraulic Engineering*. Vol. 112, (HY4), pp. 251 - 266.

Lai, Chan Ji and Yen, Chie Wei, 1993, "Propagation of Flood Wave in Compound Channel." *Proceedings of the 25th Congress of IAHR*. Tokyo, Japan. Vol. I, A-5-4 pp. 169-176.

Lean, G. H. and Weare, T. J., 1979, "Modeling Two-Dimensional Circulating Flow." *ASCE Journal of Hydraulic Engineering*. Vol. 105, (HY1), pp. 17 - 26.

Leendertse, J. J., 1967, "Aspects of a Computational Model for Long-Period Water Wave Propagation." *RM-5294-PR*, The Rand Corporation, Santa Monica, Calif.

Leopold, L. B., 1973, "River Channel Changes with Time: an Example." *Geological Society of America Bulletin*. Vol. 84, pp. 1845-1860.

REFERENCES (continued)

Lesleighter, E. J., 1983, "Flood Plain Flow using a Two-Dimensional Numerical Solution." *Proceedings of the Int. Conf. on the hydraulic Aspects of Floods and Flood Control,* London, UK. Paper No. G2, pp. 207 - 215.

Liggett, A. J., 1975, "Basic Equation of the Unsteady Flow." *Unsteady Flow in Open Channels,* K. Mahmood and V. Yevjevich, Eds., Vol. 1, Water Resources Publications, Fort Collins, Colorado, pp. 29 - 62.

Lighthill, M. J. and Whitham, G. B., 1955, "On Kinematic Waves: I-Flood Movements in Long Rivers." *Proceedings of the Royal Society of London,* (A), Vol. 229 (1178), pp. 281-316.

Linsley, R. K., Kohler, M. A. and Paulhus, J. L. H., 1982, "*Hydrology for Engineers.*" 3rd ed. McGraw-Hill Book company, New York, NY. 482 pp.

Martin, L. A. and Myers, W.R.C., 1991, "Measurements of Overbank Flows in a Compound River Channel." *Proceeding of the Institute of Engineers.* Part 2, Vol. 91, pp. 645, 657.

McGuirk , I.j, and Rodi , W., 1978, "A Depth-Averaged Mathematical Model for the near field of side discharges into Open Channel Flow." *Journal of Fluid Mechanics.* Vol. 86, part 4, pp. 761 - 781.

McKeogh, E. and Kiely G. K. 1989. "Experimental Study of the Mechanisms of Flood Flow in Meandering Channels." *Proceedings of the 23rd IAHR Congress,* Ottawa, pp. B491 - 498.

REFERENCES (continued)

Meselhe, A. and Holly Jr., F. M., 1993, "Simulation of Unsteady Flow in Irrigation Canals with Dry Bed." *ASCE Journal of Hydraulic Engineering*. Vol. 119, (HY9), pp. 1021-1039.

Naaim, M. and Brugnot, G., 1994, "Free surface modeling on a complex topography." In *Modeling of Flood Propagation Over Initially Dry Areas.* Proceedings of the Specialty conference co -sponsored by ASCE - CNR / GNDCI - ENEL spa. Paolo Molinaro and Luigi Natale Eds. pp. 298 - 308.

Ogink, H. J. M.1985, "The Effective Viscosity Coefficient in 2-D Depth Averaged Flow Models." *Proceedings of the 21st IAHR Congress*, Melbourne, Australia, Vol. 3, pp. 474-479.

Pasche, E., Rouve, G. and Evers, P., 1985, "Flow in Compound Channels with Extreme Flood Plain Roughness." *Proceedings of the 21st IAHR Congress.* Melbourne, Australia, Vol. 3, pp. 383 - 389.

Patankar, S. V., 1980, "*Numerical Heat Transfer and Fluid Flow.*" Hemisphere Publishing Company, 1980, 197 pp.

Pezzinga, G., 1994, "Velocity Distribution in Compound Channel Flows by Numerical Modeling." *ASCE Journal of Hydraulic Engineering.* Vol. 120, (HY10), pp. 1176-1197.

Pizzuto, J. E., 1987, "Sediment Diffusion during Overbank Flows." *Sedimentology*, Vol. 34, pp. 301-317.

REFERENCES (continued)

Ponce, V. M. and Simons, D. B., 1977, "Shallow Wave Propagation in Open Channel Flow." *ASCE Journal of Hydraulic Engineering*. Vol. 103, (HY12), pp. 1461 - 1476.

Ponce, V. M., Li, R. M., and Simons, D. B., 1978, "Applicability of Kinematic and Diffusion Models." *ASCE Journal of Hydraulic Engineering*. Vol. 104, (HY3), pp. 353 - 360.

Ponce, V. M., and Yabusaki, S. B., 1981, "Modeling Circulation in Depth-Averaged Flow." *ASCE Journal of Hydraulic Engineering*. Vol. 107, (HY11), pp. 1501-1518.

Ponce, V. M., 1986, "Diffusion Wave Modeling of Catchment Dynamics." *ASCE Journal of Hydraulic Engineering*. Vol. 103, (HY8), pp. 716-727.

Ponce, V. M., 1990, "Generalized Diffusive Wave Model with Inertial Effects." *Water Resources Research*. Vol. 26, No. 5, pp. 1099 - 1101.

Popovska, C, 1989, "Mathematical Model for two dimensional dam-break propagation." *Computational Modeling and Experimental methods in Hydraulics (Hydrocomp '89)*. C. Maksimovic and the late M. Radojkovic Eds. pp. 127 - 136.

Prinos, P. and Townsend, R. D., 1984, "Comparison of Methods for Predicting Discharge in Compound Open Channels." *Advances in Water Resources*. Vol. 7, pp. 180 - 187.

REFERENCES (continued)

Prinos, P., 1989, "Experiments and Numerical Modeling in Compound Open Channel and Duct Flows." *Computational Modeling and Experimental methods in Hydraulics (Hydrocomp ' 89).* C. Maksimovic and the late M. Radojkovic Eds. pp. 255 -268

Radojkovic, M., 1976, "Mathematical Modeling of Rivers with Flood plains." *Proceedings of the Symposium on Inland Waterways for Navigation, Flood Control, and Water Diversions, Waterways Harbors and Coastal Engineering Div. ASCE,* Vol. 1, pp. 56-.64

Radojkovic, M. and Djordjevic, S., 1985, "Computation of Discharge Distribution in Compound Channels." *Proceedings of the 21st IAHR Congress.* Melbourne, Australia, Vol. 3, pp. 367 - 371.

Rajaratnam, N. and Ahmadi, M, 1981, "Hydraulics of Channels with Flood Plains." *IAHR Journal of Hydraulic Research.* Vol. 19, No. 1, pp. 43 - 60.

Rashid, R. S. M. M., and Chaudhry, M. H., 1993, "Numerical Modeling of Unsteady Compound Channel Flow." Proceedings of the ASCE Conference, H. W. Shen, S. T. Su., and F. Wen Eds., San Frascisco, USA, pp. 1254, 1259.

Rastogi, A. K. and Rodi, W., 1978, "Prediction of Heat and Mass Transfer in Open Channels." *ASCE Journal of Hydraulic Engineering.* Vol. 104, (HY3), pp. 397 - 420.

Richtmyer, R. D. and Morton, K. W., 1967, "*Difference Methods for Initial value problems.*" 2nd ed. Interscience Publishers Inc. New York, NY. 450 pp.

REFERENCES (continued)

Rijn, L. C. van, 1990, "*Principles of Fluid Flow and Surface Waves in Rivers, Estuaries Seas and Oceans.*" AQUA Publications, Netherlands, 335 pp.

Roache, P. J., 1972, "*Computational Fluid Dynamics.*" Hermosa Publishers, P. O. Box. 8172, Albuquerque, New Mexico, N. M. 87108, 434 pp.

Rodi, W., 1984, "*Turbulence Models and Their Applications in Hydraulics*" -A State of the Art Review, 2nd ed. IAHR, Delft. 104 pp.

Sabur, M. A., 1990, "*A Distributed Numerical Model for Watershed Hydrology.*" Thesis presented to the University of Alberta, Edmonton, Alberta, Canada in partial fulfillment of the requirements for the degree of Doctor of Philosophy.

Samuels, P. G., 1985, "*Modeling of river and flood plain flow using the finite element method.*" Hydraulic Research, Tech. Report No. SR61, Wallingford, U. K.

Schmitz, G., Seus, G. J., and Czirwitzky, H. J., 1983, "Simulating Two Dimensional Flood Flow." *Proceedings of the Int. Conf. on the Hydraulic Aspects of Floods and Flood Control,* 13-15 september, 1983, London, England. Paper No. G1, pp. 195-206.

Seddon, J. A. , 1900, " River Hydraulics." *ASCE Trans.*, Vol. 43, pp. 179-229.

Sellin, R. J. H., 1964. "A Laboratory Investigation into the Interaction between Flow in the Channel of a River and that of its Flood Plain." *La Houille Blanche*. Vol. 7, pp. 793 - 801.

Soulis, J. V., 1992, "Computation of Two-dimensional Dam-break flood flows." *Int. Journal for Num. Methods in Fluids.* Vol. 14, pp. 631 - 664.

REFERENCES (continued)

Stephenson, D. and Kolovopoulos , P., 1990, "Effects of Momentum Transfer in Compound Channels." *ASCE Journal of Hydraulic Engineering*. Vol. 116, (HY12), pp. 1512 -1522.

Tayfur, G., Kavvas, M. L., Govindaraju, R.S., and Storm, D. E., 1993, "Applicability of St. Venant Equations for Two-dimensional Overland flows over Rough Infiltrating Surfaces." *ASCE Journal of Hydraulic Engineering*. Vol. 119, (HY1), pp. 51 - 63.

Thacker, W. C., 1978, "Comparison of finite element and finite difference schemes." Part II : Two - Dimensional Gravity Wave Motion. *Journal of Oceanography*. Vol. 8, No. 4, pp. 680 - 689.

Tingsanchali, T. and Chaiwat, C., 1984, " Two-Dimensional Flood Plain Modeling for Eastern Bangkok Plain." *Proceedings of the fourth Congress - Asian and Pacific Division, IAHR*, Thailand, pp. 29 - 44.

Tingsanchali, T. and Lal, N. K., 1988, " Subsidence of Flood Waves in Overbank Areas." *IAHR Journal of Hydraulic Research*. Vol. 26, NO. 5, PP. 585 - 597.

Tominaga, A. Nezu, I., and Ezaki, K., 1989 , " Experimental Study on Secondary Currents in Compound Channel Flows." *Proceedings of the 23rd IAHR Congress*. Ottawa, Canada, pp. A-15 - A 22.

Tuitoek, D. K., 1995, "*Coupled Equations for Modeling unsteady Flow in Open Channels with Flood Plains.*" Thesis presented to the University of Alberta, Edmonton, Alberta, Canada in partial fulfillment of the requirement for the degree of Doctor of Philosophy.

REFERENCES (continued)

Urban, C. and Zielke, W., 1985, "Steady State Solution for Two Dimensional Flows in Rivers with Flood Plains." *The Hydraulics of Flood and Flood Control, Proceedings of 2nd Int. Conf.* Cambridge, pp. 389 - 398.

Vreugdenhil, C. B. and Wijbenga, J. H. A., 1982, "Computation of Flow Patterns in Rivers." *ASCE Journal of Hydraulic Engineering*. Vol. 108, (HY11), pp. 1296 - 1309.

Walling, D. E., Bradley, S. B. and Lambert, C., 1986, "Conveyance Losses of Suspended Sediment within a Flood Plain System." In :*Drainage Basin Sediment Delivery* , R. F. Hadley Eds, I.A.H.S. publication No.159. pp. 119-131.

Walling, D. E., Quine, T. A., and He, Q., 1989, "Investigating Contemporary Rates of Flood Plain Sedimentation." *Low Land Flood Plain Rivers: Geomorphological perspectives.* P. A. Carling and G. E. Petts Eds., pp. 165-184.

Wang, H. F. and Anderson, M. P., 1982, "*Introduction to Ground Water Modeling: Finite Difference and Finite Element Methods.*" Freeman Publishing Company, San Francisco, USA. 237 pp.

Wark, J. B., Samuels, P. G., and Ervine, 1990, "A pratical Method of Estimating Velocity and Discharge in Compound Channes." *Proceedings of the int. Conf. on River Flood Hydraulics*, W. R. White Eds., Hydraulic Research Limited, Wallingford, U.K., 17-20 September, pp. 163-171.

Wormleaton, P. R. and Merret, D. J., 1990, "An Improved Method of Calculation for Steady Uniform Flow in Prismatic Main Channel / Flood Plain sections." *IAHR Journal of Hydraulic Research*. Vol. 32, No.1, pp. 145-153.

REFERENCES (continued)

Xanthopoulos, Th., and Koutitas, Ch., 1976, "Numerical Simulation of Two-Dimensional Flood Wave Propagation due to Dam failure." *IAHR Journal of Hydraulic research.* Vol. 14, No. 4, pp. 321 - 331.